– *An international journal for New Concepts in Global Tectonics* –

NCGT JOURNAL

Editor-in-Chief: Bruce LEYBOURNE (leybourneb@iascc.org)

NCGT Journal
New Concepts in Global Tectonics

Volume 14, Number 1
January 2026

ISSN 2202-0039

WWW.ncgtjournal.com

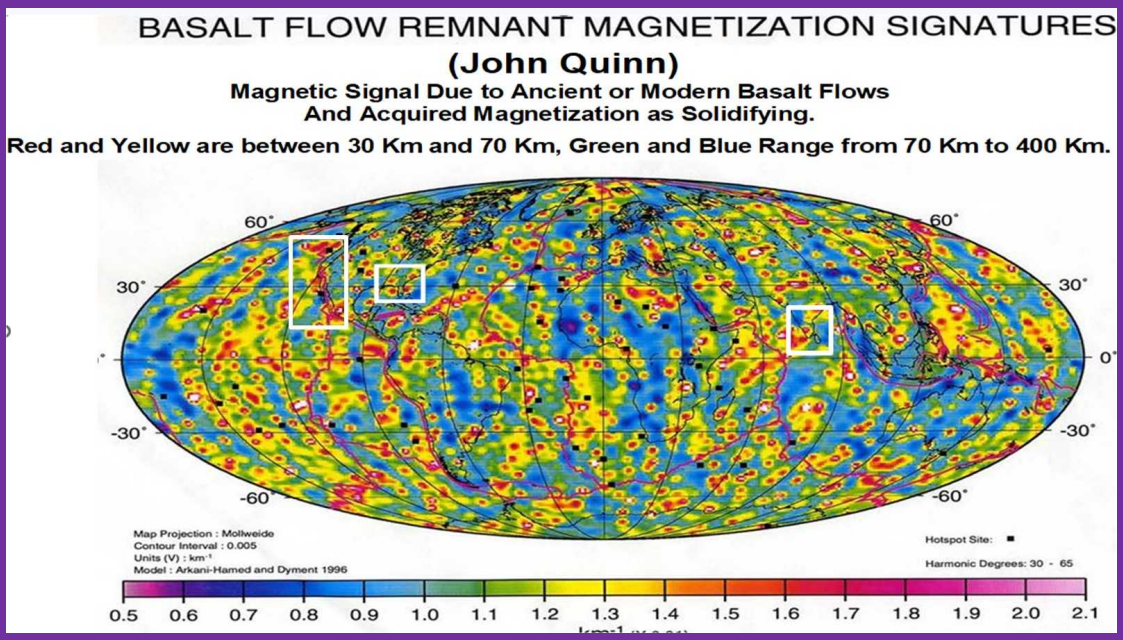

White Boxes Indicate Many Air-Earth Currents Under Geoplasma Research Investigations

Satellite monitoring of air-earth currents

by Quinn et. al.
See Fig. 86

Basalt flow remnant magnetization signatures , with a distinction in two classes of basalts , i.e., whether they are located at a depth 30 F 70 km (red and yellow), or at a depth 70 F 200 km (green and blue).

Special Issue on Air-Earth Currents

NCGT Journal
New Concepts in Global Tectonics

New Concepts in Global Tectonics Journal
Volume 14, Number 1, January 2026

ISSN number; ISSN 2202-0039

– An international journal for New Concepts in Global Tectonics –

NCGT JOURNAL

Volume 14, Number 1, January 2026. ISSN 2202-0039.

CONTENTS

For donations, please feel free to contact the Research Director of the Geoplasma Research Institute, Mr. Bruce Leybourne, at leybourneb@iascc.org. For contact, correspondence, or inclusion of material in the NCGT Journal please use the following methods: *NEW CONCEPTS IN GLOBAL TECTONICS.* 1. E-mail: leybourneb@iascc.org (files in MS Word or ODT format, and figures in gif, bmp or tif format) as separate files; 3. Telephone, +61 402 509 420. *DISCLAIMER*: The opinions, observations and ideas published in this journal are the responsibility of the contributors and do not necessarily reflect those of the Editor and the Editorial Board. *NCGT Journal* is a refereed quarterly international online journal and appears in March, June, September and December. *ISSN number*; ISSN 2202-0039.

NCGT Journal
New Concepts in Global Tectonics

New Concepts in Global Tectonics Journal
Volume 14, Number 1, January 2025

ISSN number; ISSN 2202-0039

EDITOR's CORNER: - Comments by Editor in Chief - Bruce Leybourne

Announcements on Upcoming Conferences - "CALL FOR PAPERS"

Next year - 21-24 September 2026 – NCGT in Italy is being organized by Valentino Straser (valentino .straser @gmail. com). Please contact Valentino if you wish to become involved in any aspect of the conference . Again , we are looking for Session Topics , Abstracts , Papers , Session Chairs , Organizers , Workers , Financial Contributions etc. Let me and Valentino know how you' d like to be involved, and we may accommodate.

September 2026 in Italy we currently have several sessions being locally organized by Valentino Straser

1.) Straser - EQ forecasting (Abstracts requested)

2.) Leybourne - Stellar Transformer - Global Space Weather interactions (6 Abstracts in Editor's Corner within New Concepts in Global Tectonics Journal - Volume 12, Number 4, December 2024)

3.) Anokhin - Lake Ladoga - Siberia (2 Abstracts in Editor's Corner within New Concepts in Global Tectonics Journal - Volume 13, Number 1, March 2025 pp. 5-8, more abstracts requested)

4.) Longhinos - Indian Tectonics (Abstracts requested)

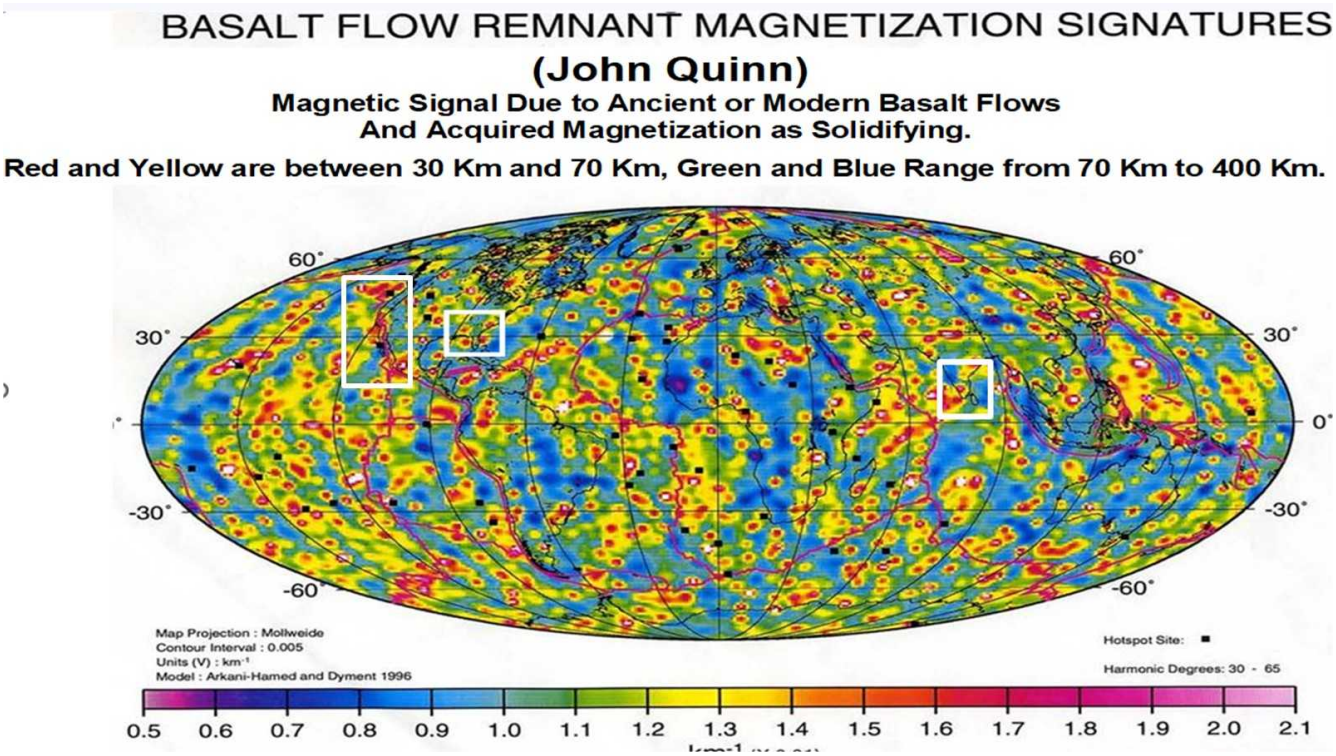

Cover Image : Satellite monitoring of air-earth currents by Quinn et. al. this issue. See Fig. 86. Basalt flow remnant magnetization signatures, with a distinction in two classes of basalts, i.e., whether they are located at a depth 30 F 70 km (red and yellow), or at a depth 70 F 200 km (green and blue).

NCGT Journal
New Concepts in Global Tectonics

New Concepts in Global Tectonics Journal
Volume 14, Number 1, January 2026

ISSN number; ISSN 2202-0039

Letters to the Editor: Giovanni Gregori discusses research papers

Dear Editor: The present special issue on air-earth currents contains two papers:
• Quinn, J.M.,† G.P. Gregori, and B.A. Leybourne, 2025. Satellite monitoring of air-earth currents
• Gregori, G.P., B.A. Leybourne, and J.R. Wright, 2025d. Generalized Cowling theorem and the Cowling dynamo.

I met John Quinn in 1995 at the IUGG General Assembly in Boulder (CO). He was looking at – and quite appreciating - a poster of mine, which anticipated the rationale to be later fully exploited in my book Gregori (2002). After our first meeting I had the honor of having several other email contacts.

He spent a large part of his life at the World Data Center for Solar -Terrestrial Physics in Boulder, being thus acquainted with handling a huge database. When he retired, he could manage to exploit some heavy data handling that he could not carry out while serving according to his official job. Thus, he carried out quite an original approach to the inversion problem of geomagnetic records collected by satellite.

It is well known that every inversion problem is per se indeterminate – as the signal of a shallow source is identical to the signal of a more intense, although deeper, source. John Quinn, however, considered that the electrical conductivity of the crust and lithosphere must in any case be within some reasonable physical range. By this, he afforded to get rid of a large drawback deriving from the mathematical indeterminacy. This resulted to be a very astute approach. Thus, he published a series of long reports that remained almost unnoticed by a large fraction of the scientific community, due also to his premature passing away (when one looses a friend, it is like loosing a part of himself). We feel sad, while being honored of filling this gap!

I do believe that this investigation by John Quinn is the most important achievement in geomagnetism since the time of Gauss, as he showed that a huge amount of air-earth currents flow across the Earth' surface, mostly in region of heavy crustal fracturing. When I wrote him this, he thanked me. However, he did not agree with me. In fact, my feeling is that he was a very kind person and he did not like to contradict his colleagues, in particular the models computed by Stefan Maus of the National Geophysical Data Center (NGDC), whom he estimated very much. Indeed our disagreement is related to the argument explained Fig. 3, and I do confirm my interpretation, even though – I must stress - this is not against the important and learned model carried out by Stefan Maus, who implemented a very careful and exhaustive analysis by assuming the Gauss classical hypothesis of a supposedly negligible mean role of air -earth currents on the planetary scale.

While writing the present long paper, based on John Quinn 's long reports, we tried to fully acknowledge the viewpoint of John Quinn, even though we must emphasize the paramount relevance of his study. I repeat: this is the most important investigation in geomagnetism since the time of Gauss, and we hope that the scientific community will soon acknowledge the memory of John Quinn for his astute inversion approach.

The second short paper derives from an invitation of Bruce A. Leybourne to give a self-contained account of the " generalized Cowling theorem".

I must give a short historical account. In 1919-1920 Larmor proposed an explanation of the magnetic field of the Sun and of stars, by envisaging that the internal plasma dynamics inside a star is in a fact a powerful dynamo. The idea was correct and it is still the object of huge astrophysical investigations. However, in the 1930s, Cowling showed a theorem, and proved that a physical system with perfect cylindrical symmetry cannot originate a dynamo. This " Cowling theorem" soon became almost a nightmare for every solar or stellar modeler. A few tens additional proofs became available in subsequent years, every one relying on slightly different approximations, although all of them gave the same result.

Only in 2002, in my book Gregori (2002), I afforded to prove a "generalized Cowling theorem", even though I did not realize it. Only at a later time, I realized what I had found. This is explained in detail in this short paper, including the agreement with the former Cowling theorem.

I hope the reader has a good reading.

ISSN number; ISSN 2202-0039

New Book

G. P. Gregori (born 1938), Degree in Physics (1961, Univ. of Milan),

B. G. Gregori (born 1967), Degree in Medicine and Surgery (1992) and Specialization in Neurology (1999)

Science is suffering an identity crisis. Our "widespread scientific knowledge" is "static".

Our mind dislikes uncertainty. Not relying on the mainstream is uncomfortable, but we gain better awareness of the world and of ourselves. This book is challenging. It stimulates the reader also on a psychological level, and tries to explain concepts that to most people consider abstruse. It is a journey where mind can dance between quantum physics, cosmology, theology, Greek philosophy and the mystery of life and death. Science is logic, and a scientist can never give up. Many present unsolved paradoxes can find a solution.

At present, we are biased by: 3 "original sins" in Newton's principles, by an Einstein's mistake, and by a misconception of "absolute" time and of the perception of time passing. A new formulation is presented, which is a substantial advancement compared to Galileo, Newton, Maxwell and Einstein.

https://www.europebookstore.com/products/the-universe-out-of-the-box-worlds-and-anti-worlds-g-p-gregori-and-b-g-gregori/

.

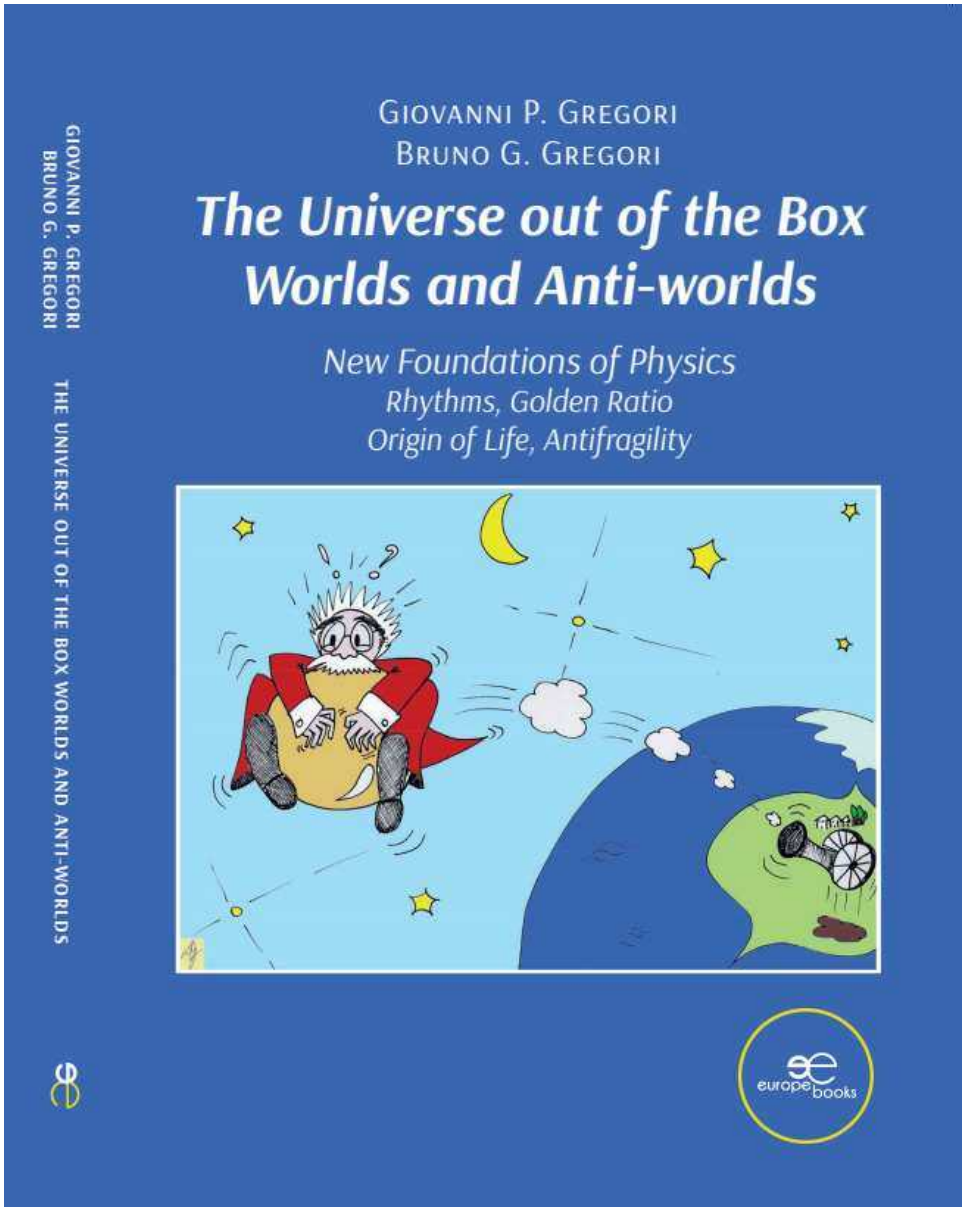

ISSN number; ISSN 2202-0039

Company Profiles:

Tesla 3D, Inc. is an independent research and development company with a strong applied science foundation, enabling rapid and practical innovation in the energy and exploration sectors. While not a large enterprise, Tesla 3D, Inc. stays well informed about breakthroughs in electrical generation, storage, and mining technologies. When called upon, the company can comprehend complex challenges and develop strategic, real-world plans that effectively navigate regulations, funding mechanisms, and policies. Tesla 3D, Inc. actively contributes to national and industry advancement through volunteer leadership, including participation in the Homeland Security Taskforce focused on energy resilience and EMP (electromagnetic pulse) threats. The company also set a precedent by independently qualifying for federal Innovation (R&D) Tax Credits; demonstrating that small, agile innovators can leverage these incentives to streamline regulatory solutions and tackle critical infrastructure challenges. This involvement underscores Tesla 3D, Inc.'s commitment to advancing energy security and shaping the transformative role of technology in resource development. Founded: 2011 Colorado by R. Miller.

Geo-Transect LLP (www.tgeo.co.in) Geo-Transect LLP is a knowledge-driven geoscience consultancy, specializing in subsurface exploration and environmental intelligence across India. With core expertise in subsurface mapping, groundwater zonation, aquifer recharge quantification, coastal and shoreline analysis, landscape and topological planning, and island conservation, the firm delivers data-driven insights that empower sustainable planning and development. Representing the forefront of India's earth-science services sector, Geo-Transect blends scientific precision with advanced technologies to support governmental, industrial, and research-based initiatives across southern India and beyond. Integrating indigenous knowledge with global best practices, the firm is committed to environmental stewardship and responsible resource management. Guided by the ethos "With Wisdom in Nature," Geo-Transect envisions a future where scientific understanding harmonizes development with the natural world.

Stellar Transformer Technologies (https://stellartransformertechnologies.com/) is a private geophysical modeling company specializing in modeling the dynamic electro-magnetic Stellar Transformer interactions between Earth-Sun and planets within our solar system. Original research started in 1995 by the current owner and founder during investigations of the seafloor as a geophysicist with the Naval Oceanographic Office at Stennis Space Center. Leading to an understanding and application of new tectonic theories. Later research confirmed dynamic links to space weather affecting a myriad of environmental factors: such as everyday weather; hurricanes; tornadoes; sever weather outbreaks; earthquakes; global climate-change; and certain types of wildfire outbreaks from passing coronal mass ejections induced by internal core generated Electro-Magnetic Pulses (EMP). Current and planned services include mapping of Stellar Transformer circuits; innovative modeling of deep earth magnetics, forecasting Earth's natural hazards listed above; database development and more. Combining big data and AI to find inter-relationships. Developing algorithm inputs for forecasting, data visualization and simulations. All leading to new forecasting technologies. We are actively assisting the EMP Task Force power grid protection efforts with direct input and evaluation of EMP threats. Our company comprehends the complex challenges of geophysical modeling and development of real-world forecasting applications. Electro-magnetic or magnetic induction is the production of an electromotive force, or voltage, across an electrical conductor in a changing magnetic field. The Stellar Transformer Concept contends that simple step-down energy induction occurs between Sun and Earth, much like the transformer process that steps down your household energy from higher voltage transmission lines sourced from the power company. The Sun represents a large coil from the power company, while the Earth represents the smaller coil to your home. The larger coil element generally excites current into the smaller coil element by induction of "step down energy", although lesser feedback mechanisms occur due to the action/reaction principles. Layers within the Earth hold and release charge acting as condensers, or capacitance layers. Thus, the Earth operates somewhat like a battery where energy is either stored or released through time-change of state-of-matter. We combine new Geophysical Intelligence with AI for a winning combination of innovations that will bring new mitigation strategies for space weather to the forefront. Bringing a paradigm shift to the business community for global environmental forecasting based on solar and planetary effects. This will save lives and mitigate property damage using new science and innovative technologies. Many of these ideas were first presented at EU2015 - Electric Universe (https://www.youtube.com/watch?v=IoqgZhbxhhU). Followed up at EU2016 with discussions on geometrical modeling applications, adhering to golden ratio principles (https://www.youtube.com/watch?v=Q355Haapq-0). Founded: 2023 in Colorado by Bruce Leybourne – Owner/Operator.

NCGT Journal
New Concepts in Global Tectonics

New Concepts in Global Tectonics Journal
Volume 14, Number 1, January 2026

ISSN number; ISSN 2202-0039

Satellite monitoring of air-earth currents

John Michael Quinn† (posthumosly) [1], Giovanni Pietro Gregori [2], Bruce Allen Leybourne [3]

[1] *Solar-Terrestrial Envionmental Research Institute, Lakewood, CO*
[2] Former Senior Researcher at *IDASC-Institute of Acoustics and Sensors O. M. Corbino (CNR), Rome,* now merged with the *INM-Institute of Marine Engineering "Section of Acoustics and Sensors O.M. Corbino"- (CNR Rome)*; and *ISSO-International Seismic Safety Organization*, Italy
[3] *Stellar Transformer Technologies, Geoplasma Research Institute, Aurora, CO, USA*

Corresponding Author: G. P. Gregori, *IDASC-Istituto di Acustica e Sensoristica O. M. Corbino (CNR), Roma,* now merged into *IMM-Istituto per la Microelettronica e Microsistemi (CNR);*
Email: *giovannipgregori38@gmail.com*
leybourneb@iascc.org

† means deceased

Dedication – This paper is dedicated to the memory of John M. Quinn (May 8th, 1946 - March 31st, 2020) and of the founder - and former Chief Editor - of *New Concepts of Global Tectonics,* Dong Choi (February 15th, 1945 - August 28th, 2018). We feel deeply indebted to them for the learning, encouragement, and great help they gave us. This paper is based on a long report, poorly known in the international scientific community, by John M. Quinn. We believe that it contains the most important contribution on geomagnetism since the time of Gauss. We wonder that no obituary is available of John M. Quinn. Therefore, for historical memory, we include a brief obituary, coordinated by Bruce. A. Leybourne, based on inputs from John M. Quinn's sister and brother and from a few of his former colleagues at the *WDC-A Data Center for Geomagnetism and Aeronomy* in Boulder.

Abstract: The focus of the present paper is on intense air-earth currents directly influenced by space weather that are revealed by an original inversion technique developed by John M. Quinn and Don Shiel (Quinn and Shiel, 1993a; 1993b) of 3-component satellite records of the geomagnetic field. Intense air-earth currents permanently flow mainly in regions of heavy crustal fracturing. The treatment here given is according to a detailed illustration of the content of a few reports and papers (mainly Quinn, 2014) by the late John M. Quinn, including several subsequent emails with him. We believe Quinn's contribution is a milestone in the history of geomagnetism and Earth science, although some disagreement still exists between our interpretation and Quinn's original arguments. The key of the disagreement is briefly outlined in Fig. 3. We claim that he underestimated his finding that – in contrast - represents the likely most important achievement in geomagnetism since the times of Gauss. Similar analyses may soon be carried out for achieving a realistic picture of the role of intense soil exhalation in the balance of solar-terrestrial space weather relations. Other evidences of coupling between soil and atmosphere are discussed and compared with Quinn's detailed geophysical and geological analysis.

Keywords: inversion technique (physics *vs.* mathematics) - *CHAMP* records - soil exhalation - crustal fractured areas - crustal total magnetization - magnetic-source-depth - geomagnetic anomalies - basalt flow remnant magnetization signatures – astroblemes – hotspots - tectonic implications - *l.o.d. – IGRF* - Gauss working hypothesis on air-earth currents - permanent intense air-earth currents - atmospheric condenser - Joule heat - friction heat - Svensmark effect - atmospheric discharges - Cowling dynamo – space weather - electrostatic charge of the solar wind - positive charge of the ionosphere - atmospheric precipitation phenomena - *BL* (ball lightning) - lightning, *IC* (intra-cloud) and *CG* (cloud-ground) - *TLE*s (transient luminous emissions) - *TGF* (terrestrial gamma flash) - *WMT* (Warm Mud Tectonics) - *TEC* (Total Electron Content) - seismicity and volcanism

Introduction

This paper is the result of separate contributions by every coauthor, the most important part relying mainly on Quinn (2014) who reports about a gigantic study. His report is poorly known inside the wide scientific community and deserves to be acknowledged as a most important achievement in geomagnetism. John M. Quinn passed away on March 31st, 2020 - otherwise he had been invited to contribute the present paper. Since he cannot correct our

ISSN number; ISSN 2202-0039

draft and we want to acknowledge, very respectfully, his original thought and interpretation - we faithfully include several long quotations from Quinn (2014) and other related papers and reports, including reference to long discussions by email that we had during the past several years. In this respect, we feel happy to witness and to inform the scientific community about the thought and feelings of John M. Quinn, a true astute and often unconventional great scientist. Owing to these reasons, he must be the first author of this paper.

For clarity, we stress that we deal with three different items.

One key item is the *original* mathematical *inversion* technique envisaged by Quinn to invert $6\,months$ of records of the magnetic satellite *CHAMP*. This is a remarkable and astute, innovative approach for solving the mathematically undetermined problem of inversion by means of a sound physical argument. This is, perhaps, the most relevant and crucial aspect of Quinn's study.

A second item deals with the *physical interpretation* of the results, i.e., the focus is on the basic physical model used by Quinn, compared to the alternative interpretation that we envisage. Our effort is to respect as much as possible the original Quinn's thought, and to emphasize the different interpretation by which we claim that Quinn's results are likely to be the most important finding of geomagnetism since the times of Gauss. Quinn was aware of our thought, and several long emails were exchanged between him and one coauthor (GPG). He was very humble and he did not like to be overestimated, but our arguments are sound and certain. That is, we do not criticize Quinn's analysis. In contrast, we claim that he underestimated and downplayed the true relevance of his achievements.

A third item deals with the *tectonic implications*, applied all over the globe, based on a large set of maps and plots originally prepared by Quinn that are here fully reported in detail. In some respect, this is, perhaps, the least realized aspect of his revolutionary inversion technique.

In general, the greatest innovative point is the observational proof of the existence of huge air-earth currents, mainly in areas of large crustal fracturing. This is one of Quinn's best innovations.

The three items outlined - all based on aspects of a new physical tectonic e.m. interpretation - often seem mixed together , although we attempt to avoid , as much as possible, every possible confusion.

Quinn's results are also compared to evidences inferred from *TEC* (total electron content) records and from the standard models of the geomagnetic field.

The physical basis of our interpretation – Permanent, huge air-earth currents

We like to stress three key arguments needed to explain our physical interpretation:

- the magnetic effect of air-earth currents;
- how air-earth currents are generated and propagate through the atmospheric condenser; and
- how air-earth currents can be detected by a magnetic satellite.

The magnetic effect of air-earth currents is well represented by the geomagnetic anomaly in every volcanic area (see Gregori et al., 2025r). The rationale is symbolically represented by Fig. 1, and refers to subsoil currents associated to a bunch of sea-urchin spikes. The associated morphological signature on the geomagnetic anomaly map is a double-eye pattern. Several examples are shown in Gregori et al. (2025r).

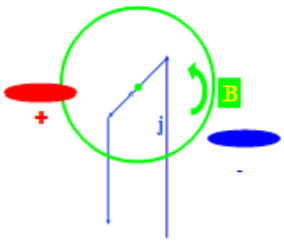

Fig. 1 - Cartoon showing the scheme of the shallowest extension of a DC circuit supplying the top point underground of a sea-urchin spike. A field ***B*** is shown by a green circular pattern located in the plane of the figure. Positive and negative anomalies are indicated by red and blue colour, respectively. The DC electric current ***j*** of the spikes is perpendicular to the plane of the figure. After Gregori and Paparo (2021) and Gregori et al. (2025r), with kind permission of *AJEAS*.

On the other hand, air-earth currents are propagated from soil through the atmospheric condenser up to the ionosphere and magnetosphere. The problem is obvious inside volcanic plumes (Gregori et al., 2024t), while, in general, the electrical discharge between ground and the ionosphere is part of a multifaceted phenomenon, which is extensively discussed in Gregori and Leybourne, (2025e, 2025f, 2025g) and can hardly be simply denoted as "plasma physics".

A synthesis is as follows. Consider heat flow from underground, deriving, e.g., from Joule heat or friction heat. Heat flow causes conspicuous atmospheric convection. Air is ionized, either by cosmic rays (Svensmark effect) or by friction due to interaction with Earth's surface. Convection of an ionized medium is an effective dynamo – i.e., the Cowling dynamo (Gregori et al., 2025d). In principle, the dynamo can equally generate positive or negative electric charge to be supplied to the ionosphere. In contrast, the effect is one sided, as the ionosphere already has a positive charge, because the solar wind is positive (Gregori and Leybourne, 2025b). This implies that atmospheric dynamics (convection) is the leading responsible cause for the observed positive charging of the ionosphere.

This is the physical framework for the primary energy supply. A variety of consequent morphological features must be considered. An "atmospheric discharge" is more than just lightning. Even the motion of one electron is a discharge. The morphology of observable signatures includes atmospheric precipitation phenomena (fog, rain,

NCGT Journal
New Concepts in Global Tectonics
New Concepts in Global Tectonics Journal
Volume 14, Number 1, January 2026
ISSN number; ISSN 2202-0039

snow, hail), ball lightning (*BL*) and lightning, both *IC* (intra-cloud) and *CG* (cloud-ground) discharges, the faint *TLE*s (transient luminous emissions), and the deadly *TGF*s (terrestrial gamma flashes). See Gregori and Leybourne (2025e, 2025f, 2025g).

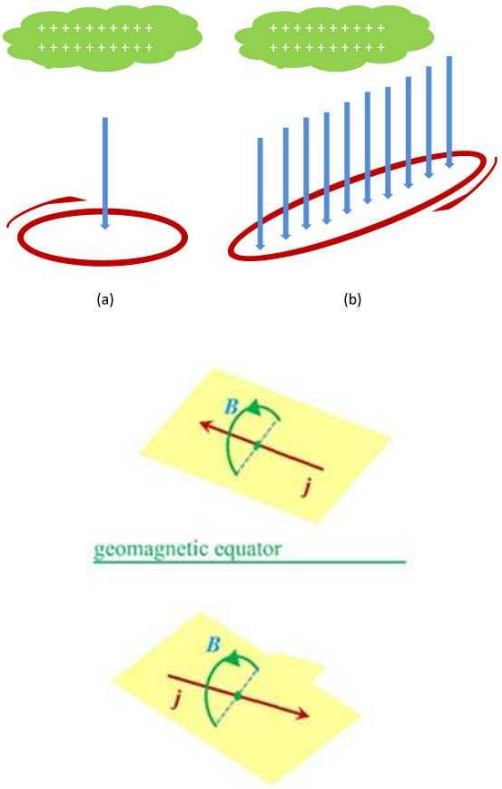

Fig. 2. The cartoon shows the effect of the disturbance produced on *CHAMP* records by a large air-earth current. *(a)* Case history of a point-like "double E-eye" pattern. *(b)* Case history of an elongated pattern of soil exhalation, and of the consequent elongated "double E-eye". The most frequent occurrence is here shown of a positive charge in the ionosphere, with a downward pointing $\boldsymbol{E}$ and $\boldsymbol{j}$, although its symmetrical figure with reversed $\boldsymbol{E}$ and $\boldsymbol{j}$ can be representative of some comparatively seldom occurring eventual case histories. The $\boldsymbol{B}$ field generated by these air-earth currents is summed to the pre-existing ambient $\boldsymbol{B}$. Thus, a sharp discontinuity is originated just at the location of the intense air-earth current. A shallow horizontal conductor implies a magnetic anomaly as shown in the lower panel. A telluric current $\boldsymbol{j}$ in the northern geomagnetic hemisphere generates on the right side of $\boldsymbol{j}$ a magnetic anomaly with $Z < 0$, and $Z > 0$ on the left side of $\boldsymbol{j}$. In the southern geomagnetic hemisphere, the signs of the Z anomaly are reversed between the right and left side of $\boldsymbol{j}$.The geomagnetic anomaly map displays a double-eye pattern with an extended linear discontinuity between a positive and a negative "egg"-feature, separated by a sharp line coinciding with the linear soil exhalation. This feature is a very effective tool to monitor the location of large and almost permanent air-earth currents on the globe. See text. Unpublished figure.

These are, however, occasional occurrences. In contrast, Quinn (2014) showed the existence of an intense effect associated with soil exhalation with no light emission. In general, fluid exhalation occurs inside comparatively wide areas and can hardly be monitored by records at Earth' surface. Quinn's inversion technique produced to evidence – by means of magnetic records from a satellite – of a double-eye feature associated with a similar argument outlined in Fig. 1, according to the principle idea illustrated by the sketch in Fig. 2.

Consider that Fig.2 denotes the existence of a comparatively shallow conductor that, in principle, must be expected to contain currents approximately parallel to Earth's surface, so that the effect illustrated in Fig. 1 is expected. In fact, it would be singular if no horizontal currents ought to occur. Hence, the double-eye pattern must be expected, as a standard.

Fig. 2 explains why air-earth currents can be detected by a magnetic satellite. Quinn's maps show a large number of double-eye (or, better, double-"egg") patterns all over the world, and he stresses that they are correlated with area of greater crustal fracturing. This is consistent with a more intense soil exhalation - and more intense air-earth currents that are likely to occur along linear deep faults.

This result is of paramount importance, as it changes the overall perspective of geomagnetism. This is a revolution since the former logical setting proposed by Gauss. In fact, this result contradicts the working hypothesis – reasonably introduced by Gauss – of a *mean* negligible role of air-earth currents. This has been the well-known logical foundation of the classical and great development of the study of geomagnetism by means of the *SHE* (spherical harmonic expansion) of the geomagnetic potential. This hypothesis permitted to Gauss to separate the origin of internal and external magnetic fields. This same rationale is used today for computing – every 5 *years* – the *IRGF* (*International Geomagnetic Reference Field*).

This general criticism to the original Gauss' working hypothesis has a long historical precedent. The former proposal by Schuster of the so-called "curl-free" test (i.e., computing the circulation of the magnetic field $\boldsymbol{B}$ along a loop at Earth's surface) was aimed at checking this hypothesis. However, owing to practical operational difficulties, it was never carried out. See, e.g., Chapman and Bartels (1940) or Matsushita and Campbell (1967), and references therein. The hypothesis was never suitably tested. This concern was authoritatively stressed, e.g., by the late Naoshi Fukushima (see e.g. Fukushima, 1989).

The skeptical reader may complain that as far as no "smoking gun" proof exists, one is always concerned with speculation bias. Three recent findings, however, agree and independently lead to the identical conclusion. Three clear hunches are unlikely to be only a matter of a coincidence.

One finding deals with the results discussed in the present paper. The two additional findings are, respectively, *(i)* earthquake precursors associated with the coupling between soil and atmosphere (an extensive literature is now available; see Parrot, 2025, Straser et al., 2026, Wu, 2025, Gregori et al., 2025h), and *(ii)* a likely explanation of several unexplained features considered in

New Concepts in Global Tectonics Journal
Volume 14, Number 1, January 2026
ISSN number; ISSN 2202-0039

the origins of wildfires, tropical cyclones, or hurricanes (see Gregori and Leybourne, 2025i, 2025j, Gregori et al., 2025v).

The present paper deals with a skillful, original and astute – approximate although physically significant and realistic - analysis carried out by John M. Quinn by means of an original inversion technique. An extensive description is given by Quinn (2014) and is here reported in detail. Owing to the very innovative character of his study, several aspects – and a discussion of its physical implication - deserve detailed discussion. A previous account was given in Quinn (2012), with some additional information in Quinn (2013).

Quinn gave a different interpretation of the several double-eye (or double-"egg") patterns. He appealed to hypothetical huge reservoirs of different magmatic inclusions, associated to several huge hyper-volcanos. A varied interpretation he considered is in terms of huge astroblemes that could cause huge volcanic eruptions. However, he could not explain the sharp linear separation between the two "eyes" or "eggs", nor why no geological evidences are known that can support such an interpretation. Geological evidence should apply to a great number of locations all over the world. That is, some case histories can be explained according to Quinn's hypothesis, although we claim that the sharp "double-eye" features constitute a credible support for intense and steady air-earth currents along bands of relevant crustal fractures.

Quinn's objection – according to several long emails with one coauthor (GPG) - was that the *SHE* geomagnetic model he used – based on 6 $months$ of *CHAMP* results – was carefully computed by his reliable colleagues who carefully excluded from the computed $\boldsymbol{B}$ model the disturbance associated with air-earth currents, by rejecting perturbed periods, reflected by the Kp index, etc. Hence, Quinn claimed being confident that the air-earth currents can be excluded.

We respectfully contend such a conclusion on the basis of an argument illustrated by the cartoon of Fig. 3 - and we respect also John M. Quinn, who was a very kind gentleman and felt unhappy whenever he eventually had to contradict some friend or colleague.

In fact, we stress that no mathematical procedure can distinguish – in any way - between the magnetic effect of the $\boldsymbol{B}$ disturbance originated by a $\boldsymbol{j}$-loop either crossing or not at Earth's surface. That is, independent of the great skill applied by the modelers – who deserve respect and admiration – in principle, *it is strictly impossible to recognize, or to separate and to reject the effect of air-earth currents.*

The Quinn's maps were obtained by a $\boldsymbol{B}$ model computed with a very careful selection of quiet periods. The records were excluded that were collected while a particle flow crossed through the satellite. The Quinn's result denotes that huge air-earth currents exist all over the globe at any time – and, therefore, are to be expected to be even more intense during disturbance periods.

Summarizing, we clarified the disagreement between the two interpretations – i.e., huge, permanent, and diffuse air-earth currents mainly in regions of heavy crustal fracturing *vs.* hypothetical hyper-volcanoes. Now, let us report in detail the highly accurate and astute gigantic analysis carried out by John M. Quinn.

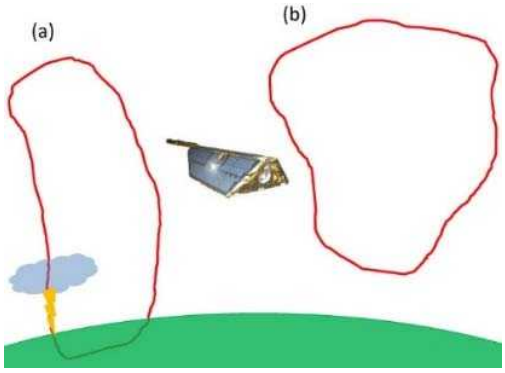

Fig. 3. A satellite magnetometer detects the effect of every closed $\boldsymbol{j}$-loop that can indifferently flow everywhere, either crossing [case *(a)*], or not [case *(b)*], through the Earth's surface. The $\boldsymbol{B}$ records are unreliable only when the satellite crosses through a region where a flow occurs of charged particles. All other records monitor the effect of every current, either air-earth or not. This is just a simple matter of principle. In contrast, Quinn claimed that the *SHE* models he used had been computed by excluding the role of air-earth currents. See text. Unpublished figure.

The leading rationale for inversion

Just the title of Quinn (2014) is expressive: "*Global remote sensing of Earth's magnetized lithosphere*". The leading focus is on the physical motivations behind the original inversion procedure, which cannot be simply mathematical, as *per se* the inversion problem is indeterminate.

Quinn (2014) introduces the problem and claims that "*bathymetric and topographic surveys, and to a lesser extent ocean and land seismic surveys, have revealed a wide range of geologic features such as ocean ridges, trenches, fracture zones, plateaus, etc. Yet, in most cases, these features are obscured by ocean and land sediments that were accumulated over millions of years such that only small portions of these features actually rise above the sediment cover. Deeper structures, which may reach depths of several tens of kilometers, thus remain largely unexamined.*

Geologic layer 1 *sediments in ocean areas are typically non-magnetic, being largely composed of* Ca *deposits from the decay of marine organisms and plant life, while in continental regions these sediments are largely composites of nonmagnetic erosion materials. Geologic layer* 2 *on the other hand is composed of basalt and other minerals that are highly magnetic in comparison. Via a suitable inverse-modeling procedure conducted on global geomagnetic-survey satellite-data, the morphology (i.e., depth variations and vector magnetization) of geologic layer* 2 *can be uniquely revealed. The distance between the top of this layer and the known marine-bathymetry/continental-*

NCGT Journal
New Concepts in Global Tectonics
New Concepts in Global Tectonics Journal
Volume 14, Number 1, January 2026
ISSN number; ISSN 2202-0039

topography also yields an approximate global estimate of sediment thickness beneath both the oceans and continents.

The magnetic inversion procedure presented in this manuscript is applicable to global vector-magnetic satellite-surveys (e.g., MAGSAT, ØRSTED, CHAMP*, etc.). The inversion method is a variation of that developed by Quinn and Shiel (1993a and 1993b), which was originally applied to a low-altitude (*$500\ ft = 152.4\ m$*),* 1981 Project MAGNET *aeromagnetic-survey of the Juan de Fuca and Explorer Plates. That problem used a regional rectangular-harmonic model derived from the survey data and the* FFT *to generate both vector-magnetic and magnetic gradient-tensor data at a finely spaced lat. – long. grid interval. These data were used as input to the inversion problem. The global problem addressed in this report requires the use of a* SH *model. The* CHAMP*-derived, third-generation* $\boldsymbol{B}$ *(*mf3*), degree-and- order* 90, SH *model (Maus et al., 2005, 2006, and 2006a) was used for this purpose.*

The spatial resolution of the lithospheric inversion depends primarily on the highest degree-and-order adopted from the chosen SH *model. This model is phenomenological and is itself derived via its own inversion procedure from satellite, geomagnetic, survey-observations after various fields* $\boldsymbol{B}$ *generated external to the Earth's surface and related induction fields have been removed. Magnetic fields originating in the lithosphere are associated with SH degree* $n = 16$ *and above. This report is confined to a wavelength band corresponding to degrees* $n = 31$ *through* $n = 60$ *of the m model. Clearly, much more geophysical information can be obtained by performing the identical lithospheric-inversion procedure presented here to higher harmonics which, from the* CHAMP *survey data, now reach degree-and-order* 720 *(Maus et al., 2008, and Maus, 2008). In due course, one may reasonably expect* SH *geomagnetic-field models derived from single satellite missions to be in the realm of degree-and-order* 1500 *and higher ...* "

Quinn (2014) gives an overview of his inversion technique, with a focus on the *physical* implications of his algorithm. He implements his analysis on a point-to-point basis, where he represents the characteristics of $\boldsymbol{B}$ by the magnetization of a suitably defined "*prism*".

Since Quinn uses *SH*s of limited degree-and-order, the spatial detail that he achieves is implicit in his choice, i.e., ~$670\ km$ at Earth's surface. Finer details ought to require higher degree-and-order terms. Therefore, it is nonsensical to choose very small "*prisms*". Rather, it is important to choose a "*prism*"-size in such a way that the computed parameters correctly refer to that location, and are representative of a local feature with little contamination by respective surrounding areas.

Thus, after a trial-and-check procedure, Quinn (2012) finally claims that "*the prism's lateral dimensions are assigned the value of* $450\ km$ *(height of the satellite's orbit plus the average depth of layer 2, i.e.* $425\ km + 25\ km$*), while the prism's thickness is* $2\ km$*.*"

Note that, since the *CHAMP*'s mean orbit is ~$425\ km$ above layer *2* (see below), Quinn implicitly conforms to the same argument of Fig. 4 by which it is claimed that ground-based records can realistically provide with no significant ionospheric detail on a space-scale approximately smaller than the average height of the ionosphere. In fact, an electric charge $[\rho d\tau]$ is located at a height h over an observer located at a point A at Earth's surface (ρ is an electric charge density, and $d\tau$ is an infinitesimal volume element). Another observer is located at C, at a distance *L* from A on a flat Earth. Refer to the symbols defined in Fig. 4, and call V_A and V_C the electric potential at A and C, respectively, and p the percent of $V_C = V_A$. By simple computation shows that for $L \sim h$ it is $p \sim 1/\sqrt{2} \sim 70\%$.

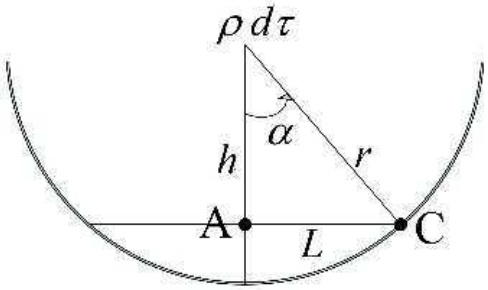

Fig. 4 - Estimating the linear distance *L* at Earth's surface where the ionospheric signal has significantly changed. See text. Unpublished figure.

In this respect, note that the *SHE* models for the geomagnetic potential - which are computed by magnetic satellite data - often specify also a greater detail than it is permitted by this argument. Indeed, the argument considered in Fig. 4 implies that the magnetic signal - which is originated at the *ALB* (asthenosphere-lithosphere boundary; see Gregori et al., 2025a) - is better monitored by satellite than by ground based observatories. In fact, satellite records, owing to the distance between source and detector, are less perturbed by crustal sources. Conversely, compared to satellite altitude, the sources due to crustal magnetization are better monitored at ground. Therefore, the best *SHE* models can be computed by combining ground based and satellite records. Satellite data can be treated in such a way that they can be likened to ground based data, and every *SHE* model is computed by putting altogether all available "good" data. Thus, compared to the constraint expressed by Fig. 4, the final result can specify better details than by means of ground based records alone.

For a correct interpretation of the final findings of the Quinn's inversion, it is also important to stress that the "*prism*" is chosen to be $2\ km$ thick. That is, Quinn looks for the role of crustal magnetization. In this respect, a reminder is needed about the *LN* plot (acronym of Lowes-Nevanlinna; see Gregori, 2002) that can be summarized as follows.

Consider a *SHE* of the geomagnetic field $\boldsymbol{B}$. Evaluate $\boldsymbol{B^2}$ at every point at Earth's surface, which is proportional to the local magnetic energy density. Separate the contribution that derives from the terms of a given degree n, while the contribution of all terms (for fixed n but of varying order m) are summed altogether. For every give n, compute $\boldsymbol{B^2}$ for every point at Earth's surface, and call E_n the planetary mean. Plot $log\ E_n$ *vs.* n (Fig. 5). This is called

NCGT Journal
New Concepts in Global Tectonics

New Concepts in Global Tectonics Journal
Volume 14, Number 1, January 2026

ISSN number; ISSN 2202-0039

LN plot, as it was formerly plotted by Frank Lowes who evidenced two lines, for $n < 14$ and $n > 14$, respectively. Subsequently Heikki Nevanlinna stressed the existence of a third line (for $n = 1, 2$). It can be shown that the Nevalinna's line corresponds to the *IC* (inner core) $\boldsymbol{B}$, while the first Lowes line (for $n < 14$) corresponds to the $\boldsymbol{B}$ originated inside the *OC* (outer core) and lithosphere, and the second Lowes' line (for $n > 14$) corresponds to the crustal $\boldsymbol{B}$.

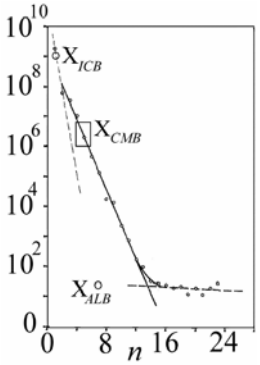

Fig. 5 - Lowes-Nevanlinna's (*LN*'s) plot. The $\boldsymbol{B}$ observed at the Earth's surface (i.e. at $r = a$) is described by means of a potential, when air-earth currents can be neglected. Such potential is expressed in terms of a *SHE*, every term of which is denoted by a degree n and order m. The trend of these terms *vs.* m depends on the choice of the frame of reference, unlike that trend *vs.* n, which is invariant. The present plot displays on abscissas n and on ordinates the corresponding associated fraction of $\boldsymbol{B^2}$, measured at $r = a$ (Earth's surface) and averaged over the entire planet (i.e., this corresponds to a value proportional to the mean magnetic energy density). Such a $\boldsymbol{B^2}$ fraction is defined for every fixed n by summing up over all $m = 0, 1, \ldots, n$ contributions. The *SHE* here considered is based on the $\boldsymbol{B}$ records collected by the *MAGSAT* satellite, epoch *1979.85* (Gregori *et al*., 1999). All points result to be aligned along *3* straight lines. One line through $n = 1, 2$ is called *Nevanlinna's line*, and it is denoted by an index $k = 0$. The $k = 1$ line is called *first Lowes' line* and it goes through points with $n = 3, 4, \ldots, 13$. The third line, $k = 2$, is called *second Lowes' line* and it goes through points with $n = 14, \ldots$ When considering *SHE*s that refer to different epochs, it is found that the tilt of every line changes *vs.* time, even by some relevant amount. However, every such "historical" line always results to cross through some fixed cross-point here denoted as X_{ICB}, X_{CMB}, and X_{ALB}, respectively. This implies that every line ought to be associated with some relevant change of the internal structure of the Earth, although always allowing for one specific n, and for a corresponding energy contribution by that given n, which results invariant in time. Figure redrawn after Gregori *et al*. (2000c) and Gregori (2002). *ESA* copyright free policy, and kind permission of the late Wilfried Schröder.

Concerning Quinn's computation, when reference is made to one given "*prism*", every *SHE* term results from the sum of four contributions. The two leading contributions (at these high degrees n) are, respectively, from the *ALB* currents and from crustal magnetization. Two additional much lesser (to the "*prism*") contributions are originated by the *CMB* currents (first Lowes' line), and even less by the *IC* (Nevanlinna's line).

Quinn (private communication, 2015) also makes an important comment: "*the computation of the prism and magnetization parameters are limited to a single prism. This inversion process is not of the harmonic variety.* [In fact, the "harmonic" regularity of the field is already intrinsic in the *SHE* model that he uses. In contrast, the approximate physical argument about "calibration" that Quinn makes in the next paragraph clarifies the physical meaning of this comment about single "*prism*" computation.] *Each solution of each point on the Earth is acquired independently of all other grid points around the Earth. In order to introduce waviness, adjacent grid points must have some connection. Only the geology provides this connection through a magnetic domain structure ...* [i.e., he stresses the role of local observations, opposite to mathematics].

I did experiment with different lateral dimensions of the prism. The choice of this parameter does affect the inversion outcome. So, in effect there is still some non-uniqueness left in the modeling process. However it can be removed. This is resolved by introducing a calibration technique. The idea is that a small set of known volcanic islands, the average height of which are known to be $< 0.5\ km$ *in height (i.e., near sea-level), can be compared with the source-depth at these island locations. The average height of the source depths for these locations should be* $1\ km$ *depth. That is, the prism, being* $2\ km$ *thick will have its top just at sea-level. The lateral prism width of the prism that accomplishes this as the average of all the source depths corresponding to these islands, is the lateral width chosen. This is the general idea.*

Of course, as one roams around the world, the thickness of the Earth's magnetized lithosphere will not be constant. So, $2\ km$ *is a first approximation based mostly on geological surveys of ocean data. Even here, within this* $2\ km$ *there are two layers that are being averaged as one. Their relative thickness could also vary from place to place ...* "

Quinn (2014) explains these items in detail as follows.

"*In the global case, the Earth's ellipsoidal surface is divided into a set of equally spaced (* $1/4°\ lat.\times 1/4°\ long.$ *) grid points. Fixed, low-altitude (* $50\ km$ *) observation points are established directly above these grid points. At these observation points, the vector and gradient-tensor fields* $\boldsymbol{B}$ *are computed from the* SH *model. The assumption is that the magnetic vector and gradient-tensor fields computed from the survey-based* SH *model at a specific observation point are effectively due to a uniformly-magnetized rectangular prism centered directly beneath the grid point in question at an unknown depth. The unknowns are the prism's geometry (length, width, thickness, and depth beneath Earth's ellipsoidal surface), and the prism's three vector-magnetization components.*

Using both the magnetic vector and gradient-tensor fields from a SH *model as input-data permits the inversion problem to be broken-up (i.e., decoupled) into two parts: one nonlinear part involving the prism's geometrical parameters, and one linear part involving the prism's*

New Concepts in Global Tectonics Journal
Volume 14, Number 1, January 2026

ISSN number; ISSN 2202-0039

geophysical parameters (i.e., the three magnetization vector components). The prism dimensions (i.e., length, width, and thickness) are constrained a priori *using geophysical arguments, leaving the prism's depth as the only remaining geometric unknown. Thus, the total number of unknowns is whittled down to just four, the prism depth and the prism's three magnetization components.*

The thickness of the Earth's magnetized layer, and thus of the prism, is taken from the Ocean Drilling Program *and ocean seismic results to be* $2\ km$ [*i.e., layer* 2a *(*$0.5\ km$*) and layer* 2b *(*$1.5\ km$*)*]. *This assertion is carried over to the continents as well, although layer* 2 *is generally deeper beneath the continents. The inversion results tend to validate this continental extension. One could of course refine the results by including the thickness as an additional unknown.*

The prism's lateral dimensions are chosen sufficiently large that fields $\boldsymbol{B}$ *generated by any magnetization located beyond the prism's lateral boundaries are negligible along a vertical line through the prism's center, which is the primary region of interest. This leaves just the prism's central depth as the only remaining geometric unknown. It is easily determined by minimizing a decoupled least-squares function involving the magnetic intensity vector* $\boldsymbol{B}$ *and the magnetic gradient-tensor* $\boldsymbol{B}$ *both of which are known from the model. The minimization is performed by stepping the center of the prism from* $1\ km$ *beneath the Earth's surface (meaning that the top of the prism is at the Earth's surface) at* $0.1\ km$ *intervals to some maximum depth (e.g.,* $500\ km$*). The deepest depth was found to be* $196\ km$*. Having obtained the source depth, a simple liner matrix inversion is all that is necessary to determine the three magnetization vector components.*

The decoupled inversion results in a unique solution at each grid point. This process is repeated for each and every grid point covering the entire Earth. This totals 1.036.800 *grid points.*

The inversion procedure is not calibrated. To do so globally requires an a priori *knowledge of the sediment thickness by some independent means. Ground-truth data would necessarily consist of numerous* Deep Sea Drilling *and* Continental Land Drilling *core samples of exceptional depth. The deepest marine core-sample to date reaches to only ~*$7\ km$ *(*$2\ km$ *of water and* $5\ km$ *of solid Earth) (*The Economist*, 2010). Some isolated near-surface features yield depth uncertainties on the order of ~*$1\ km$*.*

Based on special situations, such as exposed igneous islands (e.g., Fiji), a depth uncertainty limit on the order of $\pm 1\ km$ *seems reasonable. The magnetization uncertainties are not likely to be much more than* $\pm 0.2\ A\ m^{-1}$*. In either case one must keep in mind that only a small* SH *wavelength band has been used. The addition of higher harmonics in the analysis will alter the results slightly by adding more detail/finer spatial-resolution, which in any case is already quite good for the span of harmonics used in this report. One of the largest sources of error in the procedure is the constraint on the prism thickness. The thickness of layer* 2 *does vary around the Earth. Altering the inversion procedure to include this parameter as an additional unknown should improve the overall accuracy of the inversion technique.*"

Quinn's computation is impressive, and also the great care in taking account of observational local evidence, compared to every mathematical smoothing and interpolation. This is the logical key by which he affords to get rid of the mathematical indeterminacy of the inversion problem by means of the input of concrete observational data. Quinn (2014) also specifies the geological aspects that are an important additional information when dealing with crustal features.

"*It is known from the* Ocean Drilling Program *and seismic results that the ocean crust is composed of several layers, which for this analysis are extended to continental regions as well. Layer* 1 *consists of an assortment of non-magnetic sediment types depending on whether it is a marine environment, and thereby is composed of non-magnetic* Ca*-based shells formed from marine animals and organisms, or land areas that consist mainly of well-mixed erosion materials. Over time, these sediments may be compressed into rocks.*

Layer 2 *is an approximately* $2\ km$ *thick magnetized layer (Fowler, 2005). In ocean regions, its depth varies between* $10\ km - 20\ km$*, while beneath continental regions, its depth is typically much deeper. It is most deep beneath mountain ranges (Hamoudi et al., 1998). Flood basalt regions are an exception (Agrawal et al., 1992). Overall, oceans and continents combined, the global average depth of this layer is on the order of* $25\ km$*. Layer* 2 *is divided into several sub-layers, of which the most important are layers* 2a *and* 2b*. Layers* 2c *and* 2d *are considered to be transition layers with respect to layer* 3 *and are considered to be of negligible importance for the present analysis.*

Layer 2a *is composed primarily of pillow basalts, having a global average magnetization of ~*$6\ A\ m^{-1}$ *that results from the volcanism associated with seafloor spreading at ocean ridges (Dyment and Arkani-Hamed. 1995 and Hemant and Maus, 2005). It is ~*$0.5\ km$ *thick. Layer* 2b *lies beneath layer* 2a *and is approximately* $1.5\ km$ *thick. It is composed of diabase dykes, which are essentially magmatic intrusions from the deeper lithosphere. It has a magnetization on the order of* $1.5\ A\ m^{-1}$*. The global thickness variability of layer* 2 *is not well-known. So, in this manuscript as a first approximation, its thickness is taken as a global constant of* $2\ km$*, with layers* 2a *and* 2b *being combined into a single layer. Thus, the combined layer is expected to have a global average magnetization of approximately* $2.6\ A\ m^{-1}$*.*

Layer 3 *resides beneath layer* 2 *and is approximately* $5\ km$ *thick. It is composed primarily of gabbro which consists of coarse-grained and crystalline basalt, rich in non-magnetic aluminum, and has a magnetization on the order of* $1\ A\ m^{-1}$ *(Fowler, 2005; and McDuff and Heath, 2009). This layer, being deeper, is nearer to the Curie isotherm than the layers above and is therefore warmer, which disrupts the ability of magnetized minerals to align themselves to yield coherent magnetization. The isotherm has temperatures on the order of* $560 - 600\ °C$*. Below this isotherm, magnetization is essentially non-existent. So, the*

NCGT Journal
New Concepts in Global Tectonics

New Concepts in Global Tectonics Journal
Volume 14, Number 1, January 2026

ISSN number; ISSN 2202-0039

magnetization of layer 3 *is not strong. On the other hand, with respect to fields* **B** *observed at or above Earth's surface, the thickness of this layer may compensate for the low-magnetization due to its proximity to the Curie isotherm. However, a screening effect provided by the magnetization of layer* 2 *may mute some of the enhanced* **B** *observed at Earth's surface due to layer* 3*. In any case, for the purpose of the present analysis, layer* 3 *is assumed to have a negligible effect at Earth's surface.*

The lateral prism dimensions are chosen to be 450 km*, which corresponds approximately to the* 425 km *average* CHAMP *orbit altitude above Earth's surface plus an additional* 25 km *to account for the average lithospheric source depth beneath Earth's surface. Thus, along a vertical line through the prism's center, fields* **B** *due to the prism's lateral edge effects will be negligible. Likewise, fields* **B** *due to portions of the magnetized lithosphere beyond the prism's lateral dimensions will also be negligible. The vertical line through the center of the prism is the only region of computational interest.*

For purposes of this source-depth inversion, the observational grid's altitude computed from the mf3 *model is chosen to be* 50 km *above Earth's geoid surface, referenced to the* World Geodetic System, 1984 *(*WGS-84*) ellipsoid (Featherstone and Claessens, 2008). This computational altitude is not entirely arbitrary since, if it is much higher (lower), the lateral prism limits might have to be extended (contracted). In any case, for the best spatial resolution for the inversion, it is desirable to keep the lateral prism dimensions as short as possible*."

The computation

Quinn's computation is carried out by means of tensor calculus.[1] Detailed technicalities are explained in Quinn (2014) and are not here repeated, as the leading concern is here about the physical implications.

A previous application of the same principle is exploited according to the procedure explained by Quinn and Shiel (1993a), while Quinn and Shiel (1993b) applied it to the specific case history of the northern Juan de Fuca and Explorer plates, using airborne geomagnetic survey off the coast of Vancouver.

"*Quinn and Shiel (1993a) derives the arithmetic associated with potential field for electric, magnetic and gravity fields due to a prism and examines the fields associated with single prism and collections of prisms.* [It] *shows various relations among the electric, magnetic and gravity fields and the physical parameters associated with them like electric conductivity, polarization, and magnetization. It also develops the least-square technique that leads to inversions that* uniquely[2] *determines magnetic source depth and vector magnetization*" (Quinn, private communication, 2015).

They used a rectangular coordinate system in a plane with the origin-point tangent at Earth's surface, at a suitable location on the plane. "*At each grid point a least-square problem is formulated using the relations between the vector and the gradient tensor components which allows the magnetization vector to be eliminated so that only the depth is left as an unknown. The grid is made as finally spaced as possible, depending on survey line spacing etc. Then a prism is centered directly beneath a particular grid point referred to as the observation point. The vector and gradient tensor fields* **B** *due to a prism (* $450\ km \times 450\ km \times 2\ km$ *thick) are computed and compared to the observation grid point. The prism-generated field components are computed at the specified altitude of the observational grid-point generated by the* FFT *from the harmonic model.*

The depth of the prism is varied until the least-square problem is minimized. Having found the source-depth, which is unique, one goes back to the vector magnetic-field equation containing the magnetization vector and computes the magnetization vector, which is also unique. This process is then repeated for all of the grid points. From a computer programming point of view, this is a very easy procedure and it is fast" (Quinn, private communication, 2015). [Note the astute and skillful combined use of physical arguments with algorithms in order *(i)* to constrain mathematics into realistic boundaries and *(ii)* to get rid of the indeterminacy of the inversion.]

Quinn used a degree and order 90 *SHE* model computed by *CHAMP* data (Maus and Weidelt, 2004), but he used only degrees and order $31 - 60$, although he specifies[3] that Maus et al. later generated a 720 *SHE* model that provides with much finer details.

"*The global lithosphere's magnetic source-depth and vector magnetization have been mapped using the degree-and-order* 90 mf3 SH *magnetic-field model (Maus et al., 2005a, 2006, 2006a), 2005 which is based on early* CHAMP *satellite magnetic-field survey data ...* " (Quinn, 2012).

The "*geologic layer* 2 *is a magnetically anomalous,* ~2 km *thick shell that surrounds the entire Earth. It is magnetically isolated, being sandwiched between non-magnetic geologic layers above and below*" (Quinn, 2013).

Quinn (2012) describes in better detail his available geomagnetic information as follows.

"*... The degree and order* 90 mf3 *model used in the present case ... is based on* CHAMP *satellite magnetic-survey-data collected during the early part of that survey at an average altitude of* ~425 km*, the initial orbit insertion being* 454 km*. Various tidal effects have been removed from these data. Subsequent models (i.e.,* mf4, mf5*, and* mf6*) are available which extend the* SHs *to degree-and-order to* 120 *(Maus et al., 2007 and 2008). The most recent models are various refinements of the* mf3 *through* mf6 *models and have been extended even further to degree and order* 720*. The higher degree and order models result from the lower altitudes as the German* CHAMP *satellite orbit decays ...*

[1] See a short mention and symbol definition in the Appendix.

[2] Emphasized character is Quinn's original.

[3] "*I would point out that in the 1980s the harmonics that I am using were considered to be high degree-and-order*" (Quinn, private communication, 2015).

NCGT Journal
New Concepts in Global Tectonics
New Concepts in Global Tectonics Journal
Volume 14, Number 1, January 2026
ISSN number; ISSN 2202-0039

... While the mf3 *model is of degree and order* 90*, only the* SH*s between degree-and- order* 31 *and degree-and-order* 60 *were actually used in the lithospheric inversion analysis. Thus, there is a great potential to achieve much higher spatial resolutions ...*

From Ocean drilling data it is known that geologic layers 2a *and* 2b *are magnetic. Layer* 2a *consists of pillow basalts and is* 0.5 km *thick, while layer* 2b *consists of diabase dikes and is* 1.5 km *thick. Their combined thickness is taken to be* 2 km*. Layer* 2a *has the stronger magnetization. It is assumed that layer* 2 *forms a spherical shell* 2 km *thick around the entire Earth. Above layer* 2 *are non-magnetic sediments. Below layer* 2 *is non-magnetic gabro material. While this shell's depth may vary, its thickness is presumed constant as a first approximation. Subsequently, the Earth's surface is endowed with a global set of grid points with a* $1/4°$ *latitude by* $1/4°$ *longitude grid spacing."*

Note that the detail that can be achieved is strictly determined by the available highest degree and order coefficients - while also the "leopard skin" effect, which is strictly unavoidable in every truncated expansion, is correspondingly reduced (the term derives from the appearance of patches that remind about a leopard skin, and are the consequence of the truncation of the *SHE* to comparatively low degree-and-order). For order 720 the peak-to-valley size of the "leopard skin" effect is $\sim 360°/720 = 0.5°$, equivalent to ~55 km, which is the highest spatial resolution that can be achieved.

Quinn and Shiel (1993b) report several maps that show the great detail that they afforded to achieve by means of their astute analysis. Their results are here explained in no better detail, as the results reported by Quinn (2014) are more directly pertinent (they are more general and updated) for the present discussion.

Quinn (2014) gives a very detailed description of the arithmetic of the formal treatment for whole Earth, with no approximation dealing with a tangent plane etc. Only the leading logical, computational and physical principle of the whole procedure is here concisely outlined, mainly relying on the brief account given by Quinn (2012).

"*The remaining unknowns of the problem are the depth of the prism's center below the Earth's surface using the* WGS-84 *ellipsoid as reference, and the three components of the prism's vector magnetization. The prism is treated as being uniformly magnetized, which means that the three vector magnetization components are constant* M^{λ} *(*$\lambda = 1, 2, 3$ *corresponding to* x*-North,* y*-East, and* z*-vertically down) ...* [Hence] *the* $\boldsymbol{B}$ *vector components* B_{μ} *due to the magnetized prism at the* 50 km *altitude observation point, referenced to geodetic coordinates, is just*

$$B_{\mu} = \Lambda_{\mu\nu} M^{\lambda} \qquad (1)$$

The Λ *matrix contains all of the geometric information, while the magnetization vector* M *contains all of the geophysical information ...* [This astute separation of geometrical and physical information is fundamental in order to get rid of the indeterminacy of the inversion problem. It is, maybe, the logically most remarkable aspect of the skillful original Quinn's inversion method.]

The same is true for the magnetic gradient-tensor field that is obtained by taking the derivatives of the $\boldsymbol{B}$ *components, yielding*

$$\mathcal{B}_{\mu\nu} = \Lambda_{\lambda\mu/\nu} M^{\lambda} \qquad (2)$$

where the slash (/) notation simply denotes ordinary partial differentiation with respect to a particular coordinate (e.g., $_{/\sigma} = \partial/\partial\sigma$*)."*

However, note that the "curl-free" condition $curl\, \boldsymbol{B} = 0$ imposes specific relationships on B_{μ} through its derivatives $\mathcal{B}_{\mu\nu}$. The "curl-free" condition is imposed as a strictly needed requirement during the whole derivation of the *SHE* model by satellite records: every disturbance that does not fit with this requirement is just rebutted. Therefore, in principle, according to the primary leading perspective of the *SHE* model computation, the eventual presence of some relevant amount of air-earth currents - that substantially violates the "curl-free" condition - ought to imply that the associated $\boldsymbol{B}$ records are excluded from the model. This, however, often does not occur, as per the argument symbolically represented by the cartoon of Fig. 3. That is, there is a real hazard that some observed features do reflect the substantial, even large, effect of steady air-earth currents, even of possibly large intensity, that were not rejected during the computation of the *SHE* model.

On the other hand, the Quinn's inversion is carried out on a point-by-point basis, by referring to every given "prism" ($450\ km \times 450\ km \times 2\ km$ thick) and by minimizing the influence originated by other "prisms" at its boundaries. That is, concerning the relationship between contiguous "prisms", the "harmonic" requirement is physically minimized. As mentioned above, Quinn states that *" ... the computation of the prism and magnetization parameters are limited to a single prism. This inversion process is not of the harmonic variety. Each solution of each point on the Earth is acquired independently of all other grid points around the Earth. In order to introduce waviness, adjacent grid points must have some connection. Only the geology provides this connection through a magnetic domain structure ... "*

Note that not only geology, but, symmetrically, also a local amount of unwanted air-earth currents can cause a relevant physical trend as per the argument related to Fig. 3, because their associated $\boldsymbol{B}$ records were not rebutted during the *SHE* model computation. Compared to the former assumption of mere "curl-free" condition, this is a severe bias. This fundamental fact has consequences of paramount importance in the following.

"*The troublesome non-uniqueness is removed by decoupling the magnetization* M *from the geometric matrix* Λ *by inverting eq. (1), which yields* [note that this inversion, i.e., computing the matrix $\bar{\Lambda}$ which is the inverse of Λ, suffers by the same non-uniqueness problem of every inversion problem. However, this drawback is avoided if one takes for granted the constraint represented by the known physical value of $|M|$. This is a remarkable example of skill while keeping in mind first of all the physical constraints of the problem, and of how the indeterminacy of mathematics can and must be circumvented by additional

NCGT Journal
New Concepts in Global Tectonics
New Concepts in Global Tectonics Journal
Volume 14, Number 1, January 2026
ISSN number; ISSN 2202-0039

observational information (i.e., either physical or geological).]

$$M^{\lambda} = \bar{\Lambda}^{\lambda\sigma}\,\mathcal{B}_{\sigma} \qquad (3)$$

and inserting this result back into eq. (2) ... yields the decoupled equation:

$$\mathcal{B}_{\mu\nu} = \Lambda_{\lambda\mu/\nu}\,\bar{\Lambda}^{\lambda\sigma}\,\mathcal{B}_{\sigma} \qquad (4)$$

[where $\mathcal{B}_{\sigma}$ and $\mathcal{B}_{\mu\nu}$] *are known from the* SH *model* [although with the aforementioned possible bias by air-earth currents]."

Therefore, Quinn applies a least-square-fit procedure in order to compute the magnetic source-depth by minimizing

$$\sum_{\mu=1}^{3}\sum_{\nu=1}^{3}\left[\mathcal{B}_{\mu\nu} - \Lambda_{\lambda\mu/\nu}\,\bar{\Lambda}^{\lambda\sigma}\,\mathcal{B}_{\sigma}\right]^2 \qquad (5)$$

"*In this manner, the source-depth becomes known. Consequently, $\bar{\Lambda}$ also becomes known and can be inserted into eq. (3) to uniquely determine the magnetization's vector components.*

The derivation of the Λ *matrix elements and their derivatives is given in Quinn and Shiel (1993a), where similar equations for the gravity and electric fields are also obtained. The $\bar{\Lambda}$ matrix, incidentally, is related to the Reimann curvature tensor (space part). The inversion process was implemented from the North Pole to the South Pole around the world. The inversion results are quite stable. Consequently, the images obtained are virtually noiseless, giving the appearance of photographs*" (Quinn, 2012).

"*The greatest depth encountered was* 196 *km, while the shallowest was at or near the Earth's surface* [The physical meaning of these very shallow $\boldsymbol{j}$ is considered here below.] *... The total magnetization is computed as the square-root of the sum of the squares of the three components of the vector magnetization generated by the global inversion process*" (Quinn, 2013).

This information is needed for the discussion of the Quinn's maps. The reader who is interested only in the physical interpretation may directly refer to the results shown below.

However, an astute computation - which has been envisaged by Quinn (2014) although it was not yet applied to real observational data - can provide with a quantitative evaluation of the current $\boldsymbol{j}$ and of the electrical conductivity σ on the outer boundary of the sea-urchin spikes. The leading idea still relies on consideration of realistic typical values for the electrical properties of lithosphere and crust.

As emphasized by Quinn (2014), owing to the limited spatial resolution implied by the highest degree and order of the *SHE* which he considered, the estimate resulting from this computation refers to some average over a bunch of sea-urchin spikes, rather than to a single spike.

The Quinn's algorithm can be briefly summarized as follows. He uses the *cgs-sym* (i.e., *cgs* symmetric) unit system, where the Maxwell's equations get the form

$$\begin{aligned} curl\,\boldsymbol{H} &= \boldsymbol{D} = \epsilon_r\,\boldsymbol{E} \\ &= (4\pi/c)\boldsymbol{j} + (1/c)\,\partial\boldsymbol{D}/\partial t \\ curl\,\boldsymbol{E} &= -(1/c)\,\partial\boldsymbol{B}/\partial t \qquad \boldsymbol{B} = \mu_r\boldsymbol{H} \\ div\,\boldsymbol{D} &= 4\pi\,\rho_{el} \qquad \boldsymbol{j} = \sigma\boldsymbol{E} \\ div\,\boldsymbol{B} &= 0 \end{aligned} \qquad (6)$$

that he re-writes in tensor formalism, i.e.

$$\varepsilon_{\mu\nu\lambda}\,H^{\lambda/\nu} - (1/c)\left(\partial D_{\mu}/\partial t\right) = (4\pi/c)j_{\mu}$$

$$\varepsilon_{\mu\nu\lambda}\,EH^{\lambda/\nu} + (1/c)\left(\partial B_{\mu}/\partial t\right) = 0 \qquad (7)$$

$$D^{\mu}_{./\mu} = 4\pi\,\rho_{el}$$

$$B^{\mu}_{./\mu} = 0$$

The derivation proceeds through the following relations (every reader who is a little bit acquainted with tensor formalism can understand the logical procedure, hence there is no need to specify here any additional detail):

$$\begin{aligned} &D_{\alpha} = \epsilon\,E_{\alpha} \\ &B_{\alpha} = \mu\,H_{\alpha} \\ &j_{\mu} = \sigma\,E_{\mu} \\ &j^{\mu}_{./\mu} + \frac{\partial\rho_{el}}{\partial t} = 0 \\ &j_{\mu} = \frac{c}{4\pi}\varepsilon_{\mu\nu\lambda}H^{\lambda/\nu} - \frac{1}{4\pi}\frac{\partial D_{\mu}}{\partial t} \\ &D_{\mu} = \frac{c\epsilon}{4\pi\sigma}\varepsilon_{\mu\nu\lambda}H^{\lambda/\nu} - \frac{\epsilon}{4\pi\sigma}\frac{\partial D_{\mu}}{\partial t} \\ &j_{\mu} = \frac{c}{4\pi}\varepsilon_{\mu\nu\lambda}H^{\lambda/\nu} - \frac{c\epsilon}{(4\pi)^2\sigma}\varepsilon_{\mu\nu\lambda}\frac{\partial H^{\lambda/\nu}}{\partial t} + \frac{\epsilon}{(4\pi)^2\sigma}\frac{\partial^2 D_{\mu}}{\partial t^2} \\ &D_{\mu} = \frac{c\epsilon}{4\pi\sigma}\varepsilon_{\mu\nu\lambda}H^{\lambda/\nu} - \frac{c\epsilon^2}{(4\pi\sigma)^2}\varepsilon_{\mu\nu\lambda}\frac{\partial H^{\lambda/\nu}}{\partial t} + \frac{\epsilon^2}{(4\pi\sigma)^2}\frac{\partial^2 D_{\mu}}{\partial t^2} \end{aligned} \qquad (8)$$

and, by neglecting the second order derivatives,

$$\begin{aligned} &j_{\mu} = \frac{c}{4\pi}\varepsilon_{\mu\nu\lambda}H^{\lambda/\nu} - \frac{c\epsilon}{(4\pi)^2\sigma}\varepsilon_{\mu\nu\lambda}\frac{\partial H^{\lambda/\nu}}{\partial t} \\ &D_{\mu} = \frac{c\epsilon}{4\pi\sigma}\varepsilon_{\mu\nu\lambda}H^{\lambda/\nu} - \frac{c\epsilon^2}{(4\pi\sigma)^2}\varepsilon_{\mu\nu\lambda}\frac{\partial H^{\lambda/\nu}}{\partial t} \end{aligned} \qquad (9)$$

a consequence of which is

$$\begin{aligned} j^{\mu}_{./\mu} &= 0 \\ D^{\mu}_{./\mu} &= 0 \end{aligned} \qquad (10)$$

If one neglects all time derivatives, this is the quasi-stationary approximation that applies to conducting media, because insulators develop conspicuous displacement currents. In the present case, only the second order time derivatives are neglected. Thus, the computation refers to a conducting medium, where, however, also displacement currents can play a role. This is taken into account, although upon neglecting some lesser effect. "*The approximation is valid in conducting media such as an ore body or an electrically conducting fluid, such as magma. The electrical conductivity and related parameters such as the electric current density will vary throughout the lithosphere. However, within the confines of a small prism they are taken for constant.*"

Finally, by some algebra, Quinn (2014) promptly finds

$$j_{\mu} = \frac{c}{4\pi\mu}\varepsilon_{\mu\nu\lambda}B^{\lambda/\nu} - \frac{c\epsilon}{(4\pi)^2\sigma\mu}\varepsilon_{\mu\nu\lambda}\frac{\partial B^{\lambda/\nu}}{\partial t} \qquad (11)$$

"*... Since the vector* $\boldsymbol{B}$ *and its* SV *are also known, eq. (11) can be solved straight away for* σ*, if some reasonable estimates can be given for both the electric permittivity* ϵ *and the magnetic permeability* μ *of the conducting medium. The results is:*

$$1/\sigma = \bar{\bar{B}}_{\lambda\sigma}\left\{\frac{4\pi}{\epsilon}\left[B^{\lambda/\sigma} - \frac{2\pi\mu}{9}\bar{\Lambda}^{\alpha\sigma}B^{\lambda}_{./\alpha}\right]\right\} \qquad (12)$$

ISSN number; ISSN 2202-0039

where the first factor on the right-hand side of eq. (12) is the inverse of the ***B*** *gradient-tensor* SV *...*

The key to solving for σ *is having available several high degree-and-order* SH ***B*** *models that are created from the same satellite survey at several widely spaced epochs. The higher the harmonic in the model, the greater the epoch separation must be. Three* ***B*** *models are necessary, one at time* t_1*, one at time* t_2*, and one at time* t_3*, preferably equally spaced in time by at least* $5\ years$*. The focal point is on the time* t_2*. That is, epochs* t_1 *and* t_3 *are used to compute the* SV *at epoch* t_2*. Then, both the geomagnetic field and its* SV *are known at the same epoch* t_2 *and eq. (11) can then be evaluated for ...*

This fractal inversion technique to determine the electric-current density and σ *has yet to be implemented. So, unforeseen difficulties may still lay head.*"

Note that Quinn (2014) intuitively considers as a fractal the distribution of sea-urchin spikes, although no formal proof can be available concerning self-similarity independent of scale-size, as it is requested by formal fractal definition. In any case, the Quinn's result is impressive, and it shows the great innovative and heuristic potentiality of the Quinn's inversion.

The method presumes, as an *a priori* paradigm, that ***B*** is curl-free at Earth's surface.

In the final analysis, the ***B*** model is derived by considering $6\ months$ data, recorded only during "quiet" time, and by rebutting data correlated with intense particle fluxes detected by onboard instruments. Then, iteratively, several tests are carried out, and the final model is progressively corrected with minor adjustments in order that it must satisfy the aforementioned curl-free hypothesis. The primary motivation is that a model ought to use satellite data similarly to ground based observatory records, according to the classical Gauss' former computation and working hypothesis.

However, even if these compulsory criteria are applied to Quinn's inversion – owing to the argument related to Fig. 3 - Quinn's inversion can also give evidence of air-earth currents. Similarly, it is reasonable to guess that it affords to provide also with quantitative estimates of electric currents and of σ. No other method is presently known suited for such a performance. This Quinn's result is a real unprecedented milestone in the study of geomagnetism.

Maps of total magnetization and of magnetic source depth - Interpretation - "*Double E-eye*" features

Consider in detail the results of the Quinn's inversion. As a premise, a mention is deserved about a more recent modeling of the lithospheric ***B*** carried out by means of the records by the three *SWARM* satellites. At present, we are aware of two movies that are available concerning the ***B*** generated, respectively, by ocean tides (*Anonymous*, 2018b), and by lithospheric sources (*Anonymous*, 2018c). No real comparison can be made with the Quinn's maps. The precise details are not available of the complicated multidisciplinary models used for the aforementioned movies.

In any case, those authors apply a skillful separation of the tiny ocean tide contribution by means of a model for ocean tides, and they represent the lithospheric ***B*** by subtraction of the main deep-origin ***B***, evaluated according to the standard *SHE* procedure by neglecting air-earth currents etc.

Consider, rather, the original algorithm envisaged by John M. Quinn who applies a concrete inversion computation that *per se* is indeterminate. However, he affords to manage the indeterminacy upon considering the physical range of the electrical conductivity σ of the shallower Earth's layers. That is, compared to the standard approach to the data handing of geomagnetic records, the substantial originality should be stressed of the Quinn's skillful physical inversion. Indeed, the Quinn's results show some unexpected details that have no correspondence with the traditional, mainly mathematical and less physically oriented, algorithms.

Therefore, no real comparison can be made with the aforementioned maps, as they are computed by a physically different approach. The basic reason relies just in the substantially more physical arguments that rely behind the Quinn's inversion, compared to the traditional, and mainly mathematical, description that is applied by the conventional approach that critically relies on the – unreliable - assumption of a negligible mean planetary role of air-earth currents.

As a key warning, when dealing with the evaluation of the physical implication of the results, one should always keep in mind that a *SHE* model of the geomagnetic potential for the internal origin field relies on the *a priori* implicit assumption that air-earth currents can be presumed to cause only a mean negligible perturbation.

On the other hand, we stress that the eventual presence cannot be excluded of some relevant amount of air-earth currents, as per the argument related to Fig. 3. Air-earth currents violate the assumption that $curl\ \boldsymbol{B} = 0$, while $curl\ \boldsymbol{B} = 0$ implies that, owing to definition, some suitable elements of the aforementioned "*Earth's magnetic gradient-tensor*" must be mathematically and non-physically related one to another. Therefore, this drawback can be suspected to generate sometimes some unwanted instability of the computed results and of their maps (two kinds of maps were drawn by Quinn, respectively, for the total magnetization and for the magnetic source-depth, respectively).

The focal question is, therefore, about the temporary (or not) location at Earth's surface of possible air-earth currents, about their origin, and about how they can be monitored.

Refer to the physical meaning and implication of Quinn's maps. His computation was carried out at some grid-points ($1/4° \times 1/4°$ in latitude and longitude). Then, color figures were generated by computer graphics. Quinn's maps *per se* represent continuous functions. That is, they imply no additional interpolation for graphical purposes. The physical interpolation was carried out at the epoch when the *SHE* model was computed, which was later used in Quinn's analysis. That is, the spatial detail provided by Quinn's maps is defined - and limited - by the total number of terms used in the truncated expansion of his *SHE* model.

NCGT Journal
New Concepts in Global Tectonics

New Concepts in Global Tectonics Journal
Volume 14, Number 1, January 2026

ISSN number; ISSN 2202-0039

Therefore, let us attempt to implement a physical interpretation of Quinn's maps by considering first some restricted test-area. Subsequently, a planetary analysis can be exploited. For comparison purpose, one additional map is here considered, which is complementary to both Quinn's maps. The additional map is a detail - approximately spanning the same area of interest - in Fig. 6, which is the world map of the geomagnetic anomalies.[4]

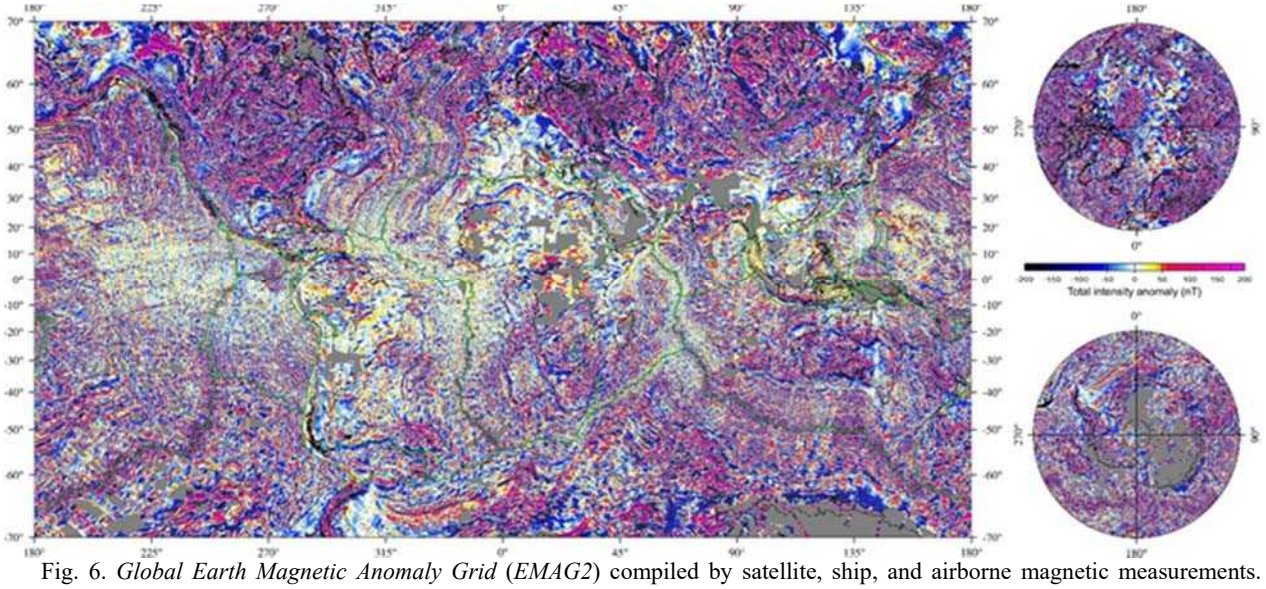

Fig. 6. *Global Earth Magnetic Anomaly Grid* (*EMAG2*) compiled by satellite, ship, and airborne magnetic measurements. Different map projections are shown of the same physical database. After *http://geomag.org, and http://noaa.gov*. See also Maus et al. (2009). *NOAA* copyright free policy.

For brevity and clarity purpose, it is worthwhile to anticipate the three different tentative interpretations that can be envisaged: *(i)* by volcanism; *(ii)* like astrobleme remnants (both mechanisms are proposed and discussed by Quinn), and *(iii)* intense air-earth currents flowing mainly over tectonically active regions (this is the mechanism that is here proposed). In reality, the two mechanisms considered by Quinn are not distinct, as a volcanic feature could have been caused by some meteoritic impact. However, for clarity purpose, it is worthwhile to discuss separately these two possibilities suggested by Quinn.

A warning is that - for completeness sake and also for a matter of respect – Quinn's interpretation is here faithfully reported according to his rationale that relies on the standard way to conceive geodynamics, as per the well-known model of plate tectonics and all its associated generally agreed schemes.

Two kinds of maps

The best way to begin, perhaps, is by considering the case history that Quinn has discussed in greater detail, i.e., the feature he calls "*Farallon hyper-volcano*" (see below). A premise is needed about his general applied criteria while drawing his maps. Some excerpts, from Quinn (2014, p. 19-21), illustrate these items.

"... The images presented consist of two types: the magnetic source depth in km *and the total magnetization in* $A\,m^{-1}$. *The total magnetization is the square-root of the sum of the squares of the three vector-magnetic components. The total magnetization image color-scales have a scale factor of* 0.01. *Thus, a value of* 100 *on the color scale corresponds to* $1\ A\,m^{-1}$. *These parameters are computed over the entire Earth at a* $1/4° \times 1/4°$ *grid spacing. However, some large-scale images (e.g., Earth Quadrants) are presented at a* $1°\ lat. \times 1°\ long.$ *resolution ...*

... The total magnetization images have imbedded in them two distinct and contrasting features. One feature consists of low-magnetization sites that are interpreted as being locations of high heat flow. These features pin-point hotspots where temperatures are near or exceed the Curie temperature, which is generally between $550°C - 600°C$. [However, the definition of the Curie point depth inside the Earth is not clear.] *They are considered to be regions of active volcanism and are referred to as hotspots even though they may not precisely match the traditional definition associated with that term. The number of such hotspots is significant, especially in the Indian Ocean. Also, the dimensions of these hotspots are often quite large, on the order of* $200\ km$ *in diameter or more*. [It is well-known that the concept of hotspot is vaguely defined, and several authors use this term with a different meaning.]

The second variety of magnetization characteristic can only be described as large-scale magnetic-domains. These represent areas of the Earth that have been persistently exposed to the Earths main (i.e., core-generated) $\boldsymbol{B}$ *over extended periods of time (i.e.,* Ga*) while at the same time having been exposed to only modest temperature fluctuations that were well-below the Curie temperature. The best examples of large-scale magnetic domains are in North America and Western Europe.*

[4] After *http://geomag.org, and http://noaa.gov*.

New Concepts in Global Tectonics Journal
Volume 14, Number 1, January 2026
ISSN number; ISSN 2202-0039

All of the images presented are in geographic coordinates without a projection. So, there is some lateral stretching in the graphics as the geographic poles are approached. In the source depth case, the color scale refers to the prism's center depth. Thus, given the $2\ km$ *thickness of the prism, a depth of* $-1\ km$ *means that the top of the prism is at the ellipsoid's surface, which is not necessarily the true surface of the Earth since the geoid undulates about the ellipsoid surface.*

While there is good global correlation between the known bathymetry/topography and the lithospheric depths presented here, the absolute uncertainty in depth still requires some analysis. An ad hoc *estimate of the uncertainty ranges from* 5% *to* 20%*, depending on the source depth itself, as well as on the lithosphere's magnetic composition, sediment thickness, the fact that only a select set of* SH*s were used, and other factors. The same uncertainty extends to the magnetization ...*

... Other observed source-depth features include east-west oriented fracture zones. North-south oriented fracture zones are not observed. The lack of north-south oriented fracture zones is most likely a consequence of the CHAMP *satellite's polar orbit. The orbit tracks are perpendicular to east-west trending fracture zones and parallel to north-south trending fracture zones. Since fracture zones are not very wide, it is more difficult to detect them if the fracture zones run parallel to the orbit tracks. Globally, several trenches that form boundaries between tectonic plates are also observed ...* [This warning is important for geophysical interpretation.]

... While there is a good correlation between these atlas images and the images presented in this report, the correlation is not necessarily one-to-one, nor should it be expected to be so, since the magnetized lithosphere often resides tens of kilometers beneath the bathymetric/topographic surfaces. Consequently, the two morphological histories near the surface and at depth may be somewhat different. Also, only a select set of harmonics were used for the lithospheric inversion. Thus, the lithospheric depth and magnetization maps have essentially been band-pass filtered."

This band-pass filtering is the same earlier reference to the so called "leopard skin" effect (see above).

An additional general comment deals with the comparative spatial detail provided by the two kinds of the Quinn's maps. Compared to total magnetization maps, the magnetic-source-depth maps show a seemingly substantially higher spatial resolution. It is difficult to justify this feature. However, in general, when some data handling is applied to an observational database, every different derived parameter displays a typical robustness. In addition, different parameters have possibly much different robustness, and this can be assessed only by means of an *a posteriori* analysis.

This is a basic issue - for map interpretation - that often is not suitably considered. It can be explained as follows. In general, let us suppose that we deal with some data analysis of a given observational database, and suppose that a parameter p is computed and mapped. At the same time, suppose that we map also another parameter defined by $log\ p$. The robustness is comparatively very different, which is displayed by the two maps, because, compared to the p map, the $log\ p$ map emphasizes the details provided by the comparatively smaller values of p and reduces the weight of larger p. In contrast, if we map e^p, the emphasis is on the larger p values compared to the smaller p. Analogous comments apply to any either positive or negative power of p, etc.

In addition, while applying any kind of graphical procedures, a color code is defined in terms of a discrete series of constant increments between different colors. Hence, the gradual change in a given map between different values of p results to be very different when either p or $log\ p$ or e^p is mapped. Thus, the physical details look substantially different, which are described by the three kinds of maps, and one chooses the map that appears better suited for the investigation of his concern.

Suppose that another parameter q is derived by means of the same observational database, and consider a few different maps, such as, e.g., of q, $log\ q$, and e^q, respectively. Compare the detail provided by either one of the p maps with the detail provided by either one of the q maps, respectively. In general, the detail is different in the two cases. Perhaps, one should compare the p map with the $log\ q$ map, or with the e^q map, etc. in order to get, maybe, a comparable resolution of details. No general rule exists, however, and the usefulness of either one map or the other has to be assessed depending on the kind of application of concern.

In the present case history, in general the magnetic-source-depth maps seem to be much more detailed and physically expressive. In contrast, the total-magnetization maps seem to display some comparably more smoothed and interpolated features.

Tectonic morphological correlations

*The "*Farallon hyper-volcano*" and North America*

The several - unprecedented and extremely interesting - maps provided by Quinn (2014) therefore need a preliminary strategy for interpretation. Begin by considering the case history of the "*Farallon hyper-volcano*", while the final target is the interpretation of all planetary features displayed by the maps.

Figs 7 through 10 illustrate the "*Farallon hyper-volcano*" according to the definition of Quinn (2013, 2014).

Quinn (2014, p. 25) claims that his figures "*show what can only be interpreted as an extinct volcano*. [We kindly disagree that this is the unique possible explanation.] *It is referred to as the Farallon hyper-volcano, so named due to what is believed to be its intimate connection with the Farallon tectonic-plate subduction process that began during the Sevier Orogeny* $130\ Ma$ *and continued on through the Laramide Orogeny which covered the period* $65 \pm 15\ Ma$ *(i.e., between* $80-50\ Ma$*). So there was some overlap between the latter part of the Sevier Orogeny and the Laramide Orogeny which lead to the extraordinary tectonic activity and magmatic (Armstrong, 1968, and Gilmer et al., 2003)*."

NCGT Journal
New Concepts in Global Tectonics

New Concepts in Global Tectonics Journal
Volume 14, Number 1, January 2026

ISSN number; ISSN 2202-0039

Note the indent feature in Fig. 7 located close to Phoenix, Arizona. It seems correlated with a remarkable pattern in Fig. 8. Indeed, in this area the geomagnetic anomalies are characterized by two large clusters, i.e., a largely-blue cluster to the North and a largely-red cluster to the South, with respect to a roughly ENE-WSW strike (see Gregori et al., 2025r). The location of this blue/red feature appears to occur slightly North of the inland prolongation of the Murray fracture zone. This geomagnetic anomaly can be interpreted as a "double eye" pattern according to the rationale of Fig. 1 in terms of an electric current ***j*** flowing along the same line. This item is discussed in better detail in the following. Note, however, that the exact location of the sea-urchin spikes runs through the line that separates the two "eyes".

Fig. 7. Relative location map: Yellowstone, Farallon, and Chicxulub. The contours have been drawn by John M. Quinn on the basis of his analysis. See text. After Quinn (2014).

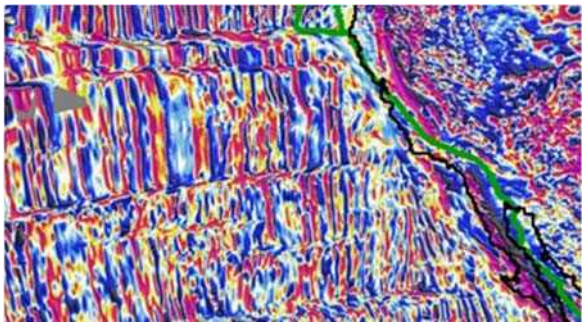

Fig. 8. Geomagnetic anomalies of the area around the Farallon hyper-volcano. Longitude span $125°W - 110°W$; latitude span $25°N - 40°N$. Detail of Fig. 6. *NOAA* copyright free policy.

This inference is to be compared to the two Quinn's interpretations in terms of two possible mechanisms, which are extensively discussed in the following.

Fig. 9 shows that crustal magnetization is minimum right at the center of this area. That is, ***B*** is originated by some source other than the crust. Indeed, this is confirmed by Fig. 10, where the huge "double eye" pattern on the upper right corner is very clearly suggestive of intense air-earth currents outflowing from sea-urchin spikes.

So, very roughly, red (blue) patches in the magnetic-source-depth map should correspond, approximately, to blue (red) patches in the total-magnetization map, although - when reference is made to some smaller and more detailed spatial scale - the correlation can be considered the exact location of the sea-urchin spikes.

This statement must be taken with some caution as the magnetic source is not unique. The estimated source-depth is just some average between the depth of different sources, and the weight of every respective source depends both on its intensity and on its distance from *CHAMP*.

In addition, possible disturbance potentially associated to air-earth currents are appealed to by the interpretation

NCGT Journal
New Concepts in Global Tectonics

New Concepts in Global Tectonics Journal
Volume 14, Number 1, January 2026

ISSN number; ISSN 2202-0039

here proposed. Indeed, these currents are reasonably expected to be more intense right on top of areas with comparably larger release of endogenous heat. This typically occurs over two kinds of areas. It occurs right on top of active tectonic areas where, depending on tectonic setting, either friction heat or sea-urchin spikes produce intense fluid exhalation.

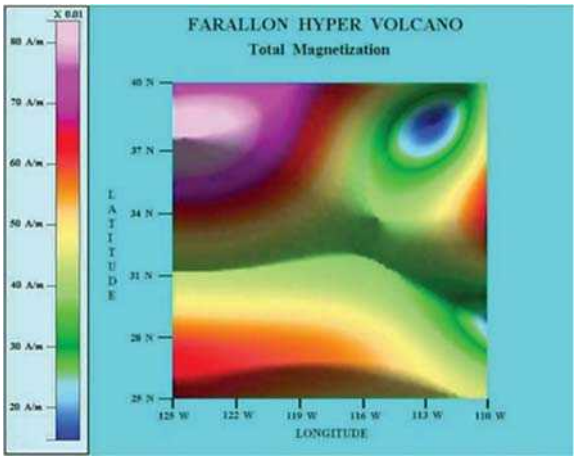

Fig. 9. The Farallon hyper-volcano: total magnetization. Longitude span $125°W - 110°W$; latitude span $25°N - 40°N$.

A warning, however, is given for the "double eye" feature in Fig. 10, i.e., a large red patch at the center of the "hyper-volcano", and a blue patch close to it (i.e., above and at the right side, with respect to it). This crucial morphological feature is extensively discussed as follows.We also point out that In general also telluric currents are an important source for the recorded ***B***. These currents are induced on the planetary scale and they are violently channeled through the comparably more conductive layers immediately below the Earth's surface, i.e., mostly through ocean waters and hydrated sediments etc. However, they are transient phenomena that have been rejected from the computation of the *SHE* model that has been used by Quinn. In addition, the Quinn's computed *SHE* model refers to an average over $6\ months$ of "quiet"-time *CHAMP* records. Moreover, it is well-known that during "quiet" time these telluric currents are likely to be less relevant than during disturbed time. Hence, in the present discussion they can be reasonably neglected.

Therefore, it is reasonable to guess that the roughly ENE-WSW linear pattern of sea-urchin spikes in Fig. 8 culminates into a large bunch of sea-urchin spikes (denoted by the blue/red boundary) that corresponds to the feature that Quinn (2013, 2014) calls "*Farallon hyper-volcano*".

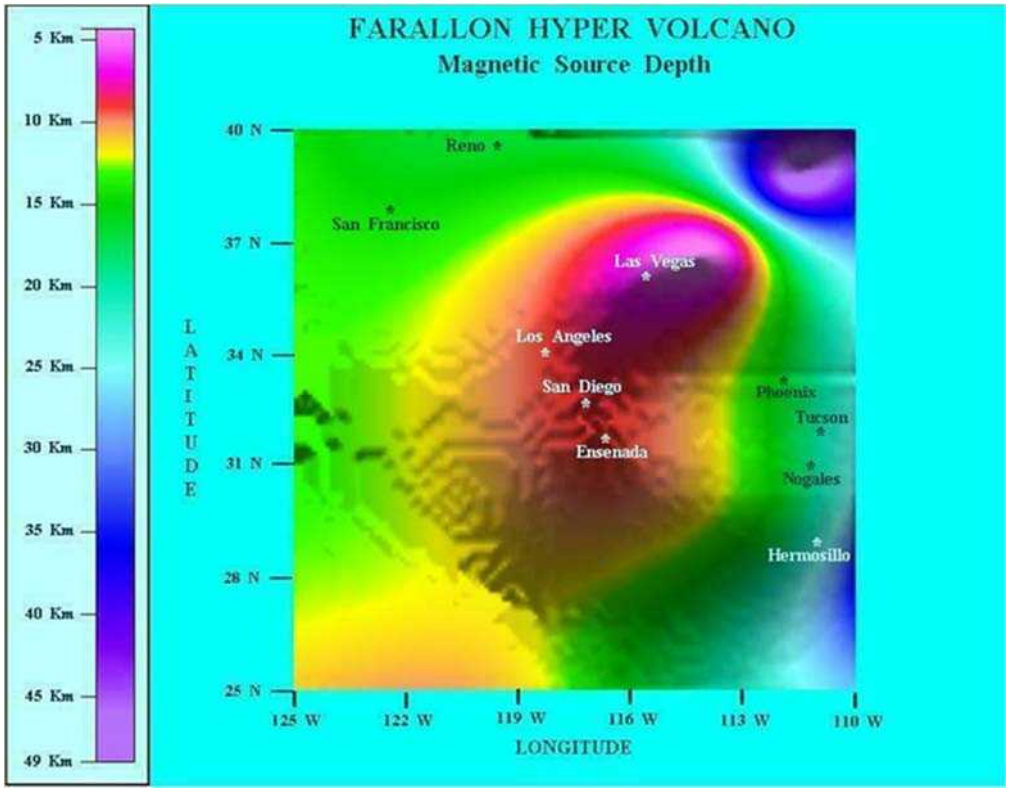

Fig. 10. "*The Farallon hyper-volcano: magnetic-source-depth (km) ... Also note the Murray fracture zone emanating from the crater's center and passing Phoenix towards the east. The crater's base is at 14 km depth. The crater's rim near Las Vegas is near 4 km depth. So, its relative height is ~10 km ... The Mendocino fracture zone is seen along 40°N leading to the Great Western Basin (blue).*" The interpretation which is here given is somewhat different. Longitude span $125°W - 110°W$; latitude span $25°N - 40°N$. See text. Figure and captions after Quinn (2014).

However, in order to avoid confusion with the "double eye" features on geomagnetic anomaly maps (see Gregori et al., 2025r), denote these new "eye" features as "E-eye", where the prefix "E" is the acronym for "external" (for a reason to be later specified). This physical feature - as it is better explained in detail in the following - is evidence of a bunch of sea-urchin spikes. However, before proposing the interpretation that is here given in terms of intense air-earth currents, let us report the two possible explanations that are proposed in Quinn (2013, 2014).

It should be stressed that every possible interpretation should be considered - in order to search for future

NCGT Journal
New Concepts in Global Tectonics
New Concepts in Global Tectonics Journal
Volume 14, Number 1, January 2026
ISSN number; ISSN 2202-0039

observational tests, aimed to focus on some missing aspects of phenomena that can enlighten the road towards truth. In any case, the space-size of every observed anomalous morphological feature is the same in every case: the space-size is just a matter-of-fact that either one interpretation - or any other – must always explain. The two possible explanations envisaged by Quinn (2013) are as follows.

"*... Among the numerous, previously unknown, geologic features revealed by the resulting global inversion is what can only* [in contrast, we guess that at least one other interpretation can be proposed] *be described as a hyper-volcano, for it far exceeds the dimensions of even the Yellowstone supervolcano. The hyper-volcano site is now extinct, but it is likely the largest, or nearly the largest, volcano ever to have existed on planet Earth and indeed within the Solar System* [note, however, that this feature might even be only an aborted hyper-volcano; see below] ... *Its NS base diameter is* $1210\ km$*, while the crater rim has a NS diameter of* $700\ km$*. These parameters are difficult to measure in the EW direction due to an apparent violent eruption that destroyed the volcano's eastern face.* [According to the aforementioned inference, this feature ought rather to be associated with the ENE-WSW linear strike in Fig. 8.] *The volcano, though eroded over millions of years, still has a crater rim that resides* ~$10\ km$ *above its base. The rim's shallowest point is* ~$4\ km$ *beneath the Earth's* WGS-84 *ellipsoid surface.*

This volcano is thought to have been created [this information may be correct even if it is only an aborted feature as mentioned above] *during the Sierra Nevada and Rocky Mountain building processes of the Laramide orogeny* $50–80\ Ma$ *(i.e.,* $65 \pm 15\ Ma$*) ...*

Due to the North American ... motion, its underlying hotspot now appears to reside in down-sized form beneath the Yellowstone supervolcano. The Farallon volcano was likely erupting off-and-on throughout the Laramide period, with the most significant eruptions occurring near two extinction events. This volcano may not only have been the chief cause of the dinosaur's demise $65.5\ Ma$*, but may also have been responsible for the Palæocene-Eocene Thermal Maximum (*PETM*) extinction around* $55.8\ Ma$. [All events occurred ~$55\ Ma$ are clearly indicative of a huge series of phenomena associated with a particularly intense peak of two heartbeats ago, when several dramatic geodynamic and climatic events occurred. See Gregori and Leybourne (2021) and Gregori et al. (2025a).]

The global effect throughout the Laramide period would have been devastating for plants and animals alike, both on land and in the oceans. While the volcano may have erupted several times, the explosive energy and catastrophic aftermath of just a single, major, Farallon volcano eruption is likely to have exceeded that of the Chicxulub meteorite impact event in the Yucatàn Peninsula (crater diameter ~$180\ km$*) many times over*."

Quinn (2013, also 2014) illustrates the tectonic history of North America, but this is not directly pertinent for the present discussion. Only a few excerpts are here reported, being more specifically concerned with the estimate of the date and of the energy release of this "hyper-volcano".

"*... In contrast to the Nevadan and Sevier orogenies, the Laramide orogeny, which spanned the late Cretaceous through the early Palæogene from* $80\ Ma$ *to* $50\ Ma$*, confined its activity primarily to the southwestern portion of North America.* [This means that the bunches of sea-urchin spikes reached Earth's surface at that time. Then, the primary main energy supply largely exhausted, and the phenomenon slowly faded off.] *During this period, the horizontal mountain building compression rate of the Earth's crust increased from* $1.4\ mm\ year^{-1}$ *to* $3.0\ mm\ year^{-1}$*. This indicates that during the Laramide orogeny, the southwestern portion of North America was in an accelerated state of tectonic activity, involving: thrusting, subsidence, and enhanced volcanism (DeCelles and Mitra, 1995, and DeCelles, 2004).* [According to the rationale of *WMT*, this means that a temporary increase of $\boldsymbol{j}$ -supply by the *TD* dynamo - consistently with the anomalous intense heartbeat - caused a more rapid uplift of the mid-Atlantic superswell. Hence, North America moved more rapidly westward, while sliding on the *ALB*, although with some relative difference when comparing different areas.]

"Also during this period there was a flattening of the Farallon slab's subduction angle in southwestern North America that was caused by the combined effects of oceanic plateau subduction and unusually great suction in the mantle wedge formed by the descending Farallon plate relative to the crustal surface (Liu et al., 2008a). Extensive plume activity resulted from this flattening [note that Quinn applies plate tectonics, but this is unessential for the present discussion; according to *WMT* a conspicuous amount of friction heat was generated, which was the leading energy source, and there is no need to speculate about subduction or suction etc.], *but the details are somewhat sketchy (Chapman et al., 2011). During the latter part of the Laramide orogeny (i.e., during the Palæocene) the convergence rate decreased along the western margin of North America, the subducted slab steepened, and hinged rollback ensued (du Bray et al., 2012).* [The relationship between drift speed and "flat-subduction" is a classical topic investigated in the Andes. A conspicuous literature is available, and cannot be here quoted.]

The Laramide orogeny is associated with uplifts and the building of the Rocky Mountains from the reactivation of earlier orogenies (Corner and Harrison, 2003) ...

Plume activity began in the latter part of the Lower-Cretaceous during the Sevier orogeny, around $110\ Ma$*, peaked during the Laramide orogeny in the upper-Cretaceous around* $70\ Ma$*, then slowly subsided as it extended into the early Palæogene (i.e., Palæocene), after which time it began to dissipate altogether around* $50\ Ma$ *(Ducea, 2001). Uplift preceded the later phases of the Sierra Nevada range building-process that occurred in the late Cretaceous and early Palæogene, during a time of rapid upwelling between* $90 - 60\ Ma$ *(Cecil et al., 2006; Mulch et al., 2006; and Cassel et al., 2009). It is suggested that the uplift, and hence the Farallon hyper volcano itself, formed as a typical explosive subduction-zone volcano* [according to *WMT* it was formed mainly by friction heat] *during this upwelling period, evolving into a hyper-volcano*

New Concepts in Global Tectonics Journal
Volume 14, Number 1, January 2026

ISSN number; ISSN 2202-0039

of deep mantle origin, while its uplift drained away the shallow sea from which the Farallon volcano emerged.

Note that during the $50\ Ma$ *prior to the late Cretaceous (i.e.,* $150-100\ Ma$*) in southwestern North America, records of sedimentation, tectonics, orogenies, and surface volcanism remained at a relatively steady level of activity, while during the late Cretaceous, plume activity reached catastrophic levels, increasing in this geographic region by a factor of a thousand (Gilluly, 1963; Prokoph et al., 2013; and Rampino and Prokoph, 2013). Consequently, the Farallon volcano probably reached its maximum energy output somewhere between* $75-65\ Ma$*, after which it became relatively quiet for* $10-20\ Ma$ *until it either erupted again or significantly out-gassed for a short period during the* PETM *around* $55\ Ma$*, but with different emission characteristics.*

The hotspot plume that gave rise to the Farallon volcano may have originated in the deep mantle or perhaps even at the CMB $110\ Ma$ *and took* $20-30\ Ma$ *to reach the Earth's surface. This suggests an estimated age range for the Farallon volcano between* $80-50\ Ma$*, which covers the Laramide orogeny*." [Note that these estimates agree with the penetration speed of the sea-urchin spikes derived by means of the *dSBT* law (see Gregori et al., 2025a). In the present case, upon assuming (as it was made for the *dSBT* law) that the depth of the *CMB* always remained (roughly) approximately the same as at present, i.e., *~2900 km*, if the penetration occurred during $20-30\ Ma$, say during $\sim 25\ Ma$, the resulting speed is of the order of $\sim 11.6\ cm\ year^{-1}$. According to the *dSBT* law the speed estimate is $\sim 10\ cm\ year^{-1}$, being almost zero at the very start of the spike from the *CMB*, and increasing up to $\sim 20\ cm\ year^{-1}$ when the spike reaches the Earth's surface.]

This completes the brief description of the first part of the volcanic hypothesis, according to Quinn (2013), which is also specified in greater detail in Quinn (2014). He makes explicit reference to plate tectonics, which is the "generally agreed" standard geodynamic model that is inconsistent with the general rationale of our approach. On the other hand, this hypothesis is irrelevant for the present concern as - owing to the several *ad hoc* assumptions that are appealed to in the aforementioned Quinn's arguments - the several geological facts that he considers can be equally well considered in the framework of *WMT* or of any geodynamic model other than plate tectonics.

Quinn (2013, 2014) also discusses the second hypothesis, i.e., the possible role of the impact of a huge meteoroid, i.e. an astrobleme. As a preliminary step, he compares the possible role of the Chicxulub event (see also Gregori and Leybourne, 2025j) with the role of the "*Farallon hyper-volcano*" in order to explain the dinosaur extinction. The following account is from Quinn (2013).

"*While the popular cause of the dinosaur extinction event* $65\ Ma$ *is that of a meteorite impact, it is still argued in some circles that volcanism, the Deccan Traps in particular, may have been responsible for the extinction. More precise dating of the Chicxulub meteorite impact event indicates that it actually predates the mass extinction at the* K/T *(or* K/Pg *or* KPB *or* KTB*) boundary (Keller et al., 2004a, 2004b, and 2007). Consequently, some focus has been diverted to the Deccan Traps as a more likely alternative cause of the* K/T *extinction, since more precise dating of this geological event places it during a time frame that straddles the* K/T *boundary. The Deccan energy emission levels rival, if not exceed, that of the Chicxulub event, with the most intense eruption phase occurring at the* K/T *boundary itself (Chenet et al., 2009; Keller et al., 2009c; and Keller, 2012).*

Due to its tremendous size and explosive potential, the Farallon hyper-volcano is suggested as another possible cause of the dinosaur's extinction at the K/T *boundary. In so doing, it may have acted independently, or it may have been acting in cooperation with the Deccan Traps eruptions ... Given that the* K/T *boundary clay layer thickness diminishes with distance from the event origin, the thickness of this clay layer, which defines the end of the Cretaceous and the demise of the dinosaurs, cannot be used to fix the geographical origin of the ash and glassy chards found in the clay due to the comparatively close geographic proximity of the Farallon volcano site to the Chicxulub meteorite impact site. The Farallon volcano may be the major source of this clay.*

The origin of the PETM *extinction is also something of a mystery. It is proposed that during the quiet period between* $65.5-55.8\ Ma$*, the Farallon volcano's magma chamber's compositional mixture changed due to tectonic and other geomorphological activity that occurred during the Palæocene. The net effects of these compositional changes were to alter the volcano's relative gaseous mixture to include more* CO_2 *and* CH_4 *and less ash,* SO_2*, sulfates, etc. This in turn favored a greenhouse environment and higher temperatures. Despite the gaseous phase change, the staggering magnitude of a Farallon eruption with altered emissions would still generate global toxic effects for both land and marine life that would have been sufficiently devastating as to eliminate* $35\% - 50\%$ *of all biota living at the time. So, for perhaps only a few* $10^3\ years$ *to a hundred* $10^3\ years$*, around* $55.8\ Ma$*, the* PETM *environment was created along with another mass extinction.* [A slow phenomenon associated to a changing greenhouse effect is also proposed in Gregori and Leybourne (2025j) although according to a different mechanism and timing.] *After this, the Farallon volcano, and its underlying hotspot, finally became extinct at the end of the Laramide orogeny. Or did it?*

The Farallon hotspot may simply have down-sized, only to re-emerge again millions of years later as the Yellowstone supervolcano. The center of the Farallon volcano is at ($32.5°\ N$, $117.3°\ W$*), while the current location of the Yellowstone caldera is at (*$44.3°\ N$, $110.0°\ W$*). If the Yellowstone hotspot is the remnant of the Farallon hotspot, then, over the past* $60\ Ma$*, the North American tectonic plate must have moved* $1406\ km$ *southwest (i.e.,* $1312\ km$ *south and* $504\ km$ *west) relative to Farallon hotspot. This corresponds to a rate of motion for the North American plate of* $2.34\ cm\ year^{-1}$ *to the southwest, which is consistent with the* U.S. National Park Service *(2013) estimate for the current North American plate motion over the Yellowstone hotspot of*

NCGT Journal
New Concepts in Global Tectonics
New Concepts in Global Tectonics Journal
Volume 14, Number 1, January 2026
ISSN number; ISSN 2202-0039

$2.5\ cm\ year^{-1}$ *to the southwest. So, the Yellowstone hotspot may actually be intertwined with the age, and possibly the demise, of the dinosaurs*." [Note that there is no need to appeal to plate tectonics, as this speed is consistent with the *WMT* viewpoint, following a comparatively rapid uplift of the geotumor associated with a temporary paroxysm of the primary energy supply by the *TD* dynamo. For completeness sake, note, however, that some intense flow of air-earth currents (as it is explained in the following being one possible explanation of these observed features) can originate a disturbance that can mimic the apparent presence of this "hyper-volcano". That is, in this case, the same existence of this "hyper-volcano" must be suitably ascertained and confirmed by some additional independent geological investigation.]

Concerning the relevant time variation of the primary heat supply to this anomalous large bunch of sea-urchin spikes - and upon referring to a much shorter epoch, i.e., to the last few centuries – a remind is deserved for the planetary distribution of Joule heat generated on the *CMB vs.* year, computed by means of the geomagnetic *SV*. It is thus found (see Fig. 3 of Gregori et al., 2025o) that the *30* hotspots (this is an exact number) envisage that - since $\sim AD\ 1400$ – every hotspot experienced a temporary period of intense activity that later diminished by some relevant amount, or it even faded off. This is suggestive of the fact that a large energy release formerly occurs when a bunch of sea-urchin spikes emerges at Earth's surface. However, during the subsequent time, the primary energy supply does not afford to sustain the same power release. Thus, the intensity of the magma emplacement rate decreases - or sometimes it seemingly stops - although, eventually, some more or less seldom, although comparatively weaker, revival can occur. This same alternation, of comparably more or less paroxysmal periods, ought therefore to have, perhaps, occurred both on the several centuries time-scale and on the geological time-scale.

The following statements after Quinn (2013) illustrate the energy estimate. In addition, in this argument, Quinn implicitly seems to make a mixture of the volcanic hypothesis with the astrobleme hypothesis.

"*The fact that the volcano is extinct is determined from an examination of the region's total magnetization presented in Fig. 9 ... Note the scale factor of* 10^{-2}. *While the lithospheric magnetization is low with a maximum magnetization of only* $0.84\ A\ m^{-1}$, *it is relatively smooth, showing no sign of suddenly going to zero as it would in a region of very high heatflow* [indeed, this means that the comparably smoother magnetic effects associated to channeled currents enter into play, consistently with the evidence from Fig. 11]. *In fact, if the geographical limits of Fig. 9 were expanded to include most of the western United States, one would observe very long East-West oriented ridges and valleys that make up magnetic domains. These domains exist only in regions that are thermally and geologically inactive."*

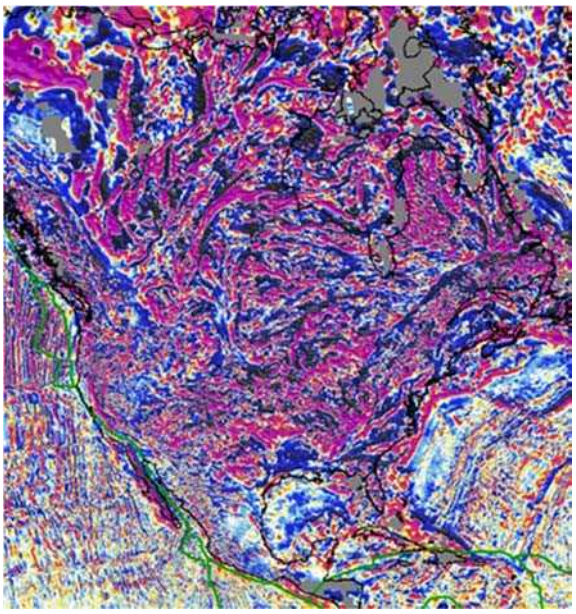

Fig. 11. Geomagnetic anomalies of North America. Longitude span $125°W - 110°W$; latitude span $25°N - 40°N$. Detail of Fig. 6. *NOAA* copyright free policy.

A related significant evidence is given by Fig. 12 that shows detailed hotspot tracks that envisage an ensemble of several sea-urchin spikes, rather than a single huge hyper-volcano. Zhou et al. (2018) carried out a 3D model of this region relying on the conventional plate tectonic paradigm etc. envisaging a pattern consistent with several other observational seismic evidences. No pattern is envisaged that reminds about the huge double "E-eye" Quinn's pattern. It is here suggested that the double "E-eye" is associated to huge air-earth currents that are a mean extended feature. In contrast, the hotspot tracks are much more restricted phenomena, caused by local episodes of sharp sea-urchin spikes that are likely to be supplied by friction heat, similarly to the typical volcanism of the whole circum-Pacific Ring of Fire.

The discussion of the North American continent is carried out at a second time (see Figs 11 and 13 through 17).

"*The Farallon volcano region is at the intersection of three magnetic domain valleys. In the northeast corner of Fig. 9, there is a circular region of depressed magnetization (blue) that indicates a small hotspot.* [This is consistent with the aforementioned inference on the signature of a hotspot, or of a bunch of sea-urchin spikes, which is the same. This is the "double E-eye" features to be here extensively discussed in the following.] *As a rule, low total-magnetization correlates with high heatflow and vice versa. Magnetic domain valleys are the exception. Hotspots tend to be localized features that disrupt the magnetic domain pattern.* [This pattern is related to the need to refer to the exact location of sea-urchin spikes, derived from the geomagnetic anomaly map, as it is discussed in the explanation in terms of air-earth currents that is here proposed.]

NCGT Journal
New Concepts in Global Tectonics

New Concepts in Global Tectonics Journal
Volume 14, Number 1, January 2026

ISSN number; ISSN 2202-0039

Fig. 12 - Hand-made indicative cartoon that shows (in red) various eruptions, with green numbers that denote the age of every eruption in millions of years. Figure simplified and based on information after Johnson (2017) and Zhou et al. (2018). Unpublished figure.

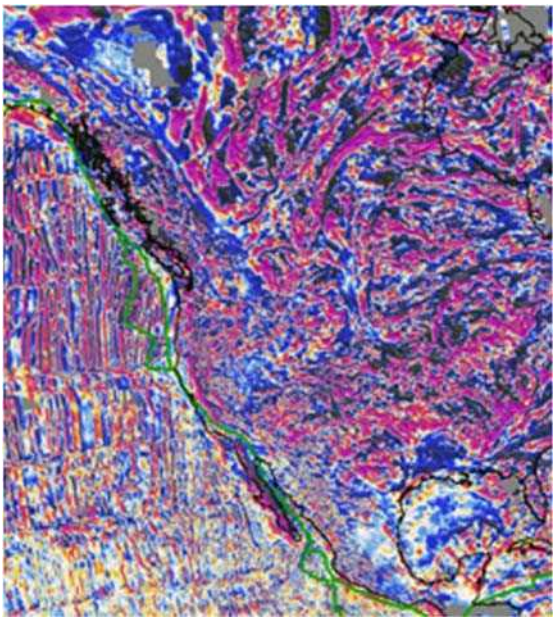

Fig. 13. Geomagnetic anomaly map for western North America. Longitude span $145°W - 85°W$; latitude span $15°N - 65°N$. Detail of Fig. 6. *NOAA* copyright free policy.

The magnetic domains evolve after long-term exposure of magnetic minerals to the ambient ***B*** *in geologically and thermally undisturbed regions. A contrasting region is the Indian Ocean which is studded with hotspots of* $200\ km$ *diameter or more, and which cause the magnetic domains to be severely broken-up. These hotspots are scattered over the entire Indian Ocean, especially between the equator and* $30°\ S$. [Concerning the Indian Ocean, see Figs 59, 60 and 61.]

Globally, the hotspot distribution varies as the cosine of the latitude. This is most evident globally in ocean areas. [This interesting comment is given by Quinn (2013) with no explanation or hypothesis. According to the rationale of the present study, it reminds about a few items: *(i)* the possible role of centrifugal force in the dynamics of the *TD* geodynamo and the consequent preferential location of the beginning of a sea-urchin spike from the *CMB; (ii)* a consistency (perhaps) with the influence on the *l.o.d.* originated by the tides on the Sun, caused by planetary alignments (see Fig. 18); and *(iii)* also the variation of the bathymetry *vs.* latitude of the *MOR*'s elevation in the Indian Ocean and its correlation with the isotopic chemism of basalt (see Gregori et al., 2025a).]

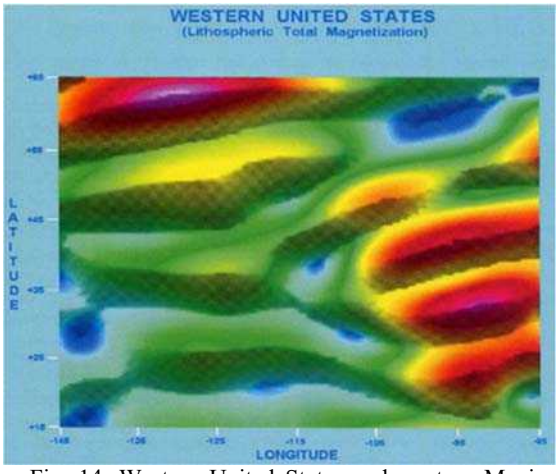

Fig. 14. Western United States and western Mexico: total magnetization map ($A\ m - 1 \times 0.01$). Longitude span $145°W - 85°W$; latitude span $15°N - 65°N$. After Quinn (2014).

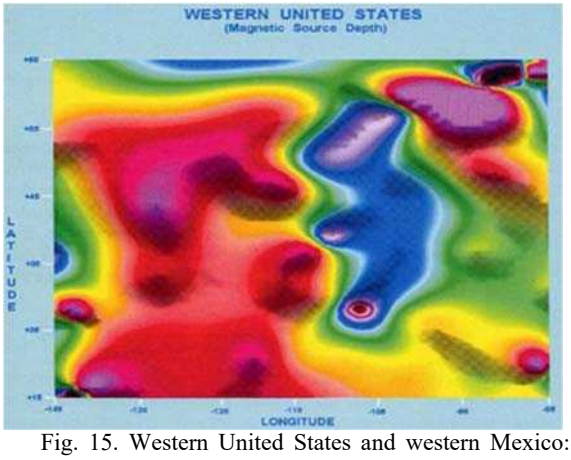

Fig. 15. Western United States and western Mexico: magnetic source depth (*km*). Longitude span $145°W - 85°W$; latitude span $15°N - 65°N$. After Quinn (2014).

As seen, using the color scale to the left of the image in Fig. 10, the Farallon volcano's base depth is $14\ km$ *below the* WGS-84 *ellipsoid surface. The volcano's peak, though somewhat warn, is* $4\ km$ *beneath the ellipsoid surface. So, the volcano's crater rim rises* ~$10\ km$ *above its base. This is despite the erosion that must have taken place during the intervening years between the Cretaceous, when the volcano is presumed to have originated, and the present. Its*

NCGT Journal
New Concepts in Global Tectonics

New Concepts in Global Tectonics Journal
Volume 14, Number 1, January 2026

ISSN number; ISSN 2202-0039

origin in a shallow sea may have limited its erosion to some degree ...

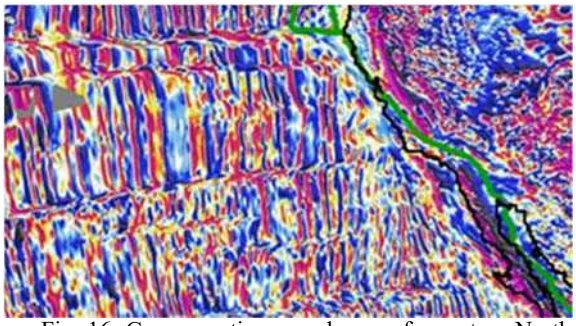

Fig. 16. Geomagnetic anomaly map for eastern North America. Longitude span $125°W - 55°W$; latitude span $10°N - 70°N$. Detail of Fig. 6. *NOAA* copyright free policy.

While the Farallon volcano is quite large, the image presented in Fig. 10 is somewhat deceptive in that the slope of the volcano is a very gentle $2.25°$ ... [In fact, a "hyper-volcano" of this size appears to be quite a singular morphological feature on the Earth. Some evidence - derived by other observations - ought to envisage the existence of similar features either in this area or in some other region. This peculiar feature shown in these Quinn's maps needs to be realistically explained, and a support should be found by other multidisciplinary information referred to the same region.]

The energy released by the Chicxulub meteorite impact was in the neighborhood of $0.7 - 3.4 \times 10^{22}\ J$, *which is sufficient to cause, when ash,* SO_2, *sulfates etc. are thrust into the stratosphere: global cooling, acid rain, ocean circulation modifications, and global mass extinctions of both land and marine life over a period of a decade or less (Pope et al., 1997 and 1999).* [The Chicxulub event is a complicated case history. See Gregori and Leybourne (2025j).] *This impact energy value is consistent with that predicted by the energy* vs. *crater diameter formula*

$$E = 4.45 \times 10^6 \times D^{3.05} \qquad (13)$$

where E *is in Joules and* D *is in meters (Taniguchi, 1993 and Sato and Taniguchi, 1997). This formula for a Chicxulub sized,* $180\ km$ *diameter impact crater, yields* $3.78 \times 10^{22}\ J$. *Applying this relation to the Farallon volcano with its* $700\ km$ *diameter crater, yields an energy of* $2.38 \times 1024\ J$ [note that this is the second Quinn's hypothesis, i.e., an astrobleme ought to have originated the Farallon hyper-volcano; see also the following]. *This is about two orders of magnitude greater than the Chicxulub impact energy.* [This conclusion is, perhaps, somewhat perplexing. In particular, the comparably much smaller Chicxulub event has left several unquestionable morphological signatures. Therefore, also this "Farallon" event ought to have left some equivalent signature that, however, to our understanding, is supported by no evidence.]

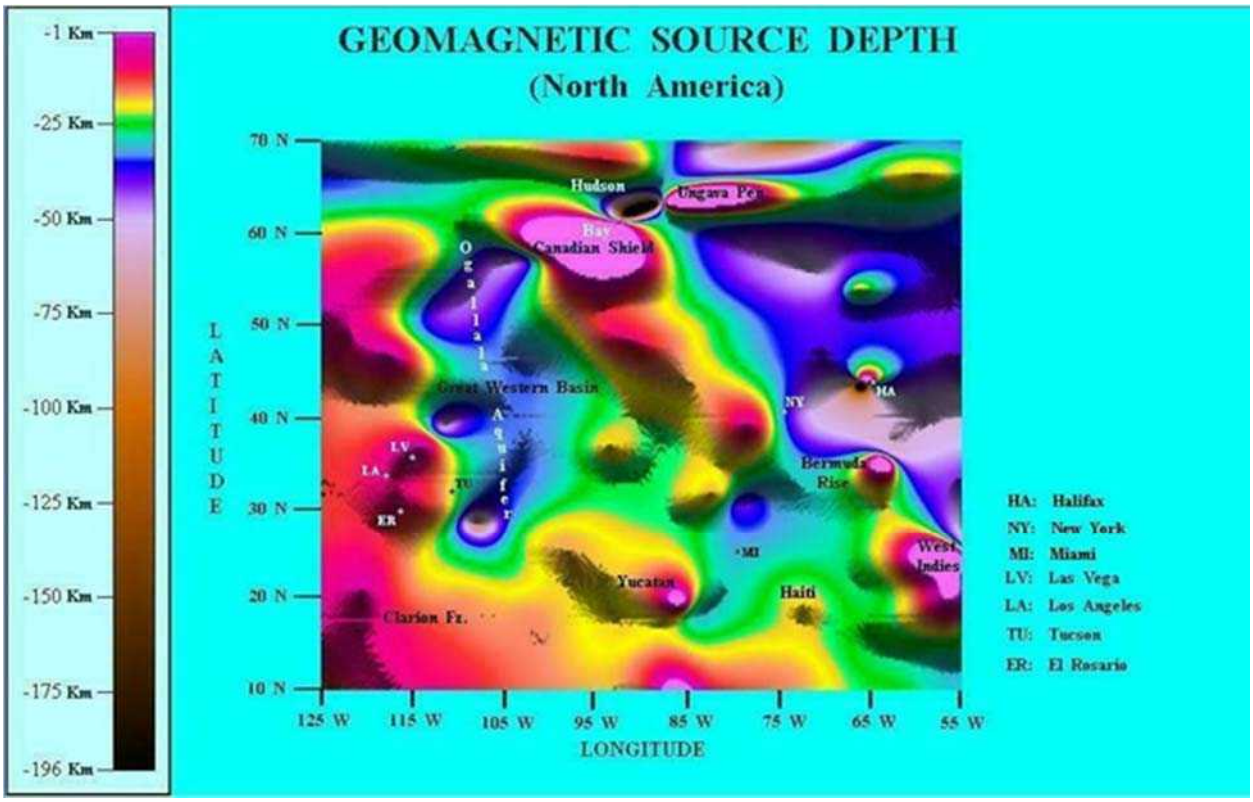

Fig. 17. Magnetic source-depth under eastern North America (km). Longitude span $125°W - 55°W$; latitude span $10°N - 70°N$. After Quinn (2014).

NCGT Journal
New Concepts in Global Tectonics
New Concepts in Global Tectonics Journal
Volume 14, Number 1, January 2026
ISSN number; ISSN 2202-0039

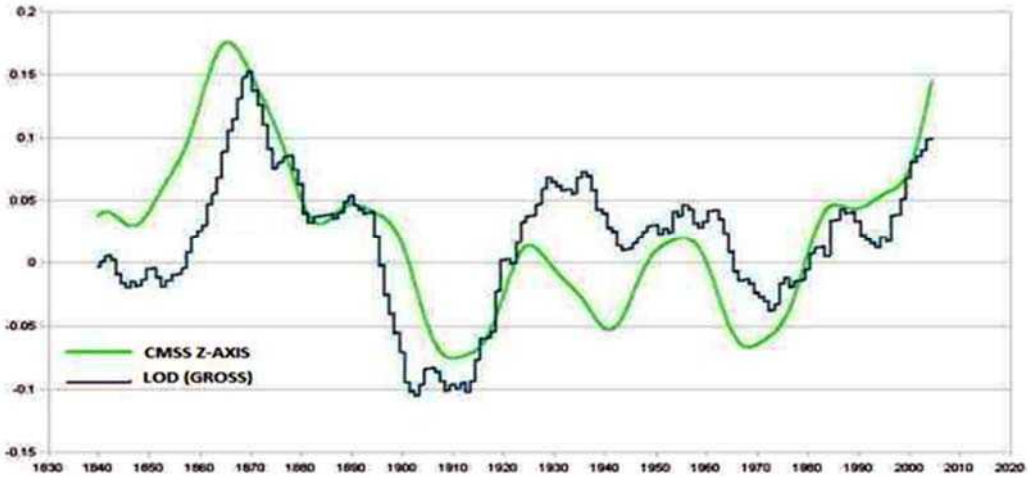

Fig. 18. "*z-axis motion of the center of mass of the Solar System (*CMSS*) relative to the solar equatorial plane plotted against* l.o.d. *(Gross, 2007) 1840-2005.*" Figure and captions after Tattersall (2013a). With kind permission of *Pattern Recognition in Physics* ("*Open Access*") and of Roger Tattersall.

Assuming a 20% *erosion factor, for the Farallon volcano, makes its original height* $12.5\ km$. *Taking its slope into account, yields an original crater diameter of* $286.25\ km$. *In this case the volcano's emission energy is reduced to* $1.55 \times 10^{23}\ J$. *This is still nearly an order of magnitude greater than the energy output of the Chicxulub impact event. Of course, Chicxulub, was just a single event, while the Farallon volcano may have had several significant eruption events. Thus, any claims that can be made concerning the destructive power of the Chicxulub meteorite impact event can also be reasonably attributed to any single major eruption of the Farallon volcano, of which, presumably, there may have been several.*

... given the comparatively close proximity of the Farallon volcano site to the Chicxulub impact site, it might be rather difficult to distinguish geological, atmospheric, biological, and other environmental effects caused by one or the other type of event. This would include such things as the distribution patterns of glassy spherule deposits, shock signatures, and iridium in the K/T *(or* K/Pg *or* KPB *or* KTB*) boundary clay.*"

The mechanism ought to be stressed, which is appealed to by Quinn. This same mechanism was also independently envisaged when writing a former draft in order to give a tentative explanation of the $300\ ka$ time-delay between the Chicxulub event and the dinosaur extinction.

It can be reasonably guessed (Gregori and Leybourne, 2025j) that the astrobleme impact originated a strong heating of the underlying Earth's body, thus increasing the local electrical conductivity σ.

Hazen et al. (2012) state that " ... *in spite of carbon's importance, scientists remain largely ignorant of the physical, chemical, and biological behavior of carbon-bearing systems a few hundred meters beneath Earth's surface. Little is known about how much carbon is stored in the Earth as a whole, how deep reservoirs form and evolve, or how carbon moves from one deep repository to another. Further, scientists are largely ignorant of the nature and extent of deep microbial ecosystems, which by some estimates rival the total surface biomass.* [Consider that also the total amount is unknown of water stored in the serpentosphere, and how it changes on the multiannual scale - as it depends on crustal fracturing, hence on geodynamic activity and endogenous energy exhalation. See below.]

Past consideration of the global carbon cycle has focused primarily on oceans, atmosphere, and shallow surface environments, with the understanding that these reservoirs exchange carbon relatively rapidly as an essentially closed system. Earth's near-surface carbon cycle undergoes transfer of carbon through biotic and abiotic reservoirs via combustion of organic matter, burial of carbonaceous sediments, exchange of CO_2 *between oceans and atmosphere, and the influence of living systems (Berner, 2004).*

Distributions of fossil fuels, organic-rich shale, carbonate rocks, and near-surface life have been mapped, their abundances and ages estimated, and their contributions to Earth's surface carbon cycle well established. By contrast, knowledge of the deep interior, which may contain $> 90\%$ *of Earth's carbon (Javoy, 1997), is limited. Carbon forms varied mineral phases in Earth's interior, yet the nature and extent of these reservoirs in space and time are poorly constrained. Even less well understood are solubilities of carbon in mantle silicates and core metals, the source fluids and mechanisms of carbonate volcanism, and chemical environments of carbon at extreme conditions ...*

The nature and extent of carbon reservoirs in Earth's deep interior (Table 1 and Fig. 17) are poorly known. Primitive chondritic meteorites, thought to reflect the basic composition of the early Solar System, contain up to several weight percent carbon, yet estimates of Earth's total carbon inventory, though poorly constrained, are much lower, ranging from $0.07 - 1.5\ \%wght$ *- more than a twentyfold uncertainty. Earth appears to be significantly depleted in highly volatile elements compared to chondrites, but uncertainty remains because of large potential reservoirs of carbon in Earth's mantle and core.*

Therefore, owing to the Hamilton's principle, the sea-urchin spikes can more easily penetrate through the upper mantle and lithosphere. The more intense electric currents

ISSN number; ISSN 2202-0039

$\boldsymbol{j}$ that flow on the outer boundary of every sea-urchin spike are a source of Joule heat that supports the comparatively higher value of the local temperature and also of σ at some comparatively shallower depth. Hence, this anomalous intense sea-urchin spike survives for some long time after its former trigger caused by the astrobleme.

This ought to have two possible consequences. On the one hand, the local steady existence of a huge bunch of sea-urchin spikes causes a permanent larger release of endogenous heat through an intensified soil exhalation. This has also long-range impact on climate change, and on the very slow evolution of the biosphere, including also eventual extinctions after a suitable time lag, etc. On the other hand, a comparatively more intense effect of this kind can also explain the eventual formation of some feature resembling (perhaps) to some structure similar to the Quinn's Farallon hyper-volcano, etc.

One related possible consequence is the formation of a kingpin for a clockwise rotation of South America (see Gregori and Leybourne, 2025j).

Note the substantial difference between *(i)* the merely Earth's endogenous process that leads to the formation, development, and evolution of bunches of sea-urchin spikes, and *(ii)* the astrobleme mechanism, although - as mentioned above - an astrobleme can trigger the indirect formation of a steady intense local large bunch of sea-urchin spikes.

In either case, these large bunches cause the uplift of geotumors and superswells (see Gregori et al., 2025a). According to *WMT*, the lithosphere slides on their slope, until thrust occurs inside huge megasynclines, leading to the formation of continents and of orogenetic processes (like "foam" in a boiling pad with a circular heat source, with foam that therefore converges towards the center of the pad). According to this rationale, an astrobleme is only an accidental event that originated a paroxysm inside deep Earth, by which the development of sea-urchin spikes was rapidly accelerated due to the local increase of internal temperature, hence of σ.

This phenomenon, with its slow impact on climate, can explain the extinction of dinosaurs with a considerable time delay after the astrobleme impact, i.e., some $\sim 300\ ka$ later (Gregori and Leybourne, 2025j).

This hypothesis by Quinn is the unique mention that we found in the literature envisaging the same mechanism - i.e., a steady anomalous large release of endogenous heat by a persistent large sea-urchin spike - that is proposed in Gregori and Leybourne (2025j) in order to explain the observed anomalous very large energy input to hurricanes in the Gulf of Mexico, which occurs by a matter of only very few hours (or maybe even more rapidly).

In this same respect, note in Fig. 11 that the aforementioned ENE-WSW red/blue pattern in Fig. 8 is repeated much more intensely roughly South - East towards the Gulf of Mexico (with respect to the former red/blue pattern). This new red/blue/red large pattern precedes a huge blue patch, slightly North of Yukatàn, and it is extended from the Pacific coast almost until Florida. This huge blue "crater" envisages a possible correlation with the Chicxulub crater. This remarkable singular feature is recalled in Gregori and Leybourne (2025j) and can be the surface signature of the kingpin.

In this same respect, note that the existence of this singular feature, which Quinn calls Farallon hyper-volcano, is an observational matter-of-fact. It might be originated by an astrobleme. In this case, the aforementioned estimate of its energy by means of (13) makes sense. On the other hand, it might also be the simple remnant of some kind of aborted *LIP* that was originated at the time of the huge Earth's paroxysm occurred approximately two heartbeats ago. That is, the Farallon hyper-volcano could be only an aborted *LIP*, much like a diamond-bearing kimberlite seems to be an aborted volcano (see Fig. 19c). However, (13) cannot be applied in the case that it is an aborted *LIP*.

Quinn (2013) finally shows how the Farallon hyper-volcano is correlated with the major fracture zones on the Pacific Ocean floor (see Fig. 7).

"*Just below latitude* $34°\ N$, *on the eastern side of the image in Fig. 10, a fault zone running through the crater can clearly be seen.* [Compare also with Fig. 11] *Though obscured by the lighting angle and the fault's narrow width, the fault actually extends into the eastern Pacific Ocean where it is known as the Murray fracture zone. The fault is* $\sim 45\ km$ *wide. Normally, widths this short cannot be resolved except by using higher harmonics. However, it is the length of the fault that is being picked up by the low and intermediate harmonics*. [As mentioned above, the degree and order 60 used by Quinn permits to detect no detail shorter than a few hundred kilometers.]

There is another fault zone residing just below $40°\ N$ *latitude. It is* $\sim 40\ km$ *wide and can be faintly seen extending into the eastern Pacific ocean as well. It is known as the Mendocino fracture zone. In the upper right-hand corner of the image is a hint of the Great Western Basin, which is adjacent to, but farther east of Fig. 10. The basin extends from northern Mexico to Southern Canada and contains the Ogallala aquifer. The dark spot within the basin appears to be a lithospheric drip site* [a warning is, however, needed about this, as these dark spots could be the result of the "double E-eye" feature discussed in the following]. *The Farallon volcano sits on the western edge of the Great Western Basin, a region that was once occupied by the Cretaceous Seaway*."

According to the astrobleme hypothesis, Quinn (2012) made a tentative discussion of the possibility to explain morphological patterns worldwide - both of the total crustal magnetization and of the magnetic source-depth - in terms of huge astroblemes occurred "*during the Late Heavy Bombardment (*LHB*) era of Earth's history around* $3.9\ Ga$*",* although he warns that *"the geological events occurring in the Late Hadean (*$4.1-3.9\ Ga$*) and Early Archæan (*$3.9-3.5\ Ga$*) Eons ... are not well studied.*" However, as he stresses, this ought to be considered only a tentative guess. Quinn (private communication, 2015) very clearly clarifies this point.

"*Girdler et al. (1992) reported the Bangui crater* [see below] *and associated anomaly as a result of a Precambrian (*$\sim 4.1\ Ga$ *during the* LHB *era) meteorite impact site, not me. They based their opinion on physical*

NCGT Journal
New Concepts in Global Tectonics

New Concepts in Global Tectonics Journal
Volume 14, Number 1, January 2026

ISSN number; ISSN 2202-0039

geological evidence. I merely point out that my images support Girdler et al. better than Regan (1978) and Regan and Marsh (1982). There are other large craters that have a similar morphology. So, one cannot rule out the possibility of a meteorite impact for them.

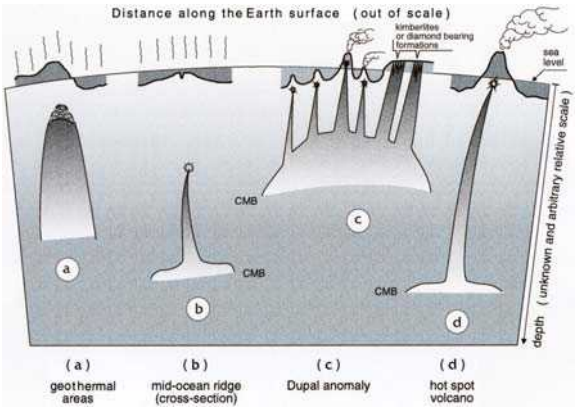

Fig. 19. A speculated model for global magmatism. An electric circuit supplies currents from deep Earth up to some shallow depth where Joule heat is released. Suppose that water and other "standard" fluids are sufficient to transport - by advection - Joule heat up to Earth's surface. This is the case observed in a geothermal area [figure *(a)*]. When these standard fluids are insufficient, some melting must occur, until a newly created fluid (i.e., magma) affords to transport the excess heat, thus originating volcanism [figures *(b), (c),* and *(d)*]. Volcanism can have a heat source at different depths. In the case of *MOR*s [figure *(b)*] the magma chamber is comparatively deeper (several tens of kilometers), magma outpours with a slower although steady and smooth spreading rate, and its chemical characteristics reflect the deep location of the melting processes: hence, the *MORB* is depleted. The entire outpouring process, perhaps, involves only hot mud (pillow lavas could be only seldom occurring events). In contrast, volcanoes from *DUPAL* anomaly [figure *(c)*] have a comparatively less deep magma chamber, their temperature is lower, and the basalts are enriched, due to the shallower depth of the region where melt occurs (see Gregori et al., 2025a). An eventual thick lithospheric/crustal layer, composed by a craton or by a continental platform, can substantially affect the morphology of volcanism, such as in *DUPAL* areas, where it can lead to formation of kimberlites. Unpublished figure.

There are generally three alternatives, either they are meteorite impact sites, in which case due to their large size they are probably very old, if they occur on land, and $< 150\ Ma$ *if they occur in the ocean. They may be the consequence of some collapsed plume. The mere motion of tectonic plates can also result in the formation of ridges and valleys that may give the configured appearance of a crater.*

In the case of Australia [see below]*, I merely focus on the most obvious feature, which is the circular shape of the land masses that surround the Australian continent. Can you account for that. I cannot*. [Australia is at the border of the tectonically dramatic region comprised between the Moluccas Sea and the Sunda archipelago, and is roughly on top of one vertex of the tetrahedron with a maximum release of endogenous heat (Gregori and Leybourne (2021).] *While the geologic history of Australia is well-studied, no geologist to date has ever been aware of this peculiar distribution of land masses. My images, permitting me to be the first to notice it, allowed me to offer-up one possibility. I do not subscribe to it. I merely point out the possibility.* [Note the understating feeling of Quinn, as a truly conscience-driven scientist.]

The only way to determine the origin of the morphology of the Australian region, in light of my work, is to send field geologists out to these sites to do a thorough geologic investigation (including drilling, since these features are at depth). This goes for any of the new features uncovered by my work, such as the Farallon volcano for instance. My comments regarding the Farallon volcano rest upon what geologists believe they have deduced about the geologic history of the entire southwest portion of North America as a consequence of extensive field studies, which, when put together, suggest that there may be a connection between the Farallon and Yellowstone volcanoes. [Such a connection is consistent also with the alternative interpretation that is here proposed.] *Obviously, in light of my images, the Bangui Region* [see below] *needs to be completely re-investigated from a geological point of view ...*

As for the Shatsky crater [see below]*, which geologists refuse to acknowledge even exists, I merely point out that it has a morphology similar to that of the Bangui Crater which geologists seem to feel really is an impact site. Therefore, one of the several possible origins is that of a meteorite impact. Hardly an outlandish conclusion.*

Another point that ought to be made is that while the Earth has no-doubt been hit by meteorites on numerous occasions, probably even more so than the Moon, very few impact sites are observed on Earth's surface due to environmental factors such as erosion. On the other hand evidence of most impacts that have impacted the Earth are very likely preserved in the lithosphere beneath initial crustal surface of the Earth on land areas. For ocean areas, only the last $150\ Ma$ *of impact evidence may be preserved due to plate tectonic subduction. I believe that the higher* SH*s will pick-up this evidence. So, I think we should be on the alert. Only the largest impacts are likely to be observable for degrees-and-orders* 31 *through* 60*. The largest ones are most likely older impacts which are more likely to be associated with the* LHB*. Hence, I discuss these more in my lithosphere report. If I had images from the higher harmonics I would no-doubt be concentrating on more recent impact events.*"

In addition, note that - according to the general rationale of our approach - there is no need to appeal to such an extreme and early *LHB* in the Earth's history. In fact, these features can be explained by the evolution of bunches of sea-urchin spikes that were developed during the geothermal history of the Earth through the most ancient geological past. On the other hand, also the astrobleme hypothesis can sometimes be the correct explanation, as the two mechanisms do not exclude each other, being operative at different sites and/or time.

Concerning several regions mapped by Quinn (2014) - and his figures are here reproduced with some brief discussion - he gives extensive details about their

ISSN number; ISSN 2202-0039

geological and geophysical setting, although he relies on the present standard geodynamic modeling - plate tectonics, etc. However, this target is outside the focus of the present paper. These items, therefore, are not here reported and the interested reader can refer directly to Quinn (2014).

Instead, let us address the "double E-eye" feature. Consider Fig. 10 and note that the large red/yellow patch appears together with the blue patch displayed at the upper right corner. This pattern is better shown by looking at a wider map.

Figs 13 through 15 refer to western North America and Mexico. Mostly Fig. 15 shows a complicated pattern that is seemingly composed of several "double E-eyes", every one characterized by a couple of "E-eyes", one "eye" red, and the other blue, and *the most impressive feature is the sharpness* of the divide between every couple of contiguous "E-eyes".

Analogous maps for eastern North America are shown in Figs 16 and 17. The "double E-eye" feature seems to be very frequent. Note that no large-scale anomalous pattern is observed to possibly correlate with the Chicxulub crater. This feature is here reconsidered in the following (see also Gregori and Leybourne, 2025j).

Analogous "double E-eye" features are observed at several other sites at Earth's surface. Quinn (2014) shows several self-explaining figures, dealing with different morphological features. They are here briefly reported in order to show the almost ubiquitous morphology of these very peculiar "double E-eye" patterns that are frequently characterized by a clear sharp divide.

The different interpretation which is here given appeals to the "double E-eye" feature that envisages an intense flow of air-earth currents through regions of great tectonic activity, associated to large soil exhalation of fluids. Before entering into a more specific discussion, it is worthwhile to report in some detail the Quinn's discussion about Australia.

Australia

According to Quinn (2012, 2014), Australia - which is a continental size region with limited anthropic pollution - perhaps can be considered as the possible remnant of a former huge astrobleme, although, compared to the Farallon hyper-volcano, the related morphological evidence is substantially different. Owing to this reason, for comparison purpose it deserves a specific consideration. In addition, as already mentioned, it is located roughly on top of one vertex of the tetrahedron with a maximum release of endogenous heat (Gregori and Leybourne (2021).

The magnetic anomaly map of the same region considered by Quinn is shown in Fig. 20.

From Quinn (2012) "*... the Australian region ... includes Australia, Indonesia, Malaysia, Borneo and the Philippines ... Fig. 21 presents the lithospheric source depth in the Australian region. Most noticeable is the ring of volcanic intrusions that generally match the seismicity that defines the Australian plate boundaries in Fig. 22 to the East, West and South. To the North, the ring extends beyond the current Australian plate to include the Indonesian plate and the Philippine plate. The crater rim actually coincides with the Australian tectonic plate boundary to the East, West, and South. To the North the crater rim reaches the northern boundaries of the Philippine and Indonesian plates. The large pink region to the northwest is in the vicinity of Malaysia, Borneo and the Sunda Sea and is part of the extreme southeastern Eurasian plate referred to here as the Indonesian plate. It is almost a microplate ... It is nearly surrounded by modern volcanic and seismic activity as indicated in Fig. 22 ...* "

Let us present the interpretation that we give according to the general *WMT* rationale of the present whole study. The ring of pink color in Fig. 21 roughly coincides with the so-called plate boundaries interpreted as fractured lineaments of intense serpentinization (see Gregori et al., 2025a).

The "*ring of volcanic intrusions that generally match the seismicity that defines the Australian plate boundaries in Fig. 22 to the East, West and South*" is just the result of the very complicated geodynamic history of this tectonically dramatic region comprised between the Moluccas Sea and the Sunda archipelago. It results from the combined action of the lithosphere that slides on the slope of the Kerguelen superswell, altogether with the southern extension of the effect associated to the gap that is left in the wake of the westward drift of Eurasia, which is pushed by the Pacific loading tide. In addition, Australia is located on top of one vertex of the tetrahedron with a maximum release of endogenous heat (Gregori and Leybourne (2021).

At present, owing to the concern about corals, a list has been prepared of *20* species that are threatened (Showstack, 2014). Some images are shown, e.g., by Bryner (2015a). A permanent monitoring is a service provided by the *NOAA*'s *Coral Reef Watch*. See e.g. *Anonymous* (2017f). It is stressed that the bleaching process occurs through "events" of various duration. A few highlights are here provided by some excerpts from *Anonymous* (2017f).

"... The first global bleaching event was in 1998, during a strong El Niño that was followed by an equally very strong La Niña. A second one occurred in 2010 ... NOAA*'s experts say* Cr*s around the world may finally catch a break from high ocean temperatures that have lingered for an unprecedented three years, the longest period since the 1980s. The latest* NOAA *forecast shows that widespread coral bleaching is no longer occurring in all three ocean basins - Atlantic, Pacific and Indian - indicating the likely end to the global coral bleaching event. Scientists will closely monitor* SST*s and bleaching over the next six months to confirm the event's end.*

NOAA *declared the beginning of the third-ever global coral bleaching event in 2015. Since then, all tropical* Cr*s around the world have seen above-normal temperatures, and* > 70% *experienced prolonged high temperatures that can cause bleaching. U.S.* Cr*s were hit hardest, with two years of severe bleaching in Florida and Hawai'i, three in the Commonwealth of the Marianas Islands, and four in Guam.*

Fortunately, some coral reef areas did not bleach despite the damaging conditions ... 'Coral reefs are not beyond help'*, said Jennifer Koss, director of the* NOAA Coral Reef Conservation Program. 'Many proactive steps to make coral reef ecosystems more resilient are being taken

NCGT Journal
New Concepts in Global Tectonics
New Concepts in Global Tectonics Journal
Volume 14, Number 1, January 2026
ISSN number; ISSN 2202-0039

around the world. We are reducing local threats to coral, and are looking into innovative ways to increase coral populations and species that are more resilient to rising ocean temperatures and acidified waters*'* ....

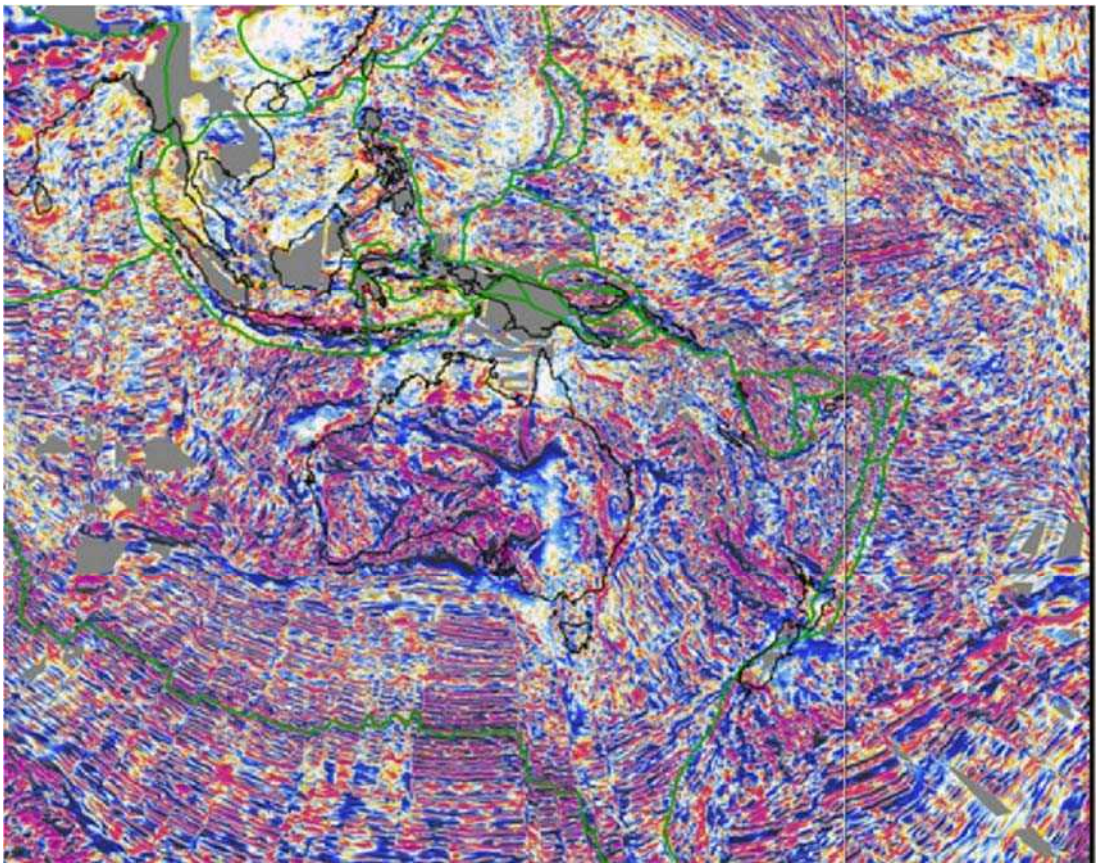

Fig. 20. Geomagnetic anomaly map for the large Australian region. Longitude span $75°E - 210°E$; latitude span $60°S - 30°N$. Detail of Fig. 6 referring to Sunda longitudinal sector. *NOAA* copyright free policy.

Despite what appears to be the end of the third global event, some U.S. Crs *are still not completely in the clear ...* 'This global coral bleaching event has been the most widespread, longest and perhaps the most damaging on record'*, said C. Mark Eakin,* NOAA*'s* Coral Reef Watch Coordinator ... *"*

Every $4\,months$ the *NOAA*'s *Coral Reef Watch* regularly provides updated maps such as shown in Figs 29 and 30. Also the behavior of reef fishes is being investigated, as a response of acidification of the reef environment (e.g., Munday et al., 2014). However, this item is not directly pertinent for the present discussion.

Also the Pekeris force, maybe, plays a role. That is, the Earth gets excessively flattened, and - if the Earth is a fluid - a poleward "Pekeris force" ought to be observed with maximum at $\sim 45°$ latitude in both hemispheres. Refer to Jeffreys (1976), or, for thermal contraction, to Bott (1971), Collette (1974), and Turcotte (1974), …

The intricate Moluccas Sea and the Sunda archipelago region has elongated stripes of comparatively greater lithospheric fracturing where volcanism is supplied by friction heat.

The large pink area, which is roughly located at latitude $0-20°N$ and longitude $90-130°E$ - and that Quinn defines "*almost a microplate*" - coincides with the Banda Sea, which is one of the areas with the largest endogenous heat release, originated by a local very efficient bunch of sea-urchin spikes.[5]

The Australian continent's main geomagnetic feature is around the large blue region in Fig. 21 in its central and eastern portion. However, also the red area around Perth (i.e. at $\sim 115°E$) is noteworthy, as this is consistent with a localized bunch of sea-urchin spikes that ought to justify the diamond-bearing kimberlites reported in this area (see Gregori et al., 2025a).

A remarkable feature is the repeated, frequent, occurrence of typical "double E-eye" features in Fig. 21. Every "double E-eye" looks to be always composed of two roughly circular areas, tangent each other. One area is roughly blue, the other roughly red or pink. According to

[5] It seems to be the result of a plugged *MOR* (Gregori and Leybourne, 2021). In addition, this seems to be a favorite candidate for being, perhaps, the trigger of El Niño. See Gregori et al. (2025a). In addition, it seems the likely trigger of the wildfire propagation that repeatedly and regularly starts from the southern tip of Indochina and moves until the two "flash" areas, respectively, north of Beijing and roughly in the Karakoram region. See section Gregori and Leybourne (2025i).

NCGT Journal
New Concepts in Global Tectonics

New Concepts in Global Tectonics Journal
Volume 14, Number 1, January 2026

ISSN number; ISSN 2202-0039

the interpretation which is here proposed, these tangent features are perfectly consistent with "blades" of air-earth currents crossing through Earth's surface at the tangency area, as per Fig. 2. In fact, these tangent features should be explained in terms either of sea urchin spikes or – we do not understand how - of past volcanic intrusions, or of astroblemes.

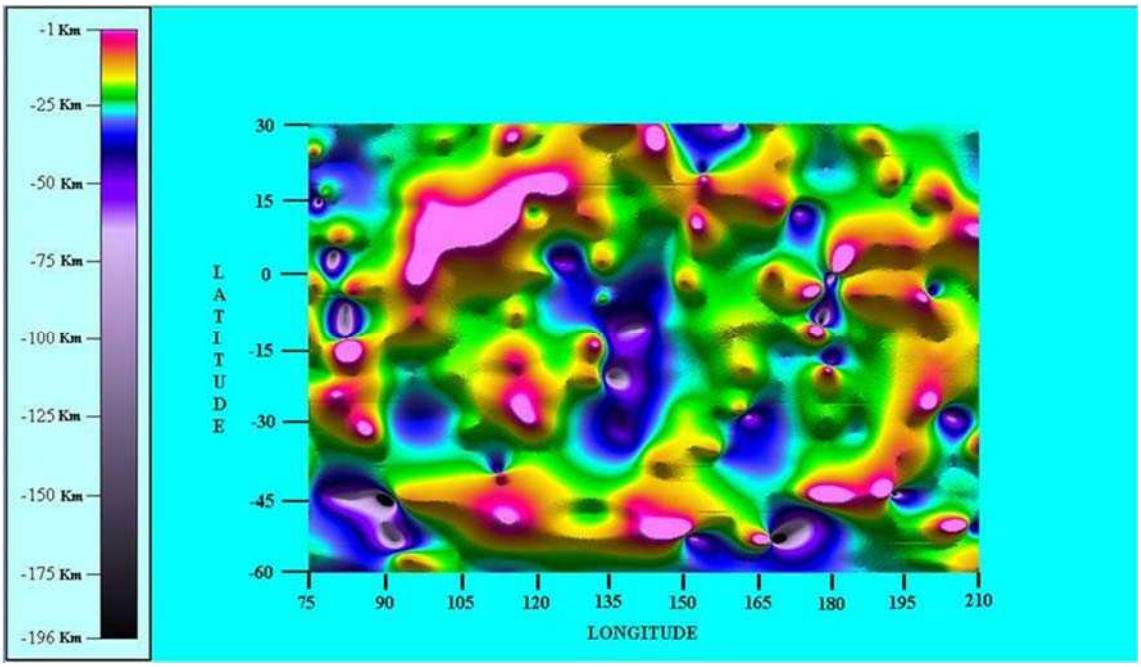

Fig. 21. Magnetic source depth (km) in the Australian region. Longitude span $75°E-210°E$; latitude span $60°S-30°N$. After Quinn (2012, 2014).

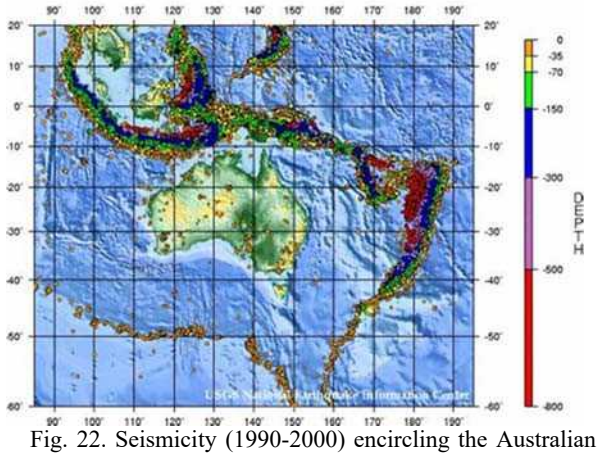

Fig. 22. Seismicity (1990-2000) encircling the Australian continent (courtesy by the *USGS Earthquake Information Center*). Also in Quinn (2012, 2014). *USGS* copyright free policy ("*Public Domain*").

Quinn (2012) notes that, if this Australia feature is a crater, it displays "*a diameter of roughly* 9000 km *in the North-South direction",* while *"in the East-West direction along* 25° S *latitude it stretches from New Caledonia to the middle of the Indian Ocean, reaching a diameter of* 13,344 km *...*

... in Fig. 21 ... the yellow, red, and pink colors denote the crater rim and volcanic intrusions through the rim ... The violet and purple colors indicate exhaust vents, presumed to have been created at the time of impact ... The shallow feature going North-South between 150° E *longitude and* 165° E *longitude is known as Lord Howe Rise. Just west of this band is a poorly resolved pair of hotspot tracts that pass near the East coast of Australia (Duncan and Richards, 1991; ...).* [See Figs 23 and 24. Duncan and Richards (1991) also shows modeled hotspot tracks for the whole globe.]

Continental Australia is centered over the central basin of Fig. 21. Lord Howe Rise was formed between 80 – 50 Ma*, long after the basin in which it resides is presumed to have been created. The hotspot tracts were formed around* 30 Ma*. Together they form the green colored ridge. The crater basin, along* 135° E*, consists of a North-South running string of very deep (*200 km*) purple/black features that may be interpreted as exhaust vent sites created at the time of the meteorite impact.*

Another North-South oriented ridge lies between 105° $E-120°$ E *longitude. This ridge is presumed to be impact generated breccia expelled westward from the string of adjacent exhaust vents to the east during the impact.* [This is here interpreted as the aforementioned bunch of sea-urchin spikes roughly close to Perth.] *On the western side of this debris ridge is a continuation of the overall basin (blue). Thus, with the exception of the debris ridge, the bluish colored crater basin prior to* 80 Ma *extends from ~*90° E *to ~*170° E *...*

These features can be observed in Fig. 25, which is a depth profile along latitude 25° S*. Mentally then, we can subtract Lord Howe Rise and other hotspot tracts out of the picture and replace it with a blue color which yields the pre-*80 Ma *depth profile of Fig. 26 along latitude* 25° S*. Then, from* 130° E *longitude to* 180° *longitude, we have the blue*

NCGT Journal
New Concepts in Global Tectonics
New Concepts in Global Tectonics Journal
Volume 14, Number 1, January 2026
ISSN number; ISSN 2202-0039

colored basin that existed prior to $80\,Ma$. [A warning, however, deals with a possible disturbance originated by the "double E-eye" pattern which is discussed in the following.] *The southeast section of the rim in Fig. 21 corresponds to the Louisville Ridge and the Tonga Trench ...* [Note that, in Figs 25 and 26 the peak at $\sim 110° - 120°E$ longitude corresponds to the aforementioned feature close to Perth. The other peaks refer to continental features, much outside the Australian subcontinent.]

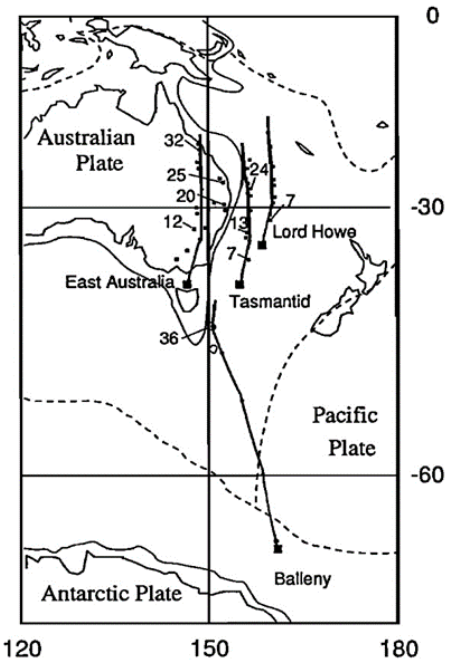

Fig. 23 - *"Modelled hotspot tracks for the eastern Australian plate ... Ages shown are radiometric age determinations (McDougall and Duncan, 1988; R.A. Duncan, unpublished data for southeast Tasmania, 1990). Solid squares are locations of volcanic centres."* Figure and captions after Duncan and Richards (1991). [Ask AGU for permission.]

Fig. 27 presents the total magnetization within the Australian region. [Quinn notes the distinct trend inside the latitude belt $\sim 15°N - \sim 15°N$. Also note the anomalous trend corresponding to the aforementioned feature close to Perth.]

The high heatflow regions (blue and violet) and the apparent active volcanic sites (violet and black spots) are primarily limited to a latitude band that stretches $\pm 30°$ *about the geographic equator. Centrifugal force due to Earth rotation may be responsible for this effect.* [Concerning the role of centrifugal force, refer to the brief comment given above, although it is perhaps difficult to apply the same argument to the comparably limited space-size spanned by Australia.]

The southern boundary of the Australian plate has relatively high magnetization compared to its northern boundary. Furthermore, the southern plate boundary has much less seismicity than at the northern plate boundary. Thus, the lithospheric peaks in Fig. 21 along the plate's southern border may be interpreted as older extinct volcanoes ... [The lesser seismic activity along the southern boundary reminds about the analogous behavior of the seismic activity of the African region of the diamond-bearing kimberlites which are likely to be "aborted" volcanic phenomena. See Fig. 19c.] *Additionally, the relative lack of seismic and volcanic activity below* $30°\,S$ *permits longer magnetic-domain lines to be formed from the persistent and undisturbed presence of the Earth's main* $\boldsymbol{B}$ *...* "

Quinn (2014, p. 33) illustrates as follows this whole morphological feature.

"*The Indonesia/Malaysia lithospheric plateau in Fig. 21 is extremely large and does not appear to have been previously identified*. [This is the aforementioned Banda Sea region that according to the rationale of the present study is interpreted in a substantially different way.] *It is the large pink feature in the northern part of the volcanic ring. It begins to rise sharply from the lithospheric basement of* $22\,km$ *depth and reaches near the* WGS-84 *ellipsoid surface over a broad geographic range that extends from the eastern Indian Ocean, beneath Malaysia and Indonesia, and into the South China Sea. It continues on beneath the Sulu Sea and the Philippine Islands, and terminates beneath the Philippine Sea. The plateau is* $3290\,km$ *long in the East-West direction, while its width at its widest point near* $110°E$ *longitude is* $\sim 1040\,km$. *Diagonally, from the southwest to the northeast, it is* $4164\,km$ *long. The base of the plateau is approximately* $4935\,km$ *long in the east-west direction, while its base width near* $115°E$ *longitude is* $3000\,km$. *So, diagonally, from the southwest to the northeast, the plateau's base is approximately* $5775\,km$ *long. The center of this plateau is located at about (*$9°N, 111°E$*).*

Fig. 27 indicates that there are two major hotspots that are extending the Malaysian/Indonesian plateau's length by generating volcanic emissions from opposite ends of the plateau. According to Fig. 27, one hotspot near the plateau's southwest end is the blue region located at ($95°E, 1°N$*), while the other hotspot near the plateau's northeast end is the blue region located at (*$122°E, 12°N$*). The low magnetization of these hotspots indicates that they are still quite active. So, presumably the plateau is still growing. Overall, this shallow lithospheric plateau occupies most of the Philippine tectonic plate seen in the northwest corner of Fig. 22 just above the Austral-Indian plate. Both plates are defined by the seismicity of the region.*"

The concern is therefore about assessing whether Australia can be considered to be a former part of Pangæa - i.e., according to *WMT,* a large region inside a megasyncline was disrupted while sliding on the slopes of superswells - or rather it is a later addition derived from a huge astrobleme.

The Quinn's (2012, 2014) argument - as he correctly stresses (see the quotation above) - is speculative. Maybe, as he comments, it will be possible to validate or deny this hypothesis when *SH*s of higher degree and order are used in the future, and an inversion similar to Quinn's analysis is carried out.

NCGT Journal
New Concepts in Global Tectonics

New Concepts in Global Tectonics Journal
Volume 14, Number 1, January 2026

ISSN number; ISSN 2202-0039

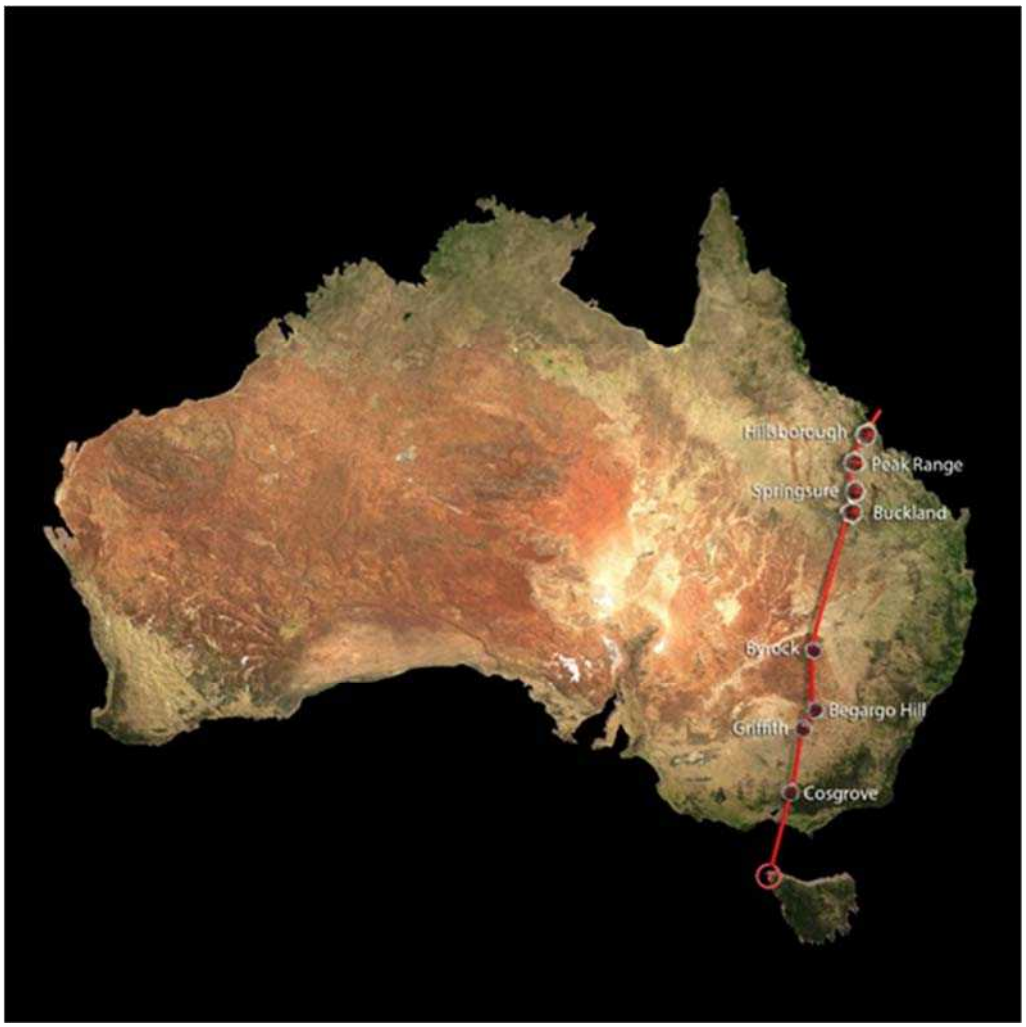

Fig. 24 - The Cosgrove Volcanic Track. Credit: Drew Whitehouse, *NCI National Facility VizLab*. After Ghose (2015a).

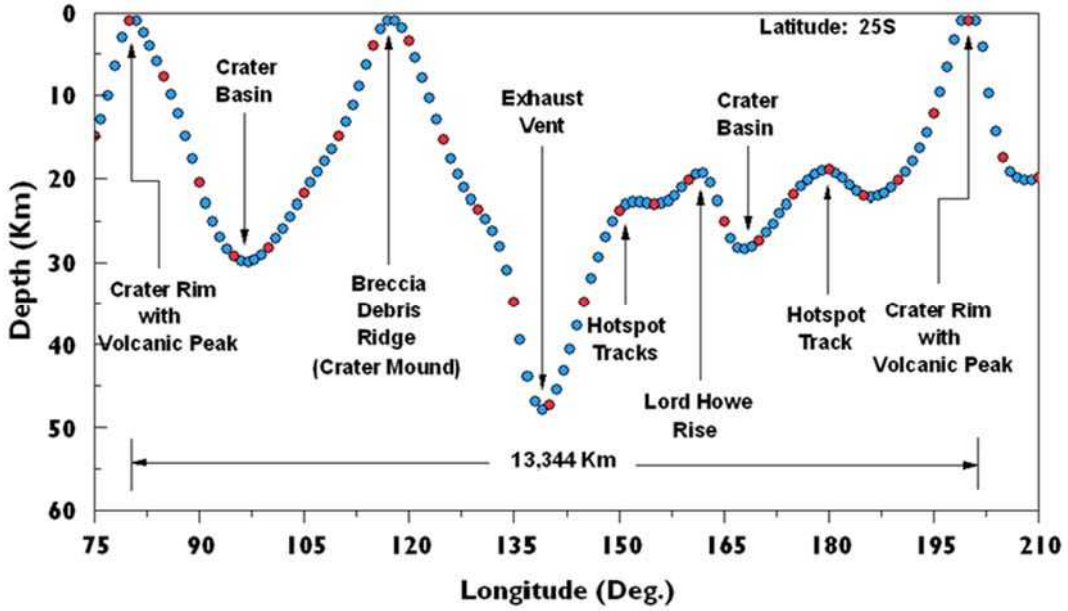

Fig. 25. Magnetic depth profile in the Australian region along latitude $25° S$. The maximum at ~$120°E$ is the bunch of sea-urchin spikes roughly close to Perth. See text. After Quinn (2012).

NCGT Journal
New Concepts in Global Tectonics

New Concepts in Global Tectonics Journal
Volume 14, Number 1, January 2026

ISSN number; ISSN 2202-0039

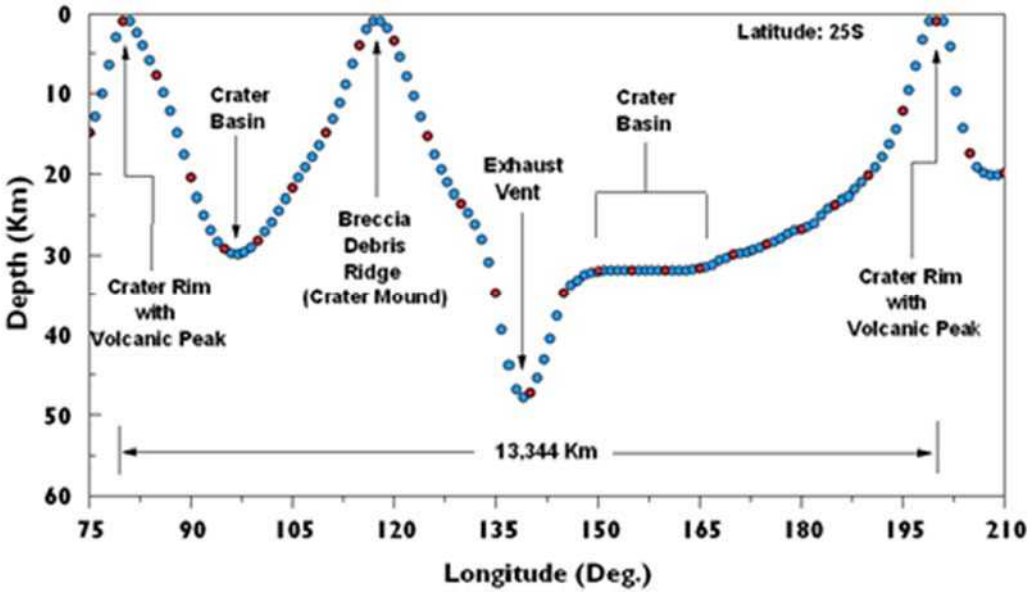

Fig. 26. Magnetic depth profile in the Australian region along latitude $25°\ S$ extrapolated to its state before $80\ Ma$. After Quinn (2012).

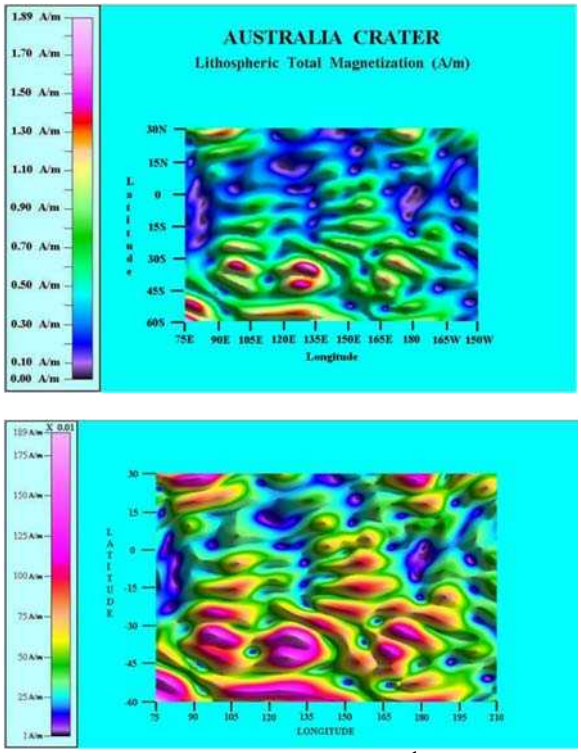

Fig. 27. Total magnetization ($A\,m^{-1} \times 0.01$) in the Australian region. Longitude span $75°E - 150°W$; latitude span $60°S - 30°N$. Two versions are here shown that use different color codes. After Quinn (2012, 2014).

The Bangui anomaly and central Africa

This is one simple case history. Fig. 28 shows a feature similar to the ENE-WSW alignment in Fig. 8. Fig. 29 is a different picture of the geomagnetic anomalies. Fig. 30 shows, indeed, a huge feature being suggestive of an extended bunch of sea-urchin spikes, which is also related to the Cameroon Volcanic Line (*CVL*), including perhaps the possibly related peculiar feature of the Oklo natural reactor.

In fact, several features display two roughly circular blue and red patterns, tangent to each other, envisaging several "double E-eyes". According to the interpretation here proposed, this is a site of conspicuous air-earth currents due to the largely fractured crust. In contrast, according to the volcanic or astrobleme interpretation envisaged by Quinn, these tangent patterns require some *ad hoc* assumption.

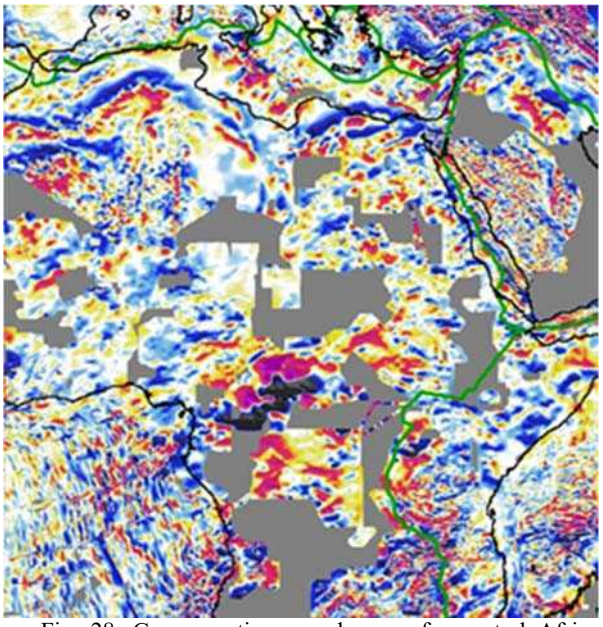

Fig. 28. Geomagnetic anomaly map for central Africa. Longitude span $10°W - 50°E$; latitude span $15°S - 40°N$. Detail of Fig. 6 referring to central Africa. *NOAA* copyright free policy.

Fig. 31 shows the Quinn's total magnetization map of this large region. In general, a larger amount of magnetization is correctly found in the region of this huge anomaly. On the other hand, it displays some regular pattern that is clearly associated to the limited number of terms of the geomagnetic *SHE*. That is, this is the same mathematical effect that is here called "leopard skin" effect (see the Introduction).

NCGT Journal
New Concepts in Global Tectonics
New Concepts in Global Tectonics Journal
Volume 14, Number 1, January 2026
ISSN number; ISSN 2202-0039

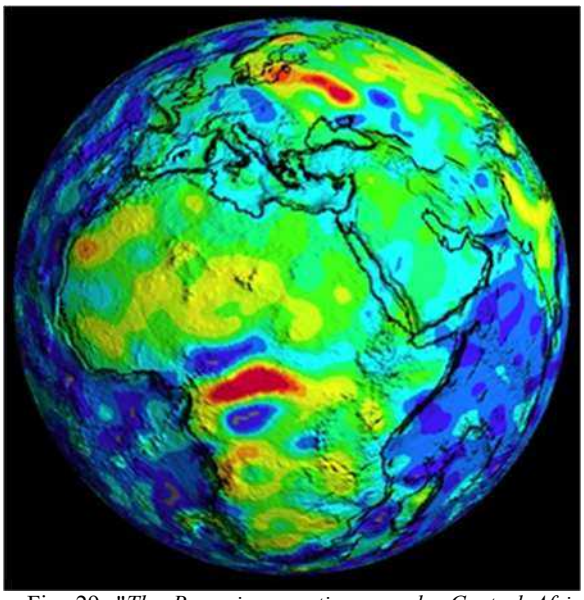

Fig. 29. "*The Bangui magnetic anomaly, Central Africa (nT). Courtesy* NASA, GSFC." Figure and captions after Quinn (2014). *NASA* copyright free policy.

This region of Africa seems to be unique and singular in several respects, including the huge gravity anomaly in Zaïre that is one of the main sources of the tropical storms that cross through the central Atlantic Ocean until the Gulf of Mexico, where they eventually transform into violent hurricanes (see Gregori and Leybourne, 2025j). Therefore, the investigation of these peculiar features is likely to deserve more specific studies and hard thinking concerning other morphological features that look comparably similar to one another.

Quinn (2014) also shows Figs 32 and 33 dealing with two profiles in order to give an estimate of the size of this "impact crater". "*The enormous size of the Bangui Crater is revealed for the first time ...* " (Quinn, 2014, p. 60).

Quinn (2014, p. 54-55) claims that "*contrary to the impression given in Fig. 30, the Bangui crater is elliptical, being* $3928\ km$ *wide in the east-west direction, as can be determined from the profile of Fig. 32, while in the north-south direction from Fig. 30 it appears to be* $5550\ km$*, extending from central Angola to the Mediterranean coast of Libya, between* $15°S - 35°N$*. However, the profile of Fig. 33 suggests that it actually extends farther south to southern Namibia, in which case its length appears to be* $6549\ km$*. Computing an average diameter from these dimensions, using the longer length, yields* $5239\ km$*, which is* 6.5 *times the* $810\ km$ *originally estimated by Girdler et al. (1992). These length and width measurements are taken from mid-rim to mid-rim. The crater has an average depth of* $\sim 40\ km$*, although some isolated spots within the crater basin go much deeper*

Concerning the interpretation which is here proposed, refer to Fig. 28 that shows that the pattern is oriented like the Cameroon Volcanic Line (*CVL*). Hence, no circular pattern has to be expected, in contrast to the requirement of the volcanic or astrobleme hypothesis. Consider also that the leopard skin effect widens a sharp line into an approximate ellipse.

In addition, the astrobleme hypothesis implies an enormous impact that could be related to the "birth" of Africa, i.e., with a significant implication on the origin and evolution of Pangæa. This is a possibility. However, one should explain why an elongated feature, such as the *CVL*, is a remnant signature, rather than some more circular pattern. In any case, this item requires harder thinking and investigation.

The Rio Grande Rise

A more interesting case history deals with the so-called Rio Grande Rise in the middle Atlantic Ocean (Fig. 34) that is located approximately in the range $\sim 28°S - 35°S$ and $\sim 39°W - 28°W$ or $\sim 321°E - 332°E$. The geomagnetic anomaly map (Fig. 35) shows some relevant perturbation corresponding to this Rise. Note the horizontal fracture zones.

One large anomaly, roughly at $\sim 27° - 28°S$ latitude, appears on the western edge of the figure, and it displays a double alignment, with red at its northern border and blue at its southern border. According to the evidence of Fig. 6 and the argument of Fig. 2, lower plot, this envisages an eastward oriented current $\boldsymbol{j}$.

It crosses another oblique (roughly SW-NE oriented) double alignment that appears to start from the lower side of the figure, with *red* at its *southern* border, and *blue* at its *northern* border. This envisages a westward oriented current $\boldsymbol{j}$ (see Fig. 6 and consider the argument of Fig. 2).

That is, a $\boldsymbol{j}$ enters on the western outskirts of the Rio Grande Rise, it flows until crossing the oblique feature, then along it, in SW direction until the southern edge of the figure.

These two anomaly alignments merge into the region of the Rise, roughly corresponding to the western portion of the Rise. Their intersection looks strongly perturbed, in terms of large either red or blue patches (reminding about a similar feature along the *CVL* in Fig. 28). However, in general, some intricate pattern is observed through the whole Rio Grande Rise, consistently with the expectation of a complicated bunch of sea-urchin spikes.

Indeed, also the total magnetization map (Fig. 36) is clearly suggestive of a large bunch of sea-urchin spikes. However, the source-depth map (Fig. 37) shows a curious "double E-eye" pattern, with an impressively very sharp divide between one "E-eye" displaying an incredibly shallow source-depth (practically zero depth) and a very close-by "E-eye" with an incredibly large source-depth ($\sim 50 - 60\ km$). All this is physically unrealistic and it reminds either about some unwanted mathematical drawback, or about some unexpected physical reason that is not yet suitably considered in the interpretation of magnetic source-depth maps.

This curious "double E-eye" feature is here interpreted as evidence of a strong air-earth current that originates a perturbation of the *CHAMP* records. The interpretation given by Quinn (2014) is substantially different. Hence, for completeness sake - and also in order to respect the parenthood of this important finding - the Quinn's interpretation is here mentioned in detail.

NCGT Journal
New Concepts in Global Tectonics

New Concepts in Global Tectonics Journal
Volume 14, Number 1, January 2026

ISSN number; ISSN 2202-0039

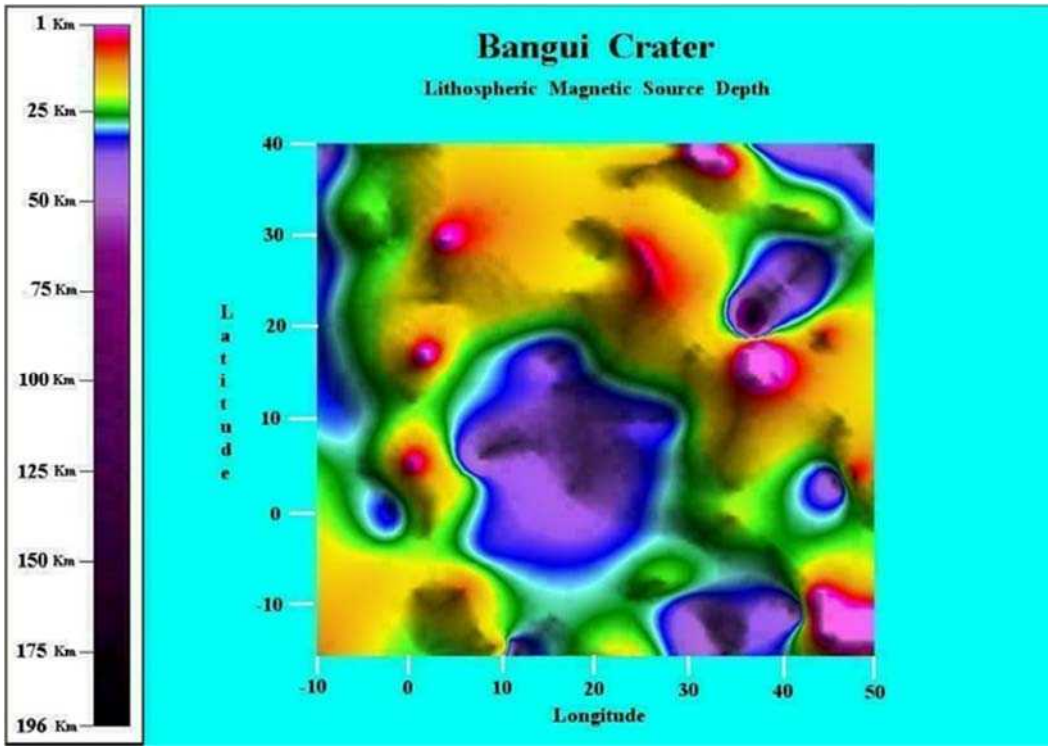

Fig. 30. Quinn's magnetic source-depth map of central Africa aimed to show the pattern associated with the Bangui anomaly, and more generally with the *CVL*. "*The Bangui crater is surrounded by a volcanic rim. An exhaust vent from the meteorite impact resides at the northeast corner on the middle of the Red Sea. Also, a trench runs along the northwest coast of Africa*." Span: Long. $10°W-50°E$; lat. $15°S-40°N$. Figure and captions after Quinn (2014).

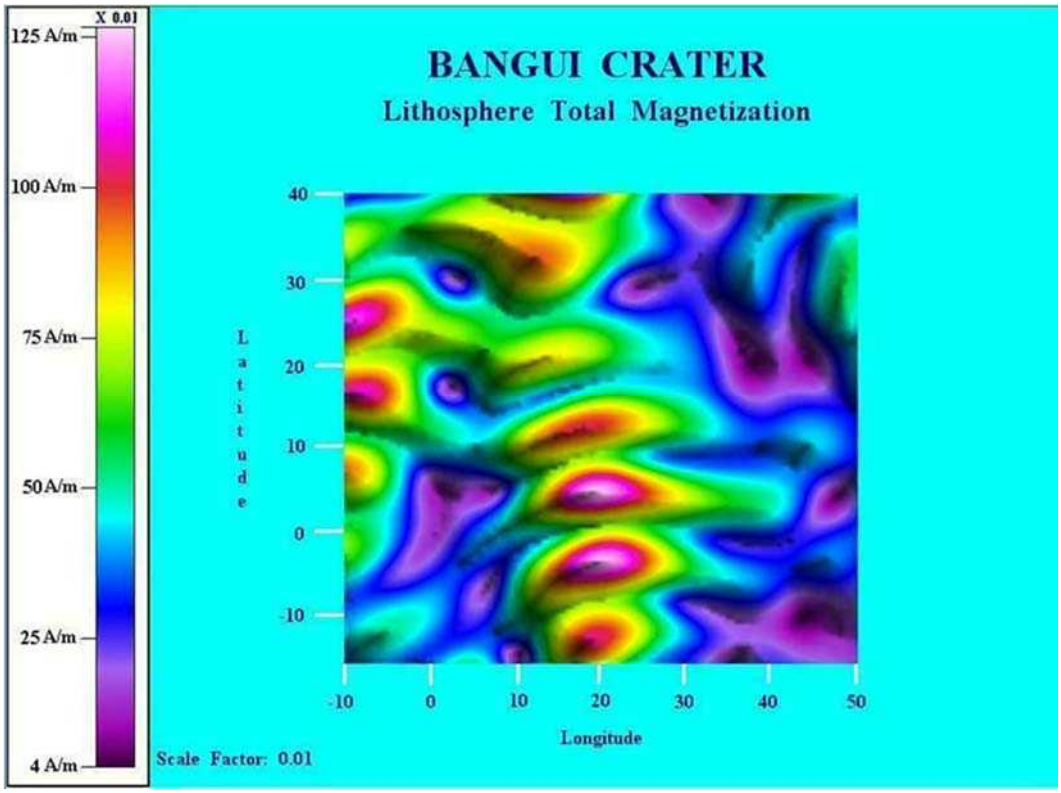

Fig. 31. Quinn's total magnetization map of central Africa (see Fig. 30). "*The crater rim exhibits undisturbed East-West magnetic domains indicating that the crater is old, while extremely low magnetization surrounds the crater, indicating high heatflow and extensive volcanism*." Span: long. $10°W-50°E$; lat. $15°S-40°N$. Figure and captions after Quinn (2014).

NCGT Journal
New Concepts in Global Tectonics

New Concepts in Global Tectonics Journal
Volume 14, Number 1, January 2026

ISSN number; ISSN 2202-0039

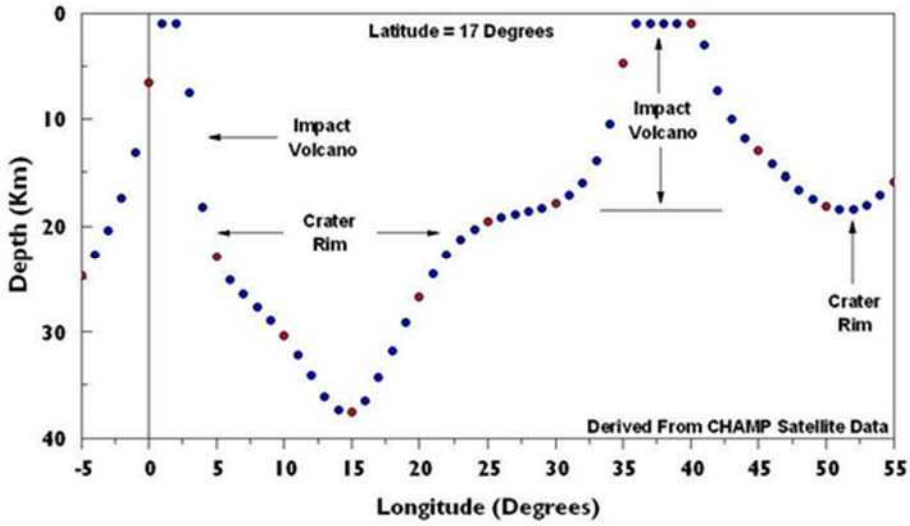

Fig. 32. Bangui crater magnetic source-depth profile along $17°N$ latitude (km). After Quinn (2014).

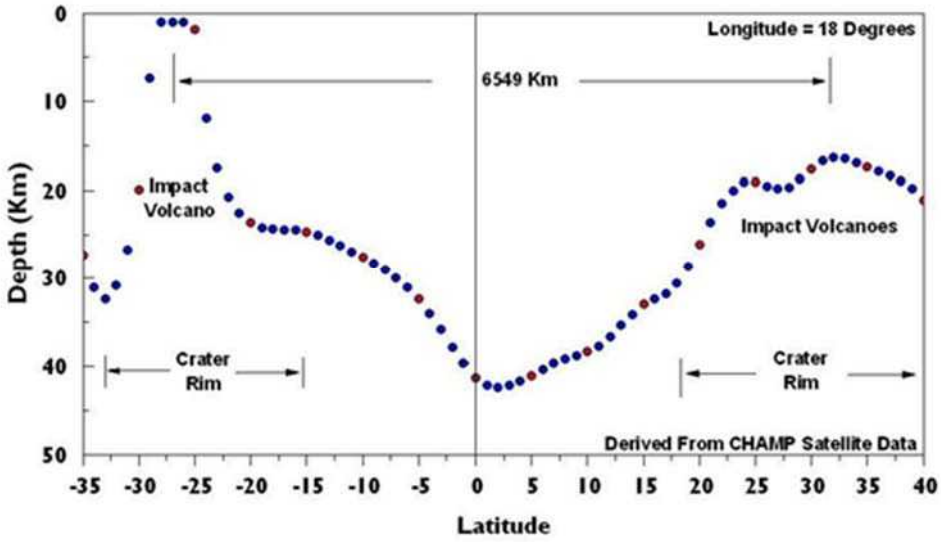

Fig. 33. Bangui crater magnetic source-depth profile along $18°E$ longitude (km). After Quinn (2014).

Quinn (2014, p. 46-49) states that "*Fig. 37 presents an image of a broad lithospheric plateau with an isolated near-surface igneous intrusion (pink) centered at (*$329°E, 29°S$*) which coincides with the Rio Grande Rise. The Sao Paulo Plateau has no equivalent intrusion associated with it. Instead, Fig. 37 shows that the Sao Paulo Plateau is just part of the Rio Grande Rise so that together they form just one* LIP. *The igneous intrusion corresponding to the Rio Grande Rise is approximately* $1\ km$ *deep, which is consistent with the bathymetry. The* LIP *corresponding to the Sao Paulo Plateau is ~*$12\ km$ *deep. This suggests that there may be a significant amount of non-magnetic sediment closer to Brazil overlaying the* LIP. *Drilling can sort this out. Directly to the northeast of the Rio Grande lithospheric plateau (igneous intrusion) there is a drip site at (*$331°E, 27°S$*). Directly beneath this location is a hotspot that is quite prominently seen in Fig. 36.*

The igneous intrusion in Fig. 37 is approximately $370\ km$ *wide in the east-west direction and ~*$400\ km$ *long in the north-south direction. It is straddled by two fracture zones. The northern fracture zone along* $26°S$ *has a length exceeding* $2530\ km$*, and is* $40\ km$ *to* $50\ km$ *wide. The southern fracture zone near* $33°S$ *is at least* $750\ km$ *long and approximately* $35\ km$ *wide. A possible underlying picture is that a pair of Bénard-Marangoni magma convection cells buried deep in the asthenosphere which are being heated from the mantle below.* [The Bénard-Marangoni convection, or thermo-capillary convection, is a mass transfer at the interface between two fluids, caused by surface tension gradient originated by temperature difference. The same effect - when the surface tension gradient is originated by any cause, also other than a thermal dependence - is called Marangoni effect, or Gibbs-Marangoni effect.]

NCGT Journal
New Concepts in Global Tectonics

New Concepts in Global Tectonics Journal
Volume 14, Number 1, January 2026

ISSN number; ISSN 2202-0039

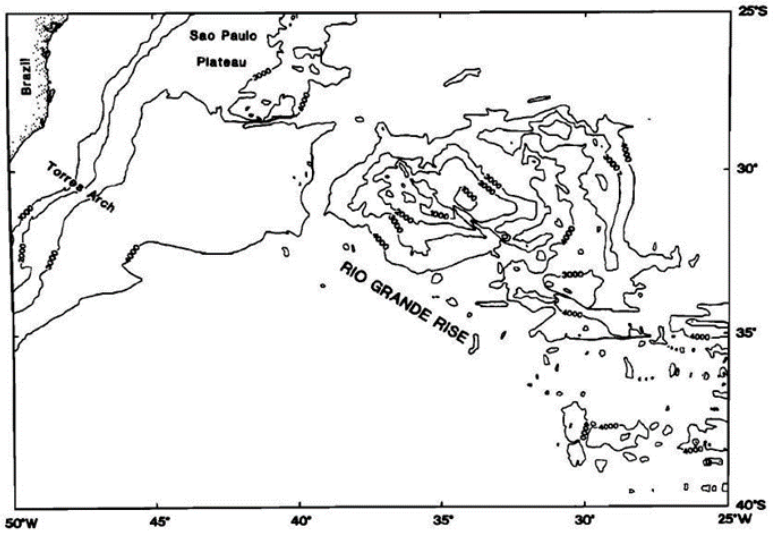

Fig. 34. Bathymetry (m) of the Rio Grande Rise and Sao Paulo Plateau in the middle Atlantic Ocean. Note that the subsequent Figs 35 through 37 deal with the longitude span that, in the present figure, is $45°W-20°W$, while their latitude span is $35°S-20°S$. After O'Connor and Duncan (1990). Also in Quinn (2014). Ask AGU for permission.

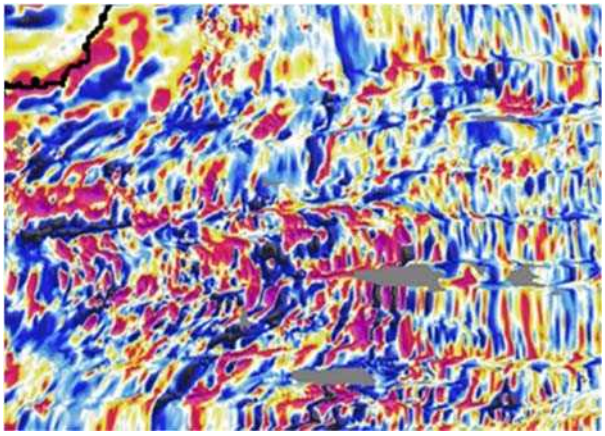

Fig. 35. Geomagnetic anomaly map for the Rio Grande Rise region. Longitude span $315°E-340°E$; latitude span $35°S-20°S$. Detail of Fig. 6. *NOAA* copyright free policy.

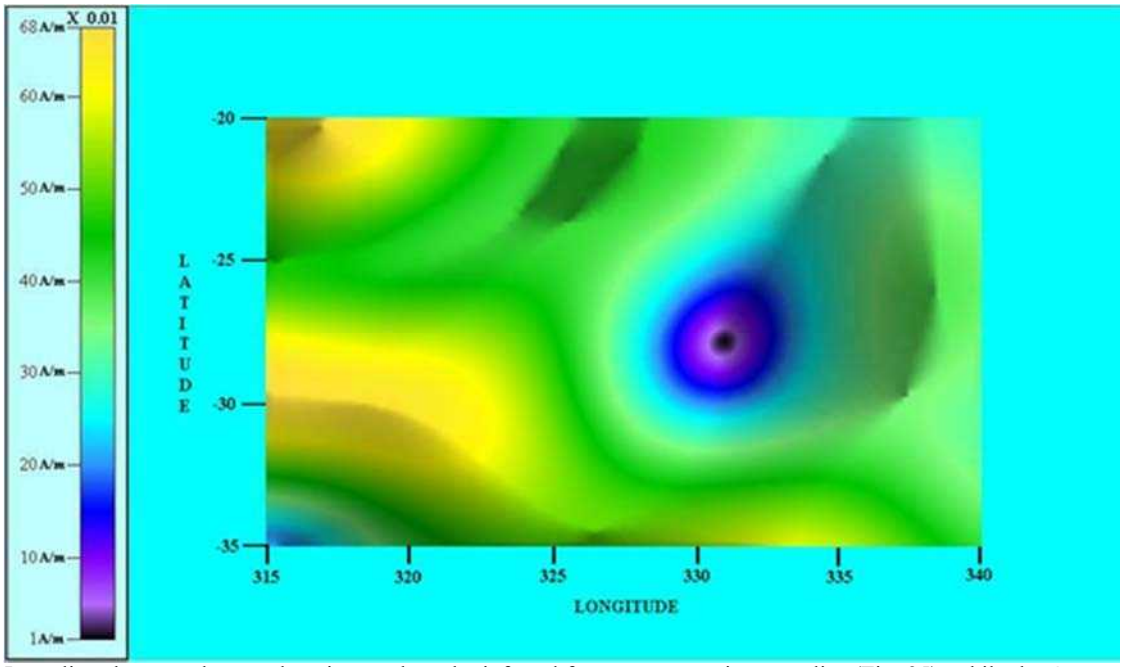

Fig. 36. Quinn's total magnetization map ($A\ m^{-1}\times 0.01$) for the Rio Grande Rise and Sao Paulo Plateau. "*Note that the center of the hotspot does not coincide with the center of the Rio Grande Plateau. Plate tectonic movement of the Plateau can account for this*." Longitude span $315°E-340°E$; latitude span $35°S-20°S$.

In reality, the exact hotspot location ought to be inferred from geomagnetic anomalies (Fig. 35), while the Ocean floor drift can be explained by several geodynamic models, including *WMT*, other than plate tectonics. Figure and captions after Quinn (2014).

NCGT Journal
New Concepts in Global Tectonics

New Concepts in Global Tectonics Journal
Volume 14, Number 1, January 2026

ISSN number; ISSN 2202-0039

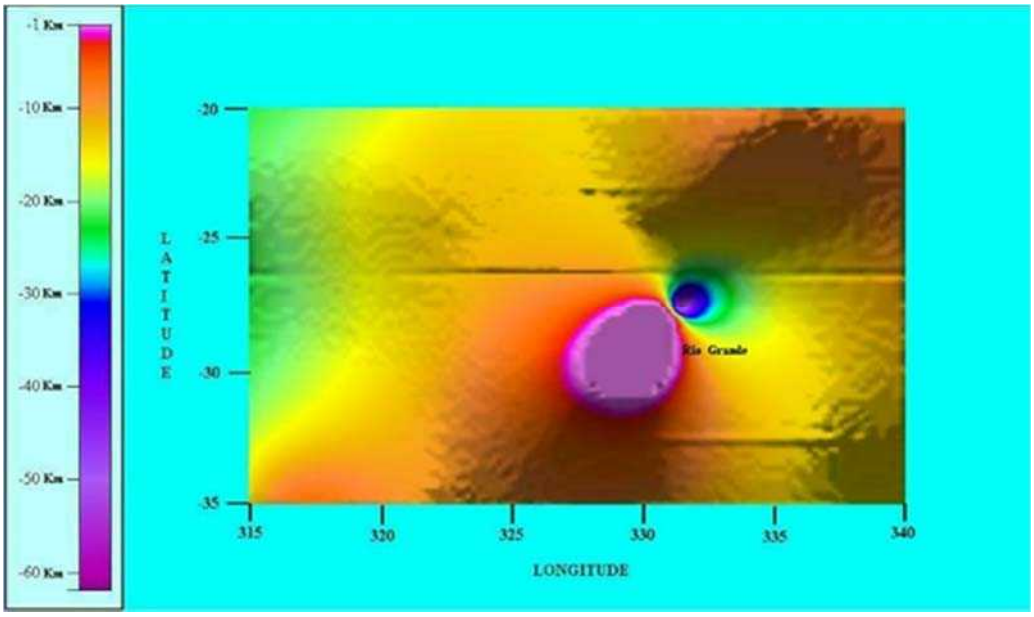

Fig. 37. Quinn's magnetic source-depth map for the Rio Grande Rise and Sao Paulo Plateau. "*The Rio Grande Plateau which lies between two fracture zones is the pink feature."* Longitude span *315°E – 340°E*; latitude span *35°S – 20°S. The Sao Paulo Plateau is the yellow region to the northwest. Note the sharp rise of the Rio Grande Plateau from ~ 7 km depth to between* 1 *and* 2 km *all around the plateau.*" Figure and captions after Quinn (2014).

Two, $225\ km$ *diameter, cylindrical cells are oriented length-wise in the east-west direction. The cell diameter is half the distance between the two fracture zones. The cylindrical cells rotate in opposite directions (i.e., the northern one toward the north, the southern one toward the south) such that along the center line between the two cells, upwelling occurs. Downwelling occurs at the two fracture zones. When a weak spot appears in the Earth's crust along the center line, a hotspot is formed and magma is permitted to flow toward the ocean surface where it becomes an igneous intrusion (i.e., a plume eruption). The magma tends to flow away from the intrusion in all directions over the course of hundreds of thousands to millions of years involving several eruptions. An igneous-province/lithospheric-plateau builds-up, which in this case adds to that which was previously created by the Tristan hotspot around the time of continental separation. The combined result can be seen in Fig. 37 as the broad yellow/orange colored* LIP. *There is a hint of a third fracture zone at (*$330°E, 23°S$*). This fracture zone is approximately* $30\ km$ *wide.*

Fig. 36 displays a pronounced region of low magnetization (blue with a black center) that is clearly interpreted as a high heatflow hotspot. Thus, the Rio Grande lithospheric plateau is still active. [This conclusion is shared also by the interpretation which is here given according to *WMT*, as the *MAR* is on top of a superswell (see Gregori et al., 2025a) and not far from an edge of the tetrahedron (see Gregori and Leybourne, 2021).] *The hotspot is isolated from other hotspot and tectonic activity in the Atlantic Ocean, which makes it a good study site. It presumably generated the lithospheric intrusion in Fig. 37. Both the intrusion and the hotspot, comparatively speaking, appear to be relatively recent additions to the lithosphere and do not seem to be part of the original separation of South America from Africa. Nor does this hotspot appear to have any connection to the Tristan hotspot.* [This statement is shared also by the interpretation that is here given.]

The presumption is that the isolated low-magnetization feature in Fig. 36 is due to high heat flow. Thus, it becomes very easy to see how the heat dissipates as one moves radially away from the hotspot's center. The hotspot has a radially diminishing effect on the surrounding magnetization up to $700\ km$ *or* $800\ km$ *from the hotspot center where the magnetization is only* $0.01\ A\ m^{-1}$*. The regional magnetization is rather low, with a maximum of only* $0.68\ A\ m^{-1}$*. This suggests that the entire region is still subject to a moderate degree of heatflow."*

The hesitancy or doubt - concerning this interpretation in terms of a hyper-volcano (or also of an astrobleme) - is basically related to the persistent, very frequent, morphological feature of the very close tangency of two approximately circular red and blue features. Indeed, this appears quite reasonable according to the air-earth interpretation, as this is what has to be expected. In contrast, either the volcano or the astrobleme model require some *ad hoc* assumption.

In any case, as mentioned by Quinn, an observational check will be perhaps carried out whenever suitable deep-drilling samples will be available. On the other hand, upon considering the very frequent occurrence of this curious morphology of "double E-eye" feature, every kind of mechanism, which is eventually guessed, must be a frequent occurrence, rather than the consequence of some peculiar and rare effect. In this respect, air-earth currents can be supposed to be a widespread phenomenon, while *a priori* it seems intuitively less likely to justify other mechanisms.

Therefore, one seemingly reasonable physical explanation is the presence of a conspicuous flow of air-earth currents associated to a huge corona effect on top a bunch of sea-urchin spikes.

That is, the $\boldsymbol{B}$ recorded by *CHAMP* is not curl-free. Differently stated, a large $\boldsymbol{j}$ exists. It flows upward for some huge extension underneath the *CHAMP*'s orbit, raising from the areas of intense soil exhalation mainly in region of

New Concepts in Global Tectonics Journal
Volume 14, Number 1, January 2026
ISSN number; ISSN 2202-0039

intense crustal fracturing. In this way, this can explain the aforementioned very sharp separation between the two "E-eyes". Moreover, this $\boldsymbol{j}$ is confined inside an ideal conductor that crosses through the atmosphere while it keeps self-collimated due to the Cowling dynamo (Gregori et al., 2025d, and Gregori and Leybourne, 2025g).

The mechanism is highlighted in the cartoon of Fig. 2. Note the similarity of the geometry of the circuits in Figs 1 and 2, although a "double eye" feature in Fig. 1 is associated with a linear DC circuit underground, while a "double E-eye" in Fig. 2 is associated with a linear conductor underground, where some $\boldsymbol{j}$ must flow, eventually due to e.m. induction from an external source. This is the reason to call "E-eye" (for "external") to be distinguished from the internal origin "eye".

This phenomenon, which is guessed to be responsible for the "double E-eye" feature, will be briefly called in the following "*air-earth current instability*".

Note that this $\boldsymbol{j}$, which seems to be closely correlated with the hotspot or bunch of sea-urchin spikes, is observed even if ocean water represents an efficient e.m. screen. Hence, the effect is likely to be even much more evident when a hotpot occurs on emerged land.

If this interpretation is correct, this seems to be, maybe, the best (or, maybe, the unique available) record ever carried out of the effect of a huge amount of air-earth currents across Earth's surface, and detected at a satellite orbit. Other attempts to measure air-earth currents are a classical topic for old books on geomagnetism, but they appear even much more complicated and problematic. The advantage of satellite monitoring relies on the possibility to detect an effect integrated over some large area that can hardly be assessed by local records at Earth's surface.

In any case, the assumption - of a negligible disturbance originated by air-earth currents in the computation of *SHE* models for the geomagnetic potential - is basically a "generally agreed" working hypothesis. This working hypothesis appeared very reasonable to Gauss, but later it was never critically checked and analyzed.

The interpretation that is here proposed is shown in the following to be effectively confirmed by other several evidences in other oceanic regions. This is the main focus of the following discussion. Note that, if the interpretation here proposed is correct, this Quinn's finding is perhaps the most important and innovative result of the last two centuries in the interpretation of geomagnetic records.

The Arctic cap

It is convenient to refer to the polar caps, where all features suffer by large deformations when displayed on other cartographic projections (Mercator's or similar). Figs 38, 39 and 40 refer to the Arctic region.

The most expressive map seems to be Fig. 40. Different "double E-eye" features are observed. The largest one at longitude ~0° approximately coincides with the Svalbard region. This is on the prolongation of the *MAR* that is certainly the site of intense sea-urchin spikes (see Gregori, 1993).

The smaller "double E-eye" located roughly at longitude $\sim 70°W$ and latitude $\sim 72°N$ is close to the Hudson Bay. The lesser feature at the same longitude and slightly northward could be associated with a "volcano" underneath Greenland, according to several indirect evidences that cannot be here reviewed, and are associated with the edge of the tetrahedron conductor that runs from the Chile Triple Junction (*CTJ*) through the geographic North Pole (Gregori and Leybourne, 2021).

The huge red/pink pattern at $\sim 170°W$ and $\sim 70°N$ coincides with the region of the Bering Straits, which is located at $\sim 170°W$. This region is influenced by the island arc process of the Eurasian boundary, due to the effect of the loading tide and the Pekeris force (see above). Hence, it is reasonable to expect a comparably thin lithosphere.

Note, however, east of this large pink pattern, the sharp red/yellow/green/blue transition: a guess is that this can be correlated with the intricate and poorly understood tectonism of eastern Siberia, including the Baikal Lake - which, maybe, is associated with the edge of the tetrahedron conductor that runs from the Australian Antarctic Discordance (*AAD*) through the geographic North Pole.

In fact, the Baikal Lake is another continental rift lake and seems to be the result of a violent uplift originated by a plugged *MOR* (see Gregori and Leybourne, 2021). This may support the Leybourne hypothesis for tectonic modulation of climate in that Baikal Lake is a "*cryogenic pump*" for climate control. That is, it may modulate the Pacific Decadal Oscillation (*PDO*), a $36\ year$ long term climate teleconnection between high atmospheric pressure node over Lake Baikal and the Aleutian Island low pressure cell. The Baikal Lake is a unique, mysterious and fascinating case history of geomorphology. Etymologically it means, in Mongolian, "*the Nature Lake*" (Murphy, 2007).

The sharp intense "double E-eye" at $\sim 155°E$ and $\sim 73°N$ is centered in the Arctic Ocean, approximately corresponding to the New Siberian Islands between the Laptev Sea and the East Siberian Sea, north of the Sakha (Yakutia) Republic.

The "double E-eye" at $\sim 80°E$ and $\sim 75°N$ is located roughly in the Kara Sea. Note, however, the contrasted pattern in this wide region. In fact, the aforementioned intense blue/red "eye" located in the Svalbard region, is followed, eastward, by the intense pink/red/blue pattern of the Kara Sea region, and also by a comparably fainter blue/red pattern that is roughly located underneath Severnaya Zemlya.

In any case, upon reconsidering Fig. 37, regions of contrast with perturbed geomagnetic anomalies are easily recognized, denoting and intense role of endogenous e.m. effects through several sea-urchin spikes. This is consistent with the several evidences envisaging ongoing increasing release of endogenous heat from the whole northern polar cap. This is also consistent with several indirect evidences that cannot be here reviewed. The present increasing trend of endogenous heat release under the northern polar ice cap is a major cause of the ongoing global climate change. See Gregori and Leybourne (2021).

A better detailed understanding is likely to be possible whenever the map of sea-urchin spikes is available (see Gregori et al., 2025a).

NCGT Journal
New Concepts in Global Tectonics

New Concepts in Global Tectonics Journal
Volume 14, Number 1, January 2026

ISSN number; ISSN 2202-0039

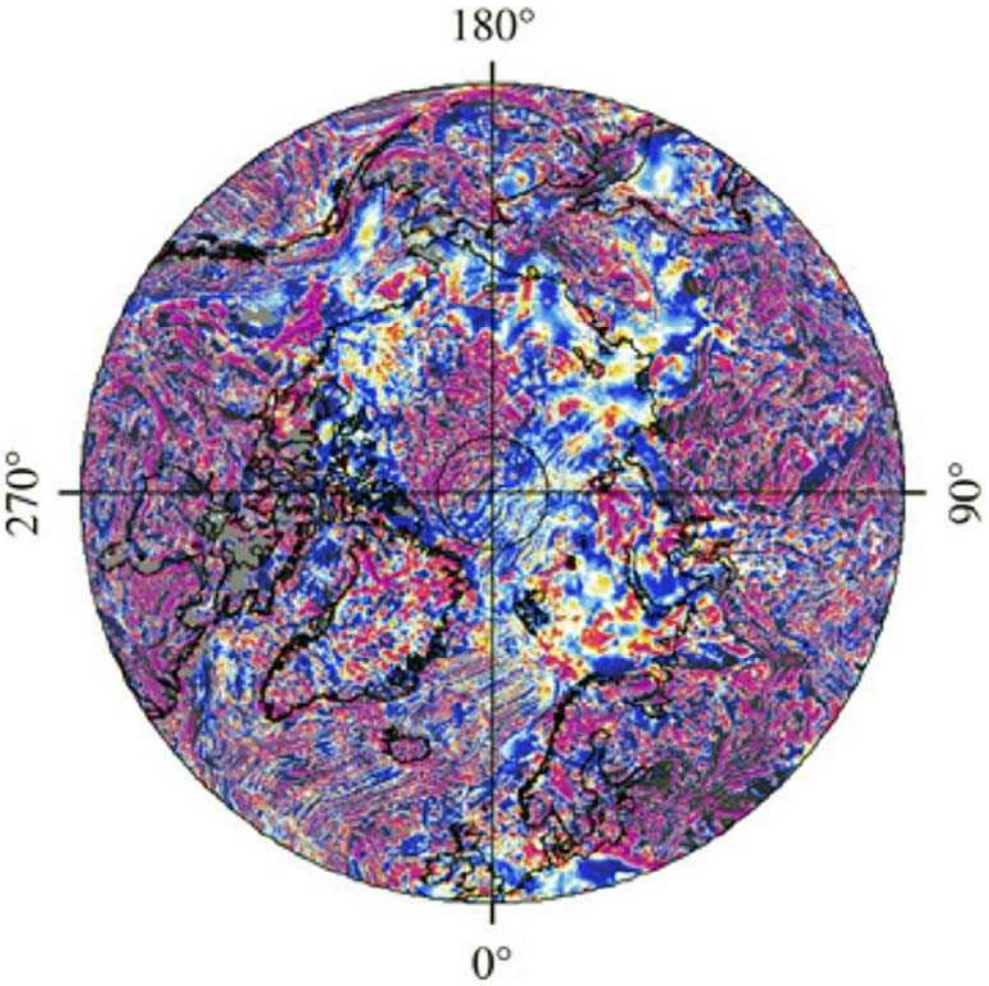

Fig. 38. Geomagnetic anomaly map for Arctic polar cap. Latitude span $70°N-90°N$. Detail of Fig. 6. *NOAA* copyright free policy.

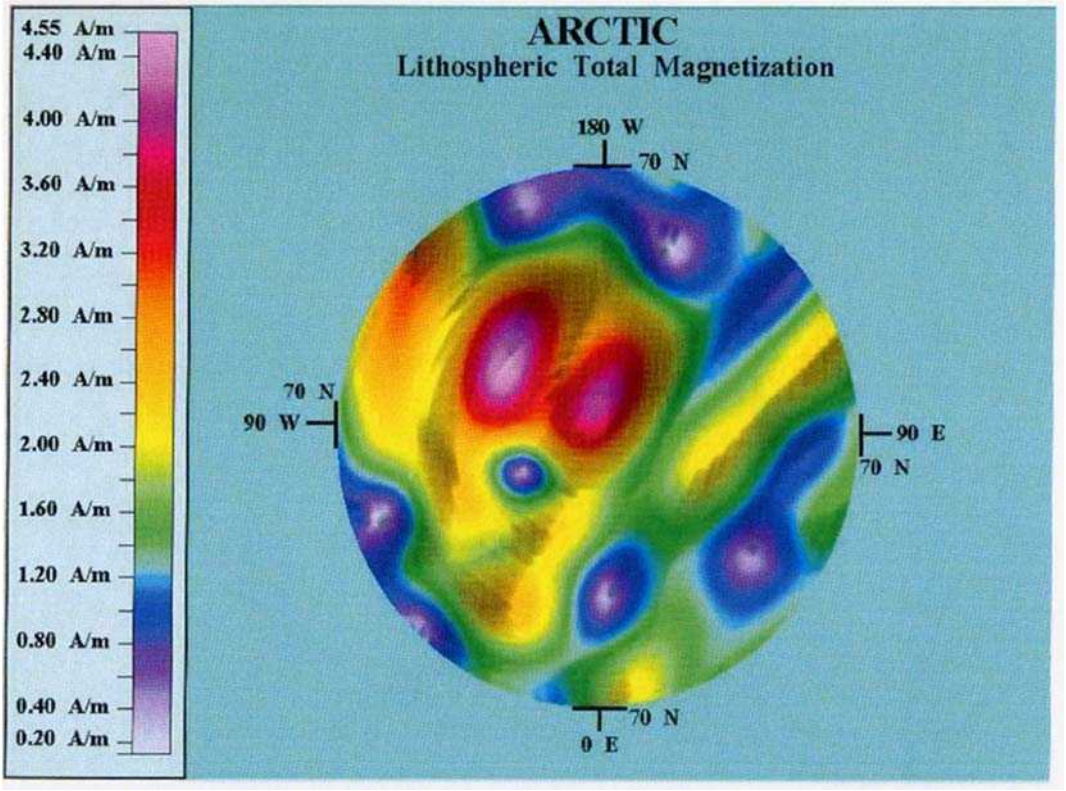

Fig. 39. Quinn's total magnetization map ($A\,m^{-1}$) for the Arctic polar cap. Latitude span $70°N-90°N$. See text. After Quinn (2014).

NCGT Journal
New Concepts in Global Tectonics

New Concepts in Global Tectonics Journal
Volume 14, Number 1, January 2026

ISSN number; ISSN 2202-0039

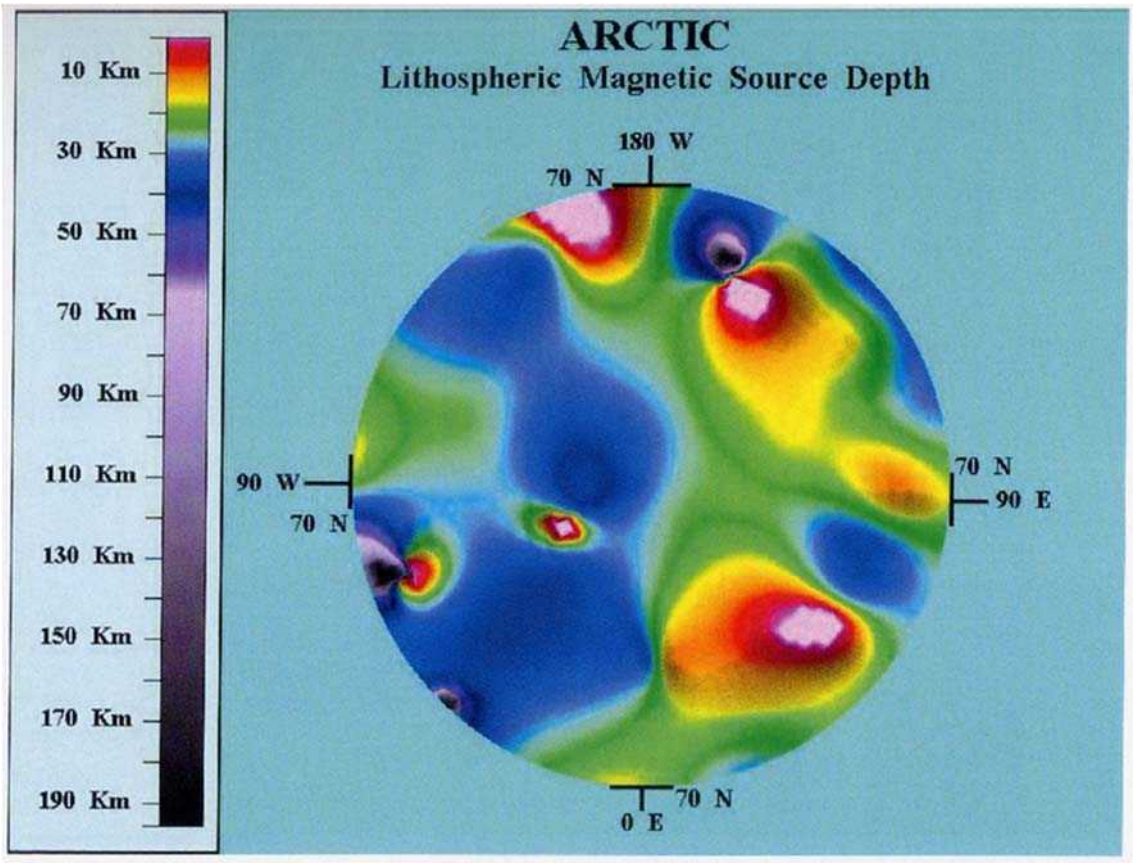

Fig. 40. Quinn's Magnetic source-depth (km) for the Arctic polar cap. Latitude span $70°N - 90°N$. See text. After Quinn (2014).

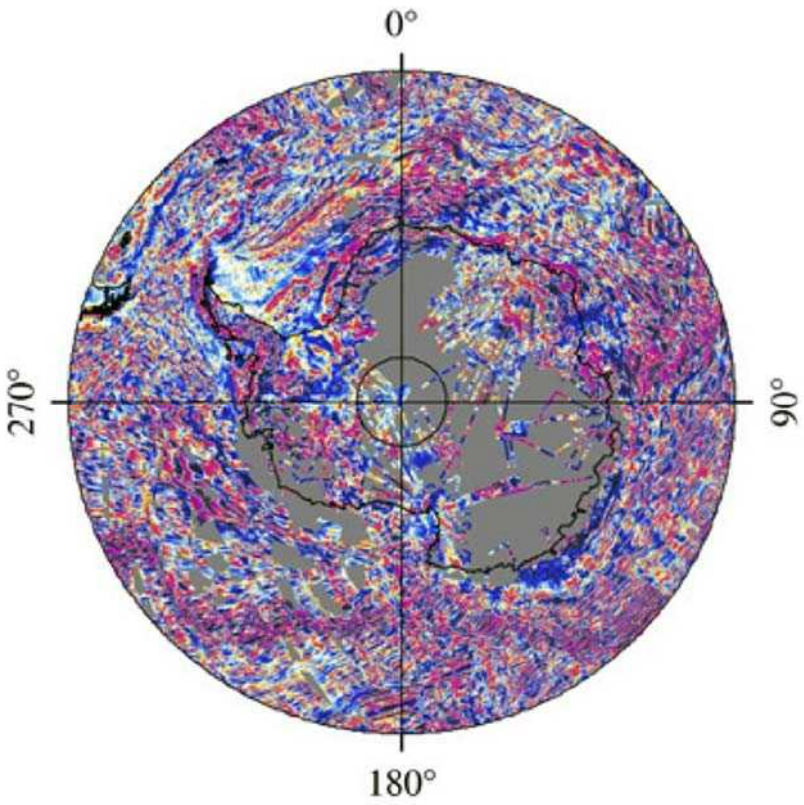

Fig. 41. Geomagnetic anomaly map for Antarctic polar cap. Latitude span $70°S - 90°S$. Detail of Fig. 6. *NOAA* copyright free policy.

NCGT Journal
New Concepts in Global Tectonics

New Concepts in Global Tectonics Journal
Volume 14, Number 1, January 2026

ISSN number; ISSN 2202-0039

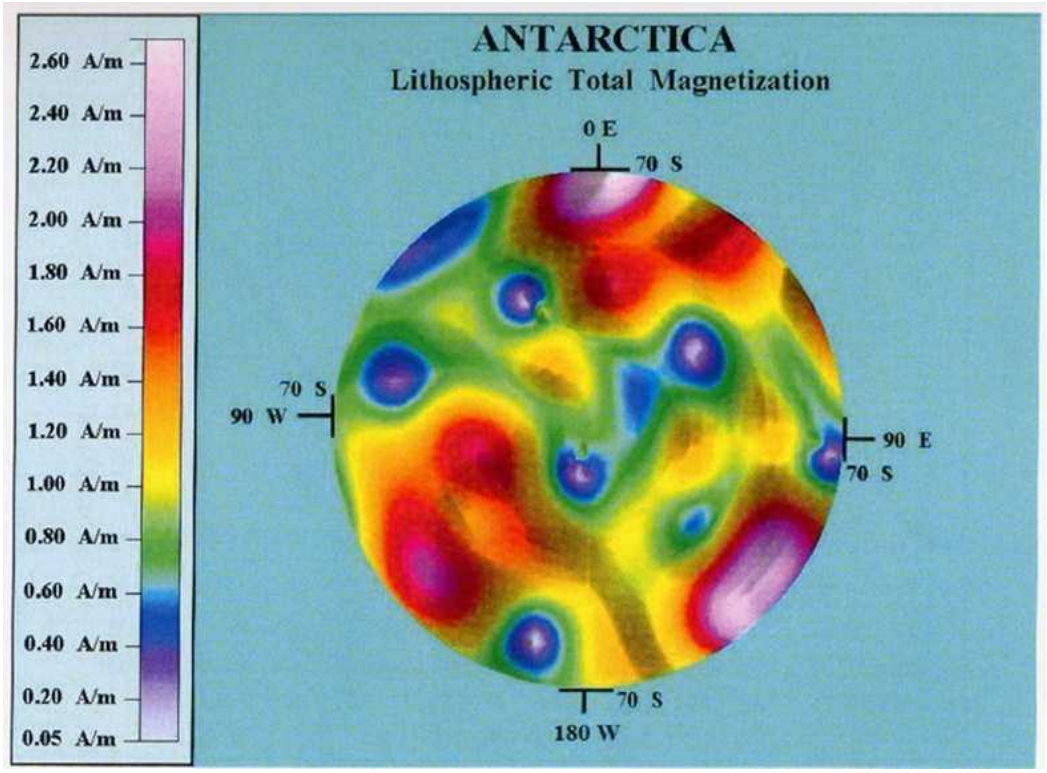

Fig . 42 . Quinn 's total magnetizatio n map ($A\ m^{-1}$) for the Antarctic polar cap. Latitude span $70\ °S - 90\ °S$. See text. After Quinn (2014).

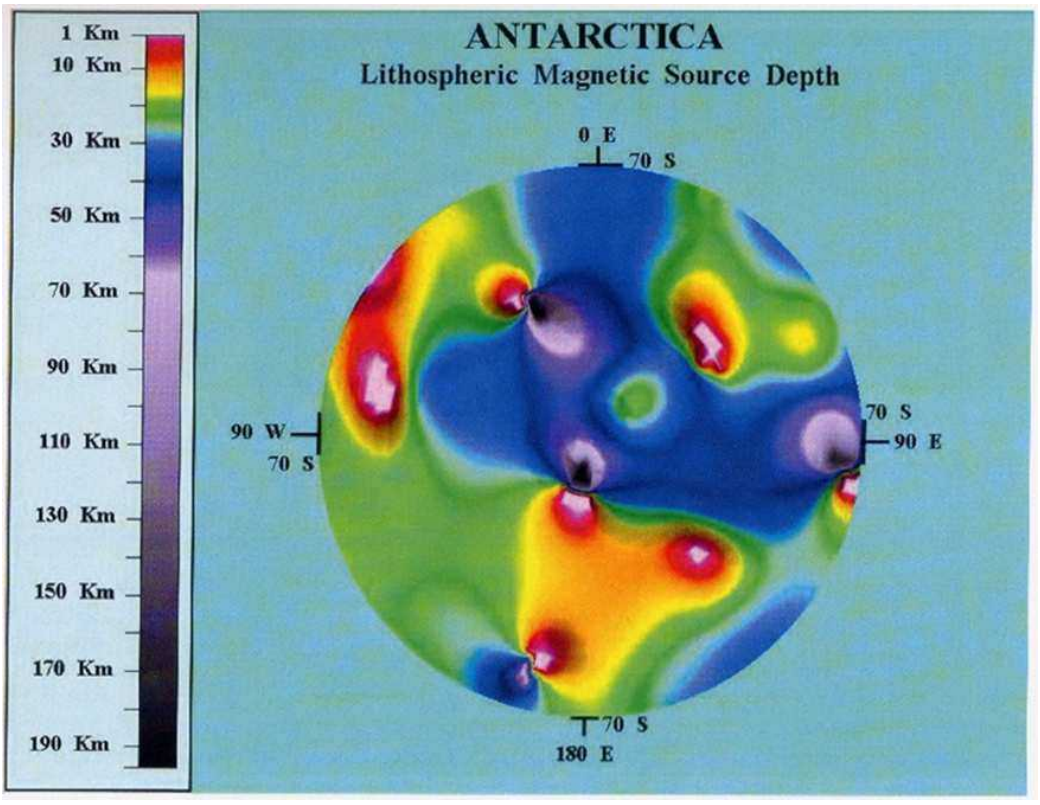

Fig. 43. Quinn's Magnetic source-depth (km) for the Antarctic polar cap. Latitude span $70°S - 90°S$. See text. After Quinn (2014).

NCGT Journal
New Concepts in Global Tectonics

New Concepts in Global Tectonics Journal
Volume 14, Number 1, January 2026

ISSN number; ISSN 2202-0039

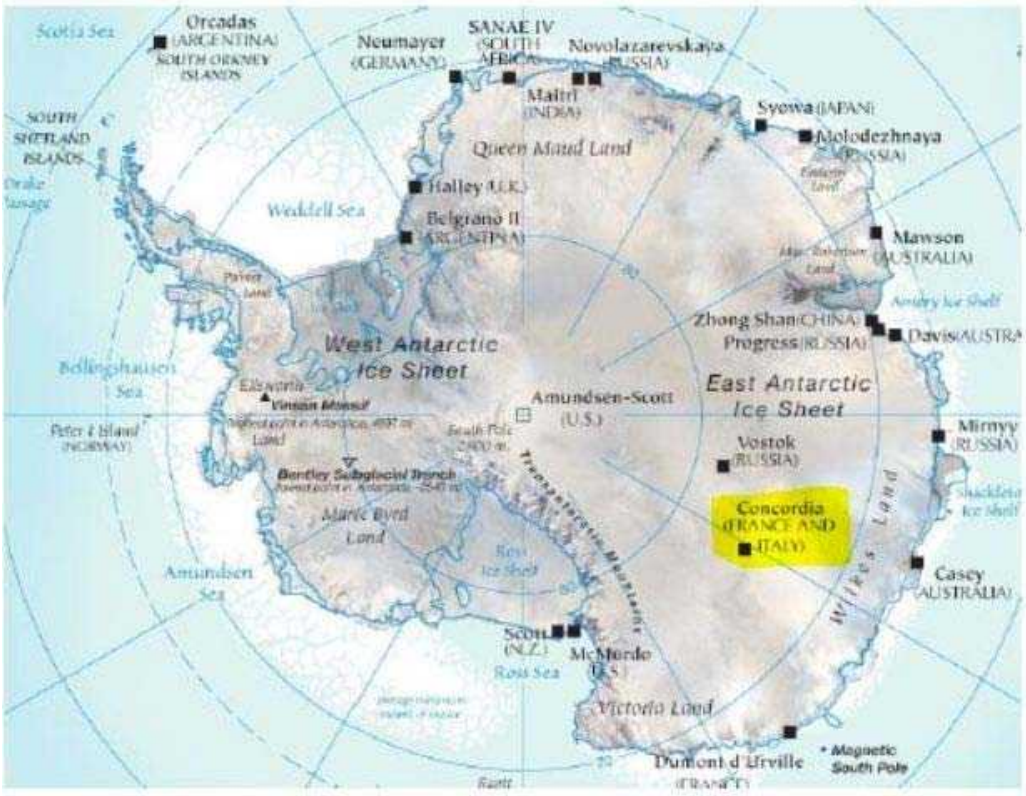

Fig. 44. Map of Antarctica. After *Honora* (2013). *ESA* copyright free policy.

The Antarctic cap

Figs 41, 42 and 43 refer to the Antarctic polar cap, while Fig. 44 is aimed to show toponyms.

The most expressive map seems to be Fig. 43. Different "double E-eye" features are observed. The large pattern at $\sim 80° - 90°W$ coincides with the Antarctic Peninsula. The huge triangular pattern close to $180°E$ coincides with the Transantarctic Mountains and the Ross Sea sector. The three remaining lesser "double E-eye" features are associated with no seemingly known structures, representing therefore a first discovery exploited by Quinn's inversion. Fig. 44 helps to associate toponym and feature. In any case, no simple relationship seems to be found with the bedrock topography (see Fig. 45).

The south-western Pacific Ocean

Quinn (2014) implements a detailed analysis of some oceanic areas. Begin to consider the case history of a large region in the south-western Pacific Ocean (Figs 46, 47 and 48). The magnetic anomaly map displays the well-known highly perturbed pattern, while total magnetization and source-depth maps show several features associated with hotspots, i.e., bunches of sea-urchin spikes. Several "double E-eye" patterns are recognized, which are associated with different oceanic islands.

However, several details are lost, due to the large size of these mapped regions, where a hotspot is just a comparably tiny pattern that can hardly be represented by the order and degree terms of the *SH*s used by Quinn.

In any case, it appears that, compared to source-depth maps, the total magnetization maps display a comparatively coarser spatial resolution. The total magnetization maps show no drawback by air-earth instability. In contrast, source-depth maps, owing to their sensitivity to this instability, are much better suited to pinpoint hotspots.

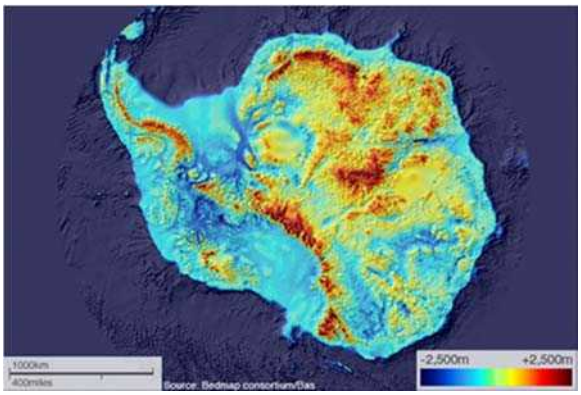

Fig. 45 - *"The digital map (*BEDMAP-2*) of the bedrock under the Antarctic ice sheet. (Image:* BEDMAP Consortium/BAS*)."* Figure and captions after *Anonymous* (2011l). With kind permission of the *British Antarctic Survey*.

The north-western central Pacific Ocean

Similar conclusions appear from the case history of a nearby region in north-western central Pacific Ocean (Figs 49, 50 and 51). The detail through the Marianas Trench is shown by the profile at $20°N$ (Fig. 52). Note the oscillation at $\sim 155°E$, associated to the Maug Islands, a group of three small uninhabited islands in the Marianas archipelago. This oscillation shows how close in Fig. 51 the two tangent approximately circular features of the "double E-eye" are displayed.

NCGT Journal
New Concepts in Global Tectonics

New Concepts in Global Tectonics Journal
Volume 14, Number 1, January 2026

ISSN number; ISSN 2202-0039

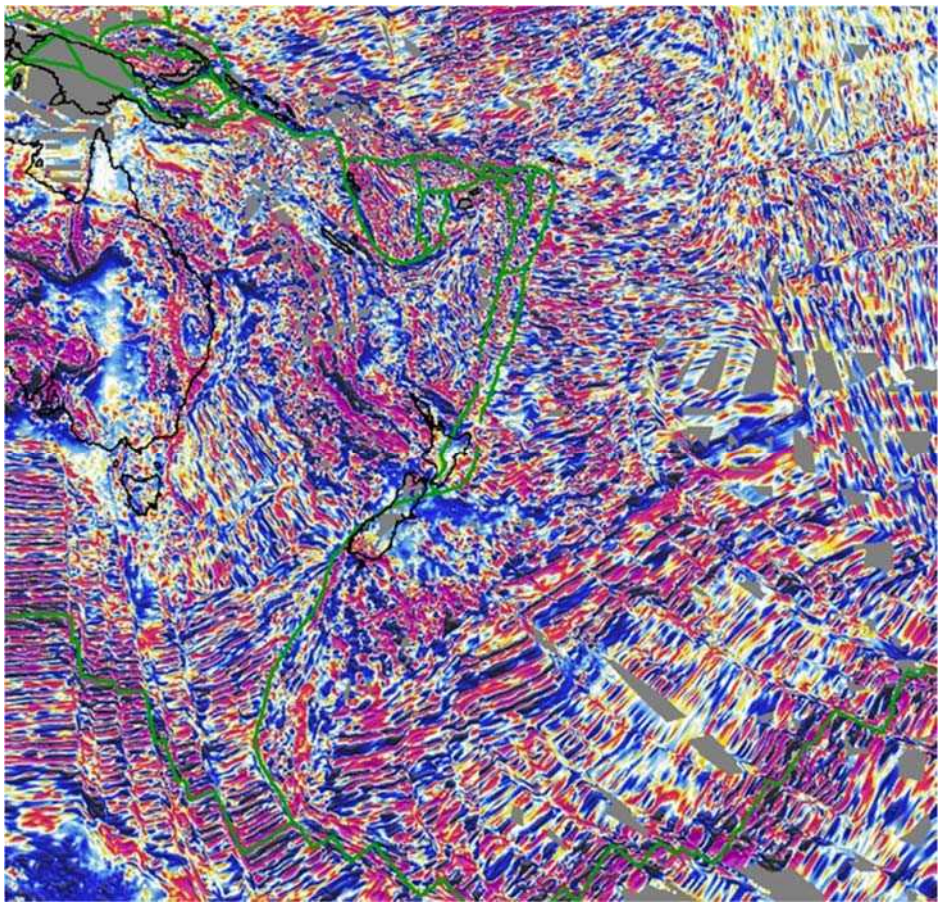

Fig. 46. Magnetic anomaly map for South-West Pacific Ocean. Longitude span $135°E-205°E$ latitude span $65°S-0°S$. Detail of Fig.6. *NOAA* copyright free policy.

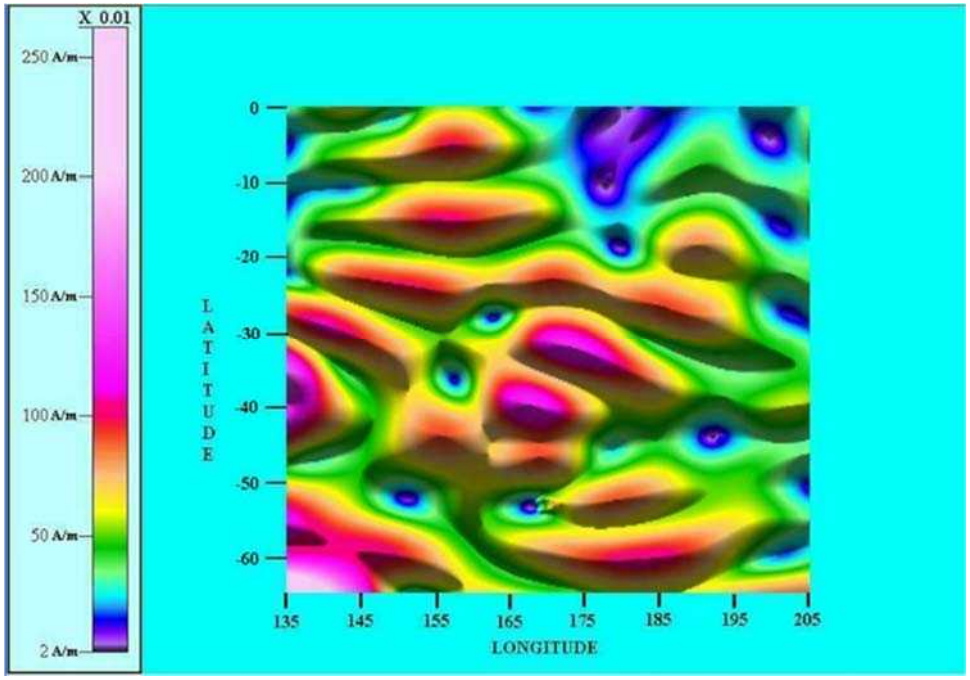

Fig. 47. Quinn's total magnetization map for South-West Pacific Ocean: "*the Fiji complex*" ($A\,m^{-1} \times 0.01$). Longitude span $135°E-205°E$; latitude span $65°S-0°S$. After Quinn (2014).

NCGT Journal
New Concepts in Global Tectonics

New Concepts in Global Tectonics Journal
Volume 14, Number 1, January 2026

ISSN number; ISSN 2202-0039

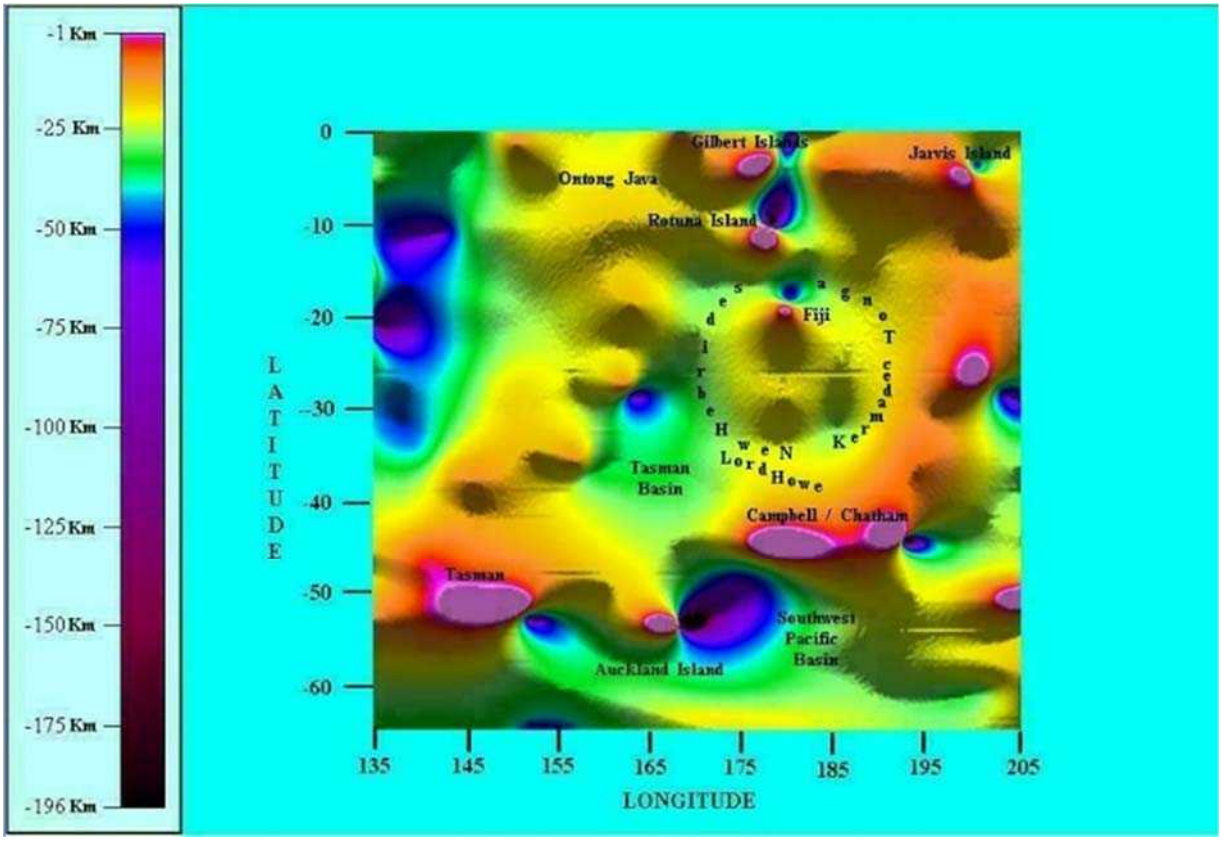

Fig. 48. Quinn's magnetic source-depth map for South-West Pacific Ocean: "*the Fiji complex*" (*km*). Longitude span $135°E - 205°E$; latitude span $65° - 0°S$. After Quinn (2014).

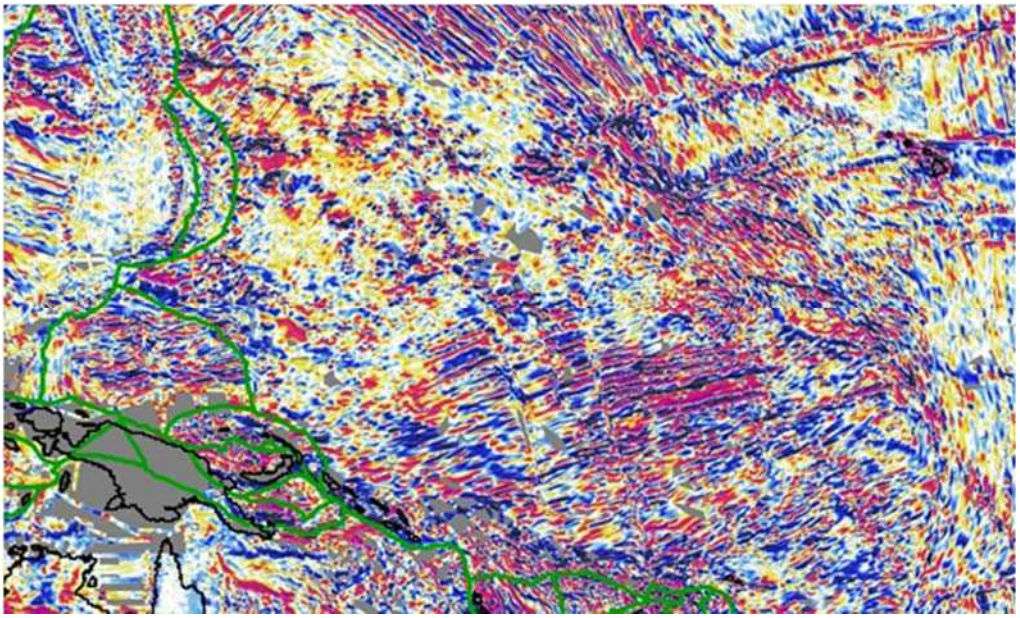

Fig. 49. Magnetic anomaly map for North-West central Pacific Ocean. Longitude span $130°E - 190°E$; latitude span $15°S - 30°N$. Detail of Fig. 6. *NOAA* copyright free policy.

NCGT Journal
New Concepts in Global Tectonics
New Concepts in Global Tectonics Journal
Volume 14, Number 1, January 2026
ISSN number; ISSN 2202-0039

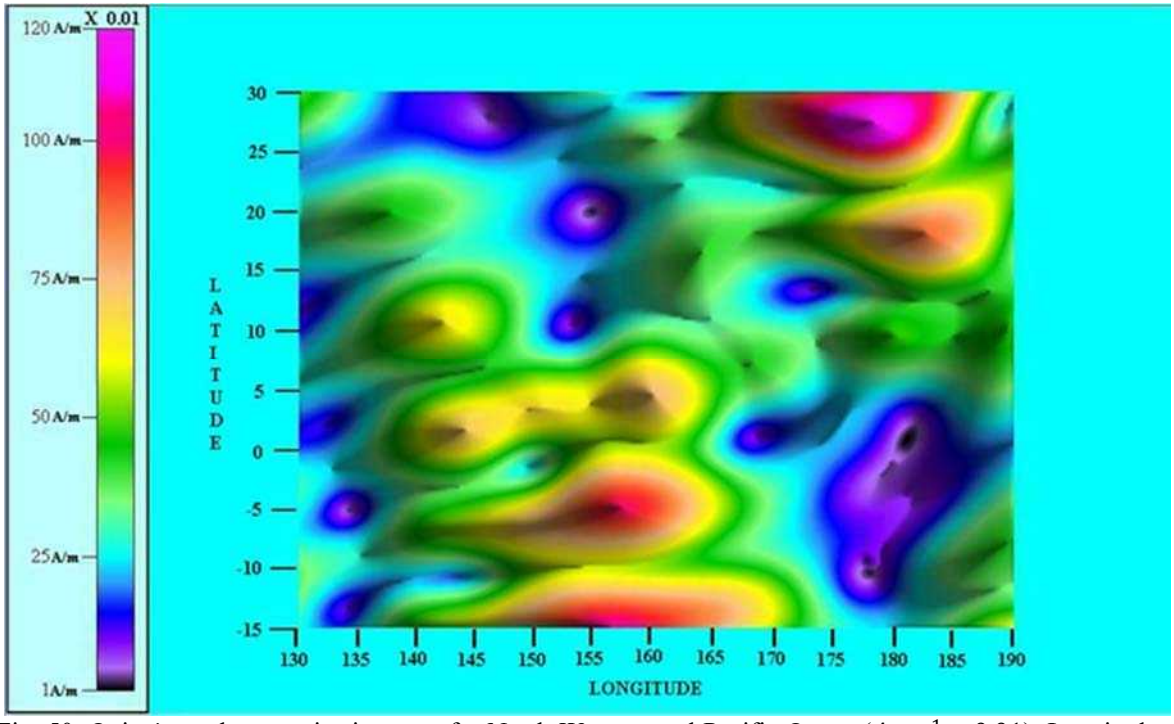

Fig. 50. Quinn's total magnetization map for North-West central Pacific Ocean ($A\ m^{-1} \times 0.01$). Longitude span $130°E-190°E$; latitude span $15°S-30°N$. After Quinn (2014).

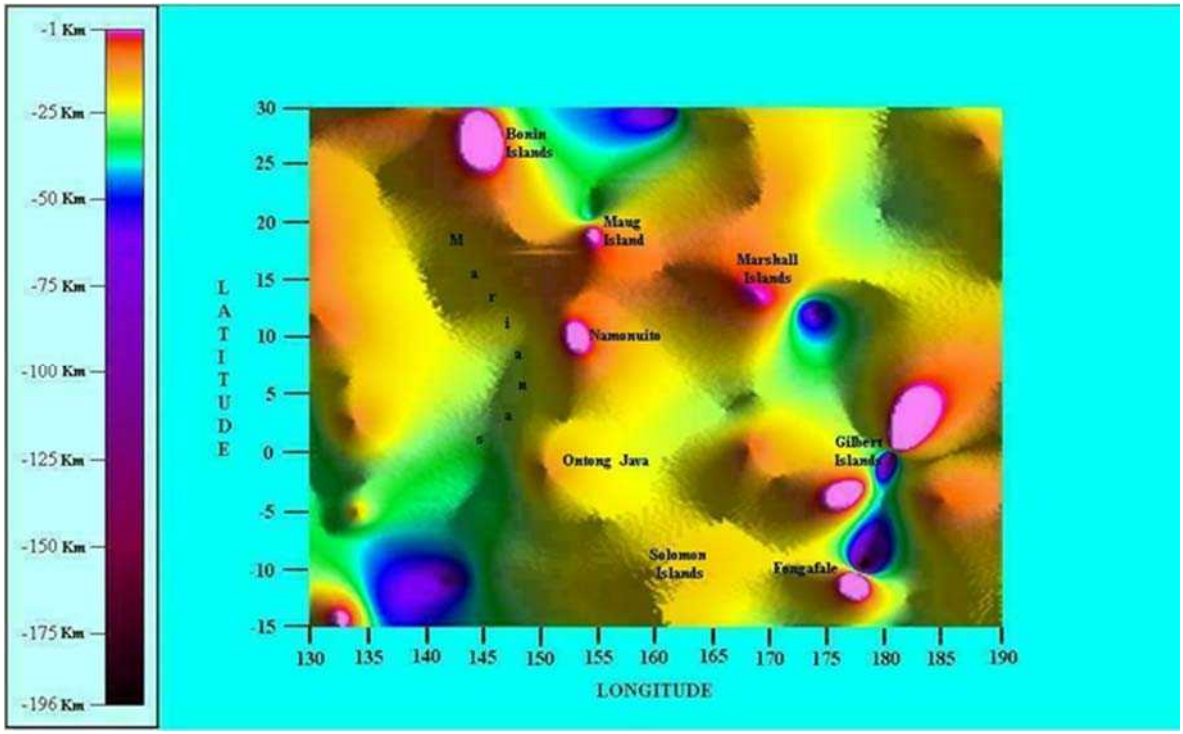

Fig. 51. Quinn's magnetic source-depth map (km) for North-West central Pacific Ocean. Longitude span $130°E-190°E$; latitude span $15°S-30°N$. After Quinn (2014).

NCGT Journal
New Concepts in Global Tectonics
New Concepts in Global Tectonics Journal
Volume 14, Number 1, January 2026
ISSN number; ISSN 2202-0039

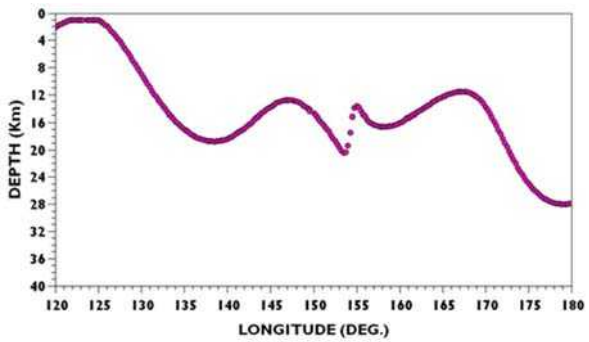

Fig. 52. Magnetic source-depth profile at $20°N$ (Marianas Trench). After Quinn (2014).

The north-western Pacific Ocean

Somewhat more complicated looks the case history of a large north-western Pacific region (Figs 53, 54 and 55).

This region displays also the feature that some authors interpret like a huge impact, the Shatsky crater. But this guess is not shared by others. The Shatky Rise, named after the Soviet geologist Nikolay Shatsky (*1895-1960*), is a Pacific Cretaceous *LIP*, considered (Fig. 56) together with Hess Rise, Magellan Rise, and Ontong Java - Manihiki - Hikurangi (Heydolph et al., 2014). The Shatky Rise is composed of three large massifs, Tamu, Ori, and Shirshov, although with little magmatism found on the Ocean floor (Ingle et al., 2007). Its chemism is investigated by Sano et al. (2012) and Heydolph et al. (2014).

Quinn (2014) shows two profiles aimed to evaluate indicatively the size of this pattern.

The debate about the Shatsky Rise is part of the more general concern dealing with the interpretation of the Pacific Ocean floor (e.g., recall the debate about the Darwin Rise). Therefore, for completeness sake, the review is here reported for the interested reader, according to Quinn (2014, p. 38-43).

Indeed - independent of the debate about its interpretation - this peculiar feature looks clear in Fig. 55. A part of this feature is very close to the older segment of the Emperor Seamount - Hawai'i chain, i.e., with the segment before the huge bending occurred ~42 Ma ago.

Therefore, such a huge rise could be the result of the effect of the Hawai'i hotspot at the time when it generated the older segment of the Emperor Seamount - Hawai'i chain.

At that time, its effect might have been more extended in space, thus generating a large geotumor, or some kind of "small" superswell.

At present, the Shatsky Rise could thus be the simple remnant of this ancient episode in the history of the heat supply to the Hawai'i hotspot. Note that this is consistent with the perturbations in the magnetic anomalies in Fig. 53.

This is speculative. In any case, for completeness sake, the following review by Quinn (2014) is here reported, which is based on the present standard plate tectonics etc.

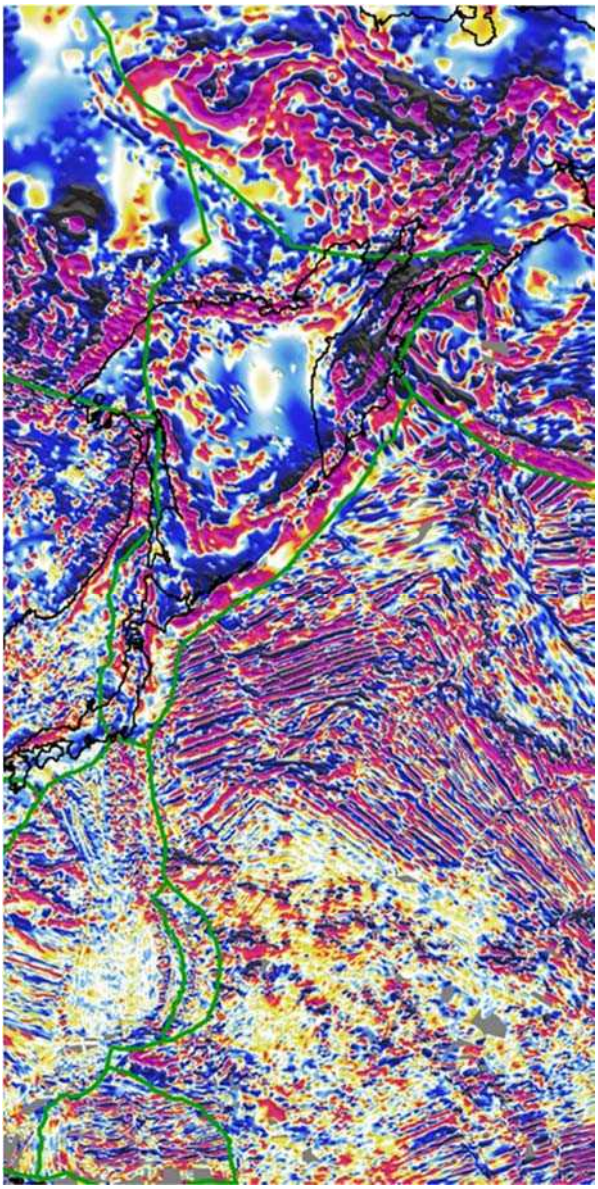

Fig. 53. Magnetic anomaly map for North-West Pacific Ocean. Longitude span $130°E-180°E$; latitude span $0°N-70°N$. Detail of Fig. 6. *NOAA* copyright free policy.

NCGT Journal
New Concepts in Global Tectonics

New Concepts in Global Tectonics Journal
Volume 14, Number 1, January 2026

ISSN number; ISSN 2202-0039

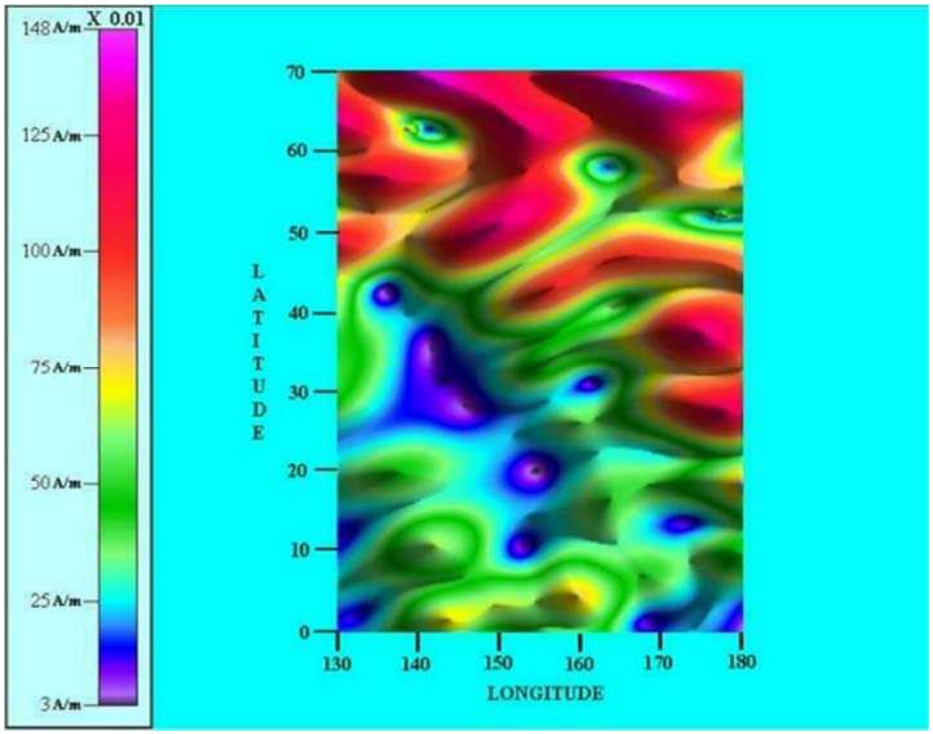

Fig. 54. Quinn's total magnetization map ($A\,m^{-1} \times 0.01$) for North-West Pacific Ocean. Longitude span $130°E - 180°E$; latitude span $0°N - 70°N$. After Quinn (2014).

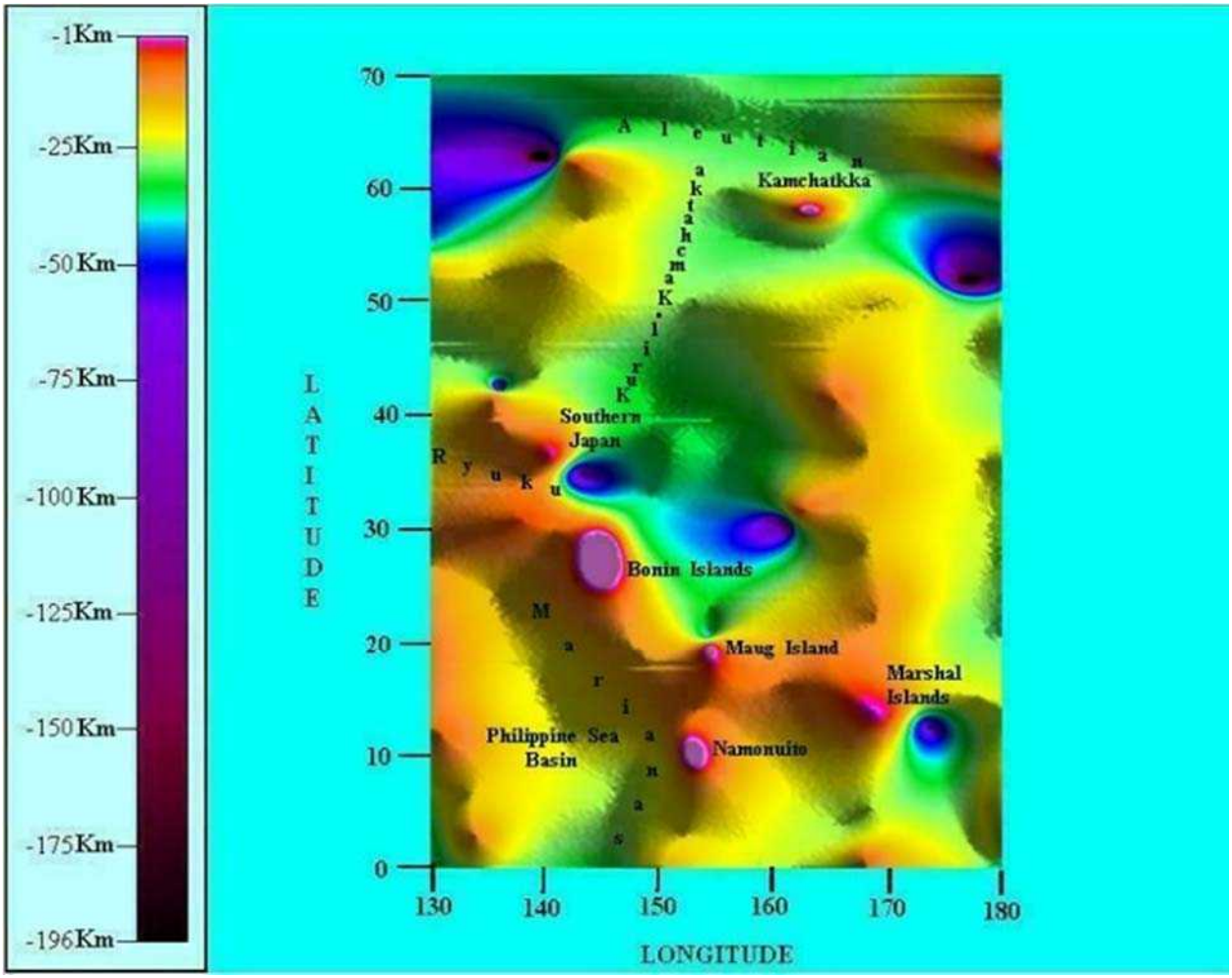

Fig. 55. Quinn's magnetic source-depth map (km) for North-West Pacific Ocean. Longitude span $130°E - 180°E$; latitude span $0°N - 70°N$. After Quinn (2014).

NCGT Journal
New Concepts in Global Tectonics

New Concepts in Global Tectonics Journal
Volume 14, Number 1, January 2026

ISSN number; ISSN 2202-0039

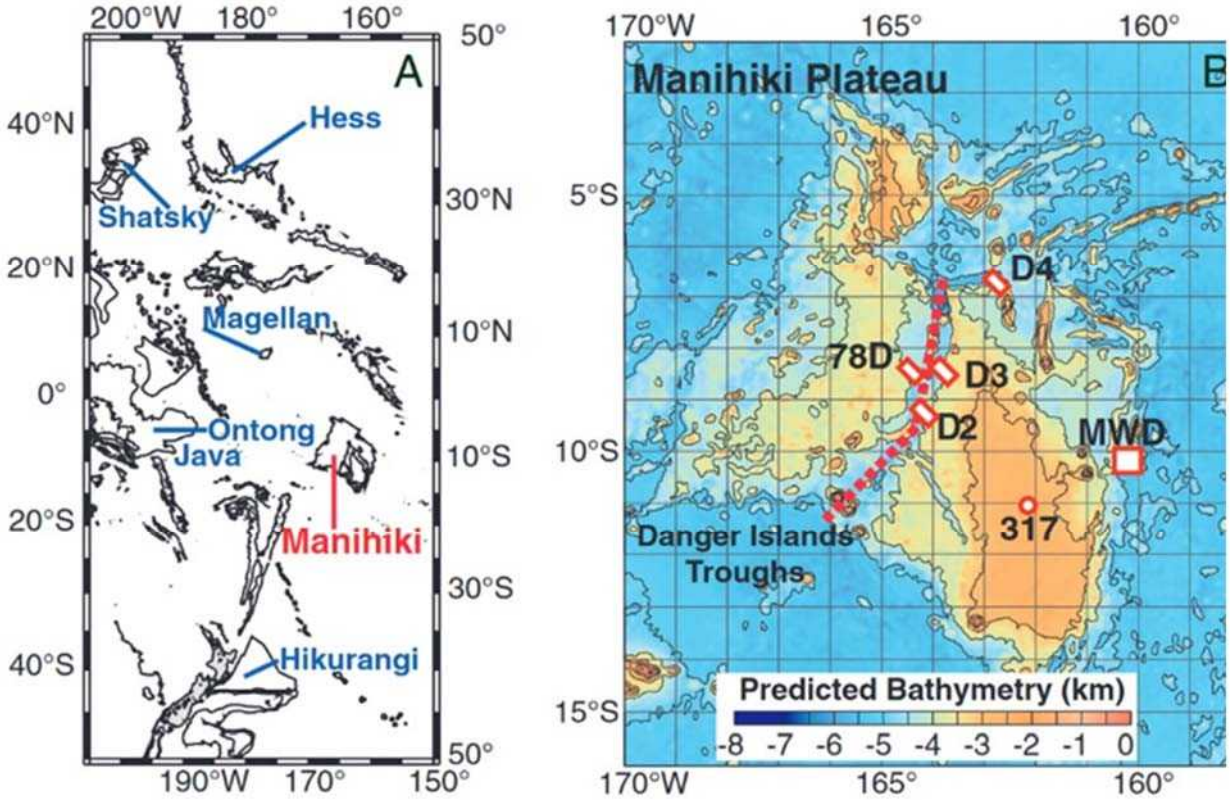

Fig. 56. *"*(A*): Locations of large western Pacific plateaus and rises. (*B*): Bathymetric map with locations of Site 317 and KH03-01 Leg 5 (D2-D4),* SOTW *(78D), and seamount (*MWD*) dredges. Strikes of Danger Islands Troughs are indicated."* Figure and captions after Ingle et al. (2007). Reproduced with kind permission of *GSA*, "*Fair Use*".

"*At the center of the northwest Pacific Ocean is Shatsky Rise. It is presumed to have either been generated by flood basalts primarily emanating from a magma plume originating in the deep mantle and which in turn was the precursor to the Tamu Massif super volcano that erupted* $145\ Ma$ *(Sager and Han, 1993 and Sager et al., 2011). Alternatively, it may have originated as the result of ridge-forming plate-tectonic activity that may be connected with a nearby Triple Junction (Nakanishi et al., 1999). The latter mechanism, however is poorly understood.*

Ocean drilling results indicate that the Shatsky Rise is composed of basalt created during a period of rapidly changing magnetic polarity [rapid changing polarity may be a local effect from rapid change in magnetic intensities of local sea urchin spikes] *that was put down in layers, some of which are roughly* $23\ m$ *thick (Nakanishi et al., 1999). The lithospheric depth morphology of the Shatsky Rise and the surrounding region is presented in Fig. 58 where, just west of the Shatsky Rise, is a very large and previously unknown crater basin which shall be called the Shatsky Crater, or alternatively Shatsky Basin. Within the Shatsky Rise is a very large shield volcano associated with the Tamu Massif (Sager et al., 2013).*

The eastern rim of this lithospheric crater is identified with the Shatsky Rise. The average bathymetric depth at the Shatsky Rise is ~$4\ km$ *(Korenaga and Sager, 2012). The lithospheric depth range taken from Fig. 58 is between* $35 - 12\ km$*. Subtracting the* $4\ km$ *average ocean depth in this region yields a thickness range for the overlying oceanic plateau of between* $8 - 31\ km$*. This compares well with the seismically determined thickness range between* $9 - 30\ km$ *(Korenaga and Sager, 2012). So, the inversion technique ... is both quantitatively and qualitatively reliable, at least in the Shatsky region.*

The crater is centered at ($150°E, 35°N$*). In the north-south direction it extends from the Caroline Islands to just south of the Arctic Circle. In the east-west direction, it extends from Japan to the Marshall Islands in the Central Pacific Ocean. The Marshal Islands are at the southern end of the Shatsky Rise* LIP *that forms much of the eastern side of the crater. The crater is ~*$4995\ km$ *in diameter along* $153°E$ *in the north-south direction. The diameter measurements are taken from mid-rim to mid-rim. The crater varies in depth between* $35 - 70\ km$*. There are also very shallow igneous intrusions (pink) protruding out of the crater's rim that reach close to the ellipsoid surface. Additionally, some isolated holes or drip sites (dark blue) that extend to nearly* $200\ km$ *depth can be seen. Comparing these features with co-located features on the magnetization map of Fig. 47 indicates that many of them are associated with low magnetization and are thus presumed to be associated with high heatflow. Consequently, they are still volcanically active.*

The fact that there is a lithospheric crater for which the Shatsky Rise appears to form at least part of the crater's eastern rim, presents a third possibility regarding the origin of the Shatsky Rise. The crater and the associated rise may be the result of an exceptionally large meteorite impact.

NCGT Journal
New Concepts in Global Tectonics

New Concepts in Global Tectonics Journal
Volume 14, Number 1, January 2026

ISSN number; ISSN 2202-0039

Large meteorite impacts are expected to generate numerous volcanoes that are likely to form on the crater's rim, thereby serving the purpose of cooling the impact site (De Carli et al., 2002). The Earth's crust, particularly in ocean areas, is relatively thin. So, it is possible that an impact large enough to create a crater diameter of 4995 *km is likely to initiate a super volcano originating from the upper mantle that subsequently would generate enormous upper mantle magma outflows (*LIP*s) along some portion of the crater run.*

The upper mantle is singled out because the Shatsky Rise igneous material is more consistent with shallow MORB*, rather than Deep Mantle Basalt that is characteristic of a naturally occurring deep mantle plume (Sager, 2005). Another factor is the exceptional speed with which the Shatsky Rise was created (Nakanishi et al., 1999).* LIP*s from deep mantle plumes take a long time to evolve, while such provinces from a meteorite impact can be generated almost overnight, geologically speaking. Long after the impact event, the geological morphology would be almost indistinguishable from that generated by a super volcano initiated by a plume head eruption. The impact might also account for the existence of the three fracture zones and even the nearby Triple Junction.*

The rest of the crater's rim is studded with lithospheric intrusions. One shallow intrusion is 300 *km long in the north-south direction and* 200 *km wide in the east-west direction, and reaches to within* 1 *km or less of the geoid surface. It is located at (*$153°E, 10°N$*), near Namonuito. The largest near-surface lithospheric intrusion is centered at (* $145°E, 27°N$ *), near the Bonin Islands. It is ~*620 *km long in the north-south direction and ~*320 *km wide in the east-west direction. A smaller intrusion is centered at (* $154°E, 18°N$ *), near Maug Island. It is approximately* 150 *km long in the north-south direction and ~*105 *km in the east-west direction. The smallest intrusion detected is near the east coast of the Kamchatka Peninsula and is ~*100 *km long in the east-west direction and ~*50 *km wide in the north-south direction. Most of these intrusions are formed from plate tectonic subductions related to the Marianas Trench, the Ryuku Trench, the Kuril-Kamchatka Trench, and the Aleutian Trench. These trenches reside east and north of the crater basin and are approximately* 30 *km deep.*

Fig. 54 presents a string of magnetization lows (blue) located below the southwestern portion of the crater rim that coincide with several volcanic peaks seen in Fig. 58. These hotspots and volcanic peaks stretch from southern Japan to Namonuito and even farther east to the Marshall Islands. At the higher latitudes the magnetization is stronger, again due to the convergence of Earth's main ***B*** *lines at the magnetic poles.*

The depth profiles in Figs 57 and 58 give a different perspective regarding the extent and depth of the Shatsky Crater. Fig. 57 is an east-west depth profile along latitude $40°N$*. It shows the average crater rim depth level below the ellipsoid surface to be ~*20 *km , while the volcanic intrusions rise through the crater rim to a depth of* 10 *km below the ellipsoid surface. The depth profile is extraordinarily symmetric. The crater's mid-rim to mid-rim diameter at this latitude is* 2636 *km, while the crater floor reaches a depth of* 33 *km. The crater's extremely large diameter would seem to rule out an origin via a magma plume head that cooled and sank to the interior of the Earth, leaving a large basin.*

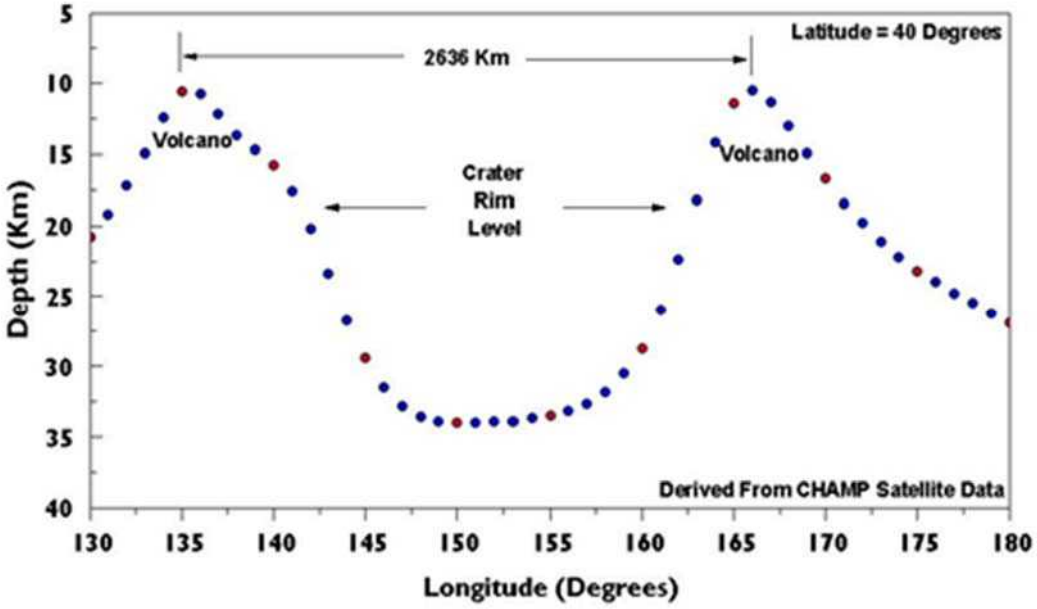

Fig. 57. Magnetic source-depth profile at $40°N$ (*km*, Shatsky crater). After Quinn (2014).

NCGT Journal
New Concepts in Global Tectonics

New Concepts in Global Tectonics Journal
Volume 14, Number 1, January 2026

ISSN number; ISSN 2202-0039

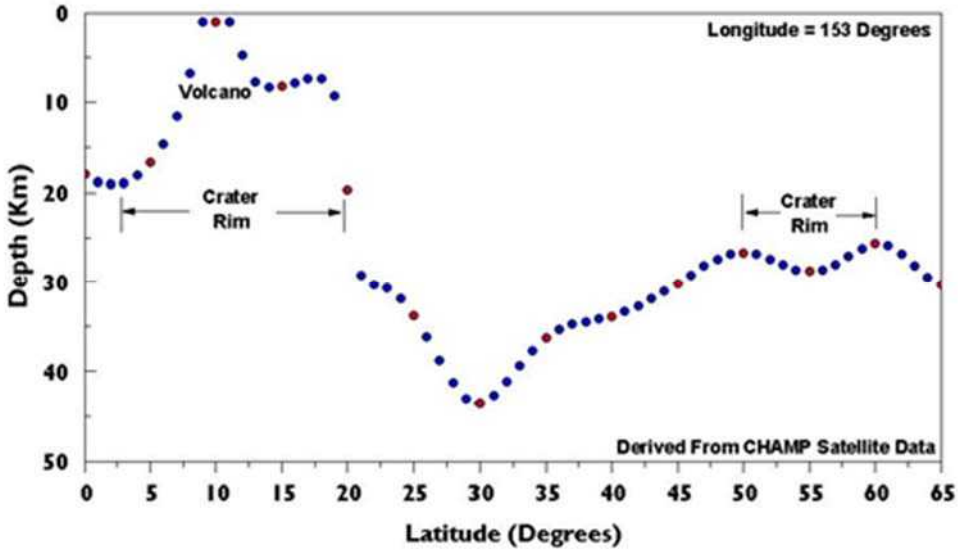

Fig. 58. Magnetic source-depth profile at $153°E$ (km), (Shatsky crater). After Quinn (2014).

Fig. 58 shows the depth profile in the north-south direction along $153°E$ *longitude. At (*$153°E, 10°N$*) a volcanic intrusion reaches the surface. It corresponds to Namonuito Island, which is part of Micronesia. This island sits upon a secondary volcanic peak that reaches to ~*$8\ km$ *depth. At about* $19°N$ *latitude the profile makes a sharp drop from the plateau of the secondary peak to* $30\ km$ *depth where the profile begins a slower drop to the crater basin, reaching* $42\ km$ *depth. At the opposite side, the crater rim intrusions appear to have been eroded away as a consequence of plate tectonic motions (e.g., earthquakes and subsequent landslides) and other factors. Beyond this rim to the north is the Aleutian Trench."*

The south-western Indian Ocean

The case history of south-western Indian Ocean leads to similar conclusions (Figs 59, 60 and 61). Specifically, several "double E-eye" patterns are found, including either oceanic islands and others associated with ongoing rifting of continental eastern Africa.

The anthropic impact

A temporary conclusion is, therefore, that - if the explanation which is here envisaged is correct - bunches of sea-urchin spikes, or hotspots, are always associated with a conspicuous air-earth current ***j***, well collimated, and their effects are clearly detectable in the ionosphere (Gregori and Leybourne, 2025g). The concern is whether other environmental factors, such as, e.g., anthropic pollution can produce any similar effect, associated, e.g., to the so-called "heat island" in the atmosphere originated by some large city or town, or industrial settlement etc.

In this respect, a previously unnoticed effect deals with the impact of urbanization on atmospheric humidity. Hao et al. (2018) carried out a detailed analysis in the Shanghai area. Urbanization has been particularly intense.

"*In 1960, about* 110 million *Chinese people - or* 16% *of the population - lived in cities. By 2015, that number had swollen to* 760 million *and* 56% ...

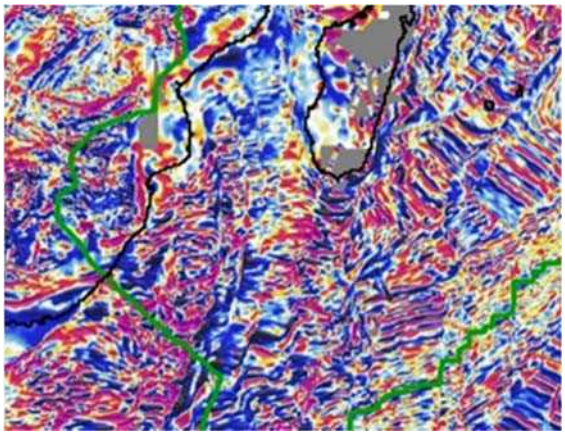

Fig. 59. Magnetic anomaly map for South-West Indian Ocean. Longitude span $25°E - 60°E$; latitude span $40°S - 15°S$. Detail of Fig. 6. *NOAA* copyright free policy.

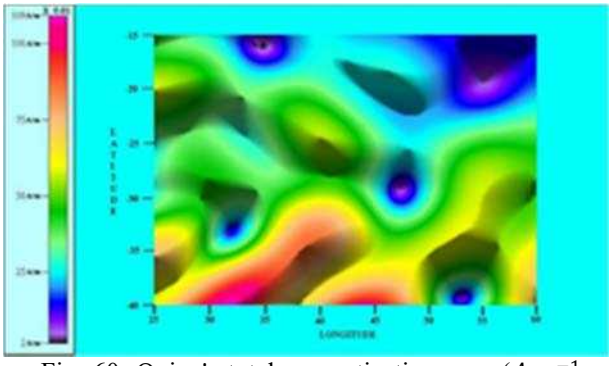

Fig. 60. Quinn's total magnetization map ($A\ m^{-1} \times 0.01$) for South-West Indian Ocean. Longitude span $25°E - 60°E$; latitude span $40°S - 15°S$. After Quinn (2014).

A 2015 World Bank *report noted that* $7{,}734\ km^2$ *in the Yangtze River Delta Economic Zone – which includes Shanghai, Suzhou, Wuxi, and several other cities - became*

NCGT Journal
New Concepts in Global Tectonics
New Concepts in Global Tectonics Journal
Volume 14, Number 1, January 2026
ISSN number; ISSN 2202-0039

urban between 2000-2010. That is an area equivalent to 88 *Manhattans. During that period, population in that zone increased by* 21 *million people*" (Underwood, 2019).Hao et al. (2018) "*define the influences of urbanization on reducing atmospheric humidity and elevating vapor pressure deficit as urban dry island (*UDI*) effects.*

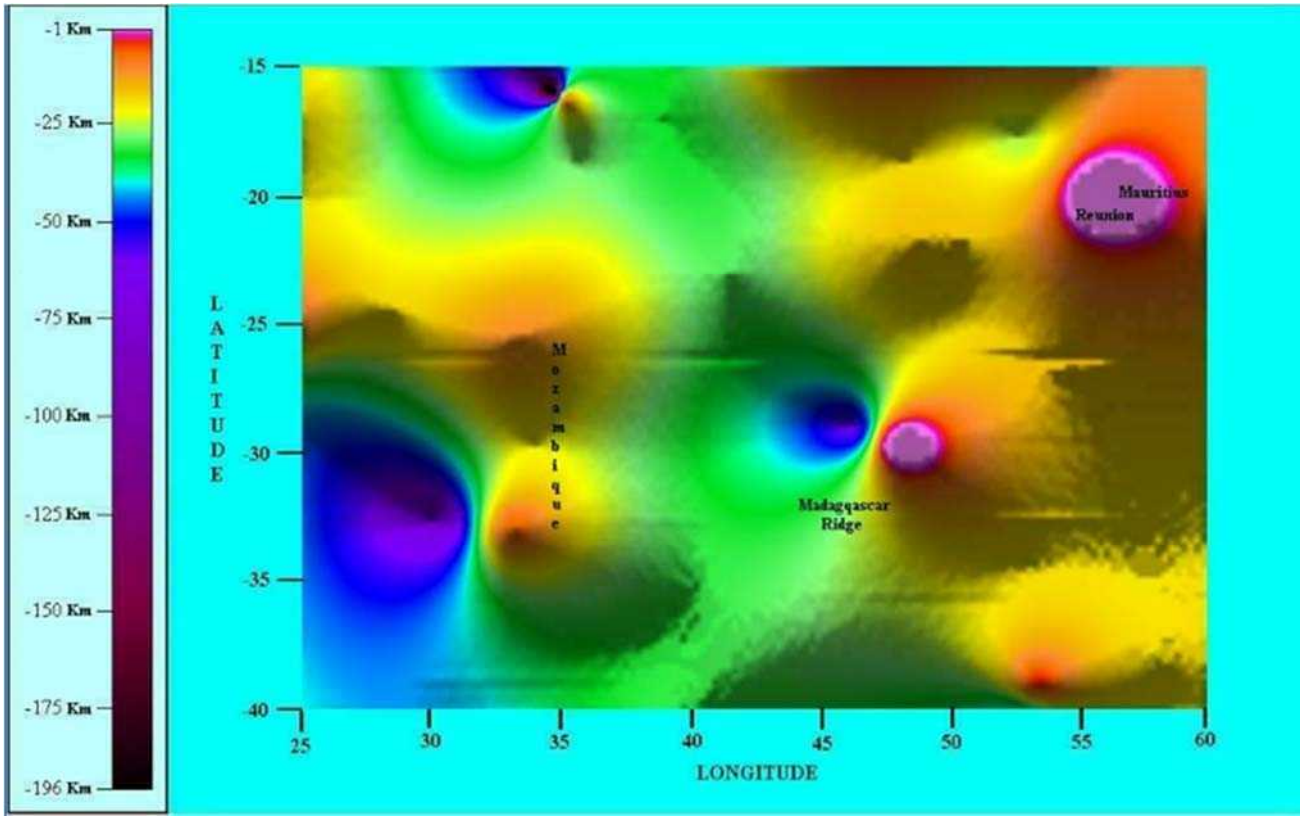

Fig. 61. Quinn's magnetic source-depth map (*km*) for South-West Indian Ocean. Longitude span *25°E – 60°E*; latitude span *40°S -15°S*. After Quinn (2014).

We conduct a case study in the Yangtze River Delta . ... We examine spatiotemporal characteristics of UDI *and identify potential drivers during 2001-2014. Relationships and interactions between variations of air temperature, atmospheric humidity, evapotranspiration, and leaf area index of different land cover were determined using correlation and attribution analyses at both station and regional levels.*

We show that atmospheric humidity decreased dramatically and vapor pressure deficit increased sharply in the urban core, resulting in enhanced UDI. *In addition to global warming and localized urban heat island,* UDI *is closely related to the loss of vegetation cover (i.e., natural wetlands and paddies). Reduction of evapotranspiration or latent heat is another important factor contributing to* UDI *effects.*

We conclude that the role of vegetated land cover and associated eco-hydrological processes in moderating UDI *and maintaining a stable climate and environment should be considered in massive urban planning and global change impact assessment in southern China*."

Differently stated, the interaction between "climate" and biosphere - and humankind is a most active part of the biosphere - is much more complicated than it can be envisaged upon referring to one chemical component alone. Even worst, it is nonsensical to be concerned with anthropic CO_2 injection in the atmosphere that, compared to the natural soil exhalation, is clearly proven to be an almost negligible contribution (see Quinn, 2010, and Gregori, 2020). A recent study [*The Cenozoic CO_2 Proxy Integration Project (CenCO_2PIP) Consortium,* 2023, illustrated by *Columbia Climate School*, 2014] shows the large decrease of CO_2 atmospheric concentration during the last 66 Ma (see Fig. 62).

Neither the role alone can be considered of greenhouse gases (CH_4 and CO_2), when H_2O has a much stronger greenhouse impact. Therefore, understanding the anthropic impact on "climate" is a great challenge for Earth scientists, especially when the drivers of natural climate change are not that well understood.

Another related item deals with nuclear reactors. It is well-known that a nuclear reactor accident is an effective way to simulate a manmade effect on the ionosphere mimicking several frequently observed earthquake precursors. Three case histories are reported, i.e., Three Mile Island, Chernobyl, and Fukushima. See *Anonymous* (2015f), Williams and Mareev (2014); Pulinets and Liu (2004); Kakinami et al. (2011); Pulinets et al. (2014); Ouzounov et al. (2011a; 2014); Takeda et al. (2011); Harrison et al. (2014); Laverov et al. (2011); Pulinets and Davidenko (2014), and references therein.

NCGT Journal
New Concepts in Global Tectonics

New Concepts in Global Tectonics Journal
Volume 14, Number 1, January 2026

ISSN number; ISSN 2202-0039

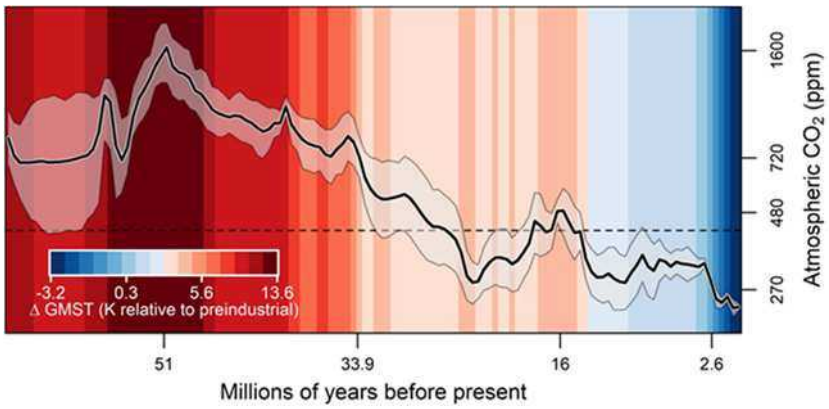

Fig. 62. "*Temperatures and atmospheric concentrations of* CO_2 *over the past* $66\ Ma$. *Bottom numbers indicate millions of years in the past; right-hand numbers,* CO_2 *in parts per million. Hotter colors indicate distinct periods of higher temperatures; deeper blues, lower ones. The solid zigzagging line charts contemporaneous* CO_2 *levels; shaded area around it reflects uncertainty in the curve. Credit: Gabe Bowen,* University of Utah." Figure and captions after *Columbia Climate School* (2014).

Quinn (private communication, 2015) comments as follows. "*No man-made / anthropic* ***B*** *have ever been observed in the internal geomagnetic field models, even at* SH *degree- and order-*720. *I expect that high degree-and-order models may contain manmade* ***B*** *information, but these would result from large-scale static features, such as industrial and military complexes containing lots of iron, metal cabling, railroad tracks and cement, which has lots of iron filings in it. Such signals would be very weak even at Earth's surface, let alone at satellite altitudes. Data selection and processing techniques would remove any transient signals (e.g., communication signals and even signals from the military's* HARP *array in Alaska and other sites around the world which sends e.m. signals into the ionosphere) from the final model*."

The concern of the present discussion, however, deals with the possible role of large "heat islands" that locally, but significantly, affect the atmospheric electrical circuit. All aforementioned case histories refer to ocean regions, with a few exceptions. The Bangui anomaly area (Figs 28 through 33) is located in central Africa, which is mostly polluted by anthropic wildfire activity (agricultural burn areas). In any case, these anomalous areas are well-known as peculiar features all over the globe, sometimes being identified with weather phenomena eventually associated with either gravimetric and/or atmospheric observations. Observations in the Horn of Arica and Zaïre region seem to suggest these anomalies may supply an energization source for tropical storms that cross westward over the Atlantic Ocean, to be eventually transformed into violent hurricanes (Gregori and Leybourne, 2025j).

Another exception deals with Australia (Figs 20 through 27) that is a continental-size region, comparably less polluted by anthropic activity. The evidences inferred by Quinn are still reasonably clear, although they might be somewhat disturbed by the "double E-eye" feature, or they might be perturbed by anthropic action, at least in the areas that are more densely inhabited.

The third exception is the source-depth map of North America (Figs 11 and 17) that displays several sharp transitions between more or less deformed and extended "double E-eyes" of different color. It seems unlikely (perhaps) that these morphological features can be interpreted in some way similar to oceanic hotspots. A reasonable suspicion is that anthropic pollution, in terms of some kind of huge and extended heat islands, altogether with ionization caused by human activity, can modify the atmosphere and favor some relevant air-earth currents that affect the *CHAMP* records.

The entire problem requires harder thinking.

Europe and Middle East

Another challenging test is represented by Europe and Middle East (Figs 63, 64 and 65), which is a tectonically, geothermally and volcanically particularly tormented continental-size region. It is also characterized by several extended densely inhabited and industrialized areas.

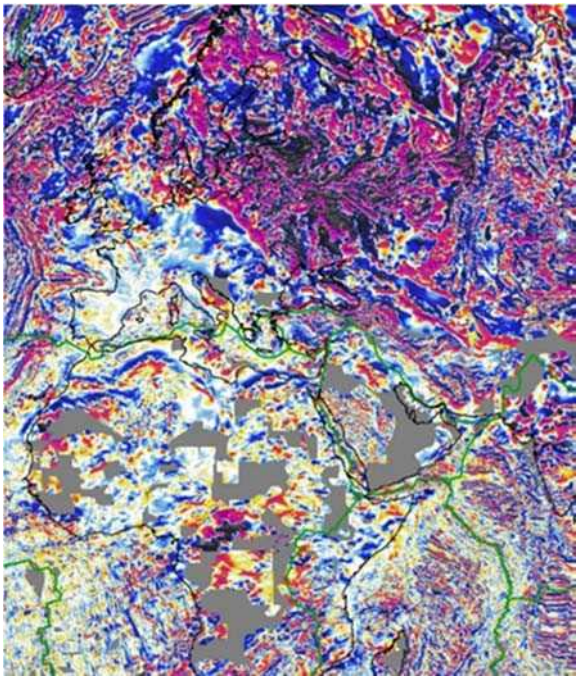

Fig. 63. Magnetic anomaly map of the European and Middle East region. Longitude span $20°W - 80°E$; latitude span $20°N - 70°N$ (note that, unlike in Figs 64 and 65, the highest latitude is $70°N$ not $80°N$). Detail of Fig. 6. *NOAA* copyright free policy.

A remarkable morphological feature is the dramatic step-wise change of style in Fig. 63. Indeed, a large belt looks almost uniform with a mainly white dominating color. It comprises a belt along the North African coast, the entire Mediterranean region, the Iberian, Italian and Balkan-

NCGT Journal
New Concepts in Global Tectonics
New Concepts in Global Tectonics Journal
Volume 14, Number 1, January 2026
ISSN number; ISSN 2202-0039

Hellenic peninsulas, and Europe until including Great Britain, central Europe, up to the Carpathians and behind them. Then, the belt extends, although somewhat sharpened, through Anatolia, Iraq, and Southern Iran.

Note that the Mediterranean volcanoes look like tiny spots. Indeed, their "double-eye" patterns are to be investigated by much more detailed maps, shown and discussed in Gregori et al. (2025r).

The southern and northern boundaries of this large belt are characterized by red/blue patterns consistent with argument of Fig. 2. The regions outside this belt include Africa, the Northern and far-Eastern Europe, plus some large fraction of Asia.

Africa has several gaps in the geomagnetic anomaly map. The most evident feature is the *CVL* and the Bangui anomaly. In contrast, the Northern and far-Eastern Europe and some large fraction of Asia display an incredibly perturbed morphology that is indicative of a past very tormented geodynamic history. The cartographical amplification should be taken into account. However, the contrast with the circum-Mediterranean region looks impressive.

According to the *WMT* mechanism that is here envisaged (see Gregori and Leybourne, 2021; Gregori et al., 2025a), this whole morphology is in close agreement with the interaction of the westward drifting Eurasia relative to Africa, and with the push on Arabia, originated from the Kerguelen superswell, which affects Anatolia until the Carpathians, etc. That is, this large anomalous belt is likely to be the site where this dramatic interaction occurs (Gregori and Leybourne, 2021; Gregori et al., 2025a).

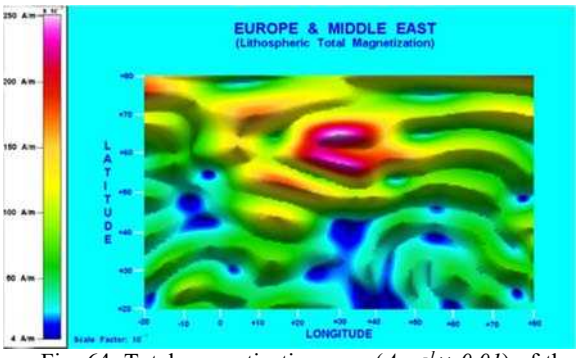

Fig. 64. Total magnetization map ($A\ m^{-1} \times 0.01$) of the European and Middle East region. Longitude span *20°W - 80°E*; latitude span *20°N - 80°N*. After Quinn (2014).

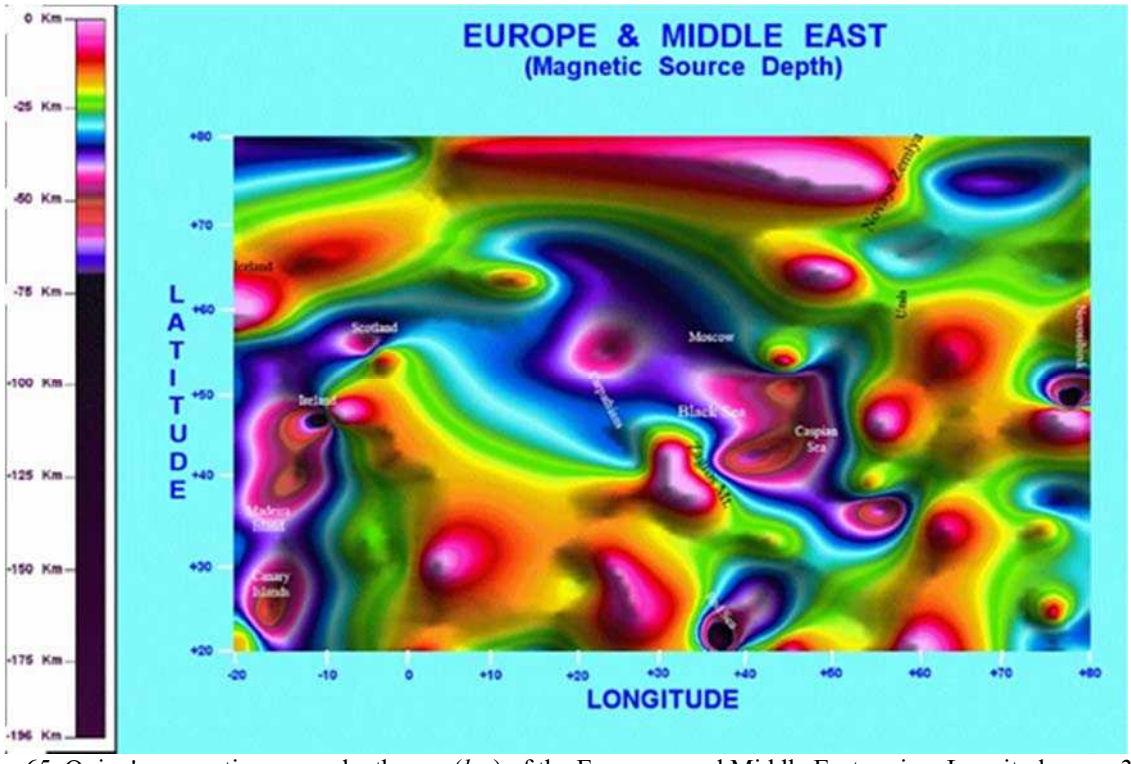

Fig. 65. Quinn's magnetic source-depth map (*km*) of the European and Middle East region. Longitude span *20°W - 80°E*; latitude span *20°N - 80°N*. After Quinn (2014).

A first relevant evidence derives from a comparison of Fig. 61 with Fig. 63. The very extended maximum of total magnetization seems to be closely correlated with the large region that in Fig. 63 appears like a wide almost fully red patch. However, the cartographic deformation should be considered, by comparison with Figs 38 through 40.

In contrast, comparably much more detailed inferences can be derived from Fig. 65. The following argument seems reasonable, although it needs for better confirmation by specific regional multidisciplinary campaigns, carried out over more restricted areas.

For the time being, a possible interpretation can be realistically envisaged as follows. In general, the possibility must be considered of the bias that is caused by the "leopard skin" effect, originated by the order and degree of the terms of the *SHE* that have been used. For instance, an effect

ISSN number; ISSN 2202-0039

could enter into play - also in these figures for Europe and Middle East - similar to the false pattern displayed in Fig. 31 and others. The huge feature that looks like an extended red patch at the northern latitudes is a cartographic deformation.

For high latitudes refer to Fig. 63. Also consider the ongoing huge release of endogenous heat over the northern polar cap that is envisaged by several other evidences that for brevity purpose cannot be here reviewed. For instance, recall the several evidences that are clearly suggestive of an increased CH_4 exhalation. However, anthropic pollution could also be co-responsible for this effect (see Quinn, 2010; Gregori, 2020, Gregori and Hovland, 2024; and, concerning the indirect evidence of CH_4 exhalation by wildfire propagation, refer to Gregori and Leybourne, 2025i).

In addition, note that the blue extended "E-eye" is perturbed by several smaller-sized features that are intermingled with one another. They are located, approximately, in the regions of the Black Sea, of the Caspian Sea, roughly in the northern Urals, and also not far and South-West of Moscow, and somewhat westward of the Carpathians. An additional almost isolated feature is observed not far from Novosibirsk. Are these natural exhalation or anthropic effects? Another distinguishable feature is roughly located in the area of Novaya Zemlya (see also Fig. 40).

A similar - although comparably less extended - "double E-eye" feature seems to be associated with Iceland. Also in this case, the blue "E-eye" contains two couples of much smaller "E-eyes", one close to Ireland, the other roughly in Scotland. In general, one can state that these features correspond to the region around Great Britain. However, owing to several independent evidences, we know that no anomalous heat flow occurs in Great Britain. Hence, it seems reasonable to conclude that these smaller "double E-eyes", perhaps, are the result of some relevant heat islands (either cities and/or industrial settlements).

A clear and well defined couple of "E-eyes" is associated with the Red Sea, and also with the Zagros Mountains. Some less clear features seem associated with the Canary Islands extending, perhaps, also to the Madeira Island and to the Azores Islands. Some maxima (not, "double E-eye") are also observed inside the continental northern Africa, although - in general - the possible drawback of the "leopard skin" effect should be realistically re-considered.

The several profiles indicated in Fig. 65 that have been considered by Quinn (2014) are shown in Figs 72 through 78, and are self-explanatory.

North America

Just re-consider the case of North America (Fig. 17) after review of the aforementioned inferences for Europe and Middle East. According to *WMT*, we know (e.g., Gregori and Leybourne, 2021; Gregori et al., 2025a) that the whole west coast of the continent is the site of a huge overthrust process that originates a conspicuous friction heat, hence soil exhalation. The huge double alignment, i.e., a red patch to the west and a blue patch inland, remind about a huge elongated "double E-eye" pattern.

Standard "double E-eyes" are observed in the West Indies and in the Bermuda Rise, and these features seem reasonable. More surprising looks the case of Halifax, or the intense feature observed in the Hudson Bay area (but sea Fig. 40). This seems likely to be associated with the ongoing large release of endogenous heat underneath the northern polar ice cap, which is structured eventually with some relevant space gradient.

Less clear is the interpretation of the complicated feature around the Gulf of Mexico, along the track from Yucatàn, through Miami, through New York - reminding, however, about the huge blue "crater" displayed in Fig. 11, which seems to be associated with the kingpin (Gregori and Leybourne, 2021). In any case, the distinction ought to be considered between two substantially different morphological features. One is the huge sea-urchin spikes that may be a remnant of the astrobleme that started the climate change that finally caused dinosaur extinction: this is an old and also very deep feature.

Conversely, a "double E-eye" reflects a present pattern of geothermal exhalation that, obviously, refers to the much shallower gradient and anisotropy of the endogenous heat release. Therefore, there is no need that any "double E-eye" pattern – which *per se* refers to lithospheric features alone - is a signature of a deep sea-urchin spike that crosses through the mantle and lithosphere. As far as the Gulf of Mexico is concerned, it is more extensively discussed in Gregori and Leybourne (2025j).

Planetary analysis

As a final item, consider Quinn's global inversion maps. Fig. 66 shows the criterion used for illustrating the planetary analysis. The choice is to map four different quadrants (North-West, South-West, North-East, South-East, respectively), plus a few profiles indicated by brown lines (the light-blue line is the Marianas Trench profile represented in Fig. 52).

Figs 67 through 72 show the Quinn's quadrant maps. Every map is repeated identically twice, with superposed some white geometrical figures to indicate the corresponding approximate regions at Earth's surface. Note, however, that this geographical information is only purely indicative, and it specifies the name of some site or feature, which is presumably known to the reader. Consider, that the features evidenced by the Quinn's maps are concerned with deep layers that, in the final analysis, nobody ever afforded to investigate. Hence, the correlation is not to be necessarily expected with any shallower surface feature.

In general, all total magnetization maps seem to be comparatively more severely biased by the "leopard skin" effect. Therefore, their interpretation is difficult, because Earth's processes and Earth's morphological features display some typical size that can hardly be pinpointed on these global maps. Conversely, the global maps of the magnetic source-depth display - just as a matter-of-fact - an impressive number of well-defined "double E-eye" features.

NCGT Journal
New Concepts in Global Tectonics

New Concepts in Global Tectonics Journal
Volume 14, Number 1, January 2026

ISSN number; ISSN 2202-0039

Fig. 66. Four quadrant representation of Quinn's inversion maps, and several profiles along a few meridians and along the $20°N$ parallel. Unpublished figure.

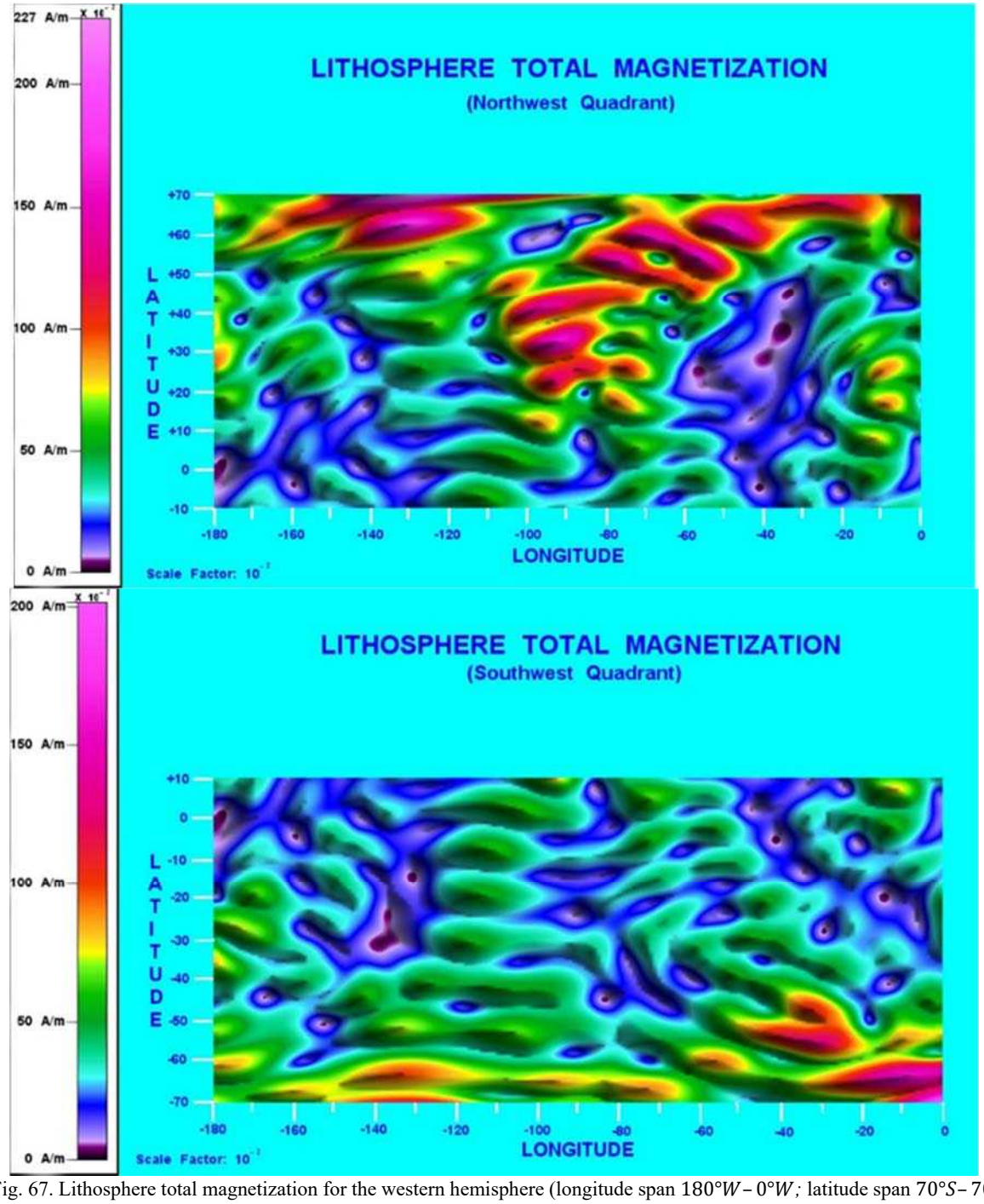

Fig. 67. Lithosphere total magnetization for the western hemisphere (longitude span $180°W - 0°W$; latitude span $70°S - 70°N$). *[upper]* Northern hemisphere; *[lower]* Southern hemisphere. After Quinn (2014).

NCGT Journal
New Concepts in Global Tectonics

New Concepts in Global Tectonics Journal
Volume 14, Number 1, January 2026

ISSN number; ISSN 2202-0039

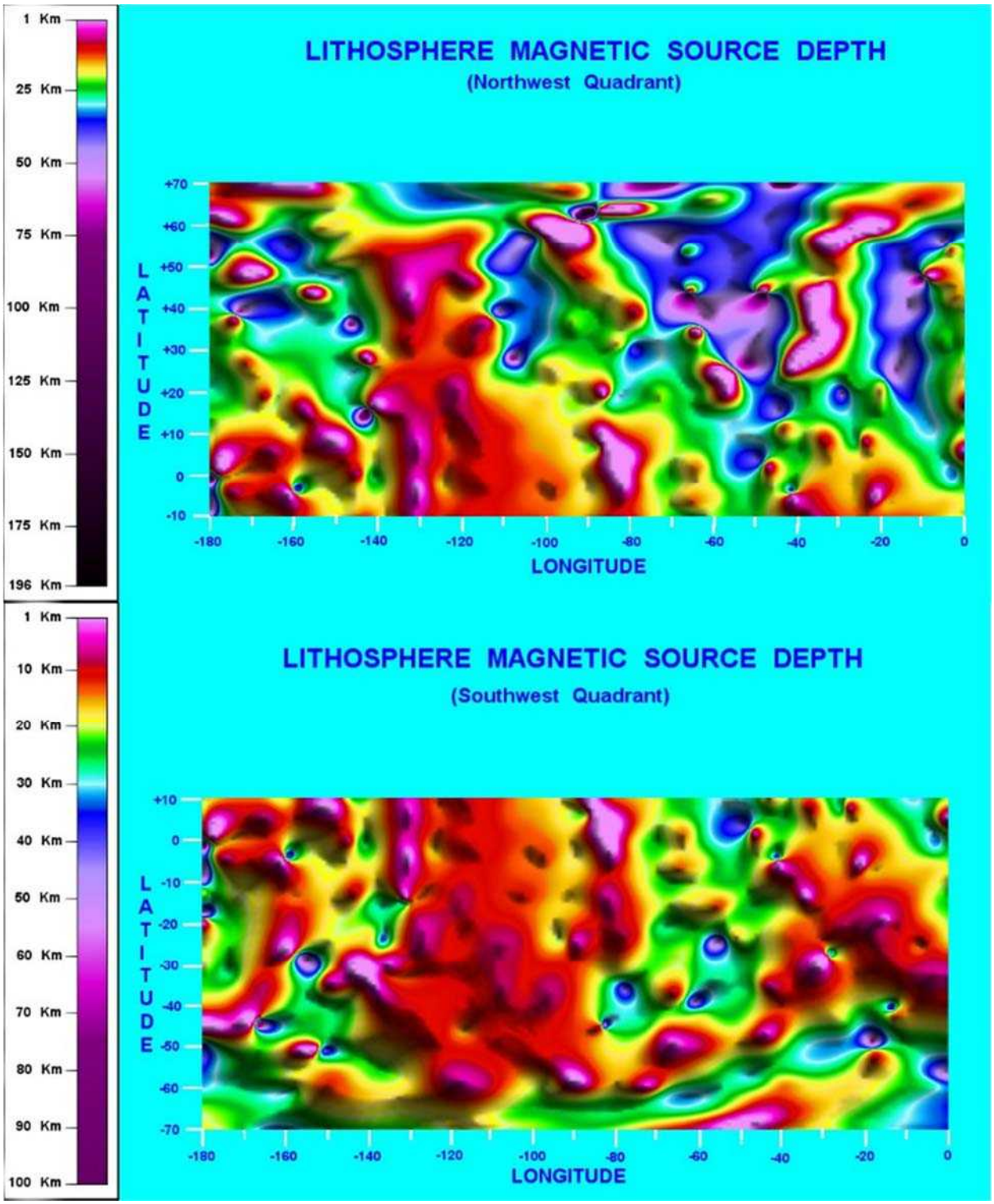

Fig. 68. Lithosphere magnetic source depth for the western hemisphere (longitude span $180°W - 0°W$; latitude span $70°S - 70°N$). *[upper]* Northern hemisphere; *[lower]* Southern hemisphere. After Quinn (2014).

NCGT Journal
New Concepts in Global Tectonics

New Concepts in Global Tectonics Journal
Volume 14, Number 1, January 2026

ISSN number; ISSN 2202-0039

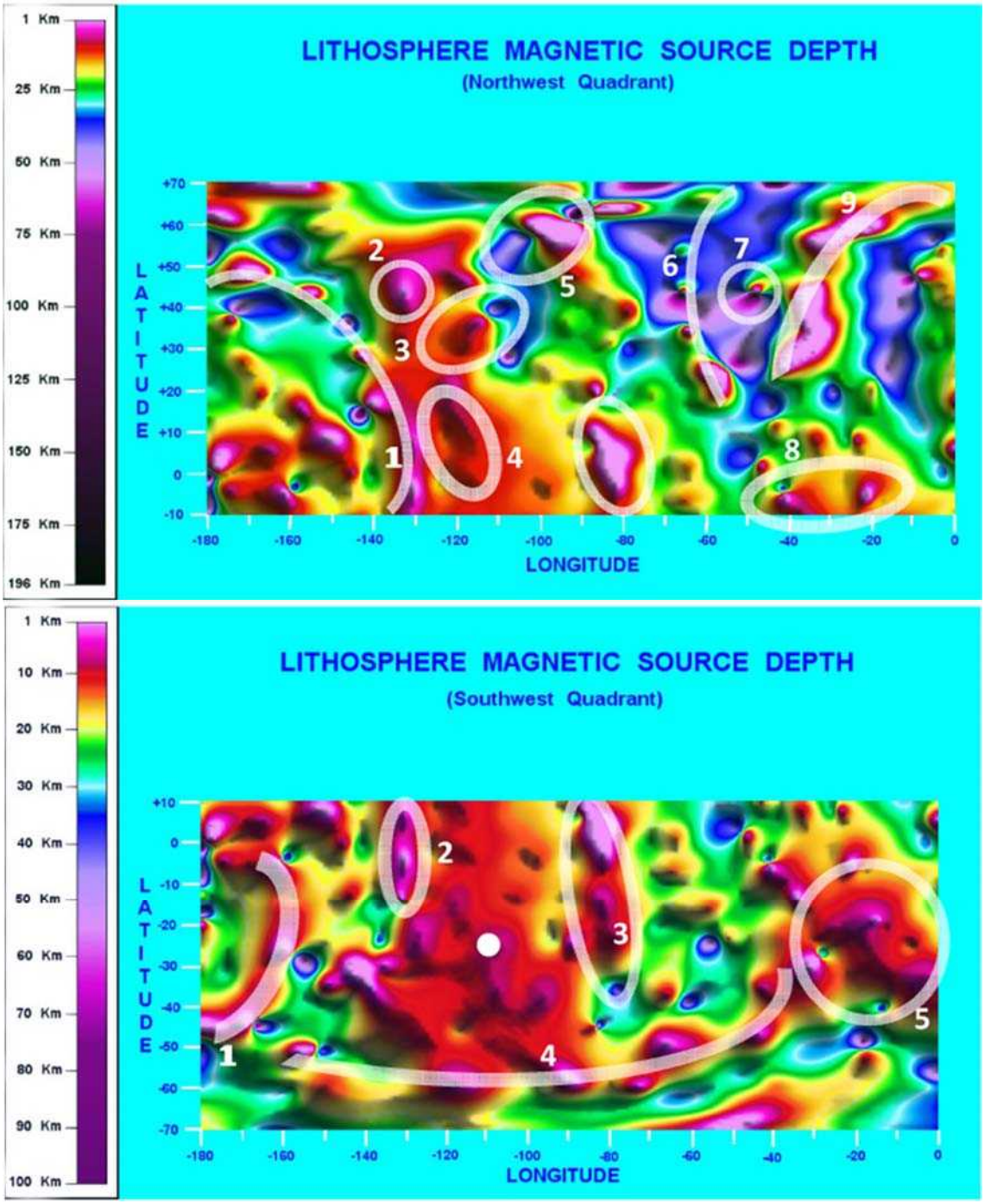

Fig. 69. Lithosphere magnetic source depth for the western hemisphere (longitude span $180°W - 0°W$; latitude span $70°S - 70°N$). *[upper]* Northern hemisphere; *[lower]* Southern hemisphere. Duplicate of Fig. 68 aimed to pinpoint specific features at Earth's surface. Modified after Quinn (2014). A few regions in the North-West quadrant *(a)* are indicatively shown as follows: *(1)* - Marquesas Islands - Hawai'i Islands - Kamchatka; *(2)* - Vancouver - Seattle; *(3)* - "*Farallon hyper-volcano*"; *(4)* - northward extension towards California of the Easter Island superswell; *(5)* - Hudson Bay; *(6)* - Caribbean Islands - Perù; Barbados - Bermuda - Greenland; *(7)* - Terranova; *(8)* - Fernando de Noronha; *(9)* - North Atlantic *MOR*. Several very sharp "double E-eye" patterns are observed, including Farallon, Hudson and Terranova. In the South-West quadrant *(b)* the codes are: *(1)* - Tuamotus Islands - northward; *(2)* – New Zealand - Line Islands or Teraina Islands or Equatorial Islands; *(3)* - Andes - Easter Island; *(4)* - "Southern belt"; *(5)* – South Atlantic superswell. A small white circle denotes Easter Island at the center of its huge superswell. Unpublished figure.

NCGT Journal
New Concepts in Global Tectonics

New Concepts in Global Tectonics Journal
Volume 14, Number 1, January 2026

ISSN number; ISSN 2202-0039

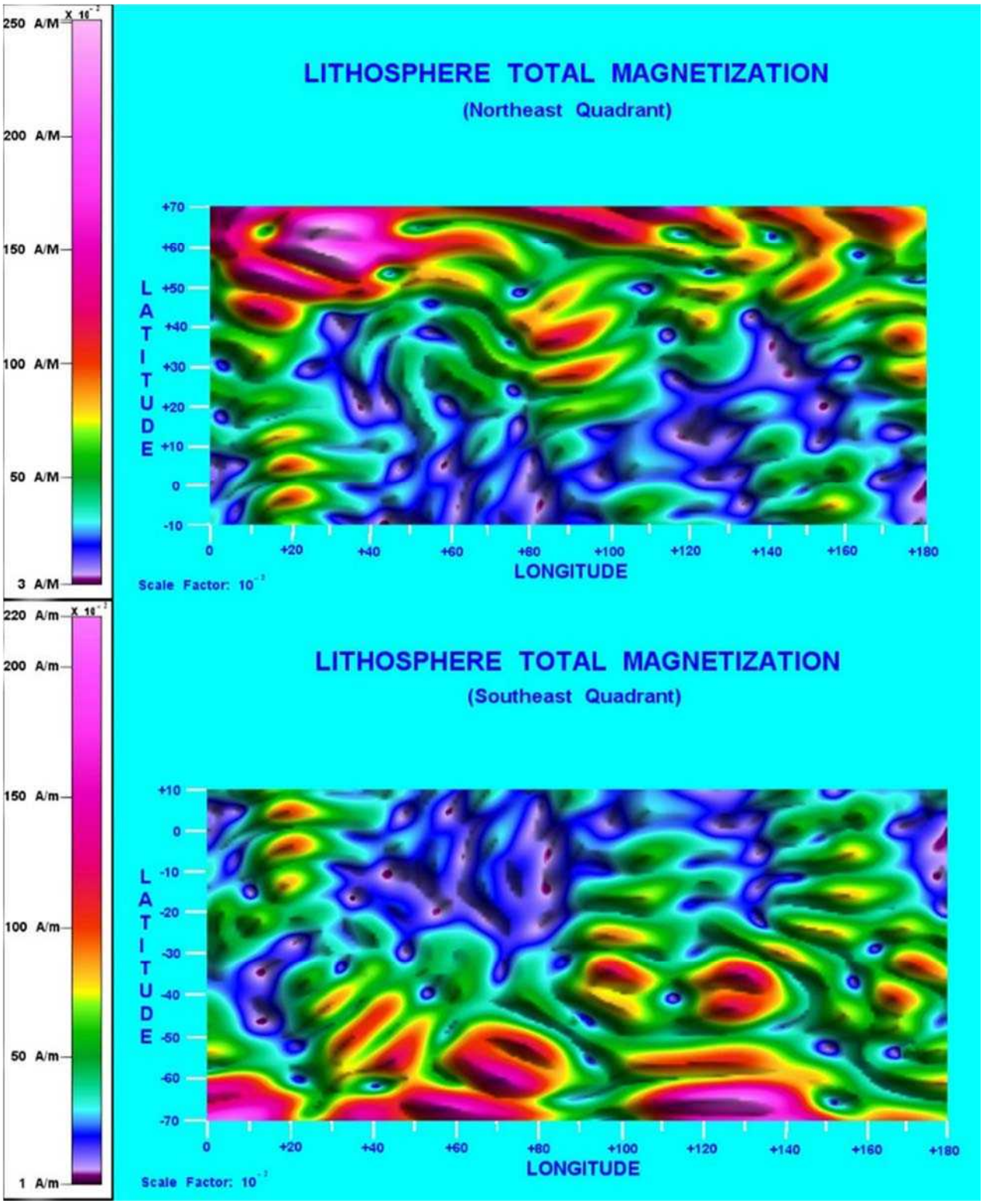

Fig. 70. Lithosphere total magnetization for the eastern hemisphere (longitude span $0°E - 180°E$; latitude span $70°S - 70°N$). *[upper]* Northern hemisphere; *[lower]* Southern hemisphere. After Quinn (2014).

NCGT Journal
New Concepts in Global Tectonics

New Concepts in Global Tectonics Journal
Volume 14, Number 1, January 2026

ISSN number; ISSN 2202-0039

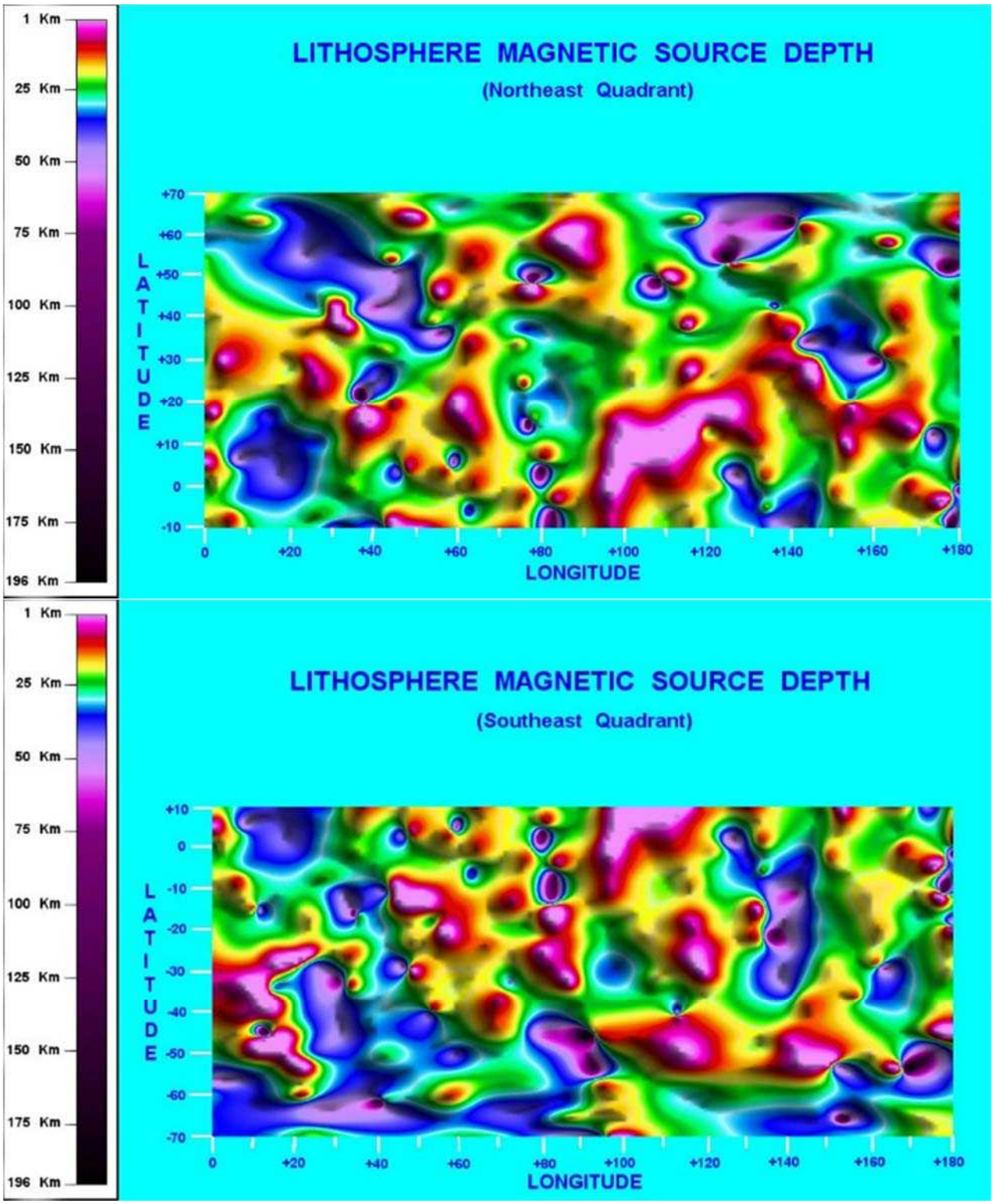

Fig. 71. Lithosphere magnetic source depth for the eastern hemisphere (longitude span $0°E - 180°E$; latitude span $70°S - 70°N$). *[upper]* Northern hemisphere; *[lower]* Southern hemisphere. After Quinn (2014).

NCGT Journal
New Concepts in Global Tectonics

New Concepts in Global Tectonics Journal
Volume 14, Number 1, January 2026

ISSN number; ISSN 2202-0039

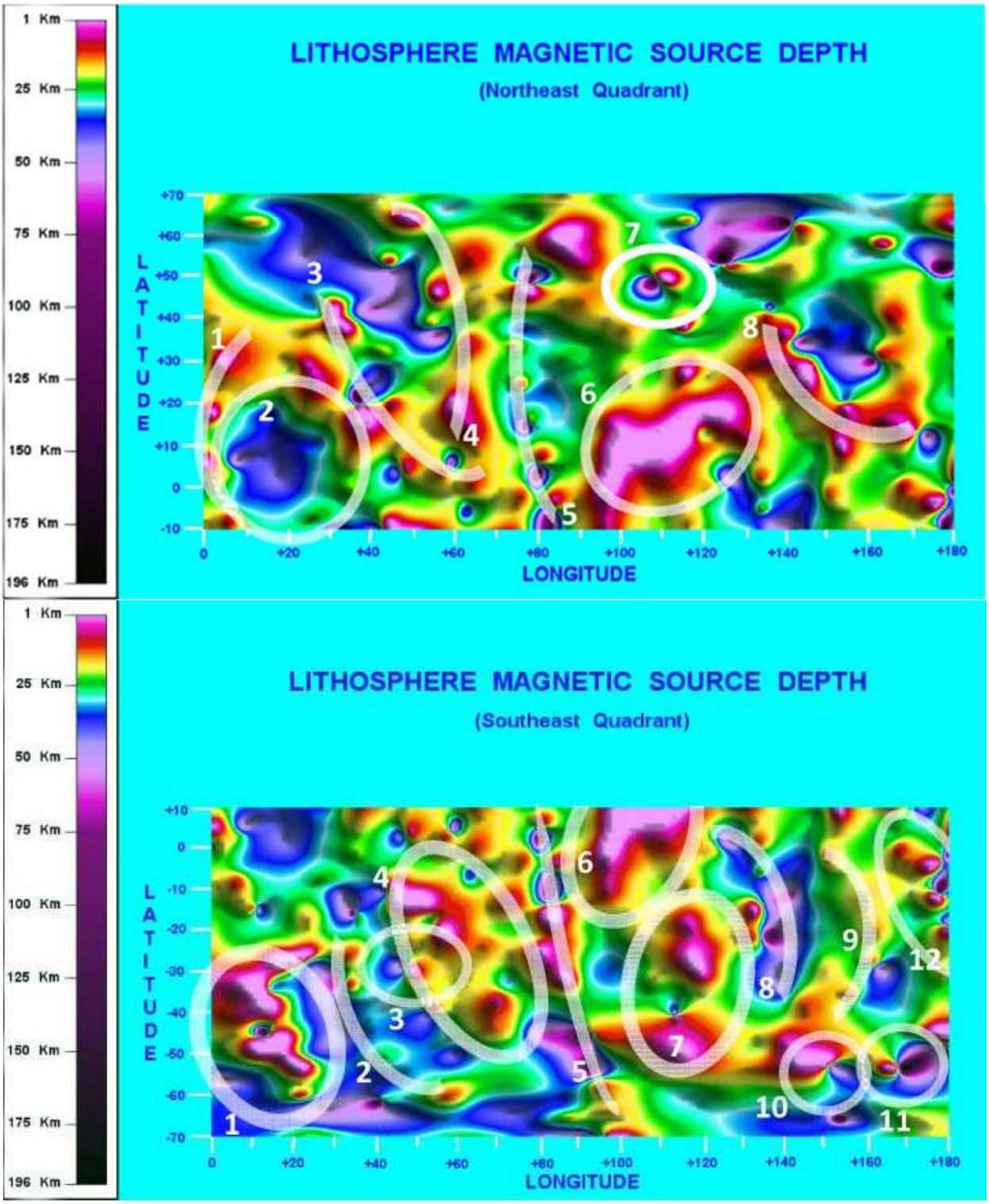

Fig. 72. Lithosphere magnetic source depth for the eastern hemisphere (longitude span $0°E - 180°E$; latitude span $70°S - 70°N$). *[upper]* Northern hemisphere; *[lower]* Southern hemisphere. Duplicate of Fig. 71 aimed to pinpoint specific features at Earth's surface. Modified after Quinn (2014). For codes and comments see text. In the North-East quadrant several very sharp "double E-eye" patterns are observed, including Zagros Mountains, Kargasok (Siberia), and Baikal Lake. In the South-East quadrant, several sharp "double E-eye" patterns are observed, including South Madagascar, southern Indian *MOR*, Western Australia, MacQuarie Island, and Campbell Island. The "double E-eye" pattern seems to be a frequent morphological feature through the whole Pacific Ocean.

NCGT Journal
New Concepts in Global Tectonics

New Concepts in Global Tectonics Journal
Volume 14, Number 1, January 2026

ISSN number; ISSN 2202-0039

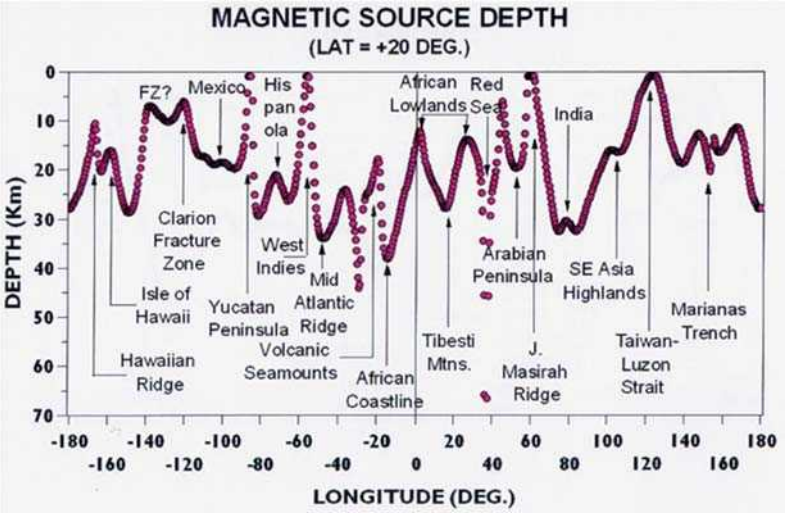

Fig. 73. Magnetic source depth profile along $20°N$ latitude. After Quinn (2014).

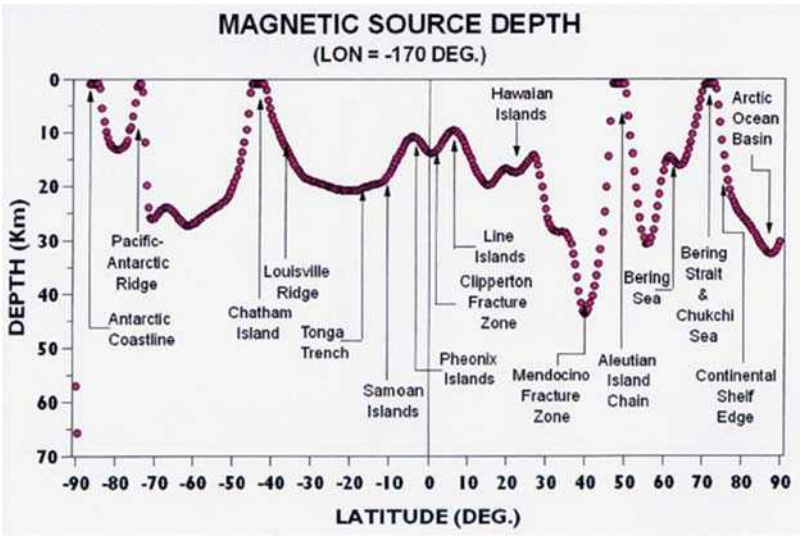

Fig. 74. Magnetic source depth profile along $170°W$ longitude. After Quinn (2014).

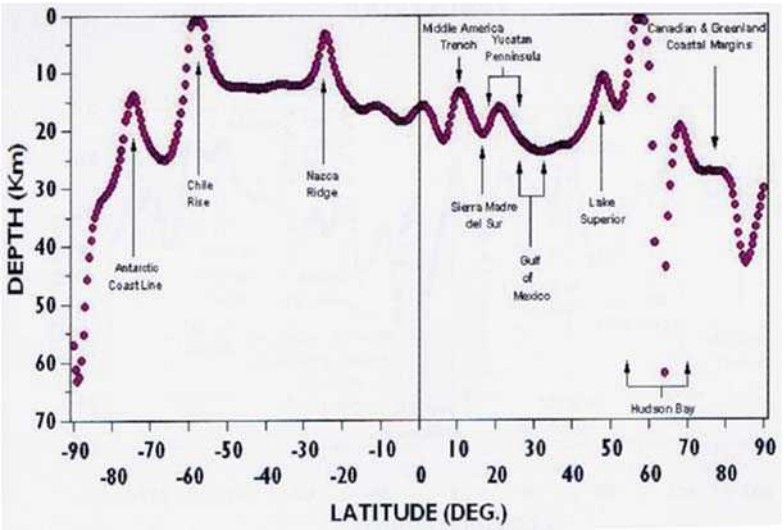

Fig. 75. Magnetic source depth profile along $90°W$ longitude. After Quinn (2014).

NCGT Journal
New Concepts in Global Tectonics

New Concepts in Global Tectonics Journal
Volume 14, Number 1, January 2026

ISSN number; ISSN 2202-0039

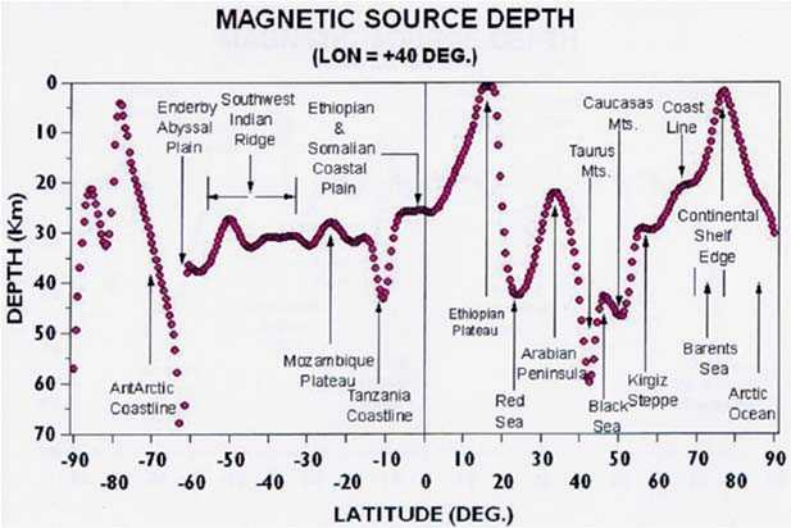

Fig. 76. Magnetic source depth profile along $40°E$ longitude. After Quinn (2014).

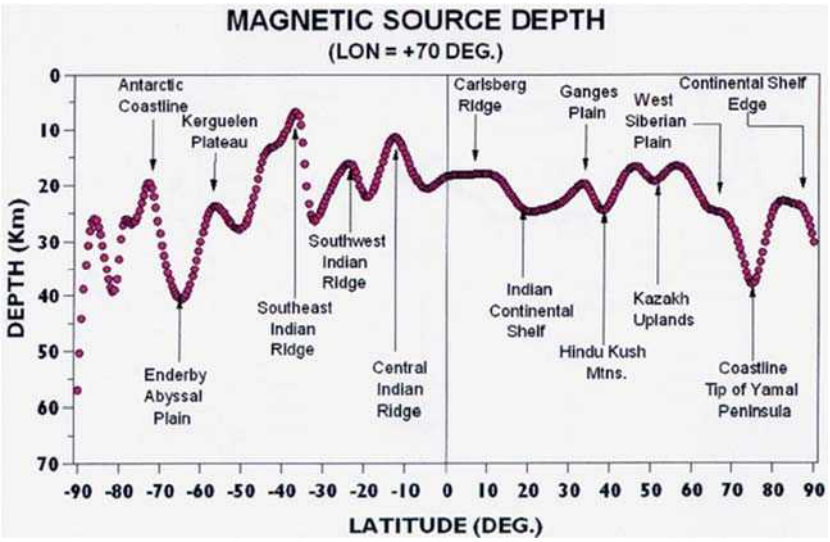

Fig. 77. Magnetic source depth profile along $70°E$ longitude. After Quinn (2014).

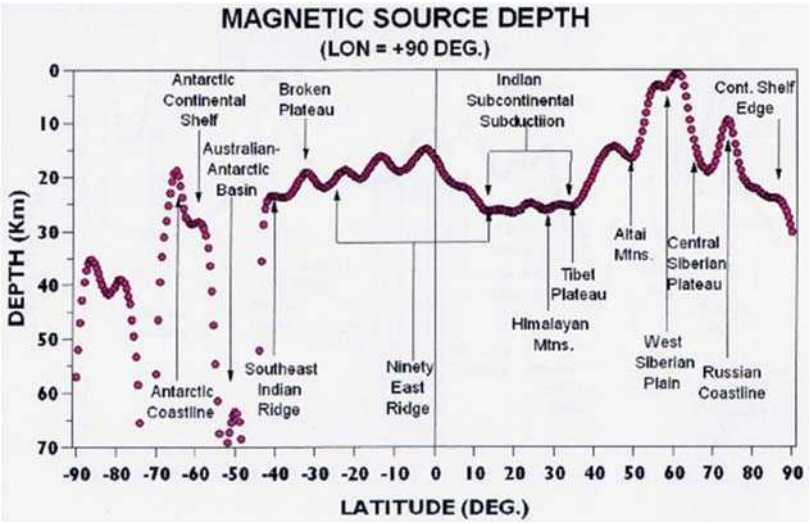

Fig. 78. Magnetic source depth profile along $90°E$ longitude. After Quinn (2014).

The term "Southern belt" denotes a longitudinal pattern, beginning from the southern *MAR*, and extended in longitude between $\sim 40° - 160°W$, reminding about the Circum-Antarctic *MOR*, although it is not interrupted by the Antarctic Peninsula and by the Scotia Arc. That is, it appears that the Circum-Antarctic *MOR* can be, perhaps, a pattern extended 360° in longitude, although its morphology is corrupted by shallow phenomena close to Earth's surface. See Gregori and Leybourne (2021).

NCGT Journal
New Concepts in Global Tectonics
New Concepts in Global Tectonics Journal
Volume 14, Number 1, January 2026
ISSN number; ISSN 2202-0039

However, the most impressive feature is, maybe, the huge extension of the Easter Island superswell that is extended northward until California, consistently with the discussion given in Gregori and Leybourne (2021).

Quinn (private communication, 2015) comments that "*the magnetic source-depth images show many well-known geologic features such as islands like Fiji, ocean trenches such as the Marianas, and ridges such as the mid-Atlantic, as well as new features such as the Farallon volcano. These are presented with unusual clarity, especially when the full resolution of the inversion is allowed to show through by selecting small geographical areas to image.*"

If the interpretation here given is correct, some conspicuous air-earth currents really appear to be a widespread characteristic on the planetary scale. However, owing to the limited spatial resolution (a few hundred kilometers) of these maps computed by *SH* terms up to degree and order ≤60, all air-earth currents that are shown by Figs 67 through 72 are representative only of some large-scale mean values. They are smoothed over some large area, and averaged over 6 $months$ of "quiet" time ***B*** records.

The codes in the North-East quadrant in Fig. 72*(a)* are as follows: *(1)* - Ghana - Algeria; *(2)* – Central Africa (blue pattern); *(3)* - Aegean - Red Sea - Maldives Islands; *(4)* - Zagros Mountains - Aral Sea; *(5)* - Chagos Islands - India - Kargasok (Siberia); *(6)* - Indonesia - Japan; *(7)* – Baikal Lake; *(8)* - Japan - Marianas Islands - Marshall Islands. Several very sharp "double E-eye" patterns are observed, including Zagros Mountains, Kargasok (Siberia), and Baikal Lake. Concerning the Baikal Lake, remind about the Leybourne's guess that the Baikal Lake is a "cryogenic pump" for climate control.

The codes in the South-East quadrant in Fig. 72*(b)* are: *(1)* - Walvis Ridge; (2) - South Africa - Kerguelen; *(3)* - South Madagascar; *(4)* - Kerguelen - Madagascar; *(5)* - Indian *MOR*; *(6)* - Indonesia; *(7)* - Western Australia; *(8)* - Adelaide - Indonesia; *(9)* – Tasmania - New Guinea; *(10)* - MacQuarie Island; *(11)* - Campbell Island group; *(12)* - Cook Islands - Line Islands, or Teraina Islands, or Equatorial Islands. Also in this case, several sharp "double E-eye" patterns are observed, including South Madagascar, southern Indian *MOR*, Western Australia, MacQuarie Island, and Campbell Island. The "double E-eye" pattern seems to be a frequent morphological feature through the whole Pacific Ocean.

Consider also that - if this interpretation is correct, - the screening by the ocean water is not sufficient to reduce the impact of soil exhalation on the atmospheric electrical circuit. Therefore the phenomenon cannot be considered like a lesser disturbance with respect to some speculated first-order approximation in terms of approximately null air-earth currents.

Other large-scale evidences of air-earth currents – TEC *observations*

A confirmation seems to be given by an investigation by the late Dong Choi (Choi, 2017) when analyzing seismicity in the Fiji-Tonga-New Zealand region. His study deserves special attention, as it is relevant also for discussions in Parrot (2025), Straser et al. (2026), Wu (2025), Gregori et al. (2025h) concerning the coupling between soil and ionosphere when dealing with earthquake precursors.

Choi (2017) reports observations of *TEC* (total electron content) in the ionosphere indicative of a large flow of electric currents (air-earth currents) between soil and ionosphere. *TEC* is the total number of electrons integrated between two points, along a tube of one meter squared cross section, i.e., it is the electron columnar number density. The so-called *TEC* unit is defined as $TECU = 10^{16}\ el\ m^{-2}$ (e.g., Hofmann-Wellenhof et al., 2001).

From Choi (2017). "*A conspicuous* TEC *high anomaly has been observed since at least early 2017 to present (June 2017), in the northwestern offshore area of New Zealand (Figs 79 and 80). This prominent long-term isolated anomaly appeared most remarkably in ionospheric* TEC *maps posted by* JPL. *Other* TEC *maps provided by* Space Weather Services, Bureau of Meteorology*, Australia and* US Weather Prediction Center *(*CTIPE *mode, or* Coupled Thermosphere, Ionosphere, Plasmasphere and Electrodynamic*) did not show this anomaly or, if appeared, only faintly. The latter two were generated with models, whereas the former does not involve models and is generated by* 'interpolating the *6-8* simultaneous *TEC* measurements obtained from each *GPS* receiver every 30 sec' *(https://iono.jpl.nasa.gov/gim.htm). Because of this very nature of the* JPL*'s* TEC *maps, they most sensitively respond to deep Earth structures. Actually, the* TEC *anomaly patterns were found harmonious with deep geological structures and geophysical data (Fig. 81).*

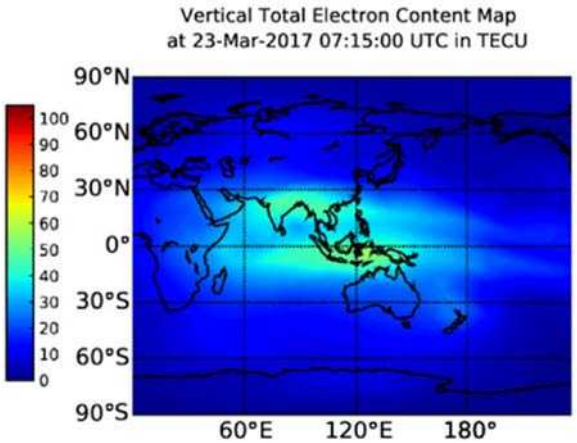

Fig. 79. "*Vertical ionospheric total electron content map, 23 March 2017, 07:15:00, posted by* JPL. *The local time at Jakarta is 13:15 (or 1:25 pm) for this specific* UTC *(London). High anomaly pattern around* 30 TECU *has been persistently maintained until the end of June 2017, at least for over four months. Note a linear NW trending higher zone, which roughly runs in parallel with a deep-seated fault zone, Vening Meinesz Fracture Zone, Fig. 81.*" Figure and captions after Choi (2017). With kind permission of *NCGT.*

[Note that, also in this case, the importance is stressed to refer to observational data that ought to be independent of every kind of modeling. The reason is that every model relies on some general rationale and "reasonable" averaging. Therefore, a model is suited to represent and interpret a smooth mean trend, while outliers are almost

New Concepts in Global Tectonics Journal
Volume 14, Number 1, January 2026

ISSN number; ISSN 2202-0039

cancelled by smoothing. In contrast, sometimes outliers are more significant than their smooth background.]

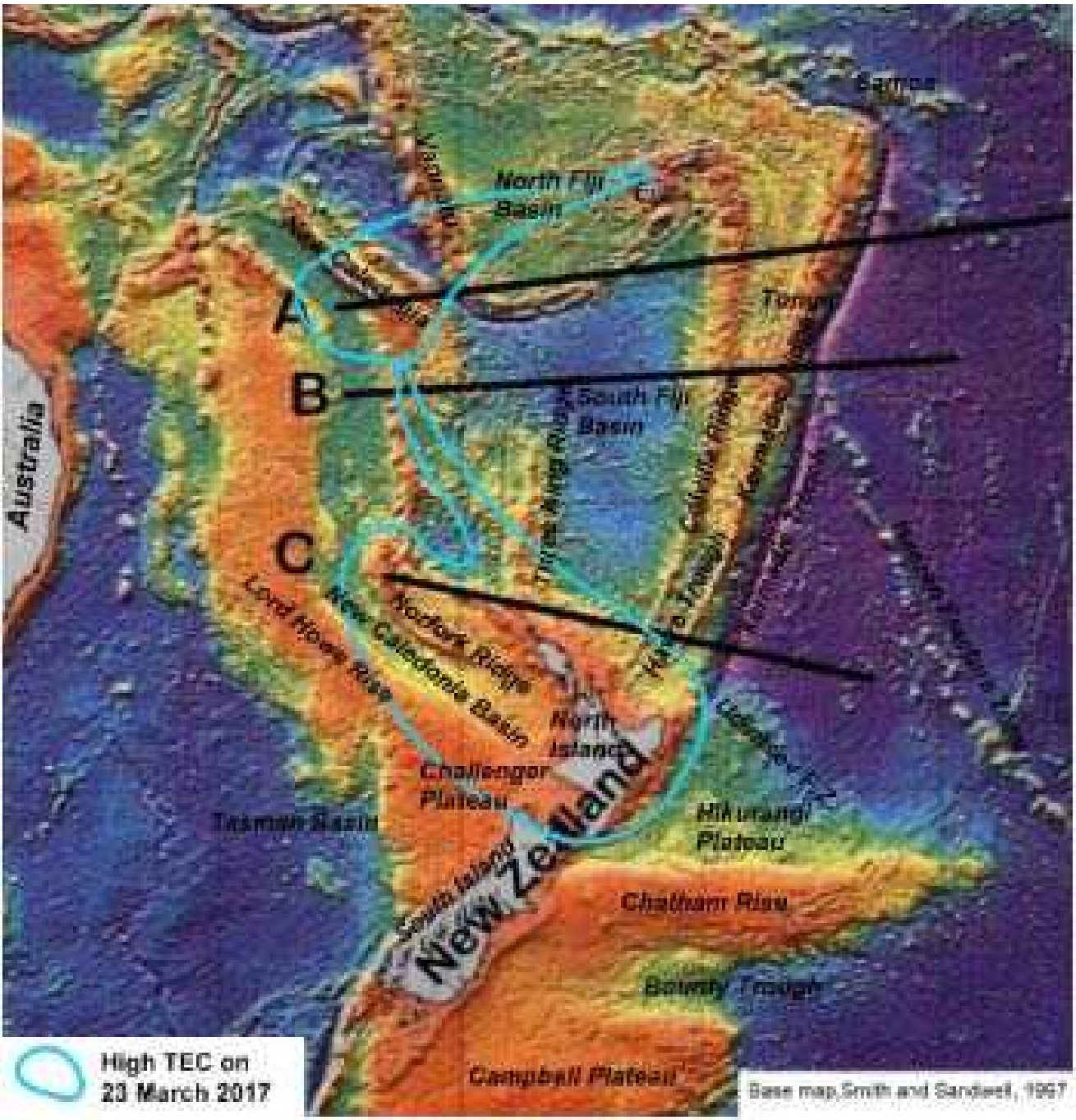

Fig. 80. "*Bathymetry of the study area and a generalized distribution of high* TEC *area (Fig. 79) drawn based mainly on the 23 March 2017 image (encircled by blue line). The high* TEC *covers the Norfork Ridge, Challenger Plateau and North Island of New Zealand.* A, B, *and* C *are tomographic profile lines of van der Hilst (1995), see Fig. 81.*" Figure and captions after Choi (2017). With kind permission of *NCGT*.

NCGT Journal
New Concepts in Global Tectonics

New Concepts in Global Tectonics Journal
Volume 14, Number 1, January 2026

ISSN number; ISSN 2202-0039

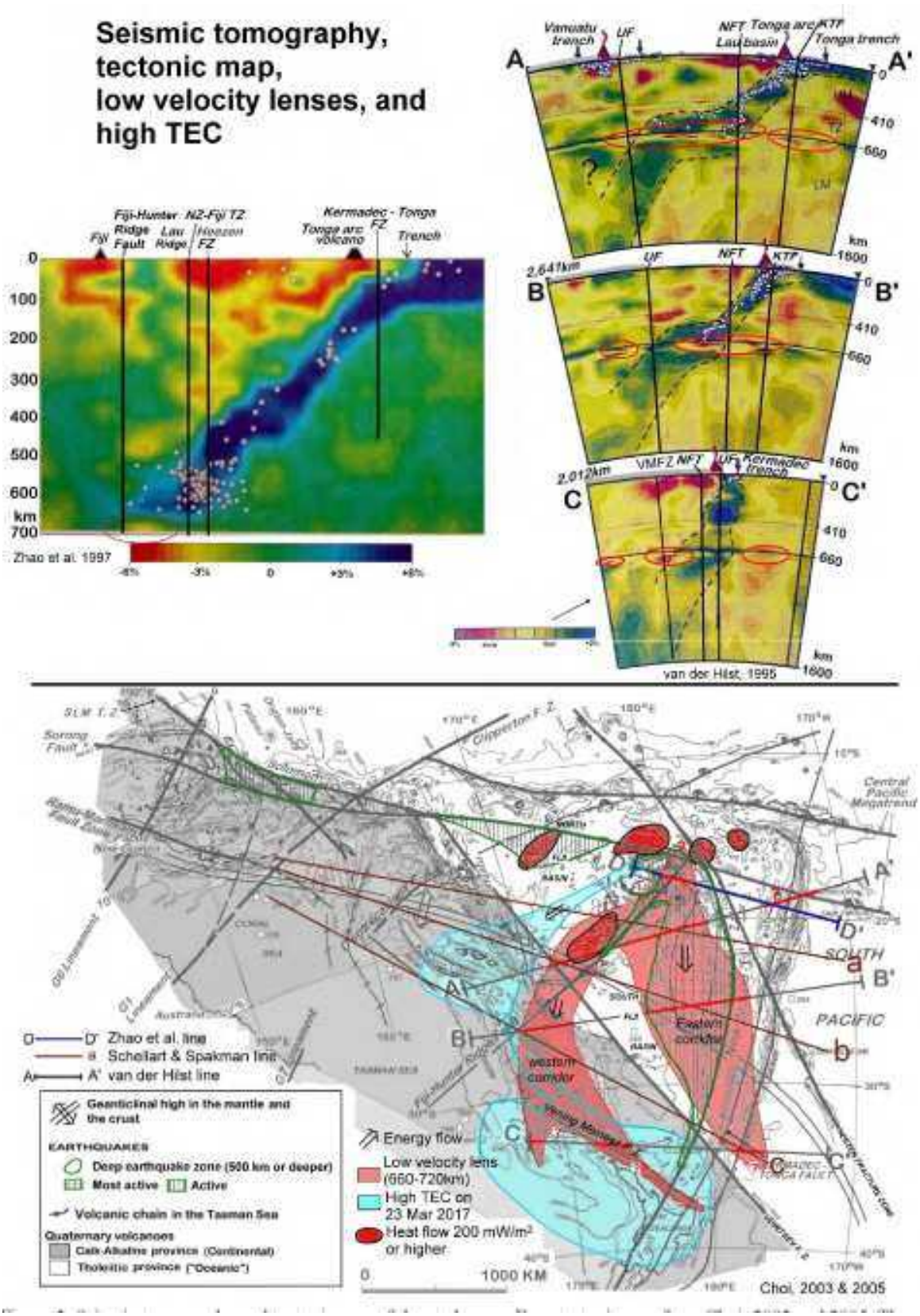

Fig. 81. "*Seismic tomography and tectonic map of the study area. Base tectonic map from Choi (2003a, 2005). The anomalous* TEC *area and the* $660-720$ *km lenses are superposed. Note that the low velocity lenses (*LVL*s) are emanating from north of Fiji Islands where three deep fracture systems meet and the highest heatflow is observed. The* LVL*s in tomographic profiles are emphasized by red circles in the top two figures*." Figure and captions after Choi (2017). With kind permission of *NCGT*.

NCGT Journal
New Concepts in Global Tectonics
New Concepts in Global Tectonics Journal
Volume 14, Number 1, January 2026
ISSN number; ISSN 2202-0039

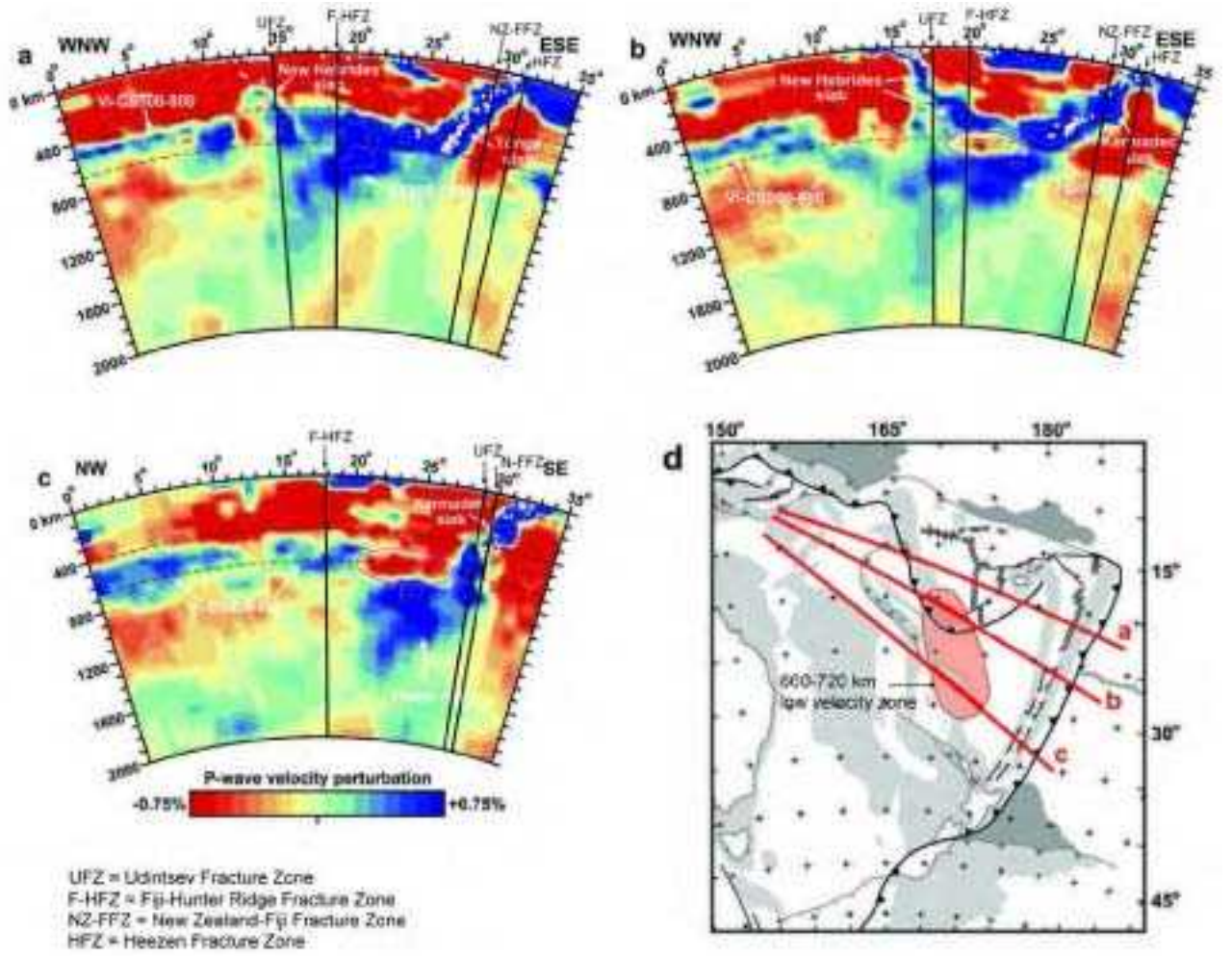

Fig. 82. "*Another set of seismo-tomographic profiles by Schellart and Spakman (2012) in the study area. Major deep fracture zones are superimposed. The* LVL*s at* $580-700\ km$ *(circled for emphasis by Choi) between latitudes* $20°-27°$ *thickens and widens southward where it fuses with overlying low velocity mantle. Note the lack of this* LVL *in the northernmost line, Line-*(a)*. Among the major fracture zones, Udintsev Fracture Zone (*UFZ*) clearly affects the mantle structure - vertical fast mantle developed along the fracture zone, and earthquake distribution is also affected. The* UFZ *also bounds the calc-alkaline province (continental) and the tholeiitic (oceanic) province (Fig. 81). Also note the compartmented fast mantle zone (intervened by slow mantle) at* $400-500\ km$ *in profile* (c)*, above which a swarm of earthquakes develops. The distribution of the* $660-720\ km$ LVL *based on the Schellart and Pakman profiles (bottom right figure) show somewhat different distribution pattern from that of van der Hilst and Zhao et al. profiles (Fig. 81). The former roughly matches the western corridor of the latter.*" Figure and captions after Choi (2017). With kind permission of *NCGT*.

The JPL*'s* TEC *images on 23 March 2017, particularly the one at 07:15 UTC (Fig. 79), showed a most remarkable anomaly pattern: a distinctive linear NWSE trending high with its northern end touching another broader high. The similar high anomalies have kept appearing at least in the last four months until late June 2017*."

According to the rationale of the present study, the interpretation of this evidence relies on a diffuse presence of sea-urchin spikes through the high *TEC* regions in Figs 79 and 80, or in the pink/red regions of Fig. 81, i.e., in the low velocity lenses (*LVL*s) and in the high heatflow areas.

Choi (2017) correctly stresses that, compared to the well-known spacetime dependence on solar radiation, this observed *TEC* trend is anomalous. This envisages an origin other than the Sun (in fact, this effect is due to air-earth currents).

Then, Choi (2017) considers in detail several available seismic profiles for this region. "*They are works by Kawakami (1994) and Ohbayashi (introduced in the frontispiece of Tsunoda, 2009, 2009a) for the whole Earth tomography. For the Southwest Pacific, three works, van der Hilst (1995), Zhao et al (1997), and Schellart and Spakman (2012) were used (Figs 81and 82).*"

Choi (2017) claims that he "*has expressed an opinion that the fast (blue) and slow (red) patterns in tomographic images reflect the content of gas/fluid (or level of chemical depletion) in the mantle (Choi, 2005, p. 103-106). The presence of even a very small amount (*1% *or less) of gas/liquid dramatically reduces seismic wave propagation speed. This is the very attribute used for detecting hydrocarbons in seismic profiles*. [This reminds about the crucial role of water in the definition of the Moho and of the *ALB*, as envisaged in Gregori et al. (2017b; 2025a).] *He considers that the low velocity layers, colored red in tomographic profiles, is effectively a closed system with gas/fluid (supercritical water?), or partial melt of global*

New Concepts in Global Tectonics Journal
Volume 14, Number 1, January 2026
ISSN number; ISSN 2202-0039

asthenosphere in the upper part of the lower mantle, 700-1000 km *(see Gordienko, 2015a, 2015b, and 2017)."*

Focus on Fig. 82. The red layers express the more brittle or solid - hence less plastic - layers, where the seismic velocity is larger. These layers are generally found in the shallower crust. In contrast, the blue layers reflect the more plastic, i.e., warmer, medium. Indeed, the sea-urchin spikes are warmer: they ought to appear blue. Wherever a sea-urchin spike affords to get closer to Earth's surface, the maximum Joule heat occurs right on top of the sea-urchin spike. Hence, right on top of a sea-urchin spike, i.e., of a blue upraising plume in Fig. £82, a *LVL* is to be expected: this is confirmed by the profiles *(b)* and *(c)* in Fig. 82. These profiles cross through the *LVL* as shown in Fig. 82d.

Note that this sea-urchin spike mechanism implies soil exhalation of electrons that supply air-earth currents originating the *TEC* anomaly. That is, this phenomenon occurs wherever the crust is more fractured - due to the thermal expansion caused by the inner heat originated by the sea-urchin spikes. In addition, no evidence is found that envisages a downward penetration of surface fluids, according to Choi (2017) who comments as follows.

"*On the other hand, the high velocity area or blue area indicates an open system with little gas/fluid or depleted mantle. It is ultimately connected to the Earth surface. This is supported by the fact that the fast mantle is often located along deep fracture zones that reach the Earth surface in tomographic images. Wadati-Benioff zone is one of the typical cases for this. It developed along the thrust or reverse fault zones: it was formed during the relative subsidence of the oceanic area and the rise of continental margins since Mesozoic (Choi, 2005). Here, attention must also be paid to innate problems with tomographic images derived from different models applied as pointed out by Foulger et al. (2015, 2015b)."*

Another relevant physical feature - at several hundred kilometer depth - is typical of these phenomena, and is consistent with the role of the serpentosphere that determines the formation of the *ALB* at a planetary mean depth of, say, *~ 80 km*, being the upper boundary of the serpentosphere (see Gregori et al., 2017b, Gregori and Leybourne, 2021, and Gregori and Hovland, 2024).

Another relevant physical issue is the different behavior, compared to heavy ions or molecules, of electrons released from soil. For instance, CO_2 exhalation from the Pacific Ocean floor - which occurs roughly in the region of the Hawai'i hotpot - is spread by ocean water circulation, and it is finally manifested as an increased CO_2 atmospheric concentration close to the Alaska coast (see Gregori, 2020 and references therein). The behavior of electrons is different, as they immediately short-circuit through air-earth currents with the ionospheric current system, and are thus responsible for the *TEC* anomaly of Fig. 79.

Choi (2017) carries out also a careful 3D analysis of the tectonism of this large region. His target is the investigation of seismic energy transmigration. Choi (2017) claims that "*the* LVL*s developed immediately below the deep earthquakes zone (Fig. 81) suggest that the earthquake energy is stored in and supplied directly from these thin lenses lying just below the upper-lower mantle boundary at* 660 km*.* [In fact, according to *WMT*, these *LVL*s are the tops of the geotumors and the lithosphere slides radially around them.] *This interpretation becomes more plausible if we take the* LVL*s as zones of partial melt (Gordienko, 2015a and b, and 2017), surge channels by Meyerhoff Hull (1996), or the top points of the sea-urchin model by Gregori (2009), which carry electric thermal energy ...* "

This region (Fig. 81) - maybe owing to the intense geothermal flow - is the presently best understood case history of tectonism according to the general rationale of the present paper. It is therefore worthwhile to report here in detail the inferences by Choi (2017).

Note that the leading rationale of the present paper is the upward thermal expansion of a geotumor, with subsequent sliding of the lithosphere along its slopes, on the lubricated *ALB*. The effect is seismic activity in the surrounding areas. This results into energy transmigration.

"*The most outstanding discovery is the energy source area in the North Fiji Basin, particularly north of Fiji Islands where three deep fracture systems meet. This is reasonably inferred from the* LVL *distribution as well. The area has also been known as a place where the world highest marine heatflow appears.* [This observational information is very important for the present discussion.] *Seismic tomography too suggests deep fractures reaching over* 2000 *km below which slower mantle occupies towards the bottom of the mantle. The most spectacular deep fracture zone that reaches the* CMB *was illustrated by Karason and van der Hilst (2001) in a profile across the Caribbean (see Choi, 2014f). Furthermore, the eastern corridor of the* LVL*s almost perfectly overlaps the* 500 *km + deep earthquake distribution in the South Fiji Basin.*

... the western corridor LVL *was linked to the concerned* TEC *anomaly in the offshore area of New Zealand. Another large high* TEC *body running north of Fiji-Hunter Ridge Fault (Choi, 2005, p. 94) in roughly E-W extension also emanates from the northeastern North Fiji Basin. This fact suggests the energy of this* TEC *anomaly was also originated from the same area.*

... we can recognize almost total match between geological, seismological, geophysical, and tomographic data. They convincingly prove that the LVL*s and the concerned* TEC *anomaly are connected to the Fiji area where energy upwelling is occurring from the* OC.

This study also shows a decisive role of deep fractures in determining the site of original energy, energy transmigration, and earthquake distribution. Among them, two NW-SE trending deep fault zones were found most significant:

1) *Udintsev Fracture Zone (*UFZ*) affecting the deep mantle velocity structure to over* 2000 *km depth and seismic foci distribution above* 660 *km as well. At the surface, it bounds the continental (west) and oceanic (east) provinces (Figs 81 and 82). Its influence is clearly felt in the earthquake foci distribution in the latitude-depth profile (Fig. 83).* [Note that this transmigration of seismic shocks derives from the upward propagation of the sea-urchin spike due to Hamilton's variation principle.]

NCGT Journal
New Concepts in Global Tectonics

New Concepts in Global Tectonics Journal
Volume 14, Number 1, January 2026

ISSN number; ISSN 2202-0039

2) *Vening Meinesz Fracture Zone. This fault zone reaches over* 700 km *in depth, as seen in the distribution of the* LVL *western corridor which follows the Vening Meinesz Fracture Zone in the northwest New Zealand (Fig. 81). The earthquake foci distribution clearly shows the impact caused by the Fracture Zone; relatively deep quakes (>* 140 km*) in the south of the Fracture Zone cannot be explained by seismic energy solely coming from the South Fiji Basin deep source where* 5000 + km *quakes are nested (Fig. 83). Another energy input must be taken into account; it is obviously the arm of the western corridor.* [Note that the phenomenon is not associated to one sea-urchin spike alone. Rather, different bunches of sea-urchin spikes simultaneously experience an increase of their respective energy supply. Thus, all consequent geodynamic phenomena are strengthened through some wide region.] *A conspicuous seismic gap is also recognized between the two Fracture Zones (Figs 83 and 84) supporting this assertion*. [Fig. 84 shows that phenomena are clustered according to the respective typical hypocenter depth of every phase during the evolution of the "transmigration" of the effect that is triggered by the uplifting sea-urchin spike.]

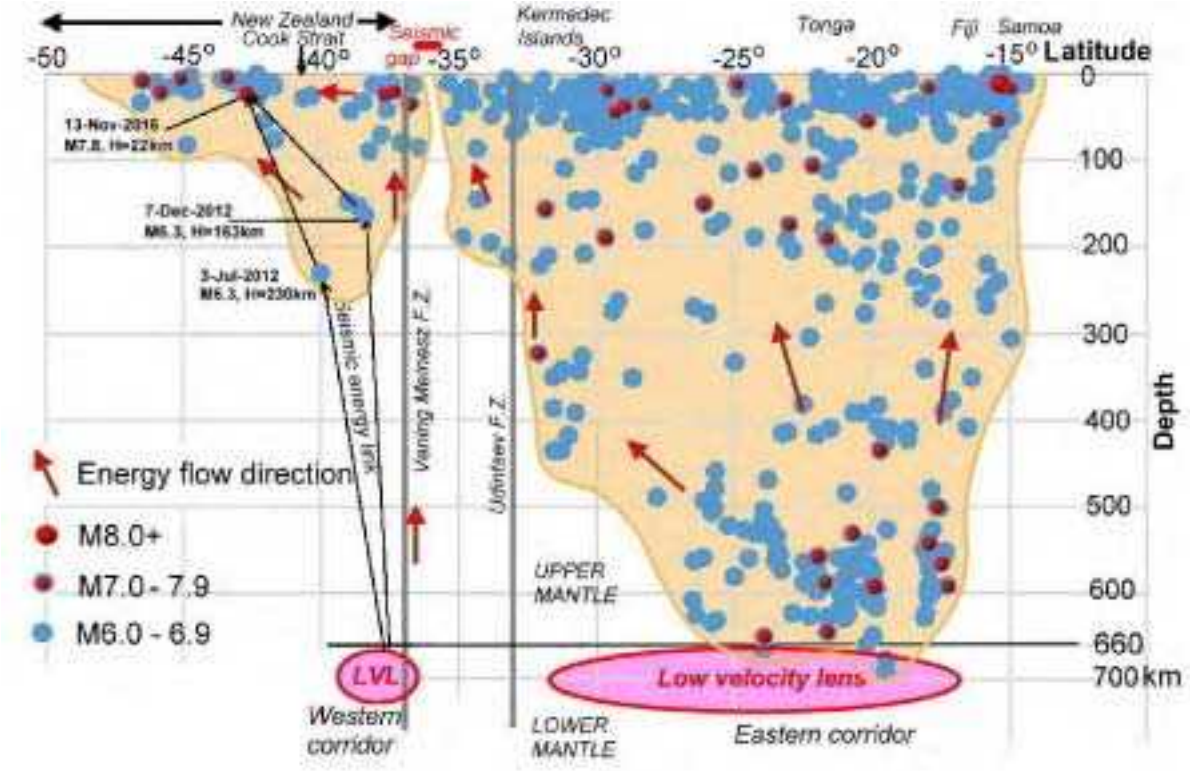

Fig. 83. "*Latitude - depth diagram of* $M = 6.0 +$ *quakes in Fiji-Tonga-New Zealand, showing two different energy channels operating in the region. Note the influence of Udintsev and Vening Meinesz Fracture Zones on earthquake foci distribution, and a seismic gap between them (see also Fig. 84). A stepwise rise of earthquake foci distribution at the boundary of* UFZ *is seen. The eastern* LVL *supplied energy for earthquakes in the Tonga-Kermadec Islands, and the western* LVL *for New Zealand quakes. The gigantic Kaikoura earthquake (*$M = 7.8$*) in 2016 is considered the result of convergence of two deeper seismic energies which manifested in 2012 in the Cook Strait and the North Island."* Figure and captions after Choi (2017). With kind permission of *NCGT*.

The anomalous TEC *pattern appeared in the early half of 2017 is now interpreted to be energetically related to the western corridor. One of the strong surges of the Earth's* OC *energy originated in the North Fiji Basin has transmigrated through the* LVL*, and reached the northwestern offshore New Zealand before early 2017. The same energy is considered to have generated a strong jet stream anomaly appeared on 11 February 2017 over the Cook Strait.*[6] *The whale beaching coincides with this day ...* "[See Wu, 2024]

[Note, however, that - as already stressed - in general the synchronism is expected to increase the energy supplied to every spike of several bunches of sea-urchin spikes. Hence, the energy transmigration can mainly be related to the sliding of the lithosphere from geotumors towards megasynclines, rather than by a timing in the energy supply to different sea-urchin spikes.]

Choi (2017) also discusses the relationship with some recent earthquakes in this region. However, Dong Choi (private communication, 2017) envisages that an

[6] Wu, https://www.facebook.com/photo.php?fbid=*1353977567987622&set=a.657516484300404.1073741826.100001261760990&type=3&theater*.

NCGT Journal
New Concepts in Global Tectonics
New Concepts in Global Tectonics Journal
Volume 14, Number 1, January 2026
ISSN number; ISSN 2202-0039

earthquake [7] that struck slightly south of the Auckland Islands was related with the *TEC* anomaly of Fig. 79. In fact, this ought to be roughly along the boundary of the crustal stress region affected by the geotumor. However, the seismic details are not directly relevant for the present discussion. Rather, it is interesting to compare the Dong Choi's *LVL* with the maps drawn by John Quinn (Fig. 85).

Except the "double E-eye" of the Fiji Islands, this region shows no anomalous feature in the Quinn's maps, envisaging that air-earth currents occur where lithosphere and crust are crossed by some volcanic island, i.e., by a bunch of sea-urchin spikes that uplifts a local small geotumor. In the opposite case, the excess Joule heat at the *ALB* is manifested like a *LVL* that affects seismology and geodynamics. In any case, the Choi maps are likely to reflect a spatial detail that the Quinn's analysis cannot achieve.

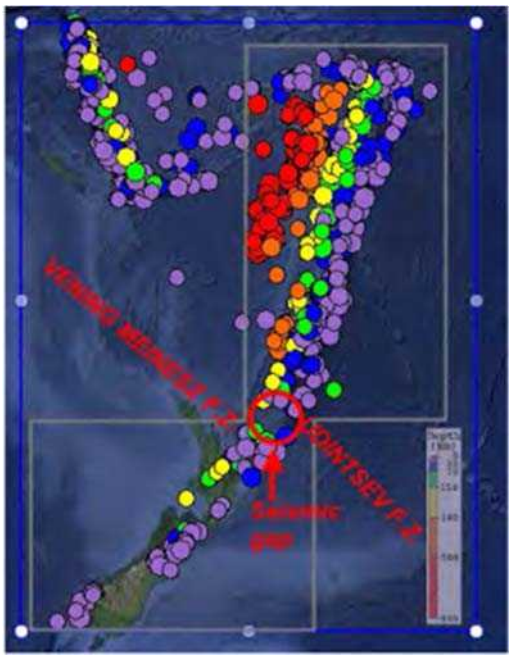

Fig. 84. *"$M = 6.0 +$ quakes from 1970 to 2016 (*IRIS *website;* http://ds.iris.edu/seismon*/). Data inside the frame were processed and plotted in Fig. 83. A seismic gap is observed between the Udintsev and Vening Meinesz Fracture Zones, see Fig. 81*" Figure and captions after Choi (2017). With kind permission of *NCGT.*

Comparing the air-earth current vs. *the volcanic/astrobleme explanation*

For comparison purpose, two analogies can clarify the state-of-the-art dealing with these huge air-earth currents. If one considers the mean water precipitation over some large region, he deals with a definitely negligible amount. In contrast, if the scatter is considered, both in space and time, the former negligible amount can justify even the most catastrophic floods, etc. Similarly, the geothermal heatflow is generally considered a negligible perturbation for climate energy balance. In contrast, it is the energetically most intense component in the energy budget of the Earth (see Gregori, 2002; Gregori and Leybourne, 2021; Gregori et al., 2025a). On the other hand, it displays also a violent scatter in space and time. The most evident case history is represented by volcanism: a volcano is a point-like feature at Earth's surface, and it can be "quiet" for several centuries. However, several other manifestations of a violent scatter characterize some phenomena that can be detected by their consequences (e.g., Palæoclimatic variations). In addition, consider that, compared to geothermal heat, volcanism plays only a tiny role in the Earth's energy balance. Hence, the much greater amount of geothermal energy must be released for the energy balance of the Earth, and this huge energy input into the Earth's atmosphere causes pressure and temperature effects that are not accounted as e.m. effects, like El Niño Southern Oscillation (Leybourne and Smoot, 2000; Leybourne and Adams, 2001). In effect natural global climate change has a large e.m. modulation component.

Much in the same way, locally, air-earth currents amperages are so tiny that it is very difficult - if possible at all - to detect them directly (see the discussion about measuring instruments in atmospheric electricity given in Gregori and Leybourne, 2025d). However, when the effect is monitored integrated over an area of linear size of a few hundred kilometers (or larger), Quinn's maps show that huge effects are propagated up to the ionosphere and the magnetosphere.

Let us just remark that the Fukushima theorem (see Gregori and Leybourne, 2025h) relies on an argument that shows that, by means of ground measurements alone, it is impossible to distinguish between a Chapman-Vestine current system and a Birkeland-Alfvén current system. However, the interpretation that is here proposed claims that *CHAMP* and ground based geomagnetic observatories are embedded in Birkeland-Alfvén current systems extended downward underground.

Differently stated, it is customary to correct satellite measurements of $\boldsymbol{B}$ in order to cancel solar effects and thus treating satellite records like ground-based observatory records. However, the paradigm of assuming a negligible mean effect of air-earth currents is an *a priori* assumption and satellite data are rejected if they violate this assumption. On the other hand, as shown in Fig. 3, in principle some $\boldsymbol{B}$ satellite records can avoid such a rejection process revealing air-earth currents. Quinn's maps show that, in reality, this is possible.

That is, these air-earth currents cannot be treated like the accidental occurrence of lightning discharges, i.e., deriving from any simple point-like occasional event. This key conceptual item requires harder thinking and critical evaluation of the details of mathematical data handling, but, owing to brevity purpose, this item cannot be here discussed. This conclusion poses serious logical constraints on the real physical meaning of the standard usual potential-model of the geomagnetic field and its *SHE*.

[7] 2017 July 11, 07:00:07.9 UTC, $49{:}30° S$, $164{:}34° E$, $15\ km$, $M = 6.6$, Auckland Islands, N.Z. region.

NCGT Journal
New Concepts in Global Tectonics

New Concepts in Global Tectonics Journal
Volume 14, Number 1, January 2026

ISSN number; ISSN 2202-0039

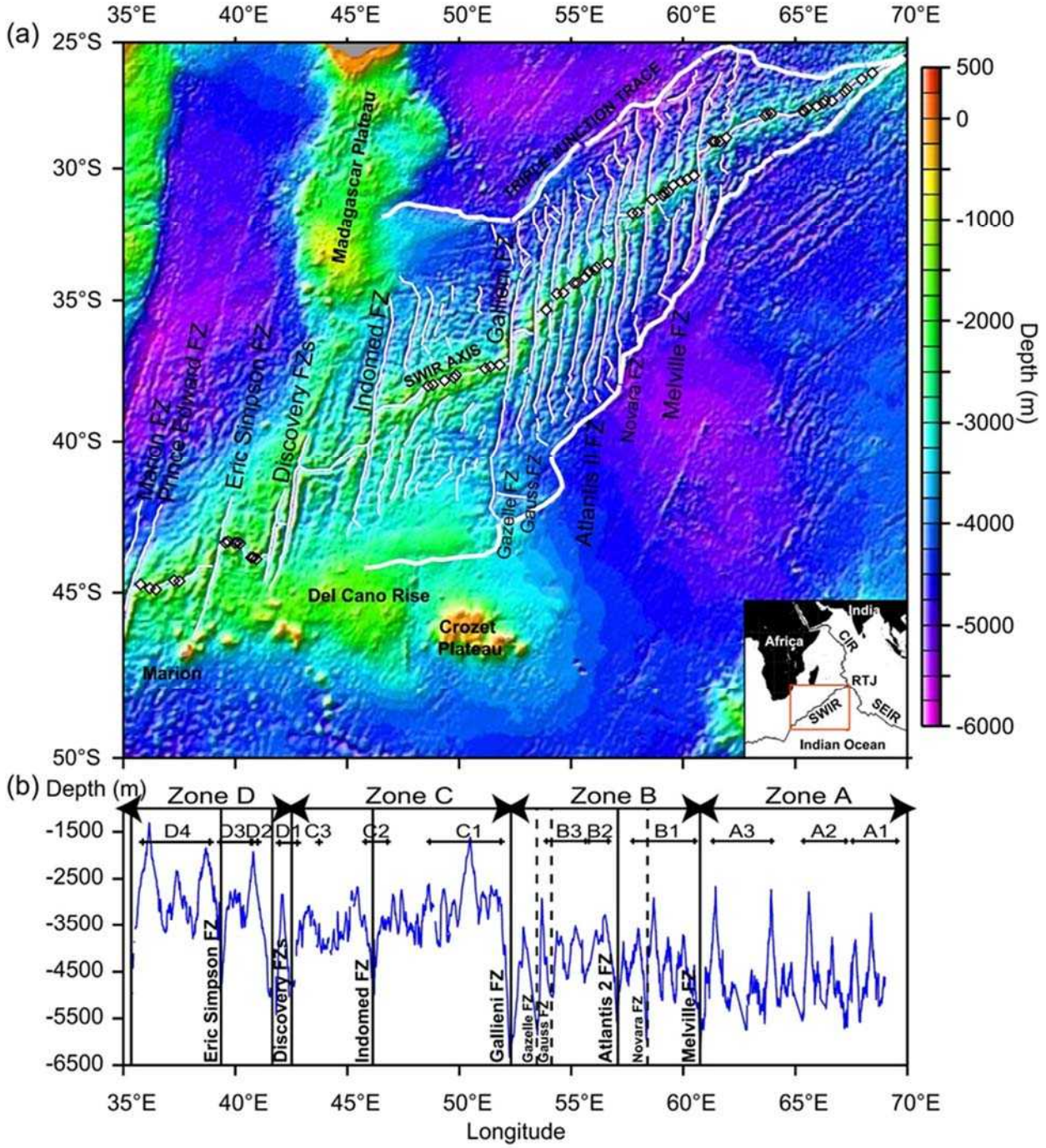

Fig. 85 - *"*(a) *Topographic map of the Southwest Indian Ridge (*SWIR*) from Smith and Sandwell (1997) showing sample locations used in this study (open diamonds).* (b) *Axial bathymetric profile* vs. *longitude (°E) (Cannat et al., 1999; Mendel et al., 2003). The zones defined by seafloor morphology variations are labeled A-D. Within these zones, isotopic domains are labeled by increasing number going westward. Major (continuous lines) and minor (dashed lines) fracture zones (*FZ*) are also shown. Inset shows regional location of the study area (box): Rodrigues Triple Junction (*RTJ*), Southeast Indian Ridge (*SEIR*), and Central Indian Ridge (*CIR*)."* Figure and captions after Meyzen et al. (2005). *AGU* copyright free policy.

Conversely, the "double E-eye" feature is a frequently occurring morphological pattern that can occur at any location at Earth's surface. Independent of its interpretation - and this is just an objective matter-of-fact.

Quinn (private communication, 2015) states what follows, while objecting against our “double-eye” interpretation in terms of air-earth currents, rather than of volcanic origin.

"*The observed waviness exhibits elongated behavior in the East-West direction with a bumpy, high/low alternating behavior in the North-South direction. I attribute this appearance to magnetically sensitive materials being aligned over millions of years into magnetic domains as a*

New Concepts in Global Tectonics Journal
Volume 14, Number 1, January 2026

ISSN number; ISSN 2202-0039

*consequence of the ever-presence of the main geomagnetic-field. This main geomagnetic-field is oriented primarily in a North-South direction at low and mid-latitudes ... As the magnetic poles are approached, the magnetization is more in the vertical direction. The relative magnetization intensity is less near the geomagnetic equator and more at the geomagnetic poles due to the fact that the **B** field-lines converge and become more intense at the geomagnetic poles. Hence the Red Patches near the geomagnetic poles.*

Judd and Hovland (2007) discuss several specific case histories – other than Lost City - that show a morphology that supports their model. This entire topic deserves a long discussion, which cannot be here reported in a few pages.

Let us just generally refer to two wide classes of phenomena: regular geometrical morphological patterns at Earth's surface, and mud volcanism.

Concerning the regular patterns observed on some soils, they can be controlled by a few among several concurrent factors, including physical, chemical, and biological drivers. For instance, a drying mud surface appears almost like a mosaic composed of tesseræ of uniform size, ... but an endless list of more or less usual or exotic case histories can be made, including permafrost areas, their seasonal morphological variations, referring both to surface appearance and underground time-varying patterns (e.g., Williams and Smith, 1989; but this item alone ought to request a long discussion and an extensive reference list). See Gregori et al. (2025u) dealing with a few related items. Permafrost phenomena are not here discussed.

This waviness is most noticeable in geographic regions that have, for the most part, been geologically inactive for millions of years. Those areas that are exposed to recent and prolonged geological activity due to such things as magma emanating from volcanoes, seismic activity, etc., have their magnetic domain structures disrupted by the high heat flow that typically accompanies geologic activity. The high heat flow regions appear as localized blue regions with isolated dark-blue/black spots. These are the hotspots. They appear larger than one might expect because they are at depth and because they are only being described by the intermediate wavelengths. Some are active, while some are dormant, just waiting for an opportunity to erupt. These hotspots are, for the most part, magma chambers and other magma related features associated with the fractal network of electric currents that are following the path of least electric resistance from Earth's interior to the surface. They are in essence the tips of your sea-urchin spikes, ... This also explains the red patches near the geomagnetic poles. The geomagnetic field-lines converge at the geomagnetic poles and disperse at mid- and low-latitudes. The magnetic alignment of the magnetically sensitive minerals becomes more and more intense as one moves toward the poles. Thus, the total magnetization intensity likewise becomes stronger at the poles than at the mid- and low-latitudes. Hence the red patches ...

*The E-eye and double E-eye images may have a geological interpretation. For instance, ... in the source depth images, there can be seen volcanic peaks that have deep holes adjacent to them. One interpretation is that the holes are the empty magma chambers after eruption. After a few million years, plate tectonics laterally separates the volcanic cone from its originating magma chamber. In some cases, the adjacent holes are not seen because the magma chamber may have collapse and been filled-in with surrounding unstable lithospheric material. In other cases, after an eruption, the magma chamber may re-fill, but has not-yet been, or never-again is, used in another eruption, in which case, there is no hole or empty cavity adjacent to the volcanic cone. One might note that ocean currents can be found in high-degree-and-order models if transient terms are added as part of the model. Otherwise these signals also, being transient (that is, they wiggle around laterally and vertically within the ocean, and the strength of the signal generated by these currents varies due to water flow-velocity, salt content of the water, etc.) signals that end-up as un-modeled **B** data in the error function. The same is true for ocean tides ...*

[A reasonable question is about the possibility that this mechanism can be applied to a large number of "double E-eye" features, observed at every latitude and longitude. In addition, since a conspicuous number of "double E-eyes" is observed over the Earth, if they are to explained by means of some kind of anomalous huge magma chambers - i.e., of a linear size from a few hundred to a few thousand kilometers - one wonders why no previous geological or seismic or geophysical campaign, e.g., for oil or mine prospecting, ever envisaged any feature of this kind. In this respect, Quinn (private communication, 2015) warns about any final inference.]

As for what is or is not unrealistic it is presumptuous for anyone to say, since we are looking at new data which begs for interpretation. lt may be real, or it may be a mathematical artifact. Time will tell. But it is too premature to attach such labels to new results. The deep portion of the 'eye', if it is real, is most certainly covered by sediments ... I give a possible explanation of this sort of feature. There may be others. If these are mathematical artifacts, this will eventually be uncovered as more such modeling is performed. [Note, however, that if these features derive from the "leopard effect", they ought to display an approximately regular repetitiveness in space, in contrast with the evidence shown by Quinn's maps.] *Given that each grid point is treated independently, it is hard to see how such a feature would arise unless it were real.* [This is an important point.] *Right now, it is best to hold ones opinions. Remember, we are looking deeper into the lithosphere than has ever been done before. Strange things are to be expected. Instant explanations should not be demanded. Nor, should one rest too hard on old paradigms ...* "

We feel sincerely honored by these extensive comments and explanations given by John M. Quinn, and we are very glad to fully acknowledge them. His final warning can be definitely fully shared, although the interpretation, which is here proposed, is fully maintained on the basis of strictly logical arguments. In any case, absolute truth is beyond human reach, and we could be wrong, although our logical doubts and concern do remain.

In addition, if the Ockham's razor can be credible - because "simplicity" unavoidably relies on a personal feeling - according to the several arguments which we

New Concepts in Global Tectonics Journal
Volume 14, Number 1, January 2026
ISSN number; ISSN 2202-0039

explained above, the Ockham's razor seems to be in favor of the explanation in terms of air-earth currents, which require a smaller amount of *ad hoc* assumptions.

As repeatedly stressed also by Quinn, a real final assessment could be achieved when additional deep-drilling information become available. Owing to the very great cost of every deep drilling facility, this is unlikely to occur soon. Maybe, it is easier and less expensive to implement an analysis of *CHAMP* records (or of any other magnetic satellite) by considering the possibilities of large regional air-earth currents (according to the principle idea of Fig. 3). That is, maybe, a possibility to attempt to interpret the same database according to different viewpoints can afford to assess what kind of analysis will eventually suggest the best possible choice.

In any case, it was here shown that, on a strict logical basis, the hypothesis, which is here proposed, is a realistic and "simple" possibility. Therefore, one cannot reject an evidence that - if it is correct - is the most important finding in geomagnetism since the times of Gauss.

Fermi claimed that when dealing with the interpretation of some observations, there is need for "*c.i.f.*" (*con intuito fenomenale*, i.e., with intuition of phenomena, or, joking, with a particular intuitive skill). Evidently, as long as no better clear observational evidence is available, everybody can only rely in his personal "*c.i.f.*", and all possibilities have to be considered like eventually correct solutions.

Quinn also kindly provided a planetary map (also published in Leybourne and Gregori, 2015) of "*basalt flow remnant magnetization signatures*" (Fig. 86), where he distinguishes two classes of basalts, i.e., whether they are located at a depth $30-70\ km$ (red and yellow), or at a depth $70-200\ km$ (green and blue). The shallower basalt can be considered to be more representative of the planetary distribution of sea-urchin spikes that have been active sometimes during a suitable geological time lag.

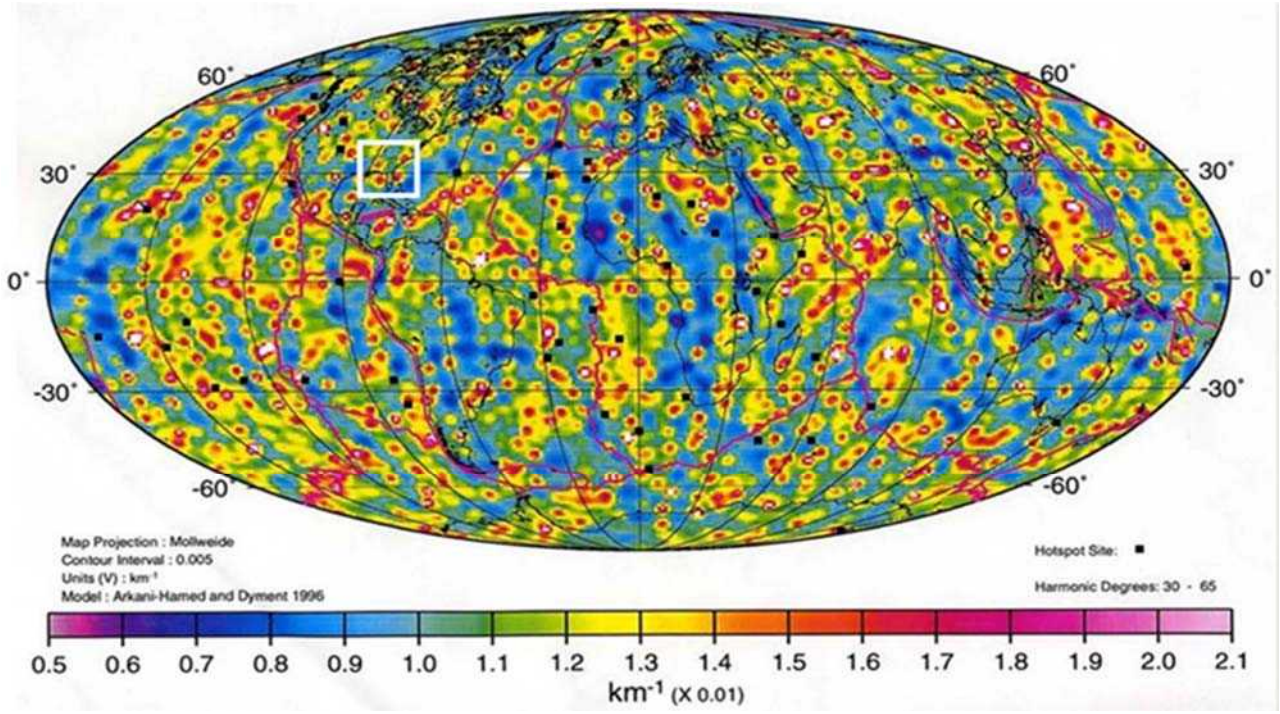

Fig. 86. Basalt flow remnant magnetization signatures, with a distinction in two classes of basalts, i.e., whether they are located at a depth $30-70\ km$ (red and yellow), or at a depth $70-200\ km$ (green and blue). The white square refers to the Florida area.

The description of this figure is given by Leybourne et al. (2017) as follows.

"*Quinn's remnant magnetization signatures are considered the tips of sea-urchin spikes ... Some may also be meteorite impacts. White square indicates ancient features in Southeast U.S. likely associated with Triassic Rifting. Quinn's remnant magnetization signatures are computed as the ratio of the total geomagnetic tensor-intensity to that of the total geomagnetic vector-intensity. This image was generated by John Quinn and distributed around the geomagnetism community in 1997. Fig. 86 was computed from the* MAGSAT *satellite model of Hamed and Dyment using* SH *degrees-and-orders between* $n,m=3$ *and* $n,m=60$. *This geomagnetic ratio parameter is described in more detail by Quinn and Shiel, (1993a). An application using their prism technique in combination with regional rectangular-harmonic modeling is given by Quinn and Shiel (1993b), while an example of the combined use of magnetic source-depth inversion using prisms with global* SH *modeling is given by Quinn (2017).*

The geomagnetic field model referred to in the legend on the bottom left-hand side of Fig. 86 was generated from MAGSAT *satellite data by Arkani-Hamed and Richard Dyment (1996). It was a degree-and-order-* 90 *geomagnetic field model. During the first decade of the* 20th century *a much higher resolution* SH *geomagnetic field model was generated from* CHAMP *satellite data to degree-and-order* 720 *(Maus et al., 2008; Maus, 2008). The most recent global, geomagnetic,* SH *field model has*

NCGT Journal
New Concepts in Global Tectonics
New Concepts in Global Tectonics Journal
Volume 14, Number 1, January 2026
ISSN number; ISSN 2202-0039

been derived from the SWARM *set of satellites (Olsen et al., 2015)."*

More recently a new map of the lithosphere was computed, with an unprecedented detail. The information is given by Geggel (2017) who states what follows.

"*The satellites, three identical spacecraft collectively known as* SWARM*, were launched in 2013 to study the Earth's many magnetic signals ... After* 3 *years of collecting data, the* SWARM *satellites were able to plot the highest-resolution map to date of the lithosphere's relatively weak magnetic signals.*

By combining SWARM *measurements with historical data from the German* CHAMP *satellite, and using a new modeling technique, it was possible to extract the tiny magnetic signals of crustal magnetization ...*

The map, presented this week (March 27th, 2017) at the SWARM Science Meeting *in Canada, shows variations in the field with greater precision than previous satellite-made reconstructions ... The new map includes magnetic field features down to roughly* 250 *km ...* "

No continental-size maps are shown, rather a movie,[8] except a detailed map dealing with the Bangui anomaly (Figs through 33 and 87). "*The map shows a red spike, indicating that the magnetic field there is especially sharp and strong ... It's anyone's guess why the lithosphere has such a strong magnetic signal under Bangui, but it's possible that the signal emanates from a meteorite that crashed into Africa more than* 540 *Ma ago ...* "

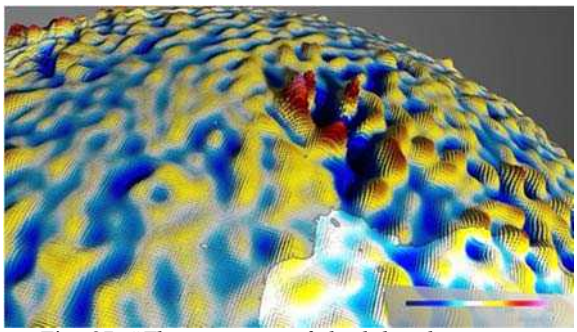

Fig. 87. "*The new map of the lithospheric magnetic field. The red area shows where the field is especially strong on the city of Bangui in the Central African Republic. It's possible that a meteorite impact more than* 540 *Ma ago led to this anomaly in the magnetic field. Credit:* ESA/DTU Space/DLR." The light area at the bottom is the Atlantic Ocean (Gulf of Guinea). Figure and captions after Geggel (2017). *NASA* copyright free policy.

However, the interpretation of the Bangui anomaly is much more intricate and difficult, as extensively discussed above.

Summarizing, it should be stressed that Figs 86 and 87 - and even better the aforementioned movie - clearly show the space distribution of sea-urchin spikes at Earth's surface, with a reasonably detailed spatial resolution, although by integrating all phenomena during some long time lag. The overall picture reminds about the surface of a boiling liquid. In particular, the movie clearly shows that the well-known stripes of the crustal magnetic field in the Ocean floors are not correlated with the sea-urchin spike distribution. In fact, the respective origin is very different of either one of these morphological features. This is in close agreement with the whole rationale of sea-urchin spikes and of *WMT*.

In contrast, Figs 67 through 72 are representative of the effect of some mean air-earth currents averaged over some large area but with a time integration of only 6 *months*.

Knowledge can be substantially improved in three ways: *(i)* by using terms of higher degree and order in order to reduce the disturbance by the "leopard skin" effect; *(ii)* by relying on small-scale maps focused on specific "local" morphological features, to be discussed everyone independently of others and also by seeking their respective correlation with other geophysical and geological information; and *(iii)* by mapping the projection at the Earth's surface of sea-urchin spikes by means of the *CGDS* analysis (see below).

The evidence of air-earth currents derived from geomagnetic field models

A similar evidence can be inferred by means of the isogonic geomagnetic maps, such as, e.g., Fig. 88.[9] However, one should consider that every map refers to a given epoch, and it is drawn by means of a planetary *SHE* model of the geomagnetic potential. Every model relies on a huge set of ***B*** records carried out either at the geomagnetic observatories, or by airborne or shipborne or satellite measurements, during a period of time that is normally 5 *years* long. In addition, data are filtered in order to reject the comparably more disturbed records. Hence, in any case every map is a mean datum smoothed over some long time lag, by considering only some reasonably quiet time alone, and by applying the *SHE* algorithm that *per se* unavoidably introduces a substantial amount of smoothing in space.

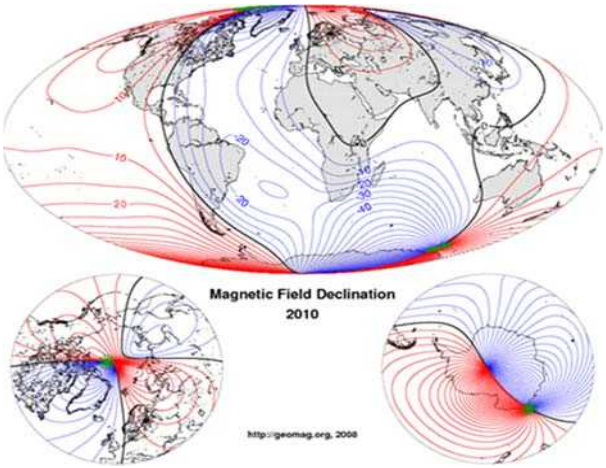

Fig. 88. Magnetic field declination 2010. After Maus (2010). *NOAA* copyright free policy.

[8] Title: "*See Earth's lithospheric magnetic field in highest resolution yet*" (not here shown).

[9] *http://geomag.org/2008.* Source: *http://forum.mutleyshangar.com/.*

New Concepts in Global Tectonics Journal
Volume 14, Number 1, January 2026

ISSN number; ISSN 2202-0039

A more detailed map (not here shown) is given by Livermore et al. (2017) who illustrate and claim they used the $\boldsymbol{B}$ field model by Finlay et al. (2016), including the *SV*. They find some daisy chain of patches of alternating sign, which encircle the north geographic pole at $\sim 70°N$. Livermore et al. (2017) emphasize that similar patterns are observed in several *SV* models by means of ground observations, and referred to the past $17\ years$.

Livermore et al. (2017) interpret these *SV* patterns in terms of westward drift of the flux lobes located between points at $80°E$ and at $120°E$, between points at $170°E$ and at $220°E$, and a weaker patch between at $280°E$ and $310°E$. They also stress that it is surprising that no corresponding counterpart is found in the Southern Hemisphere, where a uniformly low *SV* is, rather, observed. In addition, at epoch 2001, the high-latitude *SV* patches were relatively weak ($\sim 10-15\ \mu T\ year^{-1}$ in magnitude).

The amplitude of these *SV* patches notably increased between 2004-2016. This change is observed in *CHAOS-6*, and also in other field models computed by means of different data sets and by different assumptions. They explain this according to speculated rapidly changing *MHD* processes in the *OC*. They rely on the standard *MHD* Elsasser-Bullard geodynamo model that cannot be here accepted (Gregori, 2002; Gregori and Leybourne, 2021). However, the subsequent comments are closely pertinent to the present study. They are concerned with the asymmetry between the two hemispheres that - they claim - should exclude every effect related to the magnetosphere-ionosphere. They stress the seemingly close relationship with the high-latitude flux lobes, which seem close to the tangent cylinder region, and they specify that the leading part of the effect is related to *SH* degrees $11-13$.

The Northern/Southern Hemisphere asymmetry envisages, rather, a relationship with the tetrahedron pattern (see Gregori and Leybourne, 2021), which is manifested in the *MOR*'s pattern. In any case, according to the rationale of the present whole study - owing to strict physical inconsistencies - every mention must be avoided about the standard *MHD* Elsasser-Bullard geodynamo mode.

In any case, concerning the Livermore et al. (2017) analysis, the smoothing in space derived from the *SHE* interpolation is such that only comparatively large bunches of sea-urchin spikes can be evidenced. The fact that the *SH* degrees $11-13$ are the leading components associated to such an effect is closely related to the typical spatial extension of these bunches.

The asymmetry between Northern and Southern Hemisphere is consistent with several clear indications - which are often encountered (not here reported in detail) - of a presently ongoing larger endogenous heat flow under the whole northern polar cap – consistently with the aforementioned tetrahedron pattern with one vertex at the North Pole.

The conspicuous increase of the intensity of this phenomenon between 2001 ($\sim 10-15\ \mu T\ year^{-1}$) to 2015 ($\sim 35\ \mu T\ year^{-1}$) reported by Livermore et al. (2017) is consistent with the seemingly increasing speed of the present ongoing global climate change.

Upon making reference to Fig. 87, the neutral lines - which separate regions of opposite sign of ΔD, i.e., of the deviation of the declination *D* with respect to zero, i.e., with respect to an undisturbed dipolar field - are likely to be the locus of intense down-flowing air-earth electric currents (Fig. 2). They are likely to occur corresponding to regions of comparatively higher soil exhalation. That is, while computing the spacetime average by means of several different geomagnetic records, the tectonically more active regions introduce a specific and systematic disturbance, due to the air-earth currents that contribute an extra $\boldsymbol{B}$ source, according to the argument of Fig. 3. In any case, the *SHE* algorithm, as mentioned above, causes a substantial amount of smoothing in space, by which several tectonic features are unavoidably smeared out.

Air-earth currents are reasonably supposed to be mainly downward oriented due to the average positive charge of the ionosphere. The primary cause of the *downward* orientation derives from the generally positive electrostatic charge of the solar wind (see Gregori and Leybourne, 2025b). The largest fraction of the electric charge of the ionosphere is likely to be originated by the Cowling dynamo. However, this Cowling dynamo *per se* ought to supply either a positive or a negative charge to the ionosphere, but every pre-existing small amount of positive charge in the ionosphere is such that every new contribution must supply an additional positive charge.

These air-earth currents ought to be upward oriented only during the exceptional occurrence of the polar auroræ that are caused by electron precipitation. Unlike what occurs during the less spectacular proton auroræ, electron auroræ imply a corresponding local increase of the negative charge of the ionosphere. However, on the occasion of these spectacular electron auroral displays, the geomagnetic field is well-known to be severely perturbed, hence the corresponding magnetic records have been rejected from the *SHE* analysis. That is, in the auroral zone the Birkeland-Alfvén currents extend from the ionosphere into ground.

Two comments are deserved dealing, respectively, with the northern and the southern polar cap in Fig. 87.

Concerning the northern polar cap, the shrinking over the North Pole can be explained between the neutral lines, one branch moving northward from the Greenland sector, and the other branch from its 180° longitudinal opposite, i.e., from the Bering Straits sector. This feature could be a possible consequence of a mathematical bias, as the poles are well-known to pose serious stability concerns for every mathematical model by means of *SH*.

In addition, owing to independent evidence, the whole polar cap is the likely site of an increasing anomalous amount of geothermal heat flow - as mentioned above - which involves the whole 360° longitudinal extension, although with some gradient in both space and time.

New Concepts in Global Tectonics Journal
Volume 14, Number 1, January 2026
ISSN number; ISSN 2202-0039

In contrast, concerning the southern polar cap, compared to the northern cap it displays a very different morphology, characterized by two "eyes" of intense concentration of isogonic lines. Apparently, they seem to be almost the sites of two anomalous large local air-earth currents, although the spatial smoothing of the *SHE* mathematical procedure could have somewhat displaced the apparent location of these features.

No correspondence seems to be found with any feature in Fig. 43. In addition, the two "eyes" of intense concentration of isogonic lines seem to coincide, respectively, with the geographic and geomagnetic dipole poles, thus envisaging that some role is likely derived from some mathematical bias.

In any case, the existence of the Transantarctic Mountains must be considered, which seem to roughly parallel the strike of the neutral isogonic line. The Transantarctic Mountains are located close to the boundary between the so-called East Antarctica, which is the largest continental fraction of Antarctica and is characterized by an increase of ice sheet cover. The remaining part of Antarctica, the so-called West Antarctica, is characterized by a decrease of the ice cover, to be presumably associated with friction heat generated by the increased tectonic activity related to the Antarctic Mountains and to the Andes (see Gregori and Leybourne, 2021 and references therein). In any case, a glacier flow from East Antarctica through West Antarctica seems to occur through a few valleys (Winter et al., 2018).

In addition, also the anomalous feature should be considered, which is represented by the *AAD* (Australian Antarctic Discordance). It's a spectacular ridge depression, likely related to this peculiar behavior of the isogonic lines on the southern polar cap.

In this same respect, the isogonic neutral line appears to run equatorward, from Antarctica roughly along the strike of the Andes until North America and northward of it. This also can remind us about an increase of heat release caused by topographic uplift, or more generally by a land mass, originating a comparatively more intense atmospheric convection with, consequently, a more efficient Cowling dynamo that generates air-earth currents.

Indeed, concerning the possible role of topography, topography appears to play a role perhaps even on a much smaller local scale, i.e., referring to some lesser mountain relief. For instance, it seems to be responsible for animal behavior before a large earthquake being likely to be related to *ULF* radiation. That is, it seems reasonable to expect that even some lesser topographic variation always implies some more or less intense convection pattern during the diurnal thermal cycle. This is always associated to a Cowling dynamo that - in some way more or less strongly - implies a local troposphere-ionosphere current that causes an effect similar to an air-earth current. Indeed, the trigger is an energy transfer by hot fluid advection from soil into the atmosphere. This originates convective motion. When air is ionized, a Cowling dynamo is activated that generates an ***E*** from soil-surface up to the ionosphere. This amounts to trigger a steady air-earth current from the Earth's surface through the ionosphere and magnetosphere (Gregori et al., 2025d).

This same mechanism seems to occur also through some large part of Eurasia that ought to be responsible for the large-scale loop of the neutral line crossing through Siberia, the Tibet Plateau, the East Africa rift, the Red Sea, and the Mediterranean region. This whole large region, which includes a large fraction of Eurasia, is mainly covered by land and is characterized by particularly intense tectonic and/or volcanic activity.

This reasonable - although at present only guessed - speculation could be confirmed, e.g., by a more extended and systematic monitoring by means of shallow geotherms, such as it has been carried out for much over half-a-century in China by the school of Tang Maocang (see Gregori et al., 2025h). They proved that the Tibet Plateau is a region of increased geothermal heat release. This is very likely to be the consequence of an intense friction heat originated by local overthrust due to the particularly intense effect of *WMT* inside the huge megasyncline extending from Morocco through Japan.

Arrays of shallow geotherms can be operated through all land areas, except where a thick ice cover forbids to monitor the bedrock. In this respect, however, concerning Antarctica, the aforementioned asymmetry appears to be (perhaps) useful and significant, between the temporal trend of ice sheet cover in East compared to West Antarctica.

All these items need additional hard thinking and subsequent investigation. Studies must be more detailed in both space and time resolution, including the correlation with other effects to be possibly associated with soil exhalation and its relation with tectonic and/or volcanic activity.

If this interpretation is correct, a hypothetical dense network of ground-based geomagnetic recorders can provide instant information on the existence of air-earth currents that affect the *D* field pattern.

Conclusion – The coupling between soil and atmosphere

For the time being, it is reasonable to state that the coupling between soil and atmosphere (up to the magnetosphere) associated with air-earth currents is a fundamental aspect of environmental studies. In the past - since the 1920s or earlier (i.e., the so-called curl-test envisaged by Schuster) - was historically and unduly speculated to be negligible. Thus, the physical significance and implications were overestimated of the famous Gauss' algorithm of the *SHE* of the geomagnetic potential. This same inference is also supported by the recent (previously unexpected) results of the investigations on the earthquake precursors observed through the atmosphere up to the magnetosphere (see Parrot, 2025; Straser et al., 2026; Wu, 2025; Gregori et al., 2025h).

In the ultimate analysis, two competing interpretations of the Quinn's inversion of the *CHAMP* data are thus available: *(i)* the original Quinn's interpretation, which

ISSN number; ISSN 2202-0039

relies on the assumption that the data handling of the *CHAMP*'s records was such as to forbid any role for air-earth currents, and *(ii)* the interpretation which is here given based on consideration of the fact that the data handling of the *CHAMP*'s records intrinsically *cannot exclude* the role of possible air-earth currents.

The choice here made is finally in favor of huge air-earth currents, based on the Ockham's razor. That is, Quinn's interpretation, assumes the presence of several physically very "anomalous" huge "abandoned" magma chambers, mostly located in tectonically active regions, and observed by no other previous geophysical or geological investigation.

In any case, a strictly rigorous method exists that can discriminate - in an unquestionable and final way - such a dilemma. This is the Mie representation, and the Backus et al. (1996) algorithm. Unfortunately, computations are somewhat intricate and unpractical. However, the relevance of the result is such that it is certainly worthwhile to implement such a computationally heavy procedure.

Mapping sea-urchin spikes - Antennas for the e.m. coupling between solar wind and the Earth's core

A concern also deals with a way of mapping the location and distribution of sea-urchin spikes in any given area. This can be accomplished by means of geomagnetic prospecting by applying an original technique (unpublished) conceived a few decades ago by one of the coauthors (GPG) in cooperation with Louis J. Lanzerotti. This technique, called Canonical Geomagnetic Depth Sounding (*CGDS*), is a rigorous formulation of the best known *GDS* that, however, relies on a set of substantial approximations that can be fully avoided by means of the rigorous *CGDS* approach. The description of the data handling, which is needed by *CGDS,* should require a separate and lengthy treatment that cannot be here included. It will be the object of a separate treatment (in preparation).

As far as the present study is concerned, just mention that, by means of a suitable campaign of geomagnetic prospecting, it is possible to map the relative spatial distribution of underground electrical conductivity σ at different depths. Absolute values of σ cannot be known, due to the well-known non-uniqueness of every inversion technique, but relative values can be estimated with precision.

Owing to the existence of a large number of sea-urchin spikes, it is possible to show that they represent a realistic physical link by which deep induced telluric currents can modulate the *TD* dynamo, according to the analogy with a laboratory model dynamo (Gregori, 2002; Gregori and Leybourne, 2021).

If the Earth is conceived, as usual, in terms of concentric spherical shell - i.e., if it intuitively reminds about an onion-model - the σ of every comparatively shallower layer screens all underlying layers, according to the classical skin-depth effect. Therefore, it is often correctly stated that some unknown signals – of some very low frequency - are strictly required for penetrating and reaching some large depth into the Earth. For instance, it is believed that the *CMB* could be realistically reached by e.m. waves of period, say, $\gg 11\ years$ etc. However, the radial distribution of σ in the deep Earth is essentially unknown. Therefore, no reliable quantitative computation of this effect can be carried out.

Conversely, the sea-urchin spikes cross through the mantle and eventually reach at Earth's surface. Thus, they can operate like effective natural antennas that determine a concrete e.m. coupling between the solar wind and the deep Earth's interior. The very large number of spikes plays therefore a crucial role in the e.m. coupling between solar wind and the Earth's core.

Note that the geomagnetic field, which is originated in the Earth's core, acts on the solar wind. In fact, the geomagnetic field "hollows" a volume inside the solar wind flow, and this "hollow" is manifested as the magnetopause. This interaction implies that $\boldsymbol{B}$ field-lines are eventually "cut" and "reconnected", due to the crucial role of "plasma cavities" that occasionally occur through the solar wind (see Gregori and Leybourne, 2021; Gregori et al., 2025a). However, owing to the action-reaction principle, a similar reaction must occur, which is originated by the solar wind and affects the Earth's core.

Note that this is a real e.m. interaction between $\boldsymbol{j}$-loops. This interaction necessarily implies a reciprocal linking, by either one $\boldsymbol{j}$ -loop, of the $\boldsymbol{B}$ flux generated by the other $\boldsymbol{j}$-loop. Also this process requires that $\boldsymbol{B}$ field-lines are "cut" and "reconnected". Physically, this can occur because the $\boldsymbol{B}$ field-lines inside the solar wind are eventually "cut" due to the presence of sporadic "*plasma cavities*".

That is, "*plasma cavities*" in the solar wind play a twofold crucial role: *(i)* they generate the neutral sheet in the magnetosphere and they explain the morphology and development of magnetospheric substorms and geomagnetic storms (as per Gregori and Leybourne, 2021; Gregori et al., 2025a), and *(ii)* they also trigger the e.m. coupling between solar wind and Earth's core through the antennas represented by the sea-urchin spikes.

Conversely, with no antennas, the e.m. coupling can occur through much shallower telluric currents, due to the aforementioned Faraday screening by all shallower conducting layers. In this case, the energy - which is no more transported through these antennas - can no more act as a controller of the efficiency of the *TD* dynamo. Rather, its damps off rapidly through Joule dispersion inside some shallow Earth's layers.

The concern shifts therefore on the assessment of the real physical definition and meaning, when we deal with an e.m. wave of some intuitively almost inconceivably low frequency.

Consider that the solar wind is the manifestation of the expansion of solar corona. At the Earth's orbit, i.e., at $1\ AU \sim 1.5 \times 10^{11}\ m$, the solar corona is distributed over a spherical surface of $4\pi\ (1\ AU)^2 \approx 2.8 \times 10^{23}\ m^2$. Consider that the spatial distribution of the solar wind over this expanding spherical surface is very heterogeneous, both in space and time. The space-size of

NCGT Journal
New Concepts in Global Tectonics
New Concepts in Global Tectonics Journal
Volume 14, Number 1, January 2026
ISSN number; ISSN 2202-0039

heterogeneities is certainly very much larger than the size and cross-section of the Earth's magnetopause.

The Earth's magnetosphere, for simplicity, can be supposed to have a circular cross-section of ~10 RE (Earth's radii), or ~$1.3 \times 10^{14}\ m^2$. Therefore, the Earth altogether with its entire magnetosphere interacts with a tiny fraction, only ~0.45×10^{-9}, of the total surface of the expanding solar corona (see Gregori and Leybourne, 2025b).

Consider the wavelength λ of an e.m. wave of some very low frequency ν of period T. It is $\lambda = cT$ (where c is the light speed). If λ is the diameter of the Earth's orbit around the Sun, i.e., $\lambda = 2\ AU$, it is well-known that $T = 16\ min$. If it is, say, T~1 $year$, it is □~$9.5 \times 10^{15}\ m$~$6.3 \times 10^{4}\ AU$. However, we should refer to unrealistic e.m. waves of period $\gg 11\ years$.

That is, the description in terms of an e.m. wave of such a huge wavelength looks like a mathematical trick, i.e., it is the result of a formal application of Fourier algorithms. In reality, we deal only with some very slow trend. This trend changes much before the completion of one full oscillation that elapses one wavelength. Therefore, it is more realistic to consider a slow trend of the time variation of the impinging e.m. field by the solar wind on the Earth, while the phenomenon will soon be interrupted before it can complete one full wavelength cycle.

Hence, the phenomenon can be more realistically illustrated by considering an almost steady e.m. field that causes induction and can be affected by no Faraday screening due to the very low frequency.

On the other hand, the phenomenon can always be correctly and mathematically handled by means of its power spectrum. Every component of a given frequency resonates in general by a different amount inside the Earth's body. That is, the Earth reacts like a natural antenna tuned on some frequencies, better than on others. Therefore, this appears to be a physically meaningful justification for the principle idea of the *TD* dynamo, even though it is impossible to state *a priori* what frequencies are tuned inside the Earth's interior.

A method can certainly monitor the time variation of the result of this tuning. Indeed, the long-range trend - of the variation of the e.m. field of the solar wind that impinges on the Earth - depends on the spacetime scatter of the expanding solar corona, which is certainly varying in time, and in particular it depends on solar activity and on its cycle. Indeed, according to the general rationale of the whole present study, it is certain that the modulation of the *TD* dynamo implies a modulation of the endogenous energy production, which affects climate through the "internal way" (as per figure 26 of Gregori and Leybourne, 2021). Hence, some comparatively anomalous solar activity ought to be associated with a corresponding unusual or anomalous climate trend (Gregori and Leybourne, 2021)

That is, Earth's "climate" is a very effective "sensor" suited to detect the long-range of the time-varying influence on solar-terrestrial relations of these unconventional e.m. fields of low frequency that are transported by the solar wind.

For the sake of completeness a mention is deserved for the speculated "subsurface thunderstorms" (Khazanovitch-Wulff, 2007, 2007a), although the primary physical driver and process need a better explanation.

Appendix – Tensor formalism

A scalar quantity is denoted by a normal character, such as, e.g., by a, while a vector is denoted by a bold character such as, e.g., by $\boldsymbol{a}$ or, equivalently, by the symbol $\vec{a}$. Its i-th vector component of $\boldsymbol{a}$ is denoted by a_i (covariant) and a^i (contravariant). A tensor is denoted accordingly, by putting a lower index for every covariant index and an upper index for every contravariant index, such as, e.g., u^{ij}_{kl}, etc. The scalar product of two vectors is denoted by " × " (here used), such as, e.g.. $\boldsymbol{a} \times \boldsymbol{b}$, while a symbol often used in the literature is " · ", such as $\boldsymbol{a} \cdot \boldsymbol{b}$. The vector product is denoted by "∧ ", such as $\boldsymbol{a} \wedge \boldsymbol{b}$, while the often used symbol " × " is frequently reported in the literature, and it should not be confused with the same symbol here used for the scalar product.

Concerning the vector differential operators, the classical historical symbols are $grad$, div, $curl$ (or rot), □ = $(div\ grad)$ or Laplacian or Laplace' operator, and the □ or "d'Alembertian" or "d'Alembert's operator". These symbols are here preferred, as they appear much better suited for scanning the historical literature. The presently comparatively more frequently used symbols, such as, e.g., by Stratton (1941), refer rather to the operator ∇, called "nabla", by which $grad \Leftrightarrow \nabla$, $div \Leftrightarrow div\ \cdot$, $curl \Leftrightarrow \nabla \wedge$, and $\Delta \Leftrightarrow \nabla^2$ or $\nabla \cdot \nabla$ (where, however, in order to conform with the use of ∇, also the most frequent standard form is used for the scalar product, which is denoted as " · " and not as " × "). See Table A-1.

Table A-1. Symbols for the classical vector differential operators

historical symbol (here used)	most frequently used symbol	tensor symbol
$\boldsymbol{v} \times \boldsymbol{w}$ (scalar product)	$\boldsymbol{v} \cdot \boldsymbol{w}$	$a_{ij}\ v^i w^j$ $\equiv v^i w_j$ $\equiv\ v_i w^j$
$(\boldsymbol{v} \wedge \boldsymbol{w})_k$ (vector product)	$(\boldsymbol{v} \times \boldsymbol{w})_k$	$\varepsilon_{ijk}\ v^i w^j$
$(grad\ f)_j$	∇f	$\eth f/\partial x^j \equiv\ f_{/j}$
$div\ \boldsymbol{v}$	$\nabla \cdot \boldsymbol{v}$	$v^j_{/j}$
$(curl\ \boldsymbol{v})_j$	$\nabla \times \boldsymbol{v}$	$\varepsilon_{ikr}\ v^{k/r}$
Δf (Laplacian)	∇^2 or $\nabla \cdot \nabla$	$f^i_{/i\cdot} \equiv\ f_{/ik}\ a^{ik}$

The symbols that result computationally more compact and straightforward, i.e., almost immediate - as it is emphasized, e.g., by Backus et al. (1996) - rely, rather, on the formalism of tensor calculus, which is here briefly recalled, mainly relying on Finzi and Pastori (1961) (see also Moritz and Hofmann-Wellenhof, 1993), but the reference list is almost endless.

NCGT Journal
New Concepts in Global Tectonics
New Concepts in Global Tectonics Journal
Volume 14, Number 1, January 2026
ISSN number; ISSN 2202-0039

Define the fundamental tensor a_{ij} expressed by its covariant component. It is a^{ij} when it is expressed by its contravariant components, and $a^i_{.j}$ or $a^{.i}_j$ when it is expressed by its mixed components. Its formal definition is

$$a_{ij} = \frac{\partial P}{\partial x^i} \times \frac{\partial P}{\partial x^j} \qquad \text{(A-1)}$$

where P denotes the vector-position of a point. It is $i, j = 1, 2, 3$. The metric of the 3D space (either Euclidean or not) is

$$ds^2 = a_{ij} dx^i dx^j = a^{ij} dx_i dx_j \qquad \text{(A-2)}$$

where, as it is usual in tensor formalism, identical indices are supposed to be summed over $1, 2, 3$ (in 3D space, while in the 4D spacetime suitable consideration is given for the 4th coordinate and for the related metric, etc.).

Call ε_{ijk} the Ricci's tensor (its covariant components, etc.). It is defined as

$$\vec{\varepsilon}_{ij} = \frac{\partial P}{\partial x^i} \wedge \frac{\partial P}{\partial x^j}$$
$$\varepsilon_{ijk} = 0 \quad \text{(when either two indices are equal)} \qquad \text{(A-3)}$$
$$\varepsilon_{ijk} = \pm\sqrt{a} \quad \text{(when all indices are different)}$$

where a is the determinant of the matrix $\|a_{ij}\|$ and the plus (minus) sign applies when i, j, k is an even (odd) permutation of $1, 2, 3$. The Ricci tensor has the remarkable properties

$$\varepsilon_{ijk}\varepsilon^{ijk} = 3!$$
$$\varepsilon_{ijr}\varepsilon^{ijq} = 2!\, a^q_r \qquad \text{(A-4)}$$
$$\varepsilon_{ikr}\varepsilon^{ipq} =$$
$$= 2!\, a^{pq}_{kr} \equiv 2!\, \|a^{pq}_{kr}\| \equiv 2! \begin{pmatrix} a^p_k & a^q_k \\ a^p_r & a^q_r \end{pmatrix} \equiv 2!\, \left[a^p_k a^q_r - a^q_k a^p_r\right]$$
$$\varepsilon_{ikr}\varepsilon^{jpq} = \|a^{jpq}_{ikr}\| \equiv \begin{pmatrix} a^j_i & a^p_i & a^q_i \\ a^j_k & a^p_k & a^q_k \\ a^j_r & a^p_r & a^q_r \end{pmatrix}$$

The scalar product is $\times\ \boldsymbol{w} \equiv a_{ij}\, v^i w^j \equiv v^i w_j \equiv v_i w^j$. The k-th component of the vector product is $p_k = (\boldsymbol{v} \wedge \boldsymbol{w})_k \equiv \varepsilon_{ijk}\, v^i w^j$. It is $(grad\, f)_j \equiv \eth f / \partial x^j \equiv f_{/j}$. The divergence is $\boldsymbol{v} \equiv v^j_{/j}$ and the $curl$ is defined by $(curl\, \boldsymbol{v})_j \equiv \varepsilon_{ikr}\, v^{k/r}$. The Laplacian is $\Delta f \equiv f^{.i}_{/i} \equiv f_{/ik}\, a^{ik}$. Table A-1 synthesizes the different symbols.

These tensor symbols seem, however, to be generally unusual in the English literature. Backus et al. (1996) emphasize the simplicity of this formalism. They call "tensor alternator" the Ricci tensor. In reality, the formal tensor treatment (rather than a combinatorial symbol such as an "alternator") is more suited for exploiting a formal theory, e.g., in a curved space, or, e.g., in spherical or cylindrical or ellipsoidal coordinates, or in the Reimann space used in general relativity. In fact, whenever the metric is defined, formulas are straightforward and give a most direct and simple response, which is identical in every space.

In general, however, when using Cartesian coordinates in an Euclidean space, formulas get particularly simple, as covariant and contravariant components coincide, while the fundamental tensor has unit components (when its indices are identical) and vanishing components (when its indices are different), i.e., its values formally coincide with the classical Kronecker's δ^j_i symbol. However, in the general case, a warning is about a suitable logical conceptual distinction between tensor quantities and combinatorial symbols, even though such a distinction has no practical consequences when dealing with orthogonal Cartesian coordinates in an Euclidean space.

Obituary of John Michael Quinn

John Michael Quinn lived from 08 May 1946 to 31 March 2020. He is survived by a brother, Dan Quinn, and sister, Teresa Quinn, with four nephews, six grand-nephews and nieces, and one great grandniece. At the time of his passing, John was survived by his wife, Pamela Shields Quinn, a Marine Biologist for the US Government, who has since passed. John always had a soft spot for dogs and dogs loved him back, convinced they would not eat dog food, during retirement he became personal chef to his beloved dogs. John is interred at the Fort Logan National Veteran's Cemetery in Denver, CO.

John was a third-generation Coloradan. Born in Denver to parents Leonard Quinn LCDR. USN (1913-1987) and Winifred Quinn LTJG. USN (1920-1994). John graduated from *Woodson H.S.* in Fairfax VA, 1964. He received a B.S. in physics from the *University of Virginia* at Charlottesville in 1968 and an M.S. from the *University of Colorado* at Boulder in 1982. He worked during the summer breaks at the *U.S. Naval Research Laboratory* in the *Underwater Acoustics Division*. After graduating college, he served three years in the U.S. Army as a nuclear weapons specialist during the Vietnam War based in Ithaca, NY. He became a Research Physicist/Geophysicist. He worked for the *U.S. Naval Oceanographic Office* at *Stennis Space Center*, MS developing the World Magnetic Model. A model updated every $5\ years$ with global data sources assimilated at international meetings. He also worked for the *Department of Interior*'s *U.S. Geological Survey*. He had a $40 - year$ career in the sciences including $32\ years$ with the *Federal Government*.

During that period John was involved with the *Navy*'s *Acoustic and Non-Acoustic Anti-Submarine Warfare* (*ASW*) Program, the *Navy*'s *Ocean Survey Program* (*OSP*), the *Navy*'s *Fleet Ballistic Missile* (*FBM*) Program, the *Air Force Strategic Defense Initiative* (*SDI*) particle beam weapons program, the *Defense Meteorological Satellite Program* (*DMSP*), the *National Polar Orbiting Environmental Satellite System* (*NPOESS*) program, and the *Project Magnet* aeromagnetic survey program. John has been consulted by a wide range of federal government agencies, such as the *U.S. Space Command*, *NOAA*, *NASA*, and the *CIA*, as well as by all three branches of the military, military contractors, and representatives of *NATO* military forces on such diverse matters as nuclear terrorism, missile guidance, tank warfare, missile and

ISSN number; ISSN 2202-0039

anti-missile targeting/acquisition problems, as well as navigation and attitude/heading problems.

For $25\ years$ he was responsible for executing the U.S. half of the Joint US/UK *World Magnetic Modeling* (*WMM*) program on behalf of what is now the *Geospatial Information Agency* (*GIA*). The *WMM* supplies magnetic field models to the U.S. military and its *NATO* allies as well as to commercial, institutional, and private research organizations. The model provides ships, aircraft, satellites, and missiles, as well as *NASA*'s *Space Shuttle* with navigation, attitude/heading referencing, and targeting information. It is also used for basic geophysical and medical research. Fed Ex would send him a model plane every time they downloaded his most recent model reminding us that John's formulas are incorporated into the navigational *Geostationary Positioning System* (*GPS*).

John has been a member of numerous mathematical and geophysical societies and has convened sessions and presented papers at numerous scientific meetings around the world. He was a contributing member of the International *Association of Geomagnetism and Aeronomy*'s (*IAGA*'s) Committee for the *International Geomagnetic Reference Field* (*IGRF*) for $20\ years$. He was a $15-year$ member and $8-year$ chairman of *IAGA*'s *Committee on Earth and Planetary Magnetic Survey Satellites*. *IAGA* is a member of the *International Union of Geodesy and Geophysics* (*IUGG*), which meets every four years. John also worked on behalf of the federal government for the *International Standards Organization* (*ISO*), which is part of the *United Nations*, as are *IAGA* and the *IUGG*. John's scientific interests include geophysics, oceanography, solar-terrestrial physics, and more generally classical and semi-classical field theory, including General Relativity and semi-classical Quantum Field Theory. His interest in unified fields began at the age of fourteen and he self-published several related texts.

When funding for *WMM* project was transferred to the *U.S. Geological Survey* in Golden, CO, he went with the project, which was focused on geomagnetism This enabled him to move back to his home origins in Lakewood, CO were he finally retired to continue work on his theories. It was during this time that John published several papers and books. While as a guest scientist at *NOAA* John became interested in the Global Warming Problem, which resulted in a book. One of his particularly interesting and possibly most controversial books was on the topic of geophysical counterpoints to greenhouse gas driven global warming. It explains many of the geophysical relationships he explored to understand the drivers of natural climate change. This book was published in 2010 with *Dorrance Publishing* and can be found at the following link.

https://bookstore.dorrancepublishing.com/global-warming-geophysical-counterpoints-to-the-enhanced-greenhouse-theory/

His theories and his research defined most of his life and he was driven in his retirement to spend the last two decades refining and publishing his research. It was finally his time to work on the theories that were his passion. To develop his works on magnetic field modeling and unified theories, he formed a non-profit called the *Solar-Terrestrial Environmental Research Institute (STERI)* out of his home in Lakewood, CO. His work was his obsession, and he was in good company. Bruce Leybourne, one of his many good friends, was also a work colleague during his years at the *U.S. Naval Oceanographic Office*, and later an associate who helped edit some of his works and refine some of the geophysical concepts. This relationship was exemplified in a published book review of his book on global warming and a follow-on abstract in December of 2010 with the *American Geophysical Union*. See links below:

https://www.researchgate.net/publication/274532416_Book_Review_Global_Warming_Geophysical_Counterpoints_to_the_Enhanced_Greenhouse_Theory

https://ui.adsabs.harvard.edu/abs/2010AGUFM.A33A0152Q/abstract

On a professional level he was respected as a true genius. Here is a quote from Physics professor, Giovanni P. Gregori from Rome. Giovanni met John at the *International Union of Geodesy and Geophysics* (*IUGG*) General Assembly 1995 July conference in Boulder, CO, when displaying a poster on the *TD* dynamo topic, and to his surprise John was explaining his poster to a colleague. Giovanni later states, "*I am very convinced on a sound objective and logical argument – that John made the most important discovery since the times of Gauss. He showed that huge amounts of electric currents (air-earth currents) almost permanently flow between solid Earth and atmosphere/ionosphere up to the magnetosphere. The electric currents are associated to soil exhalation and occur mostly in areas with a greater crustal fracturing. When I wrote him that I considered him as being, maybe, the most important living physicist, he confessed to me - maybe with some embarrassment - that also his wife claimed the same concept….*" Giovanni went on to state…. "*Everybody lives according to what he has contributed to the welfare of others, to the progress of knowledge and civilization. I do believe - and I hope I have explained and motivated my belief - that John did a lot, and he will be always remembered for his being a true scientist, not just a 'trumpet' who likes to repeat concepts and ideas of others. John actually '*talked with Mother Nature*', as a scientist should always do*! [*The term "trumpet" is not mine, rather it is by Leonardo*.]" Giovanni also remembers John's "mild" and kind character, by which he felt very sorry, almost disappointed, by the fact that the re-interpretation of his inversion model implied a contradiction – although not a true criticism – of the geomagnetic field model made by his "*very skillful*" colleague Stefan Maus.

His brother Daniel states about Giovanni's acknowledgment, "*this blew me away and it helped me understand John in a way I didn't before. I had no idea the depth of his drive. It wasn't about letters behind his name or titles. His work was going to stand on its own. In fact, I once asked John why he didn't monetize what he's doing if it's so important. He was almost indignant that I should suggest such a thing.* 'I'm a scientist' *he said.* 'My

New Concepts in Global Tectonics Journal
Volume 14, Number 1, January 2026
ISSN number; ISSN 2202-0039

work must be out there for other scientists to see and challenge and take to the next level. That what scientists do.' " Daniel goes on to state, "*Mom asked us kids if there was anything special, we wanted for Christmas. John, without hesitation, said he wanted this very expensive physics reference book and a magazine subscription to* Scientific American*. John's future passion was going to be science and especially Physics. For the record, he didn't get the physics book due to cost, about a $100 or so (a lot back then), but he did get the subscription which he loved.*" Thus, it is important we help to preserve John's legacy and leave his mark on this world. He embraced retirement as the opportunity to devote his full attention to pursuing his "theories" that were his passion. The last year of his life he proclaimed to his sister that he would not be able to die in peace until the last of his work was complete. A dedicated scientist until the very end.

A list of some of his works can be found at *Defense Technical Information Center*:
https://discover.dtic.mil/results/?q=John+M+Quinn#gsc.tab=0&gsc.q=John%20M%20Quinn&gsc.page=1

Some references related to Magnetic Field Monitoring and other items include:

Quinn J.M. and B.A. Barrick, 1987. Spherical Harmonic modeling of the geomagnetic field using the fast Fourier transform, Physics of the Earth and Planetary Interiors, 48: 206-220

Quinn and Shiel (1993a)

Quinn and Shiel (1993b)

Quinn (2010).

Quinn (2012)

Quinn (2013)

Quinn (2014)

Quinn, J.M., 2015. A classical, non-dual, unified field theory with dark energy, ISBN: 978-1-4951-8255-6. https://bookdatabase.online/isbn.php?isbn=978-1-4951-8255-6

Quinn (2017)

Acknowledgement

The *mf3* spherical-harmonic magnetic-field model was computed by Stefan Maus at the *National Geophysical Data Center* (*NGDC*) and associates at *GeoForschunsZentrum* (*GFZ* - The German *Research Center for Geosciences*).

The model is derived from *CHAMP* magnetic satellite data.

CHAMP is a German Space Agency initiative implemented by the *GFZ*. The *mf3* model and subsequent models are available from *NGDC* and other *World Data Centers*.

Technical reports by Quinn and Shiel are available from the *Maury Library*, *U. S. Naval Oceanographic Office*, *Stennis Space Center*, MS. The base map in Fig. 7 was provided by *Microsoft*'s *Window 8* software.

We want to acknowledge all co-workers that, in different ways and at different times, contributed to the exploitation of the analyses mentioned in the present study. We like also to thank for the warm encouragement we had from several outstanding scientists.

Funding Information

G.P. Gregori is retired since 2005.

B.A. Leybourne is a semi-retired self-funded independent researcher.

Author's Contributions

This study mainly relies on the gigantic study exploited by the late John Michael Quinn.

The other coauthors contributions were derived with an independent interpretation - following after a long-lasting cooperation and discussion.

The backbone draft was prepared by GPG, and agreed with BAL, with profound respect for the original Quinn's text.

Ethics

This article is original and contains unpublished material. Authors declare that there are no ethical issues and no conflict of interest that may arise after the publication of this manuscript.

References

Agrawal, P.K., N.K. Thakur, and J.G. Negi, 1992. MAGSAT data and Curie-depth below Deccan flood basalts (India), Pure and Applied Geophysics, 138 (1): 61-75; DOI:10.1007/BF00876714

Alken, P., S. Maus, A. Chulliat, and Chandrasekharan Manoj, 2015. NOAA/NGDC candidate models for the 12th generation International Geomagnetic Reference Field, Earth, Planets and Space, 67, 68 [9 pages]; DOI:10.1186/s40623-015-0215-1

Anonymous, 2011l. Bedrock map reveals ice-free Antarctica, Australian Antarctic Division: Leading Australia's Antarctic Program, released 14 Dec 2011

Anonymous, 2015f. Chernobyl accident 1986, (updated Apr 2015), World Nuclear Association

Anonymous, 2018b. SWARM tracks elusive ocean magnetism, SWARM-ESA press release, issued 10 Apr 2018

Anonymous, 2018c. Magnetic lithosphere detailed, *SWARM-ESA press* release, issued 10 Apr 2018

Arkani-Hamed, J., and J. Dyment, 1996. Magnetic potential and magnetization contrasts of Earth's lithosphere, Journal of Geophysical Research, Solid Earth, 101 (B5): 11,401–11,425; DOI:10.1029/95JB03537

Armstrong, R.L., 1968. Sevier Orogenic Belt in Nevada and Utah, Geological Society of America, Bulletin, 79 (4): 429-458; DOI:10.1130/0016-7606(1968)79[429:SOBINA]2.0.CO;2

Backus, G.E., R. Parker, and C. Constable, 1996. Foundations of geomagnetism. Cambridge University Press, Cambridge, pp.: 1-369

ISSN number; ISSN 2202-0039

Bott, M.H.P., 1971. The interior of the Earth. Edward Arnold Pub. Ltd, London, pp.: 1-316

Cassel, E.J., S.A. Grahm, and C.P. Chamberlain, 2009. Cenozoic and topographic evolutions of the northern Sierra Nevada, California through stable paleoaltimetry in volcanic glass, Geology, 37 (6): 547-550

Cecil, M.R., M.N. Ducea, P.W. Reiners, and C.G. Chase, 2006. Cenozoic exhumation of the northern Sierra Nevada, California fFrom (U-Th)/He thermochronology: Geological Society of America, Bulletin, 118: 1481-1488

Chapman, A.D., P.I. Luffi, J.B. Saleeby, and S. Petersen, 2011. Metamorphic evolution, partial melting, and rapid exhumation above an ancient flat slab: insights from the San Emigdio Schist, Southern California, Journal of Metamorphic Geology, 29 (6): 601-626; DOI:10.1111/j.1525-1314.2011.00932.x

Chapman, S., and J. Bartels, 1940. Geomagnetism. 2 vol., Oxford Univ. Press, (Clarendon), London and New York, pp.: 1-1049

Chenet, A.-L., V. Courtillot, F. Fluteau, M. Gérard, X. Quidelleur, S.F.R. Khadri, K.V. Subbarao, and T. Thordarson, 2009. Determination of rapid Deccan eruptions across the Cretaceous-Tertiary boundary using paleomagnetic secular variation: 2. Constraints from analysis of eight new sections and synthesis for a 3500-m-thick composite section, Journal of Geophysical Research, 114, B06103 [38 pp.]. DOI:10.1029/2008JB005644

Choi, D.R., 2003a. Deep earthquakes and deep-seated tectonic zones. Part 4. Southwest Pacific. New Concepts in Global Tectonics, Newletters, (26): 16-32

Choi, D.R., 2005. Deep earthquakes and deep-seated tectonic zones: a new interpretation of the Wadati-Benioff Zone. Bollettino della Società Geologica Italiana, Volume Speciale, (5), 79-118

Choi, D.R., 2014f. Seismo-volcanic energy propagation trends in Central America and their relationship to solar cycles, New Concepts in Global Tectonics, Journal, 2 (3): 19-28

Choi, D.R., 2017. Low velocity lenses at the top of lower mantle and a new earthquake model for the Fiji-Tonga-New Zealand region, New Concepts in Global Tectonics, Journal, 5 (2): 244-254

Chulliat, A., and S. Maus, 2014. Geomagnetic secular acceleration, jerks, and a localized standing wave at the core surface from 2000 to 2010. Journal of Geophysical Research, Solid Earth, 119: 1531–1543; DOI:10.1002/2013JB010604

Collette, B.J., 1974. Thermal contraction joints in a spreading seafloor as origin of fracture zones, Nature, 251 (5473): 299-300.

Columbia Climate School, 2014. Ancient air, Modern peril: geoscientists reveal a new 66 million-year history of carbon dioxide, SciTechDaily, issued January 13, 2024

Corner, S. and C. Harrison, 2003. The origins of the Laramide orogeny, The Traprock, 2: 10-14

De Carli, P.S., A.P. Jones, N.J. Price, and G.D. Price, 2002. The Bangui magnetic anomaly is not of impact origin, American Geophysical Union, Spring meeting, Abstract #T2219-02

DeCelles, P.G. and G. Mitra, 1995. History of the Sevier orogenic wedge in terms of critical taper models, Northeast Utah and Southwest Wyoming, Geological Society of America, Bulletin, 107: 454-462

DeCelles, P.G., 2004. Late Jurassic to Eocene evolution of the Cordilleran thrust belt and foreland basin system, Western USA, American Journal of Science, 304 (2): 105-168

Du Bray, E.A., J.N. Aleinikoff, and K. Lund, 2012. Synthesis of petrographic geochemical, and isotopic data for the Boulder batholith, Southwest Montana, USGS Professional Paper, (1793)

Ducea, M., 2001. The California arc: thick granitic batholiths, ecological residues, lithospheric-scale thrusting, and magmatic flare-ups, Geological Society of America Today, 11, 4-10

Duncan, R.A., and M.A. Richards, 1991. Hot spots and mantle plumes, flood basalts, and true polar wander. Reviews of Geophysics, 29 (1): 31-50; DOI:10.1029/90RG02372.

Dyment, J., and J. Arkani-Hamed, 1995. Spreading-rate-dependent magnetization of the oceanic lithosphere inferred from the anomalous skewness of marine magnetic anomalies, Geophysical Journal International, 121, (3), 789-804; DOI:10.1111/j.1365-246X.1995.tb06439.x

Featherstone, W.E., and S.J. Claessens, 2008. Closed-form transformation between geodetic and ellipsoidal coordinates, Studia Geophysica et Geodetica, 52 (1): 1-18; DOI:10.1007/s11200-008-0002-6

Finlay, C.C., N. Olsen, S. Kotsiaros, N. Gillet, and L. Toeffner-Clausen, 2016. Recent geomagnetic secular variation from SWARM and ground observatories as estimated in the CHAOS-6 geomagnetic field model. Earth, Planets and Space, 68: 1–18

Finzi, B., and M. Pastori, 1951 and 1961. Calcolo tensoriale ed applicazioni, Zanichelli Editore, Bologna (I ed., 1951), pp.: 1-427 (II ed., 1961), pp.: 1-510

Foulger, G.R., G.F. Panza, I.M. Artemieva, I.D. Bastow, F. Cammarano, C. Doglioni, J.R. Evans, W.B. Hamilton, B.R. Julian, M. Lustrino, H. Thybo, and T.B. Yanovskaya, 2015b. What lies deep in the mantle below?, EOS, Transactions of the American Geophysical Union, 96; DOI:10.1029/2015EO034319

Foulger, G.R., M. Lustrino, and S. King (eds), 2015. The Interdisciplinary Earth: a volume in honor of Don L. Anderson, Geological Society of America Special Paper SPE514/AGU Special Publication (71)

Fowler, C., 2005. The solid Earth, 2nd ed., Cambridge University Press, pp.: 1-685, (I ed. 1997)

Fukushima, N., 1989. Memorandum on non-curl-free geomagnetic field. Il Nuovo Cimento, 12C (5): 541-546

Geggel, L., 2017. Earth's magnetic cocoon mapped in extreme detail, Space.com, issued Mar 23, 2017

ISSN number; ISSN 2202-0039

Ghose, T., 2015a. Hidden superchain of volcanoes discovered in Australia, Live Science, issued September 14, 2015

Gilluly, J., 1963. Evolution of the Western United States: Seventh William Smith lecture, Quarterly Journal of the Geological Society, 119: 113-174

Gilmer, A.K., J.R. Kyle, J.N. Connelly, R.D. Mathur, and C.D. Henry, 2003. Extension of Laramide magmatism in southwestern North America into Trans-Pecos Texas, Geology, 31 (5): 447-450; DOI:10.1130/0091-7613(2003)031<0447:EOLMIS>2.0.CO;2

Girdler, R.W., P.T. Taylor, and J.J. Frawley, 1992. A possible impact origin for the Bangui magnetic anomaly (Central Africa), Tectonophysics, 212 (1/2): 45-58; DOI:10.1016/0040-1951(92)90139-W

Gordienko, V., 2015a. Essential points of the Advection-polymorphism hypothesis. New Concepts in Global Tectonics, Journal, 3 (2): 115-136

Gordienko, V., 2015b. Advective heat and mass transfer in the Earth's tectonosphere. New Concepts in Global Tectonics, Journal, 3 (3): 282-309

Gordienko, V., 2017. Deep-seated processes and seismicity. New Concepts in Global Tectonics, Journal, 5 (2): 179-204

Gregori, G.P., and M.T. Hovland, 2025. Go for the anomaly – a golden strategy for discovery? Seepology & the origin and crucial role of the biosphere - Earth and planetary objects - Supercritical water and serpentinization. *New Concepts in Global Tectonics, Journal,* 13, (9): 1337-1491

Gregori, G.P., 1993. Geo-electromagnetism and geodynamics: "corona discharge" from volcanic and geothermal areas. Physics of the Earth and Planetary Interiors, 77: 39-63; DOI:10 .1016/S0031-9201(02)00211-X

Gregori, G.P., 2000. Geomagnetism and fundamental science. In W. Schröder, (ed.), Geomagnetism (research, past and present), *Newletter of the IDCH of IAGA*, (40), Science Edition, Bremen-Roennebeck, pp.: 12-50

Gregori, G.P., 2000c. Galaxy-Sun-Earth relations. The dynamo of the Earth, and the origin of the magnetic field of stars, planets, satellites, and other planetary objects. In A. Wilson, A., (ed.), The first solar and space weather conference. The solar cycle and terrestrial climate. *ESA SP-463, European* Space Agency, ESTEC, Noordvijck, The Netherlands, p. 329-332

Gregori, G.P., 2002. Galaxy – Sun – Earth relations. The origin of the magnetic field and of the endogenous energy of the Earth, with implications for volcanism, geodynamics and climate control, and related items of concern for stars, planets, satellites, and other planetary objects. A discussion in a prologue and two parts. Beiträge zur Geschichte der Geophysik und Kosmischen Physik, 3 (3): pp.: 1-471 [Available at http://ncgtjournal.com/additional-resources.html]

Gregori, G.P., 2006e. The Earth's interior-Myth and science. In W. Schröder, Wilfried, (ed.), Case studies in physics and geophysics. Beiträge zur Geschichte der Geophysik und Kosmischen Physik, special issue (2006/2), (Journal for the history of Geophysics and Cosmical Physics), Science Editions, AKGG, Bremen-Roennebeck, pp.: 108-126

Gregori, G.P., 2009. The Earth's interior – Myth and science, New Concepts in Global Tectonics, Newsletters, (53): 57-75. [Revised edition of Gregori (2006e).]

Gregori, G.P., 2020. Climate change, security, sensors. Acoustics, 2: 474-504; DOI:10.3390/acoustics2030026. [https://www.mdpi.com/2624-599X/2/3/26/htm]

Gregori, G.P., and B.A. Leybourne, 2021. An unprecedented challenge for humankind survival. Energy exploitation from the atmospheric electrical circuit, American Journal of Engineering and Applied Science, 14 (2): 258-291. DOI:10.3844/ajeassp.2021.258.291

Gregori, G. P., and B. A. Leybourne, 2025b. The electrostatic Sun. In press in *New Concepts in Global Tectonics, Journal*

Gregori, G. P., and B. A. Leybourne, 2025d. Measuring the electric field at ground. In press in *New Concepts in Global Tectonics, Journal*

Gregori, G. P., and B. A. Leybourne, 2025e. The physics of electrical discharges – 1. Small-scale phenomena - Fog - atmospheric precipitation – BLs. In press in *New Concepts in Global Tectonics, Journal*

Gregori, G. P., and B. A. Leybourne, 2025f. The physics of electrical discharges – 2. RB & TGFs - Runaway breakdown – terrestrial gamma flashes – GK effect. In press in *New Concepts in Global Tectonics, Journal*

Gregori, G. P., and B. A. Leybourne, 2025g. The physics of electrical discharges – 3. Sparks and lightning - electrostatics of the ionosphere – TLEs - plasma jets collimation – Birkeland currents & sea-urchin spikes - stellar and galactic alignments. In press in *New Concepts in Global Tectonics, Journal*

Gregori, G.P., and B.A. Leybourne, 2025h. The Fukushima theorem. In press in *New Concepts in Global Tectonics, Journal*

Gregori, G. P., and B. A. Leybourne, 2025i. Wildfires from the Banda Sea through Beijing and through Karakoram. *New Concepts in Global Tectonics, Journal,* 13, (6): 854-887

Gregori, G. P., and B. A. Leybourne, 2025j. The energy supply to hurricanes. *New Concepts in Global Tectonics, Journal,* 13, (5): 731-786

Gregori, G. P., B. A. Leybourne, and F. F. Bonavia, 2025v. The origin of lavakas. *New Concepts in Global Tectonics, Journal,* 13, (5): 787-811

Gregori, G.P., B.A. Leybourne, and J.R. Wright, 2025d. Generalized Cowling theorem and the Cowling dynamo, *New Concepts in Global Tectonics, Journal,* present issue

Gregori, G. P., B. A. Leybourne, Dong Wenjie, and Gao Xiaoqing, 2025h. Shallow geotherms. *New Concepts in Global Tectonics, Journal,* 13, (8): 1080-1169

Gregori, G. P., B. A. Leybourne, Dong Wenjie, and Gao Xaoqing, 2025o. Energy release from *ALB*, *CMB* and

ISSN number; ISSN 2202-0039

ICB and secular variation. V – Results, *New Concepts in Global Tectonics, Journal*, 13, (3): 433-459

Gregori, G. P., B. A. Leybourne, G. Paparo†, and M. Poscolieri, 2025a. The global Sun-Earth circuit. In press in *New Concepts in Global Tectonics, Journal*

Gregori, G. P., B. A. Leybourne, U. Coppa, and G. Luongo, 2025r. Geomagnetic anomalies: double-eyes in volcanic areas, and lineaments. *New Concepts in Global Tectonics, Journal,* 13, (6): 887-919

Gregori, G. P., B. A. Leybourne, U. Coppa, and G. Luongo, 2025t. Lightning and volcanic plumes. *New Concept of Global Tectonics,* 13, (6): 920-967

Gregori, G.P., G. Paparo, M. Poscolieri, C. Rafanelli, G. Ventrice, G. Garilli, L. Imperatori, F. Lo Castro, and G. Zimatore, 2017b. The seismic sequence in Central Italy (2016). IV – Clarifying some basic processes and concepts, New Concepts in Global Tectonics, Journal, 5 (2): 205-230

Gregori, G.P., Wen-Jie Dong, F.T. Gizzi, and Xiao-Qing Gao, 1999. The separation of the geomagnetic field originated in the core, in the asthenosphere, and in the crust. *Annali di Geofisica*, 42 (2): 191-209

Gross, R.S., 2007. Earth rotation variations-long period. Section 3.09 in T. A. Herring, (ed.), 2007. Physical geodesy. Treatise on geophysics, vol. 11, Elsevier, Amsterdam, pp.: 239-294

Hao, Lu, Xiaolin Huang, Mengsheng Qin, Yongqiang Liu, Wenhong Li, and Ge Sun, 2018. Ecohydrological processes explain urban dry island effects in a wet region, southern China. Water Resources Research, 54: 6757– 6771. https://doi.org/10.1029/2018WR023002

Harrison, R.G., K.L. Aplin, and M.J. Rycroft, 2014. Earthquake–cloud coupling through the global atmospheric electric circuit, Natural Hazards and Earth System Sciences, 14: 773-777; DOI:10.5194/nhess-14-773-2014

Hemant, K., and S. Maus, 2005. Geological modeling of the new CHAMP magnetic anomaly maps using a geographical information system technique, Journal of Geophysical Research: Solid Earth (1978–2012), 110 (B12) [23 pp.]; doi:10.1029/2005JB003837

Heydolph, K., D. Murphy, J. Geldmacher, I.V. Romanova, A. Greene, K. Hoernle, D. Weis, and J. Mahoney, 2014. Plume versus plate origin for the Shatsky Rise oceanic plateau (NW Pacific): Insights from Nd, Pb and Hf isotopes, Lithos, 200: 49-63; DOI: doi:10.1016/j.lithos.2014.03.031

Hofmann-Wellenhof, B., H. Lichtenegger, and J. Collins, 2001. Global Positioning System: theory and practice. Springer-Verlag, New York

Honora, 2013. Scientists head to the loneliest place on Earth for ESA missions, Tânia (ESA-ESTEC), Campaigns at work, issued 14/01/2013

Ingle, S., J.J. Mahoney, H. Sato, M.F. Coffin, J.I. Kimura, N. Hirano, and M. Nakanishi, 2007. Depleted mantle wedge and sediment fingerprint in unusual basalts from the Manihiki Plateau, central Pacific Ocean. Geology, 35 (7): 595–598; doi:10.1130/G23741A.1

Jeffreys, Sir H., 1976. The Earth, its origin, history and physical constitution. VI edition, Cambridge Univ. Press, Cambridge etc., pp.: 1-574

Johnson, S.K., 2017. Hunting for the reason why the Western US has so darn many odd volcanoes, *Ars Technica, issued* 22 Dec 2017

Kakinami, Y., M. Kamogawa, Jann-Yenq Liu, S. Watanabe, and T. Mogi, 2011. Ionospheric disturbance associated with radiation accidents of Fukushima I nuclear power plant damaged by the M9.0 2011 Tohoku Earthquake, Advances in Space Research, 48 (10): 1613–1616; DOI:DOI:10.1016/j.asr.2011.08.007

Karason, H. and R.D. van der Hilst, 2001. Improving global tomography models of P-wave speed I: incorporation of differential travel times for refracted and diffracted core phases (PKP, Pdiff). Journal of Geophysical Research, 106: 6569-6587

Kawakami, S., N. Fujii, and Y. Fukao, 1994. Frontiers of the earth and planetary sciences: a gallery of the planetary worlds. Journal of the Geological Society of Japan, 100, I-VIII

Keller, G., 2012. Cretaceous-Tertiary mass extinction, Chicxulub impact, and Deccan volcanism, Earth and Life: 759-793

Keller, G., A. Sahni, and S. Bajpai, 2009c. Deccan volcanism, the KT mass extinction and dinosaurs; Journal of Biosciences, 34: 709–728. DOI:10.1007/s12038-009-0059-6

Keller, G., T. Adatte, W. Stinnesbeck, D. Stüben, Z. Berner, U. Kramar, and M. Harting, 2004b. More evidence that the Chicxulub impact predates the K/T mass extinction, Meteoritics and Planetary Science, 39 (7): 1127-1144

Keller, G., T. Adatte, W. Stinnesbeck, M. Rebolledo-Vieyra, J. Urrutia Fucugauchi, U. Kramar, and D. Stüben, 2004a. Chicxulub impact predates the K-T boundary mass extinction, Proceedings of the National Academy of Sciences, 101 (11): 3753–3758

Keller, G., T. Adatte, Z. Berner, M. Harting, G. Baum, M. Praus, A. Tantawy, and D. Stüben, 2007. Chicxulub impact predates K–T boundary: new evidence from Brazos, Texas. Earth and Planetary Science Letters, 255: 339–356

Khazanovitch-Wulff, K.K., 2007. Geological consequences of large meteoric bodies approaching the Earth - the electrical factor. New Concepts in Global Tectonics, Newsletters, (43): 18-21. Also *AIG News*, (93), 21-24, 2008

Khazanovitch-Wulff, K.K., 2007a. Diatreme' trains of astroblemes or «bolide model» formation of kimberlite pipes, (in Russian). Geomaster, Petrozavodsk, pp.: 1-272

Korenaga, J., and W.W. Sager, 2012. Seismic tomography of Shatsky Rise by adaptive importance sampling, Journal of Geophysical Research: Solid Earth (1978–2012), 117, (B8) [23 pp.]; DOI:0.1029/2012JB009248

Laverov, N., S.A. Pulinets, and D. Ouzounov, 2011. Application of the thermal effect of the atmosphere ionization for remote diagnostics of the radioactive

ISSN number; ISSN 2202-0039

pollution of the atmosphere, Doklady Earth Sciences, 441, Part 1,1560–1563; DOI:10.1134/S1028334X11110183. Original Russian text Doklady Akademii Nauk SSSR, 441, (2), 245–248

Leybourne, B., J. "Mick" Davis, G.P. Gregori, J.M. Quinn, and N.C. Smoot, 2017. Evolution of Earth as a stellar transformer, *New Concepts in Global Tectonics, Journal*, 5 (1): 144-155

Leybourne, B. A., and M. B. Adams, 2020. El Niño tectonic modulation in the Pacific basin (revisited), *Systemics, Cybernetics and Informatics*, 18 (4); 107-112. 1st published in *Marine Technology Society Oceans* '01 Conference Proceedings, Honolulu, Hawai'i, November 2001

Leybourne, B.A., and N.C. Smoot, 2000. Surge hypothesis implies gravitational teleconnection of tectonics to climate: El Niño and the central Pacific geostream/jetstream, *Himalayan Geol*., 23 (1): 1-15

Liu, L., S. Spasojevi, and M. Gurnis, 2008a. Reconstructing Farallon plate subduction beneath North America back to the Late Cretaceous, Science, 322: 934-938

Livermore, P-W., R- Hollerbach, and C-C. Finlay, 2017. An accelerating high-latitude jet in Earth's core, Nature, Geosciences, 10, 62–68; DOI:10.1038/ngeo2859

Matsushita, S-, and W-H. Campbell, 1967. *Physics of geomagnetic phenomena*. 2 vol., Academic Press, New York, etc., pp.: 1-1398

Maus, S-, 2008. The geomagnetic power spectrum. Geophysical Journal International, 174 (1): 135-142; DOI:10.1111/j.1365-246X.2008.03820.x

Maus, S., 2010. Geomagnetism. Historical main field change and declination, CIRES website. Retrieved September 4th, 2021

Maus, S., and P. Weidelt, 2004. Separating the magnetospheric disturbance magnetic field into external and transient internal contributions using a 1D conductivity model of the Earth, Geophysical Research Letters, 31 (12); DOI: 10.1029/2004GL020232

Maus, S., F. Yin, H. Lühr, C. Manoj, M. Rother, J. Rauberg, I. Michaelis, C. Stolle, and R.D. Müller, 2008. Resolution of direction of oceanic magnetic lineations by the sixth-generation lithospheric magnetic field model from CHAMP satellite magnetic measurements. Geochemistry, Geophysics, Geosystems, 9 (7): Q07021; DOI:10.1029/2008GC001949

Maus, S., H. Lühr, G. Balasis, M. Rother, and M. Mandea, 2005a. Introducing POMME, the POtsdam Magnetic Model of the Earth. In C. Reigber, H. Lühr, P. Schwintzer, and J. Wickert, (eds), Earth observation with CHAMP: results from three years in orbit. Springer, Berlin, Heidelberg; DOI:10.1007/b138105,p. 293-298

Maus, S., H. Lühr, M. Rother, K. Hemant, G. Balasis, P. Ritter, and C. Stolle, 2007. Fifth-Generation Lithospheric Magnetic Field Model from CHAMP satellite measurements, Geochemistry, Geophysics, Geosystems, 8 (5)

Maus, S., M. Rother, C. Stolle, W. Mai, S. Choi, H. Lühr, D. Cooke, and C. Roth, 2006a. Third Generation of the Potsdam Magnetic Model of the Earth (POMME), Geochemistry, Geophysics, Geosystems, 7 (7)

Maus, S., M. Rother, K. Hemant, C. Stolle, H. Lühr, A. Kuvshinov, and N. Olsen, 2006. Earth's lithospheric magnetic field determined to spherical harmonic degree 90 from CHAMP satellite measurements. Geophysical Journal International, 164 (2): 319-330; DOI:10.1111/j.1365-246X.2005.02833.x

Maus, S., S. Macmillan, T. Chernova, S. Choi, D. Dater, V. Golovkov, V. Lesur, F. Lowes, H. Lühr, W. Mai, S. McLean, N. Olsen, M. Rother, T. Sabaka, Alan Thomson, T. Zvereva, and *IAGA*, Div. V, *WG VMOD*, 2005. The 10th generation international geomagnetic reference field, Physics of the Earth and Planetary Interiors, 151: 320-322

Maus, S., U. Barckhausen, H. Berkenbosch, N. Bournas, J. Brozena,V. Childers, F. Dostaler, J.D. Fairhead, C. Finn, R.B. von Frese, C. Gaina, S. Golynsky, R. Kucks, H. Lühr, P. Milligan, S. Mogren, R.D. Müller, O. Olesen, M. Pilkington, R. Saltus, B. Schreckenberger, E. Thébault, and F. Caratori Tontini, 2009. EMAG2: a 2-arc-minute resolution Earth Magnetic Anomaly Grid compiled from satellite, airborne and marine magnetic measurements, Geochemistry, Geophysics, Geosystems, 10, Q08005; DOI:10.1029/2009GC002471

McDougall, I., and R.A. Duncan, 1988. Age progressive volcanism in the Tsmanids Seamounts, Earth and Planetary Science Letters, 89: 207-220; DOI:10.1016/0012-821X(88)90173-2

McDuff, R., and G. Heath, 2009. Ocean 540: Lithosphere plate tectonics, seafloor spreading, ocean.washington.edu

Meyerhoff Hull, D., (ed.), 1996. Surge tectonics: a new hypothesis of global geodynamics. Kluwer Academic Publ., Dordrecht, etc. pp.: 1-348

Moritz, H., and B. Hofmann-Wellenhof, 1993. Geometry, relativity, geodesy, Herbert Wichmann, Karlsruhe, pp.: 1-367

Mulch, A., S.A. Graham, and C.P. Chamberlain, 2006. Hydrogen isotopes in Eocene river gravels and Paleoelevation of the Sierra Nevada, Science, 313: 87-89

Murphy, D., 2007. Silverland: a winter journey beyond the Urals, John Murray, London, pp.: 1-240

Nakanishi, M., W.W. Sager, and A. Klaus, 1999. Magnetic lineations within Shatsky Rise, northwest Pacific Ocean: Implications for hot spot-triple junction interaction and oceanic plateau formation, Journal of Geophysical Research: Solid Earth (1978–2012), 104 (B4): 7539-7556; DOI:10.1029/1999JB900002

O'Connor, J.M., and R.A. Duncan, 1990. Evolution of the Walvis Ridge-Rio Grande Rise hot spot system: implications for African and South American plate motions over plumes, Journal of Geophysical

ISSN number; ISSN 2202-0039

Research, Solid Earth (1978–2012), 95 (B11): 17,475–17,502; DOI:10.1029/JB095iB11p17475

Olsen, N., G. Hulot, V. Lesur, C.C. Finlay, C. Beggan, A. Chulliat, T.J. Sabaka, R. Floberghagen, E. Ffrisd-Christensen, R. Haagmans, S. Kotsiaros, H. Lühr, L. Toffner-Clausen, and P. Vignern, 2015. The Swarm Initial Field Model For the 2014 geomagnetic field, Geophysical Research Letters, 42, (4), 1092-1098

Ouzounov, D., S. Pulinets, K. Hattori, M. Kafatos, and P. Taylor, 2011a. Atmospheric response to Fukushima Dai-ichi NPP (Japan) accident reviled by satellite and ground observations, arXiv:1107.0930 [physics.geo-ph]

Ouzounov, D., S. Pulinets; M. Hernandez-Pajares, K. Hattori, and A. Garcia-Rigo, 2014. Geo-Space observation of atmospheric environmental effects associated with 2011 Fukushima nuclear accident, (poster), EGU General Ass. 2014

Parrot, M., 2025. DEMETER observations of the variations of the global electric circuit under various constraints, *New Concepts in Global Tectonics, Journal*, 13, (2): 355-366; ID 530865; DOI:10.1155/2013/530865

Pope, K.O., A.C. Ocampo, A.G. Fischer, W. Alvarez, B.W. Fouke, C.L. Webster, F.J. Vega, J. Smit, A.E. Fritsche, and P. Claeys, 1999. Chicxulub impact ejecta from Albion Island, Belize, Earth and Planetary Science Letters, 170 (4): 351-364; DOI:10.1016/S0012-821X(99)00123-5

Pope, K.O., K.H. Baines, A.C. Ocampo, and B.A. Ivanov, 1997. Energy, volatile production, and climate effects of the Chicxulub Cretaceous/Tertiary impact, Journal of Geophysical Research, 102 (E9): 21645-21664

Prokoph, A., H. El Bilali, and R. Ernst, 2013. Periodicities in the emplacement of large igneous provinces through the Phanerozoic: Relations to ocean chemistry and marine biodiversity evolution, Geoscience Frontiers, 4 (3): 263–276; DOI:10.1016/j.gsf.2012.08.001

Pulinets, S.A., and D.V. Davidenko, 2014. Ionospheric precursors of earthquakes and global electric circuit, Advances in Space Research, 53 (5): 709–723

Pulinets, S.A., D. Ouzounov, M. Hernandez-Pajares, K. Hattori, and A. Garcia-Rigo, 2014. Geo-Space observation of atmospheric environmental effects associated with 2011 Fukushima nuclear accident, (abstract), EGU General Ass. 2014, id.4452

Pulinets, S.A., T.B. Gaivoronska, A. Leyva Contreras, and L. Ciraolo, 2004. Correlation analysis technique revealing ionospheric precursors of earthquakes, Natural Hazards and Earth System Sciences, 4, 697–702

Quinn, J.M., 2010. Global warming. Geophysical counterpoints to the enhanced greenhouse theory. Dorrance Publishing Co., Inc., Pittsburgh, USA, pp.: 1-118

Quinn, J.M., 2012. Mapping the global lithosphere: of mega-diameter meteorite impact sites within the global lithosphere, Solar-Terrestrial Environmental Research Institute (STERI), Lakewood, CO, pp.: 1-154

Quinn, J.M., 2013. The Farallon hyper-volcano: an extinction event driver? [17 pp.], preprint (private communication)

Quinn, J.M., 2014. Global remote sensing of Earth's magnetized lithosphere, Solar-Terrestrial Environmental Research Institute (STERI), Lakewood, CO, pp.: 1-253

Quinn, J.M., 2017. Global remote sensing of Earth's magnetized lithosphere, Solar-Terrestrial Environmental Research Institute (STERI)

Quinn, J.M., and D.L. Shiel, 1993a. A unified approach to geopotential field modeling, Technical Report # 308, U. S. Naval Oceanographic Office; http://www.stormingmedia.us/35/3543/A354382.html

Quinn, J.M., and D.L. Shiel, 1993b. Magnetic field modeling of the Juan de Fuca and Explorer plates, Technical Report # 309, U.S. Naval Oceanographic Office; http://www.stormingmedia.us/70/7053/A705382.html

Rampino, M.R., and A. Prokoph, 2013. Are mantle plumes periodic? EOS, Transactions of the American Geophysical Union, 94 (12): 113-114

Regan, R.D. and B.D. Marsh, 1982. The Bangui magnetic anomaly: its geological origin. Journal of Geophysical Research, 87 (B2): 1107-1120

Regan, R.D., 1978. The Bangui magnetic anomaly, Central African Empire: final trip report. Open file report No. 78-1006. US Geological Survey.Aarons, J., 1982. Global morphology of ionospheric scintillations, Proceedings IEEE, 70: 360–378

Sager, W., and Hyun-Chul Han, 1993. Rapid formation of the Shatsky Rise oceanic plateau inferred from its magnetic anomaly. Nature, 364 (6438): 610-613; DOI:10.1038/364610a0

Sager, W.W., 2005. What built Shatsky Rise, a mantle plume or ridge tectonics? Geological Society of America, Special Papers, 388: 721-733; DOI:10.1130/0-8137-2388-4.721

Sager, W.W., Jinchang Zhang, Jun Korenaga, T. Sano, A. A. P. Koppers, M. Widdowson, and J. J. Mahoney, 2013. An immense shield volcano within the Shatsky Rise oceanic plateau, northwest Pacific Ocean, Nature, Geosciences, 6 (11): 976-981; DOI:10.1038/ngeo1934

Sager, W.W., T. Sano, and J. Geldmacher, 2011. How do oceanic plateaus form? Clues from drilling at Shatsky Rise. EOS, Transactions of the American Geophysical Union, 92 (5): 37-38; DOI:10.1029/2011EO050001.

Sano, T., K. Shimizu, A. Ishikawa, R. Senda, Qing Chang, J.-I. Kimura, M. Widdowson, and W.W. Sager, 2012. Variety and origin of magmas on Shatsky Rise, northwest Pacific Ocean, Geochemistry, Geophysics, Geosystems, 13 (8); DOI:10.1029/2012GC004235View/save citation

Sato, H., and H. Taniguchi, 1997. Relationships between crater size and ejecta volume of recent magmatic and phreato-magmatic eruptions: implications for energy partitioning, Geophysical Research Letters, 24 (3): 205-208

Schellart, W.R., and W. Spakman, 2012. Mantle constraints on the plate tectonic evolution of the

ISSN number; ISSN 2202-0039

Tonga-Kermadec-Hikurangi subduction zone and the South Fiji Basin Region. Australian Journal of Earth Sciences, 59 (6): 933-952

Straser, V., G. Cataldi, and D. Cataldi, 2026. Space weather related to potentially destructive seismic activity, In press in *New Concepts in Global Tectonics, Journal*

Stratton, J.A., 1941. Electromagnetic theory. McGraw-Hill Book Co., New York, pp.: 1-615

Takeda, M., M. Yamauchi, M. Makino, and T. Owada, 2011. Initial effect of the Fukushima accident on atmospheric electricity, Geophysical Research Letters, 38 (15); DOI:10.1029/2011GL048511

Taniguchi, H., 1993. Present situation and plan for the explosive energy estimation of phreato-magmatic explosions. In M. Akiyama, (ed.), Proceedings of the international seminar of physics of vapor-explosions, Tokyo,p. 263-269

Tattersall, R., 2013a. Apparent relations between planetary spin, orbit, and solar differential rotation, Pattern Recognition in Physics, 1: 199-202; DOI:10.5194/prp-1-199-2013

The Cenozoic CO_2 Proxy Integration Project (CenCO_2PIP) Consortium, 2023. Toward a Cenozoic history of atmospheric CO_2, Science, 382 (6675); DOI:10.1126/science.adi5177

The Economist, 2010. Inside story: plumbing the depths, Technology Quarterly, 1st Quarter, http://www.economist.com/node/15582301

Tsunoda, F., 2009. Jishin no Kuse (Habits of earthquakes) (in Japanese), 480-1 C, Y876, Kodansha, Tokyo, pp.: 1-190. Review in New Concepts in Global Tectonics, Newletters, (52): 52

Tsunoda, F., 2009a. Habits of earthquakes – Part 1: Mechanisms of earthquakes and lateral thermal seismic energy transmigration, New Concepts in Global Tectonics, Newletters, (53): 38-46. (Originally published as Tsunoda, 2009)

Turcotte, D.L., 1974. Are transform faults thermal contraction cracks? Journal of Geophysical Research, 79 (17): 2573-2577

U.S. National Park Service, 2013. Tracking the Yellowstone hotspot, http://www.nps.gov/yell/naturescience/tracking_hotspot.htm

Underwood, E., 2019. The urban dry island effect, EOS, Transactions of the American Geophysical Union, 100; DOI:10.1029/2019EO116395

Van der Hilst, R. D., 1995. Complex morphology of subducted lithosphere in the mantle beneath the Tonga Trench. *Nature,* 374: 154-157

Williams, E., and E. Mareev, 2014. Recent progress on the global electrical circuit, Atmospheric Research, 135-136: 208–227; DOI:10.1016/j.atmosres.2013.05.015

Winter, K., N. Ross, F. Ferraccioli, T.A. Jordan, H.F.J. Corr, R. Forsberg, K. Matsuoka, A.V. Olesen, and T.G. Casal, 2018. Topographic steering of enhanced ice flow at the bottleneck between East and West Antarctica, Geophysical Research Letters; *45* (10): 4899-4907; DOI:10.1029/2018GL077504

Wu, Hong-chun, 2025. Jet stream's disturbances as possible precursors of earthquakes, preprint

Zhao, Songling, Yu Hongjun, and Liu Jingpu, 1997. Origin, development and evolutionary model of shelf desertification environment in late stage of Upper Pleistocene, Science in China Series D Earth Sciences, 40 (2): 207-214

Zhou, Quan, Lijun Liu, and Jiashun Hu, 2018. Western US volcanism due to intruding oceanic mantle driven by ancient Farallon slabs, Nature, Geosciences, 11: 70–76; DOI:10.1038/s41561-017-0035-y

Acronyms

AAD - Australian Antarctic Discordance

AJEAS – American Journal of Engineering and Applied Science

ALB - asthenosphere-lithosphere boundary

Bedmap2 –British Antarctic Survey - Ice thickness and subglacial topographic model of Antarctica

BL -ball lightning CG (cloud-ground),

CGDS – Canonical Geomagnetic Depth Sounding

cgs-sym (i.e. cgs symmetric) unit system

CHAMP - CHAllenging Mini-satellite Payload

CHAOS-6 - a model of the Earth's magnetic field derived from *CHAMP, Ørsted*, and *SAC-C* magnetic satellite data

c.i.f. - con intuito fenomenale (Fermi's adage)

CMB - core-mantle boundary

CMSS - center of mass of the Solar System

CTIPE - Coupled Thermosphere, Ionosphere, Plasmasphere and Electrodynamic mode

CTJ - Chile Triple Junction

CVL - Cameroon Volcanic Line

dSBT – De Santis, Barraclough, Tozzi (law)

DUPAL –Dupré-Allègre (basalt isotopic chemism anomaly)

e.m. - electromagnetic

EMAG2 - Global Earth Magnetic Anomaly Grid

FFT – Fast Fourier Transform

GDS – Geomagntic Depth Sounding

GFZ - GeoForschunsZentrum (The German *Research Center for Geosciences*)

GPS – Global Positioning System

HARP - High-frequency Active Auroral Research Program, an array of 180 radio antennas spread over an area of 0.13 km^2

IC - inner core

IC - intra-cloud (lightning)

IGRF – International Geomagnetic Reference Field

JPL – Jet-Propulsion Laboratory

K/T - Cretaceous-Tertiary boundary (synonymous of K/Pg or KPB or KTB)

K/Pg - Cretaceous - Palæogene boundary (synonymous of K/T or KPB or KTB)

KPB - Cretaceous- Palæogene boundary (synonymous of K/Pg or K/T or KTB)

ISSN number; ISSN 2202-0039

KTB - Cretaceous-Tertiary boundary (synonymous of K/Pg or KPB or K/T)
l.o.d. - length of the day
LHB - Late Heavy Bombardment (era of Earth's history around 3.9 Ga)
LIP – Large Igneous Province
LN - Lowes-Nevanlinna plot
LVL - low velocity lens
MAGNET – MAGNET 1981 Project
MAGSAT – magnetic satellite (*NASA/USGS* spacecraft)
MAR – Mid Atlantic Ridge
mf3 - third-generation ***B*** degree-and-order 90 model for the geomagnetic potential
MHD – magneto-hydro dynamics
MOR – Mid Ocean Ridge
MORB - Mid Ocean Ridge Basalt
NCGT - New Concepts in Global Tectonics
NGDC - National Geophysical Data Center
OC - outer core
ØRSTED - Denmark's first satellite
PDO - Pacific Decadal Oscillation
PETM - Palæocene-Eocene Thermal Maximum
SH - spherical harmonic
SHE - spherical harmonic expansion
SV – secular variation
SWARM – an *ESA* satellite to study the geomagnetic field
TD – tide-driven (dynamo)
TEC - total electron content
TECU = 10^{16} *el* m^{-2} (TEC unit)
TGF - terrestrial gamma flash
TLE - transient luminous emission
UDI - urban dry island (effects)
UFZ - Udintsev Fracture Zone
ULF – ultra-low frequency (radiation)
WGS-84 - World Geodetic System, 1984 ellipsoid
WMT – Warm Mud Tectonics

NCGT Journal
New Concepts in Global Tectonics

New Concepts in Global Tectonics Journal
Volume 14, Number 1, January 2026

ISSN number; ISSN 2202-0039

Generalized Cowling theorem and the Cowling dynamo

Giovanni Pietro Gregori[1], Bruce Allen Leybourne[2], John Ricken Wright[3]

[1]Former Senior Researcher at *IDASC-Institute of Acoustics and Sensors O. M. Corbino (CNR), Rome,* now merged with the *INM-Institute of Marine Engineering "Section of Acoustics and Sensors O.M. Corbino"- (CNR Rome)*; and *ISSO-International Seismic Safety Organization*, Italy
[2]*GeoPlasma Research Institute-(GeoPlasmaResearchInstitute.org),* Aurora, CO 80014, USA
[3]*Emeritus Professor of Chemistry, Southeastern Oklahoma State University*

Corresponding Author: G. P. Gregori, *IDASC-Istituto di Acustica e Sensoristica O. M. Corbino* (CNR), Roma, now merged *into IMM-Istituto per la Microelettronica e Microsistemi* (CNR);
Email:
giovannipgregori38@gmail.com
leybourneb@iascc.org
rw4946594@gmail.com

Abstract: The classical Cowling theorem is generalized. It is rigorously shown that every system - composed of charged particles with intrinsic dynamics - is a dynamo with poloidal electric field $\boldsymbol{E}$ and toroidal magnetic field $\boldsymbol{B}$. This dynamo can be simply called "Cowling dynamo" and is a ubiquitous feature in the universe, at every scale-size. The theorem results to be a general physical property, a basic mechanism in several phenomena – from water condensation and precipitation in the atmosphere, through the physics of a spark, through galaxy alignment inside a super galactic cluster. Thus, the age-old paradox of the Cowling theorem thereby solves a nightmare for every astrophysical model of star *MHD* dynamo. Also mechanisms are discussed involving molecular interactions, leading to crystal formation and more generally involving complicated biological and cell structures. The crucial role of e.m. phenomena is emphasized, due to the key role played by the Cowling dynamo considered a leading mechanism in all these challenging processes.

Keywords: Cowling theorem - generalized Cowling theorem - dynamo with poloidal electric field $\boldsymbol{E}$ and toroidal magnetic field $\boldsymbol{B}$ - "*Cowling dynamo*" - ubiquitous feature in the universe - every scale-size - water condensation and precipitation in the atmosphere - physics of a spark - lightning - thunder blast - *TLE* - *TGF* - solar filaments - solar wind self-collimation - stellar alignments - galaxy alignment inside super galactic clusters - crystal formation - snowflakes and water forms - role of the biosphere - intricate molecular biological systems

Introduction

In 1919-1920 Larmor (1919, 1919a, 1920) proposed what is presently called an *MHD* dynamo aimed to explain the solar magnetic field $\boldsymbol{B}$, observed by means of the Babcock magnetograph (Babcock and Babcock, 1955, 1955a, and references therein). However, a few years later, Cowling (1933-1934) showed that no dynamo can be operative in the case of perfect cylindrical symmetry – such as it happens for an ideal star-model. This conclusion was traumatic for every attempt to compute an *MHD* model for the Sun or for a star. The Cowling theorem soon became almost a nightmare for astrophysicists. Several proofs were later given of the Cowling theorem, all of them with the identical result. Every proof, however, relied on suitable different approximations, and the concern has always been whether a rigorous proof can permit a non-null solution for a stellar dynamo.

The problem remained unsolved until an occasional finding reported in Gregori (2002) - where, however, the author did not realize the importance of the result, which in fact applies to natural systems within a huge range of scale-sizes. In fact, this is a generalization of the Cowling theorem, and the present paper is an attempt to synthesize the proof by relying on arguments borrowed after Gregori (2002).

Owing to the key role played by this mechanism in several applications, it is worthwhile to report the whole proof in some detail. The late Professor Raymond Hide asked for a copy and read the argument here proposed – in a preliminary although basically conclusive form - and GPG feels sincerely and very deeply indebted to him.

Anticipating the result, the generalized Cowling dynamo claims that, under very general conditions, every system of charged particles with internal dynamics[10] is an effective dynamo that, in general, can display only either one of the two patterns shown in Fig. 1. Fig. 1a has poloidal $\boldsymbol{B}$ and toroidal $\boldsymbol{E}$, while Fig. 1b has poloidal $\boldsymbol{E}$ and toroidal $\boldsymbol{B}$. The theorem states that case *(a)* is *unstable*, hence never observed, while case *(b)* is *stable*. However, the argument shows that, in the case of ideal cylindrical symmetry, the

[10] An internal energy source is essential to supply dynamics in order to avoid the implication of the virial theorem applied to plasmas (Chandrasekhar and Fermi, 1953) that claims that no plasma can be self-contained by the magnetic field $\boldsymbol{B}$ generated by itself.

NCGT Journal
New Concepts in Global Tectonics
New Concepts in Global Tectonics Journal
Volume 14, Number 1, January 2026
ISSN number; ISSN 2202-0039

stable case *(b)* has null energy, i.e., the classical Cowling theorem is correct.

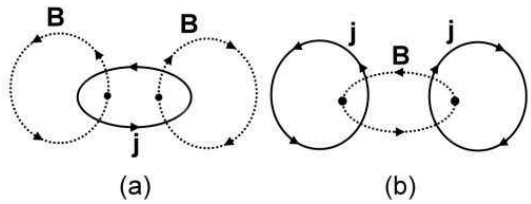

Fig. 1 – Idealized scheme of every most general dynamo composed of charge matter with some internal dynamics. Only two configurations are possible. Case *(a)* has a mere poloidal $\boldsymbol{B}$ and toroidal $\boldsymbol{j}$ or $\boldsymbol{E}$. Case *(b)* has a mere toroidal $\boldsymbol{B}$ and poloidal $\boldsymbol{j}$ or $\boldsymbol{E}$. The generalized Cowling theorem here shown states that case *(a)* is *unstable* while case *(b)* is *stable*. Concerning the classical Cowling's theorem, it is shown that, in either case, the perfect cylindrical symmetric configuration attains the maximum possible dynamo performance, even though the total energy of the stable dynamo of case *(b)* is null. In contrast, with no cylindrical symmetry the energy for case *(b)* is not null. For instance, no cylindrical symmetry occurs when the axis of symmetry of figure *(b)* is not the same as the rotation axis of the system. After Gregori (2002). With kind permission of the late Wilfried Schröder.

Preliminaries - The role of quasi-stationarity (*QS*)

A concise synthesis is here given of some arguments that are more extensively discussed in Gregori (2002, p. 41-88). The leading item deals with the dynamo process that generates the magnetic field $\boldsymbol{B}$ of stars and, maybe, of some planets. More specifically, the focus is on a few crucial physical aspects related to the physical implication of symmetry.

Symmetry is a basic feature in the following discussion and is at the heart of the generalization of the classical Cowling theorem. A comparison is therefore also required with the previous approach, in order to focus on a few key logical items.

The focus of the literature on stellar and planetary dynamos is on the well-known standard *MHD* homogeneous model. Except a few exceptions, the literature exploits mostly the deductive approach, i.e., it starts from the axioms of *MHD* and it attempts to compute the observed effects. This entire problem, however, has been - and is still - the object of great concern, controversies, paradoxical inferences, etc.

The history of the Cowling theorem is a central item in stellar and planetary dynamos, and is reviewed by Gregori (2002, section I-2, p. 44-47). No unique formulation exists even for the definition of this theorem. Some proofs were sometimes authoritatively claimed to be incorrect, etc. One crucial physical concern deals with the quasi-stationary (*QS*) approximation.

GPG feels sincerely indebted for a crucial remark by Professor Eugene N. Parker (private communication, 2000) about the use, or not, of *QS*. His remark dealt with the fact that GPG was using *QS*, unlike what is presently assumed for stellar dynamo models. Professor Parker's comments resulted crucial. Owing to this remark GPG afforded to close the logical circle (Gregori, 2002), which relates the inductive approach with the standard deductive approach used in the literature. In fact, the GPG approach was based on a mere phenomenological investigation of the available observational database, being a preliminary step before attempting to infer subsequent theoretical conclusions.

Another fundamental physical concern is strictly related to the meaning of the term "dynamo". Every author uses a somewhat different definition, and this drawback results into one additional cause of eventual discrepancy or controversy. No concise description can give an exhaustive account of this long discussion. The interested reader ought to refer to the aforementioned monograph (Gregori, 2002). We report here only the information that is needed for the present discussion.

The basis for the present approach relies on a straight implication derived from symmetry and from the classical electromagnetic (e.m.) induction and Joule heat dispersion. In addition, the concern is about some very general energy balance, independent of the constitutive properties of the system.

We first assume the requirement of *QS*. This constraint sometimes can be weakened. In particular, under special circumstances, symmetry alone can have implications almost similar to *QS*. However, it does not seem easy to include these new inferences into the framework of the general aforementioned and often intricate scenario of the historical theory of the dynamo. In any case, the most general form of the Cowling theorem - which is here proposed – does not completely overlap with the previous formulation. The older form is, rather, a particular case history of the generalized theorem here shown.

The *QS* approximation can be applied whenever, in the Maxwell laws, the $\partial \boldsymbol{D}/\partial t$ term can be neglected with respect to the $\boldsymbol{j}$ term. In the case of a pure wave of frequency $\nu = \omega/2\pi$ (where ω is the angular speed), the *QS* approximations holds whenever[11] the frequency $\upsilon \ll (2\sigma)/(\mathsf{K}_{el,0}\,\epsilon_r)$.

Therefore, the *QS* approximation is correct outside the Earth, where σ is very large (or "infinite"). In contrast, as far as the interior of the Earth is concerned, the typical values for soil (rocks) are $\sigma \approx 10^{-4}\ Mhos/m = 10^{-15} e.m.u.$ (see Fig. 2), and $\epsilon_r = 7.0 - 105.0$, while for sea water $\sigma \approx 4\ Mhos/m = 4 \times 10^{-11} e.m.u.$ and $\epsilon_r = 60 - 80$. Hence, *QS* holds for essentially all frequencies $\nu \ll 10^5 Hz$ for rocks, and $\nu \ll 10^9 Hz$ for sea water.

Whenever *QS* is adopted, every eventual non-null electric charge-density ρ is strictly neglected. As a direct consequence, this merely solenoidal $\boldsymbol{j}$ can be described in terms of closed flux-tubes of varying cross-section - i.e., of $\boldsymbol{j}$-loops. This is a well-known property, which is common to every kind of solenoidal field, such as the velocity field $\boldsymbol{u}$ within an incompressible fluid, or the $\boldsymbol{B}$ field, or the $\boldsymbol{E}$

[11] Expressed in the general unit system, not rationalized. See Gregori et al. (2025o).

NCGT Journal
New Concepts in Global Tectonics
New Concepts in Global Tectonics Journal
Volume 14, Number 1, January 2026
ISSN number; ISSN 2202-0039

field in regions of null ρ. This approximation applies, e.g., whenever *(i)* the medium has a large electrical conductivity σ, and *(ii)* the primary driving forces imply time scales that are longer compared to the typical time interval required by an e.m. signal to cross through some given geometrical fraction of the system. In fact, owing to these constraints, no ρ can accumulate anywhere, because it is promptly short-circuited and canceled. Let us point out that this approximation does not imply *per se* that we deal with an incompressible fluid, because incompressibility requires a vanishing time-variation of the *mass* density ρ_m, unlike *QS* that deals with the *electric* charge density ρ.

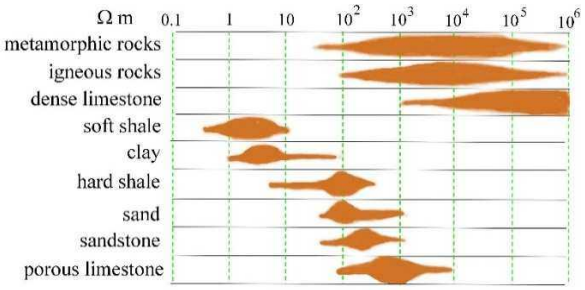

Fig. 2 - Indicative sketch aimed to focus on the resistivity ranges of different kinds of rocks or soils. The data source is Griffiths and King (1965). A similar figure is shown by Sharma (1976). Note the high resistivity of metamorphic and igneous rocks, and of dense limestone, compared to the lower resistivity of porous materials where hydration plays an important role. Unpublished figure.

In any case, even whenever *QS* is dropped, an identical picture can be applied, always in terms of ***j***-loops, although it must be suitably modified. Indeed, the term $\partial\rho(t)/\partial t$ amounts to insert a ***j***-generator into one given ***j***-loop. Moreover, all ***j***-loops in general never intersect with one another. In addition, since the system is isolated, its total Coulomb charge must be invariant. Hence, every ***j***-generator, that is associated to the term $\partial\rho(t)/\partial t$ and that injects[12] some positive charge into one given ***j***-loop, must correspondingly inject negative charges into one or a few other ***j***-loops. Therefore, reference must be made either to two, or to some bundle of several, ***j***-loops of this kind that, however, intersect with one another altogether at one given point, at which point a ***j***-generator is located, and it injects a total vanishing sum of charged particles, being distributed into parts, either positive or negative, into different ***j***-loops.

Abstraction and physical constraints

As a premise, we must consider some conceptual items. After some hard thinking and critical evaluation, it is concluded that, in the final analysis, all models that are reported in the literature imply - and often specify - a few *a priori* assumptions, or axioms, or constraints, or principles, which sometimes are the tacitly and generally agreed basis for every standard theory of a homogeneous geodynamo *MHD*. These axioms - which in general are not required by the theoretical formulation here considered – must be briefly recalled. They are, respectively:

- the *homogeneity principle* (whereby the electric charge ρ associated with every single particle can be smeared along its trajectory - that is, a ***j*** is not composed of a discrete sequence of non-infinitesimal particles and charges)
- the *non-saturation constraint* (this is assumption aimed just to avoid the Biermann's blocking[13]; see below)
- the *toroidal field assumption*, dealing with an aspect that ultimately still seems to be controversial (this assumption requires the existence of an overwhelming magnetic energy that ought to be mostly stored within the invisible dynamo, which is speculated to be associated with a toroidal ***B*** inside a planet or a star)
- the *incompressibility assumption* (that seems to be always more or less tacitly agreed)
- the *rapid rotation assumption* [whereby it is believed, with no other evidence, that some very rapid rotation always occurs inside the outer core (*OC*) of the Earth, or inside a star, etc.; that is, it is assumed that, basically, such a rotation cannot be damped by any kind of physical coupling, even though this assumption is contradictory with the aforementioned *non-saturation constraint*, i.e., with Biermann's blocking]
- the *convection assumption* (either thermal or compositional, which is believed to be the primary driver and controller of the dynamics either in the *OC* of the Earth, or inside a star).

However, under special circumstances, these axioms eventually imply some intrinsic and substantial contradiction or paradox. In particular, let us begin with the rapid rotation assumption.

"Rapid" means that Coriolis forces are supposed to play a relevant role. The concern is about the case history of a *homogeneous* conducting fluid that rotates altogether like a rigid object, where all of its parts are locked with one another by whatever kind of mutual forces. In fact, the toroidal ***B*** assumption (at least in its generally reported form, which conceives an overwhelming magnetic energy; in contrast, a *weak* toroidal ***B*** would imply no such a paradox) – or the more recently speculated large gravitational locking between eventual density heterogeneities - imply a complete, or almost complete, *blocking* of the entire system. In the case of the e.m. forces alone, this total final and very strong blocking is the aforementioned *Biermann's blocking*. A lengthy discussion of this and other critical items, with several references, is given in Gregori (2002). There is no need to repeat here this discussion.

[12] The formal injection of positive and negative particles is a formal symmetrical treatment of carriers with charge of opposite sign. In reality, one should consider that only electrons move, particularly inside strongly compacted bodies, such as, e.g., inside a planet. This physical fact, however, has no implication for the correctness of the symmetrical treatment of positive and negative carriers.

[13] Biermann (1941) pointed out a paradox, i.e., the ***B*** inside a sunspot is so large that electrons are firmly locked by ***B***. Thus, plasma cannot cool.

ISSN number; ISSN 2202-0039

In contrast, this paradox is avoided in every standard model by assuming the *non-saturation constraint,* which is more or less tacitly introduced, specifically in order to balance this severe drawback. Only in this way it is possible to avoid a full blocking of the system that should imply a total abortion of any dynamo action. In fact, it is well-known that an electrically neutral solid object - that rotates fast - generates no $\boldsymbol{B}$, i.e., it is not a dynamo, independent of every complicated and clever mathematical analysis. Indeed, a completely blocked *homogeneous* conducting fluid (and with a total neutral electric charge) behaves just like an ideal rigid object.

This *physical* difficulty is encountered by every numerical attempt to solve the *homogeneous MHD* equations. In the literature, this drawback is well-known and generally called "quenching" or "saturation".[14] Thus, every applied mathematician - who wants to compute a homogenous *MHD* dynamo - must envisage some *mathematical* "trick" capable, in some way, to provide a final solution. Therefore, he introduces some speculated "suitable" hypothetical perturbation in the equations, just in order to justify his relevant - and generally remarkable – mathematical effort. In this way, he affords to fit the generally scanty observations with the model that he was asked to "prove". However, these *ad hoc* tricks in general have no sound physical motivation other than to avoid a paradoxical final result.

In other words, the strong physical constraints and implication implied by either one axiom are balanced by some opposite equally strong implication by another axiom. How much is such an entire formulation *ad hoc*? Is it not possible - or easier or more reasonable - to appeal to some much weaker axiom, and to avoid any paradoxical constraint?

Every author likes to hypothesize the existence of an overwhelming toroidal $\boldsymbol{B}$, with rapid rotation, with $\sigma \longrightarrow \infty$, with a strong core/mantle coupling (either e.m., or gravitational). However, in this case, two difficulties must be challenged: *(i)* the aforementioned blocking (Biermann's or gravitational), and *(ii)* the Cowling theorem.

As already mentioned, one can formally get rid of Biermann's only by means of the *non-saturation constraint*, even though - in the ultimate analysis – in general this is a way to contradict other previous assumptions. In addition, as far as the gravitational coupling is concerned - that has been only comparatively recently speculated – it can be eventually introduced, e.g., only like an effect of limited amount, i.e., say, not larger than some presently unknown threshold.

As far as the Cowling drawback is concerned, some suitable failure of axis symmetry will be introduced - with the consequence that this failure acts like a perturbation on a gyroscope, i.e., implying a longitudinal drift, a phenomenon that is ultimately controlled by the kind of axis symmetry failure, or of perturbation, which was arbitrarily chosen. Indeed, it is here shown in the following that asymmetry is the key physical feature that makes operative the Earth's *MHD* dynamo.

In general, a disquieting concern of the standard treatment is about the real physical content behind these delicate mathematical decisions and handling. We can give no sound reply. The concern is about the real need to assume every one of the aforementioned axioms, or about the possibility that they only derive from some unconscious preconceived way of thinking, or from some framing of ideas and speculations, or from our cultural heritage, etc. In contrast, it is reasonable to enquire whether we should make, rather, an effort and get rid of some excess subconscious, preconceived and jointly agreed, speculation or consensus science. Do we presently violate the Ockham's razor? Elsasser (1956) and Hide (2000) make an authoritative, astute, and critical discussion of this basic and difficult logical concern.

Every realistic system $\mathbb{C}$ of currents $\boldsymbol{j}$ can be considered to have a *finite* extension, even though it is eventually contained inside some very large volume. Under *QS*, $\boldsymbol{j}$ is solenoidal and every $\mathbb{C}$ can be identified with some discrete set of closed $\boldsymbol{j}$-loops, or with some continuous distribution of $\boldsymbol{j}$-loops.

With no loss of generality - although only when dealing with the energy balance - one can divide the given system into two (or more) arbitrarily pre-defined subsystems. Then, it is rigorously possible to introduce a formal abstraction as follows.

It should be pointed out that analogous abstractions are encountered, e.g., when applying elementary geometry to natural reality. That is, a point, or a line, or a surface, never occurs *per se*, although these concepts are useful logical tools. Similarly, fractals exist in nature only like abstract models that can be applied within suitable approximations and constraints. Another abstraction is the use of the concept of "number" for counting a set of any given kind of objects; the concept of "number" is maybe one of the most primitive abstractions of our cognitive process.[15] Also the decision to use *MHD*, either by assuming $\sigma \longrightarrow \infty$ or not, or an *MHD* homogeneous dynamo, etc., is an abstraction *per se* that - in different case histories - can be more or less akin to natural reality (e.g., it applies very well to stars and galaxies, while a serious concern deals with planets), etc.

The abstraction that is here used implies to substitute every physical k^{th} subsystem D_k of $\mathbb{C}$ by one equivalent $\boldsymbol{j}$-loop C_k alone ($k = 1, 2, \ldots$). This means that every real physical k^{th} $D_k \subset \mathbb{C}$ is very different - in terms of composition and structure - compared to its formal equivalent circuit C_k. The difference, however, has no implication as far as the energy balance is concerned, as the real natural system performs in a perfectly identical way as C_k. In fact, owing to definition, the equivalence between natural reality and the simplified description in terms of equivalent $\boldsymbol{j}$-loops holds only - and strictly only - as far as the energy balance is concerned.

[14] Gregori (2002) gives several references.

[15] This is closely related to numerability, or to the concept of "time" (Gregori et al., 2022, 2022a, 2023).

NCGT Journal
New Concepts in Global Tectonics
New Concepts in Global Tectonics Journal
Volume 14, Number 1, January 2026
ISSN number; ISSN 2202-0039

The logical implications and correctness of this abstraction sometimes raised some misunderstanding. Therefore, it deserves some better explanation.[16]

There is a real physical 3D $\boldsymbol{j}$ distribution D_1, which is a subset of a larger physical real $\boldsymbol{j}$-distribution $\mathbb{C}$. The subset $D_1 \subset \mathbb{C}$ is associated with a total magnetic selfenergy U_{s1}, and with a joint magnetic energy U_j concerned with its e.m. induction interaction with the complementary subset $D_2 = \mathbb{C} - D_1$ that has a total magnetic selfenergy U_{s2}. Let us call *equivalent circuit* some hypothetical $\boldsymbol{j}$-loop - no matter how it is physically composed - that must satisfy the requirement of manifesting its presence within the entire system only - and strictly only - by means of its associated values of self- and joint energies that must be identical to the aforementioned U_{s2} and U_j .

Every *equivalent* circuit, which has thus been formally defined, can even be composed of several $\boldsymbol{j}$-loops, i.e., there is no concern about the detailed geometry, composition, and morphology. It is only - and strictly only - required that this unique $\boldsymbol{j}$-loop, which represents just one given *equivalent* circuit, reacts while respecting the aforementioned *energy* requirements and balance. Neither one can be concerned about the real physical existence of these equivalent circuits, i.e., with the real practical possibility of their definition, because they only formally replace real physical 3D $\boldsymbol{j}$ distributions, although only for energy balance estimates.

The given *equivalent* circuit can be considered only like a simple "*representation*" of the real physical 3D $\boldsymbol{j}$ distribution, in terms of a materialization of these abstract concepts. That is, one or a few equivalent circuits are analogous to some kind of modeling of a mathematical concept by means of an analogue-computer - or they are analogous to the "representation" of a thin string by means of the concept of line, or to the "representation" of a group by means of matrix formalism, etc.

One can even state that the equivalent circuit C_1 (or C_2) is just a verbal convention, as in reality it is not one single circuit, rather it is a real 3D physical $\boldsymbol{j}$ distribution D_1 (or D_2) to be identified with either one of the subsets D_1 or D_2 themselves that for simplicity are just called in the same way as two simple circuits alone, while in reality their morphology is much more complicated.

In any case, the use of the wording "*equivalent circuit*" helps in the fact that the entire subsequent discussion deals only, and strictlyplas only, with U_{s1}, U_j, U_{s2} and not with the $\boldsymbol{B}$ structure and with its general detailed geometry and morphology. Differently stated, talking about two circuits helps to recognize - in a perfectly rigorous way - the ultimate essential logical content of the *energy balance*, while forgetting about the unnecessary complications of the real physical geometry and morphology of the 3D $\boldsymbol{j}$-system and of its real $\boldsymbol{B}$.

This is a logical process, resembling, the advantage of the formulation of classical dynamics by means of the Hamilton-Jacobi variational formalism, compared to the more common treatment by means of Newton's principles, Maxwell's equations, etc.

Nevertheless, if the reader prefers, he can also identify every "equivalent circuit" C_k with the real original 3D $\boldsymbol{j}$ distribution D_k much like (in terms of the aforementioned abstractions in elementary geometry) he can equivalently eventually prefer to avoid to talk about a point, and he prefers rather the refer to a real atom, or to a dust grain, or to a huge planet, etc. - when the size of that real object is negligible compared to the space-scale that he is considering.

In the following - taken for granted such an *equivalent circuit* abstraction - reference is made only to the electromagnetic (e.m.) interaction between any two given equivalent **j**-loops C_k $(k = 1,2)$. By this, it is also implicitly supposed that every inference can be promptly extrapolated and applied to every arbitrary continuous 3D $\boldsymbol{j}$ distribution, composed of an infinite (denumerable) set of closed $\boldsymbol{j}$-loops, everyone with an infinitesimal cross-section, always contained within some finite space-domain.

Every C_k $(k = 1,2)$ has a current J_k that flows inside it, and it originates its respective fields $\boldsymbol{H_k}$ and $\boldsymbol{B_k}$, respectively. There is need to refer now to a general principle.

We call "*principle of equal variations of the magnetic selfenergies and of the opposite of the joint magnetic energy*", - or, more concisely, "*principle of magnetic energy variation*" - a rigorous result, i.e., it is a theorem although it can be applied in suitable case histories. It can be derived by college electromagnetism through a long pupil-exercise. The detail is not here given and is reported in Gregori (1999) or in Gregori et al. (2025l). The computation refers to two $\boldsymbol{j}$-loops C_1 and C_2, (Fig. 3) and to the respective self- and joint-energy, U_{s1}, U_{s2} and U_j, respectively.[17]

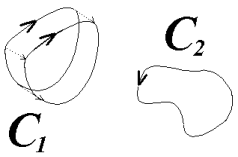

Fig. 3 - Two rigid $\boldsymbol{j}$-loops C_1 and C_2 interact with each other by e.m. induction while C_1 moves relative to C_2. After Gregori (2002). With kind permission of the late Wilfried Schröder.

In addition, consider every other kind of energy content, either kinetic, or by Joule heat, etc. Formally perform *14* Gedankenexperimenten, by changing either one $\boldsymbol{j}$-loop, either by displacing it (as in Fig. 3), or by deforming it, either when neglecting, or not, Joule heat, etc., and consider the associated variations δU_{s1}, δU_{s2}, δU_j and the variation of other forms of energy - i.e., for every respective Gendankenexperiment consider a suitably changed figure

[16] On quite a few occasions GPG had some nonsensical reaction from some referee.

[17] The concepts of (magnetic) self- and joint-energies of circuits, and of the comparatively negligible contribution by the electric energies, are taken for granted from college physics.

ISSN number; ISSN 2202-0039

similar to Fig. 3. After some lengthy formal algebra, the result is as follows.

Given any two most general distributions (in 2D or 3D) of electric current C_1 and C_2,

I) - when Joule heat can be neglected, either it is

$$\delta U_{s1} \equiv \delta U_{s2} \equiv -\delta U_j \equiv -\delta W \quad (1)$$

or either one of the following conditions hold

$$Max\ U_j \qquad min\ U_{s1} \qquad min\ U_{js2} \quad (2)$$

being

$$\delta U_{s1} + \delta U_{s2} + \delta U_j + \delta W = \delta E \quad (3)$$

where W is kinetic energy, and E includes all other forms of energy that are eventually either supplied to the system (when positive) or released by it (when negative).

II) - Whenever Joule heat cannot be neglected, U_{s1} and U_{s2} progressively damp off, while U_j is transferred step-by-step into either U_{s1} or U_{s2}, where it later decays by Joule heat. By this same principle, it is inferred that, e.g., if the permanent magnet of an AC power generator is exceedingly small compared with what ought to be needed by the conductivity and by the kinetic energy of the coil (which moves relative to it), the stray currents within the permanent magnet can severely damage it. As well, the permanent magnet of a transformer, or of an electric motor, must have dimensions suited to the output-power, otherwise the stray currents can damage it.

III) - In a third case history, one $\boldsymbol{j}$-loop is substituted by a permanent magnet, or by a "magpol" source. [18] A "magpol" object has zero electrical conductivity σ, because it has no free electrons that can move through it. In addition, a "magpol" object has a high mechanical performance. Its rheology is different compared to "solid" structure. The structure of a "magpol" object is fibrous, as every “fiber” is along the direction of all nuclear magnetic moments that must be strictly and firmly aligned one another. Therefore, if a displacement is triggered along the fiber direction, every applied mechanical deformation is irrelevant. Conversely, in the case that an external stress is applied transversally with respect to the fiber alignment, every deformation is strongly opposed. Owing to this reason, seismic S waves can propagate through the *IC*, if the *IC* is in "magpol" state.[19]

Since σ is null, no induced currents enter into play, and no transfer of magnetic energy can occur, just like it happens in the case of perfect ideal magnetostatic source. That is, all this is a strict logical requirement implied by the basic - and generally unanimously accepted - present axiomatic formulation of particle physics.

In fact, just consider that the mere magnetostatic assumption implies relevant and well-known paradoxes in terms of energy balance. Historically, magnetostatics was the former formulation of classical magnetism according to the Coulomb rationale, in terms of mere analogy of magnetostatics and electrostatics, and of the speculated existence of magnetic charges, etc. Later, the theory of electromagnetism got rid of this paradox by adopting the formulation in terms of Ampère law, i.e., of $\boldsymbol{B}$ generated by a $\boldsymbol{j}$, etc.

Summarizing, refer to the "*principle of magnetic energy variation*". The subsequent proof, which is here given, of the generalized Cowling's theorem is not a straight derivation by means of a few arguments etc. Rather, the following discussion implies a repetitive, almost obsessive, application of this "*principle of magnetic energy variation*", intermingled with a specific concern about the role of cylindrical symmetry. The focus relies therefore on a list, and discussion, of several possible case histories.

In the ultimate analysis, however, for a concise description it is sufficient to remind only about two case histories among the several possibilities that must be considered in the aforementioned *14* Gedankenexperimenten, i.e., *(i)* when one neglects Joule heat one gets

$$+\delta U_{s1} \equiv -\delta U_{s2} \equiv +\delta U_j \equiv -\delta W \quad (4)$$

or *(ii)* when one also considers Joule heat and gets

$$-\delta U_{s1} \equiv +\delta U_{s2} \equiv -\delta U_j \equiv +\delta W \quad (5)$$

Consider perfect circular $\boldsymbol{j}$-loops. Fig. 4b represents a condition of stable equilibrium, whereby U_{s1} and U_{s2} must be minimum, and U_j maximum. Joule heat in either case C_k ($k = 1,2$) is operative[20] according to (5). The result is that U_{s1} is damped by Joule heat within C_1, while U_j is transferred into U_{s2}. Analogously, Joule heat damps U_{s2} within C_2, while U_j is transferred into U_{s1}. The conclusion is that U_{s1}, U_{s2}, and U_j entirely decay.

In contrast, consider Fig. 4c that represents a condition of unstable equilibrium, whereby U_{s1} and U_{s2} must be maxima, and U_j minimum. On the other hand, U_{s1} is damped by Joule heat within C_1, and simultaneously U_{s2} is transferred into U_j (i.e., the direction of the energy transfer is opposite to the case of Fig. 4b), and analogously for the damping of U_{s2} within C_2. The conclusion is that U_{s1}, U_{s2}, and U_j entirely decay. In either case, the same relation (5) holds, although the different sign of U_j - in these two case histories - requires a different transfer of energy between selfenergies and joint-energy.

[18] Consider nuclei that are compressed by gravitation, such as it occurs, e.g., inside the inner core (*IC*) of the Earth. Whenever atoms loose the entire cloud of electrons around them, the interaction of “naked” nuclei occurs through electrostatic repulsion, but repulsion is overwhelmed by the magnetic attraction of the nuclear magnetic moments. Such a state of matter can be called “magpol” (acronym for magnetic polarization). In fact, attraction prevails, and the *IC* looks like a source of $\boldsymbol{B}$ that reminds about a permanent magnetized sphere. This explains the origin of the dipolar component of the geomagnetic field. See Gregori et al. (2024w).

[19] According to the best assessed knowledge of solid-state physics, the generally claimed statement that the *IC* is “solid” is just nonsensical.

[20] Note, however, that (5) refers to the Joule heat released within C_1 while an analogous relation applies for the Joule loss within C_2.

NCGT Journal
New Concepts in Global Tectonics
New Concepts in Global Tectonics Journal
Volume 14, Number 1, January 2026
ISSN number; ISSN 2202-0039

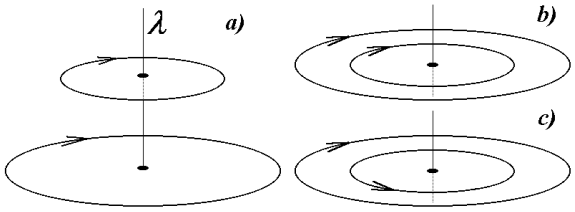

Fig. 4 - *"Both C_k ($k = 1,2$) are plane, circular, either coplanar* [*Fig.* (b) *and* (c)] *or lying on parallel planes* [*Fig.* (a)]*, and in either case with their respective center located on the same axis perpendicular to their respective planes. The* ***j*** *directions within C_k ($k = 1,2$) in Fig.* (a) *can be either the same or opposite of each other*." Figure and caption after Gregori (2002). With kind permission of the late Wilfried Schröder.

The same analysis applies to every set C_k ($k = 1,2$) of ***j***-loops that have any arbitrary shape other than the simple geometry of Figs 4b and 4c. Therefore, the system evolves while searching for final stable equilibrium, and (4) applies by e.m. induction. In the meantime, Joule heat is operative inside C_1, and (5) applies - and analogously when dealing with Joule heat inside C_2.

However, whenever the system is eventually blocked in a state of unstable equilibrium, the relation applies for the Joule loss within C_2, and Joule heat inside C_1 just applies according to (5) - and analogously the Joule heat inside C_2, although the transfer of energy by U_j has the opposite sign. In every case, the system always tends to entirely damp off U_{s1}, U_{s2}, and U_j. The system always behaves as an electric heater, never as a dynamo.

One next crucial physical concern deals with the definition of dynamo. This item cannot be entered here in great detail. Different authors used different definitions. The definition here used can be stated as follows: "*a system performs like a dynamo whenever it transforms kinetic into magnetic energy, the output being eventually varying in time, and being however 'steady' during a time range consistent with the empirical constraint. Moreover, during its action, mere e.m. induction* [*i.e., (4)*] *dominates, while the Joule loss* [*i.e., (5)*] *has a lesser, although strictly never vanishing, role. In fact, Joule heat is strictly needed in order to avoid the Biermann paradox, unless some specific other circumstances do forbid the occurrence of Biermann's blocking.*"

This definition includes the central role of the empirical constraint, i.e., the fact that the available observational evidence is always intrinsically limited - and a "dynamo" is defined whenever the output is above the detectability threshold.

For instance, in the case of the geomagnetic field, the geodynamo must have some "steady" performance. In principle, even a phenomenon dominated by (5), rather than by (4), generates a ***B***, although its time duration is comparatively very short, because it is a transient phenomenon. In fact, the definition of dynamo results to have some subtle implication, in the fact that - unlike e.m. induction that is a fundamental law - it is concerned with the concept of *steadiness* of the ***B*** generated during an adequate time lag sufficient for permitting its observation.

Different criteria were used in the literature. For instance, Hide (1981) and Hide and Palmer (1982) defined a dynamo in terms of the unsigned flux integral (the symbol × denotes scalar product)

$$N(S_0;t) = \int_{S_0} \left| B \times \overrightarrow{dS} \right| \to \neq 0 \qquad (t \to \infty) \qquad (6)$$

where S_0 is the finite surface of the volume that contains the as dynamo system, and $\overrightarrow{dS}$ is its surface element. The advantage of this definition is that N is invariant (e.g., even in the case of a contracting star), although it cannot account for the eventual generation of a toroidal ***B***, that seems to be a fundamental key feature to be assumed by every proposed standard *homogeneous MHD* dynamo model (see above).

The quantity (6) is called "*pole strength*" in the case that S_0 confines the *CMB* (core mantle boundary) of the Earth. Hide (1981) makes a clever analysis in terms of $N(S_0 0;t)$ whereby he even affords to lower the constraint $\sigma \to \infty$. In addition, he specifies that "*there is some slight arbitrariness in the literature concerning the definition of dynamo action. Some authors require that magnetic energy, and others that the effective magnetic dipole moment of the system, shall not decay (see Moffatt, 1978). There are advantages in defining self-exciting dynamo action in a fluid bounded by S_0 over the time interval $t = t'$ to $t = t''$ as requiring that the average value $N(S_0 0;t)$ shall be nonnegative (see Fig. 5), i.e.,*

$$\left(t'' - t'\right) \int_{t'}^{t''} \dot{N}(S_0;t)\, dt \geq 0 \; t'' - t' \qquad (7)$$
$$\gg Max(\tau_d, \tau_e)$$

[According to this definition introduced by Hide (1979a), the process of ***B*** amplification directly associated with the gravitational collapse of a conducting fluid does not constitute dynamo action. In the limit of perfect conductivity, while $N(S_0 0;t)$ remains constant during the collapse, the magnetic energy increases, but the magnetic moment decreases, the former being inversely proportional and the latter directly proportional to the size of the system.]" After a careful discussion Hide (1981) concludes that "*even if the dynamo action is possible in the limit when $\sigma \to \infty$, it is unlikely to be particularly efficient.*" This conclusion reminds us about the Biermann's blocking that - as mentioned above - must be avoided by means of some suitable assumption or counter-effect.

The definition of dynamo that is here adopted focuses on the magnetic energy U_s and on the e.m. induction process that occurs inside every component of the system, either fluid or not.

The difference between the substantially distinct fundamental behaviors (4) and (5) can be further highlighted by considering Fig. 4 in better detail. Let us neglect Joule heat. For instance, let either one C_k ($k = 1,2$) is either moved along λ or it is homothetically transformed in its plane into a circle of different radius (i.e., it is either expanded or contracted). Then, (4) applies in both these circumstances, independent of axial symmetry.

In contrast, let, e.g., C_1 to rotate within its plane and around its center in either Fig. 4b or 4c while its radius is kept constant. Two arguments can be applied.

NCGT Journal
New Concepts in Global Tectonics
New Concepts in Global Tectonics Journal
Volume 14, Number 1, January 2026
ISSN number; ISSN 2202-0039

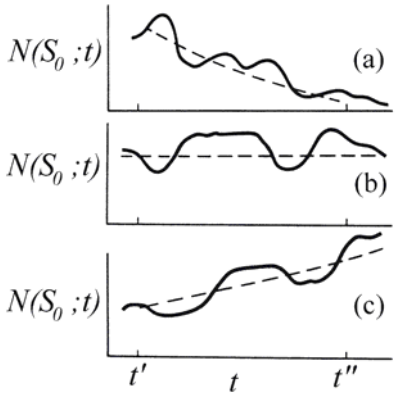

Fig. 5 - Illustrating a criterion for the definition of self-exciting dynamo according to Hide (1981). The pole strength $N(S_0 0; t)$ (i.e., the unsigned $\boldsymbol{B}$ flux across S_0) should not damp off, hence a dynamo occurs in cases *(b)* and *(c)*, not in case *(a)*. The time interval $[t'' - t']$ greatly exceeds $Max\ (\tau_d\ ,\ \tau_e)$ where τ_d is the Ohmic decay time of the system, and τ_e is the time interval within $[t'' - t']$ during which other sources are present, i.e., either permanent magnets, or the generated by e.m.f. due to noninductive effects. After Gregori (2002), being redrawn after Hide (1981). According to the present study, case *(c)* is not a dynamo as it ends into Biermann's blocking, unless a suitable energy sink is envisaged.

I. - Either it is claimed that both C_k $(k = 1,2)$ are the same, before and after such a rotation of C_1 because J_k $(k = 1,2)$ are not changed by it. In addition, no energy has been either spent or supplied. Differently stated, this is the same as to assume that no rotation of C_1 occurred, or that no real experiment was carried out. In this case, no argument can be applied. In the following, this will be briefly denoted as the "trivial" case, and it applies whenever the rotation speed of C_1 is negligible compared to the speed of the conduction charges that flow inside both C_k $(k = 1,2)$. That is, such a trivial case is often encountered in standard laboratory configurations, unlike under special circumstances in natural reality such as, e.g., inside a star.

II. -Otherwise, the motion of the externally imposed rotation must be vectorially composed with the motion of the conduction charges. Thus, it contributes to the energy balance by some suitable (positive or negative) energy amount. For instance, suppose that in this way the net J_1 is *reduced* by the rotation that is externally imposed on C_1. This is equivalent to the case in which Joule heat determines a reduction of J_1 and its corresponding energy is released outside, etc. Hence, (5) applies. The same argument holds also in the case that the conduction charges inside C_1 are rotated in order to *increase* rather than to decrease J_1, although all signs are reversed, and no analogy holds anymore with Joule dispersion (it is like the occurrence of a reverse Joule process). An ideal implementation of such a last case history can be imagined, e.g., in terms of a small ball having an electrostatic charge on it, located on top of a bar perpendicular to an axis around which it rotates, while the entire system always is strictly immaterial. Since the system has vanishing mass, a change of the rotation speed implies no kinetic energy variation, rather a variation of the magnetic self-energy of C_1, i.e., C_1 behaves like an emitting antenna and C_2 like a receiver.

In terms of intuitive variational concepts, natural reality tends to minimize the potential energy (U_{s1} and U_{s2}) and to transfer it into kinetic energy – but "kinetic energy" exists only if the system has some massive component. Since under some general circumstances a perfect frictionless system has no energy loss, it eventually oscillates back and forth up to infinity. In contrast, Joule heat - on its side - tends to destroy as much as possible the potential energy (U_{s1} and U_{s2}), and to transfer it into thermal energy, eventually by using U_j as an intermediate exchange-reservoir, which, in any case, at the very end of the whole process, must be completely empty.

Summarizing, if one wants to assess when and how a dynamo is effectively operative, this is synonymous - just by a matter of definition - of investigating when and how (4) applies rather than (5), although the additional conditions must be required of the empirical constraint, of steadiness, and of non-vanishing Joule heat.

The role of symmetry - 2D case histories

Given all the previous premises, it is possible to focus on the Cowling theorem. Consider Fig. 6a where both C_k $(k = 1,2)$ are equilateral triangles (but, the same argument applies with every other geometry), coplanar, and concentric and with some very large σ. Rotate either one C_k with respect to the other. Mere e.m. induction occurs and (4) applies. In the case of a uniform rotation speed with period T, all U_{s1}, U_{s2}, and U_j vary in time according to the qualitative sketch of Fig. 7. Hence, this case history is concerned with a real dynamo.

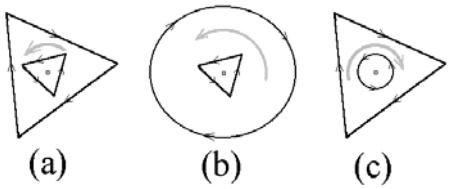

Fig. 6 - "*The indicated* ***j*** *and spin directions are arbitrary. See text.* (a) *Both* C_k $(k = 1,2)$ *are plane, coplanar, and concentric, with very large σ, and with a simple shape (equilateral triangles, but the argument applies to every other geometry). Rotate either one with respect to the other, e.g., at a uniform speed with period T. Owing to e.m. induction their respective* U_{s1}, U_{s2}, *and* U_j *vary in time according to the (qualitative) sketch of Fig. 7b and 7c. Figs* (b) *and* (c) *are the same as Fig.* (a)*, although either one* C_k $(k = 1,2)$ *is circular*." Figure and caption after Gregori (2002). With kind permission of the late Wilfried Schröder.

In Figs 6b and 6c one C_k $(k = 1,2)$ is triangular as above, the other circular. In the case that the circular C_k is rotated, (5) applies (unless one wants to consider the trivial case). In contrast, in the case that the triangular C_k is rotated, mere e.m. induction leads to straight consideration of the trivial case, which does not make sense. In principle, however, a concern is that this statement eventually holds only if one neglects some lesser effects that imply some role by (4). Such a possibility, however, can be better focused and clarified by the correct approach, i.e., in terms of a change

NCGT Journal
New Concepts in Global Tectonics

New Concepts in Global Tectonics Journal
Volume 14, Number 1, January 2026

ISSN number; ISSN 2202-0039

of reference frame, whereby one considers the rotation of the circular C_k relative to the triangular C_k, and the previous case history is obtained, where only (5) applies. Hence, in this case, no dynamo can work. Moreover, there is no need to deal with an axisymmetric $\boldsymbol{j}$-distribution. It is just sufficient that one C_k is circular (or it has a cylindrical symmetry, i.e., only this C_k is axisymmetric) and no dynamo can work (except that the other C_k acts alone like a dynamo, due to its internal processes independent of the circular C_k).

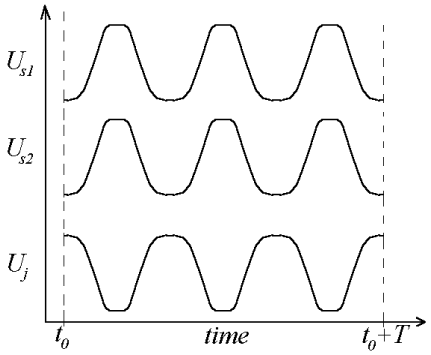

Fig. 7 - "*Qualitative sketch of the U_{s1}, U_{s2} and U_j variation* vs. t *in the case of the uniform relative rotation with period* T *of* C_k $(k = 1,2)$ *as in Fig. 6a around their common center. It is* $U_{s1} = U_{s2} = -U_j$ *apart eventual suitable additive constants.*" Figure and caption after Gregori (2002). With kind permission of the late Wilfried Schröder.

For a strict matter of completeness, however, this is not fully correct, because the definition of dynamo requests that $\boldsymbol{B}$ (not $\boldsymbol{E}$) is generated during some suitable time interval in order to match the empirical constraint. However, when we apply a transformation of the reference frame, $\boldsymbol{B}$ and $\boldsymbol{E}$ are mixed up and transformed into each other. Hence, in principle, $\boldsymbol{B}$ could vanish just because of a different choice of the reference frame, although such an extreme condition only occurs under very peculiar circumstances.

Differently stated, in principle the choice of the frame of reference is necessary in order to give a correct formal definition of dynamo, although in general a dynamo performance cannot be paradoxically canceled by any simple change of frame of reference, except at most in some very special and seldom occurring case histories. Therefore, the argument holds in general, apart the exceptional possibility that a change of frame of reference eventually cancels $\boldsymbol{B}$ and transforms it entirely into $\boldsymbol{E}$.

For instance, consider an electron located on top of an immaterial bar that makes it to rotate along a circular orbit. According to the continuity approximation of *MHD*, smear the electron charge along this circular orbit. This is the most elementary dynamo that transforms into $\boldsymbol{B}$ the kinetic energy applied to the electron mass by the immaterial bar. Change the reference frame and identify it with the rotating immaterial bar. No $\boldsymbol{B}$ is anymore generated, rather $\boldsymbol{E}$ alone, that will be different depending on whether the electron charge was smeared or not along a circle.

In any case, before applying any inferred implication dealing with the generated $\boldsymbol{E}$, $\boldsymbol{H}$, and $\boldsymbol{B}$, one should formally always apply the back transformation of reference frame. However, these details often are not of direct concern for the computation of the energy balance, because the equivalent circuit model is correct *only* when dealing with energy balance, *not* with the $\boldsymbol{E}$, $\boldsymbol{H}$, and $\boldsymbol{B}$ morphology. This fact is an additional relevant logical advantage, which is consequent to the equivalent circuit abstraction.

Summarizing, for the present purposes it can be concluded that in general no dynamo can exist in the case of all aforementioned configurations.

Consider Figs 8a and 8b, identical to Figs 6b and 6c, except that the triangular C_k is substituted by a C_k of some arbitrary shape. In either case, the same conclusion applies, i.e., no dynamo can operate whenever either one C_k $(k = 1,2)$ is circular, independent of the shape of the other C_k.

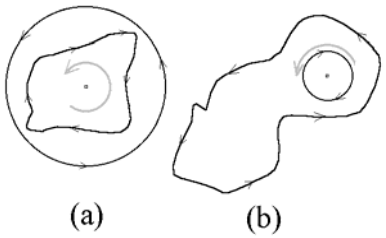

Fig. 8 - "(a) *and* (b), *the same as Figs 6b and 6c, except that the noncircular* C_k *(*$k = 1$ *or* 2*) is no more triangular, rather it has some arbitrary general shape. The indicated* $\boldsymbol{j}$ *and spin directions are arbitrary.*" Figure and caption after Gregori (2002). With kind permission of the late Wilfried Schröder.

Consider Fig. 9, identical to Figs 8a or 8b, where however both C_k $(k = 1,2)$ are coplanar, they can rotate around a common center, but their shape is general and arbitrary. Whenever either one is rotated with respect to the other, e.g., with uniform speed with period T, mere e.m. induction applies, i.e., (4), which implies a periodical output of U_{s1}, U_{s2}, and U_j according to Fig. 10. This is a dynamo.

Fig. 9 - "*The same as in Figs 8a and 8b, although both* C_k $(k = 1,2)$ *have any general shape, i.e., non-circular, non-triangular, etc. The indicated* $\boldsymbol{j}$ *and spin directions are arbitrary.*" Figure and caption after Gregori (2002). With kind permission of the late Wilfried Schröder.

That is, the deformation resulted physically determinant, of both circuits with respect to a strictly circular pattern, in order that the system acts like a true dynamo.

The following argument - which, in the 2D case history, appears redundant or almost obvious - will result crucial if its generalization is considered when dealing with a 3D dynamo.

Indeed, in Fig. 8 the concern is about the dynamo efficiency, which depends on the geometry of both C_k $(k =$

NCGT Journal
New Concepts in Global Tectonics
New Concepts in Global Tectonics Journal
Volume 14, Number 1, January 2026
ISSN number; ISSN 2202-0039

1,2). In order to get a better focus on it, suppose that one additional C_{1s} is both added and subtracted, in such a way that the system remains physically the same. It is supposed that C_{1s} is circular, or it displays some specific symmetry properties such that, by a matter of definition, it implies *per se* the regime (5), rather than (4). That is, instead of C_1 and C_2 let us deal with $C_1 = [C_1 - C_{1s}] + C_{1s} \equiv C_1^* + C_{1s}$ and C_2.

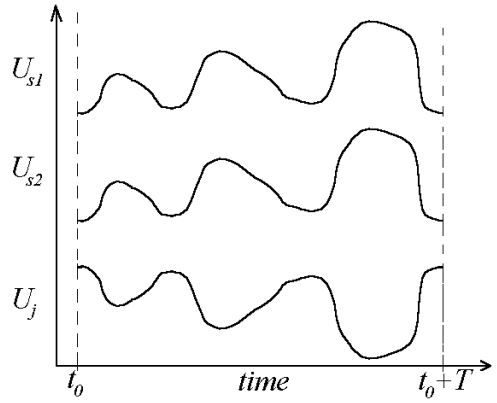

Fig. 10 - "*Qualitative sketch concerned with a uniform relative rotation between two general C_k ($k = 1,2$) with period T as in Fig. 9 (it is analogous to Fig. 7 when referring to Fig. 6).*" Figure and caption after Gregori (2002). With kind permission of the late Wilfried Schröder.

Now, one can choose C_{1s} in order to maximize the dynamo yield, or - which is the same - in order to minimize the loss W of stray energy. Symmetrically, the same argument can be applied also to C_2 similarly to C_1 as above. In general, one should deal, instead of C_1 and C_2, with C_1^* and C_2^* and search for suitable C_{1s} and C_{2s} in order to maximize the dynamo yield. For such a purpose, *a priori* four possible criteria can be tentatively considered.

I. - Either $U_s(C_{1s})$ and/or $U_s(C_{2s})$ be maximum (where the argument within the brackets of U_s specifies the **j**-loop with which U_s is concerned). This does not make sense, as one can choose both C_{1s} and C_{2s} in such a way that either $U_s(C_{1s}) \to \infty$ and/or $U_s(C_{2s}) \to \infty$.

II. - Either $U_s(C_{1s})$ and/or $U_s(C_{2s})$ be minimum. Also, this is a senseless condition, as it has the obvious solution of both C_{1s} and $C_{2s} \to 0$. Moreover, concerning both the present and the previous criterion, one should obviously be concerned with some criterion that involves also C_1 and C_2 and not only C_{1s} and C_{2s} alone.

III. - Either $U_s(C_1 - C_{1s}) = U_s(C_1^*)$ and/or $U_s(C_2 - C_{2s}) = U_s(C_2^*)$ or their sum be maximum. This amounts to search for a condition of unstable equilibrium because the system tends to cancel the self-energies of all circuits. Whenever C_1 is circular, one can increase $U_s(C_1 - C_{1s})$ as much as he likes, always keeping a condition of perfect circular symmetry of C_1^*. Hence, also this is a nonsensical solution. Moreover, it attains a maximum, rather than a minimum, of energy loss.

IV. - Either $U_s(C_1 - C_{1s}) = U_s(C_1^*)$ and/or $U_s(C_2 - C_{2s}) = U_s(C_2^*)$ or their sum be minimum. Whenever C_1 is circular, choose $C_{1s} = C_1$ and $U_s(C_1 - C_{1s}) = 0$ and the system can be reduced to the case of a dynamo system with vanishing magnetic selfenergy. In fact, owing to the Cowling's theorem, this is the correct result that had to be expected.

Summarizing, in the general case the *correct choice* is the *fourth criterion*. The given system attains the maximum efficiency, or maximum dynamo yield and minimum stray energy dispersion, whenever it requires vanishing C_{1s} and C_{2s}.

Differently stated, every system that displays circular symmetry unavoidably must perform like an electric heater, and never like a dynamo. If we want to maximize the dynamo performance - and minimize every stray energy loss - we must define C_{1s} and C_{2s} in such a way as to cancel the role of any circular symmetric component of the original given whole ***j***-distribution.

In any case, let us claim that in general we should choose C_{1s} and C_{2s} in order to get minimum $U_s(C_1 - C_{1s})$ and/or $U_s(C_2 - C_{2s})$ and/or their sum. It must be stressed, however, that, owing to the discussion of Fig. 4, these C_{1s} and C_{2s} imply only and strictly only charged particles that move azimuthally, and never either radially or along λ (i.e., the particle orbits must be circular).

However, this can be generalized. Indeed, in the case that one wants to include either one of these additional effects, the corresponding additional effects have also to be considered, and must be added to the whole - real and non-vanishing - $\mathbb{C}$ dynamo effect. That is, *a priori* all currents ***j*** that flow either radially or along λ in principle can also imply some effective dynamo action. This is shown also by the following argument.

The role of symmetry - 3D case histories

The generalization to 3D is straightforward. Indeed, let us begin and consider first every aforementioned experimental 2D configuration, and - *before* carrying out every aforementioned Gedankenexperiment - just displace either one C_k ($k = 1,2$) in such a way that its respective center is located somewhere along their common rotation axis λ, always by keeping their respective planes parallel to each other. During every experiment, however, no motion should occur along λ. Just repeat the same Gedankenexperiment as in 2D while keeping fixed the distance between these two parallel planes. Such a new 3D configuration leads to the same conclusion as for the aforementioned 2D case.

The same can be repeated by transforming homothetically all ***j*** -loops, although the homothetic transformation must be carried out always before every aforementioned Gedankenexperiment, etc.

The last concern deals therefore with the transformation of either one C_k ($k = 1,2$) into a circuit that does not lie in a plane perpendicular to λ.

This target can be achieved by considering a suitable sequence of elementary, small, stepwise deformations of a former planar circuit in order to get a progressively non-planar circuit. Consider, however, that every elementary step implies a contribution to the final dynamo efficiency,

New Concepts in Global Tectonics Journal
Volume 14, Number 1, January 2026
ISSN number; ISSN 2202-0039

and this contribution must be added in the overall energy balance of the system. In addition, every small stepwise deformation must always be applied before carrying out every aforementioned Gedankenexperiment.

That is, in the aforementioned 2D case history, both C_k were supposed to lie each one in one plane. Equivalently one can imagine any couple of two most general C_k. The only additional constraint is that their geometry must remain fixed during the entire exploitation of a Gedankenexperiment. In contrast, if they are to be modified due to their mutual interaction, a preliminary Gedankenexperiment has to be carried out in order to deform them until their final geometry. Only after this preliminary action, we can carry out the same Gedankenexperiment applied in the 2D case history.

In this way, the preliminary Gedankenexperiment changes the amount of the dynamo action provided by the system $\mathbb{C}$. In contrast, the final Gedankenexperiment affords to distinguish the fraction of $\mathbb{C}$ that ends into stray energy dispersion, and the fraction of $\mathbb{C}$ that performs like a dynamo. This distinction is, in fact, what is needed for the Cowling theorem, and for its generalization.

In any case, the final target is to attain a last-step representation of the original system in terms of two equivalent circuits alone, and both of them ought to display an internal structure that no more changes *vs.* time. This is possible, if a correct sequence was correctly defined of suitable elementary transformations to be carried out before the Gedankenexperiment.

In addition, in principle this can be made in an infinite number of different ways. One required additional property is, therefore, that one of the two circuits ought to move like a rigid body around the axis λ, and it ought to be composed of several planar circuits that are axisymmetric with axis λ.

Therefore, while referring to every pertinent 3D case history mentioned above, one can substitute every circular C_k with any arbitrary pre-chosen 3D, by a sum of two circuits C_k ($k = 1,2$) where one of them displays a perfect axisymmetric $\boldsymbol{j}$-distribution, which should always move only in terms of azimuthal rotation around λ, never along λ, nor radially (i.e., homothetically).

Owing to the same reasons that hold for the 2D case history, every perfectly axisymmetric component gives no contribution to the dynamo.

One can then optimize the 3D dynamo performance, and reduce every other stray-energy dispersion, by substituting every general $\mathbb{C}$ by a new $\boldsymbol{j}$-system where all perfectly axisymmetric parts or components have been subtracted.

In every case, the conclusion is always the same and can be summarized as follows.

I. - Given any arbitrary $\boldsymbol{j}$ distribution $\mathbb{C}$ in 3D space, suppose that it can be separated into two subsets D_1 and D_2, respectively. One subset, say D_1, displays axisymmetry around an axis λ, and moves only (and strictly only) azimuthally around it, while the other subset D_2 is composed of $\boldsymbol{j}$-loops that do not move with respect to one another. In this case no dynamo can work.

II. - Suppose that every aforementioned D_1 and D_2 is general, i.e., even nonaxisymmetric, although each subset D_1 or D_2 satisfies the aforementioned condition of being composed of $\boldsymbol{j}$-loops that do not move with respect to one another. Consider some arbitrary pre-chosen axisymmetric $\boldsymbol{j}$-distributions D_{1s} and D_{2s} (and it is intended that both these D_{1s} and D_{2s} move only azimuthally around their symmetry axis λ) and require that both $U_s(D_1 - D_{1s})$ and $U_s(D_2 - D_{2s})$, or more precisely their sum, be minimum. The system composed of the two $\boldsymbol{j}$-distributions $D_1^* = (D_1 - D_{1s})$ and $D_2^* = (D_2 - D_{2s})$ is the configuration that gives the maximum dynamo performance. Every system derived from this optimum configuration by adding any given axisymmetric $\boldsymbol{j}$-distribution (that implies only and strictly only azimuthal rotations around their symmetry axis λ) can only imply Joule dispersion, and strictly no additional dynamo action. Differently stated, such an entire operation amounts to subtract a suitable axisymmetric 3D $\boldsymbol{j}$-distribution $\mathbb{Q}$ from the given $\mathbb{C}$, and $\mathbb{Q}$ should be as large as possible in order to lower, as much as possible, the magnetic self-energy of $[\mathbb{C} - \mathbb{Q}]$.

III. - However, these two configurations composed of D_1 and D_2 alone do not fit with natural reality. A more realistic model should require consideration of a set $\{C_k\}$ ($k = 1,2, \dots K$) with K even very large, almost infinity. In this case, we should refer to every couple of these systems C_k at a time. Then, according to some clever strategy, through an error-and-trial approach, we should progressively substitute every suitably chosen couple of systems C_k (not all of them) by one respective equivalent circuit, to be later considered just like one C_k alone altogether with all remaining others. In this way, iteratively reduce - by one element at a time - the set composed by the total number K of the systems C_k, until eventually affording to reduce them only to $K = 2$. Upon a lengthy detailed analysis, it can thus be shown that this boring, and in principle logically correct, procedure must keep memory of the sequence of the systems C_k that were progressively chosen during the new definition of equivalent circuits (in addition, this procedure holds only, and strictly only, for energy balance alone). The details rely on some lengthy formal algebra, not here given, with no conceptual difficulty. From a practical viewpoint, every physical configuration is very complicated, and no simple rule can explain its entire structure, morphology, and complication. This approach is capable to manage every given system - and it appears to be maybe the only way capable to do it, although at the expense of some lengthy mathematical formalism, the complication of which, however, is just the mirror-image of the intrinsic complication of the natural physical system.

A (temporary) generalized formulation of the Cowling theorem

According to the entire previous analysis, one most general formulation of the Cowling theorem ought therefore to be as follows.

Assume *QS* and refer to a charge distribution $\mathbb{C}$ in space that, owing to *QS*, can be described in terms of closed $\boldsymbol{j}$-loops of arbitrary and varying cross-section (both in space

NCGT Journal
New Concepts in Global Tectonics
New Concepts in Global Tectonics Journal
Volume 14, Number 1, January 2026
ISSN number; ISSN 2202-0039

and time), all contained inside some given volume of finite extension, while $\mathbb{C}$ eventually moves and evolves *vs.* time t. Transient phenomena should be negligible. Also, define some arbitrary pre-chosen axis λ.

(i) Whenever $\mathbb{C}$ has axial symmetry around λ, and particles move in terms of currents $\boldsymbol{j}$ that flow azimuthally around λ and never along λ nor radially, $\mathbb{C}$ cannot be a dynamo, rather it can behave only as an electric heater.

(ii) Instead, when dealing with any most general configuration, $\mathbb{C}$ can operate eventually as a dynamo, eventually as an electric heater, eventually in both ways. It is possible to subtract from $\mathbb{C}$ some arbitrary charge distribution $\mathbb{Q}$ that is axisymmetric around λ, and such that its currents $\boldsymbol{j}$ are directed only azimuthally around (but not along λ nor radially). The system $[\mathbb{C} - \mathbb{Q}]$. acts like a dynamo only as much as $\mathbb{C}$ alone does, while, compared to $\mathbb{C}$ alone, it releases a different amount of Joule heat.

(iii) The best dynamo performance is attained whenever the system $[\mathbb{C} - \mathbb{Q}]$ has minimum magnetic selfenergy. This amounts to subtract from $\mathbb{C}$ its entire physical component that operates like an electric heater thus leaving only its component that acts like a dynamo.

Dropping quasi-stationarity

Consider whether, at least on special circumstances, the *QS* constraint can be weakened. In the final analysis, the proof given in the previous sections relies on the comparison between (4) and (5), and on the fact that in the case of an axisymmetric $\boldsymbol{j}$-loop (such as in Fig. 4) a rotation of the $\boldsymbol{j}$-loop has the same effect of a reduction, by Joule's, of the speed of the conduction charges within a wire. Whenever a $\boldsymbol{j}$-loop is moved in some arbitrary way, a dynamo effect (4) occurs. Whenever conduction charges are moved along the $\boldsymbol{j}$-loop itself, although with no change of its geometry and/or position in space, the case (5) occurs, as it is typical for an electric heater.

The same conclusion applies whenever, as a first condition, the electric energy density is negligible. Otherwise, one should introduce a different variational relation compared to (4) and (5). The second condition is that $\boldsymbol{j}$ should be at least approximately solenoidal, i.e., $div\, \boldsymbol{j}(t) = 0$ should hold. In general, these conditions are satisfied, except on special circumstances, such as inside a stellar interior where phenomena are strongly dominated by the release of thermonuclear energy. This implies that the energy balance is mostly a matter of thermodynamics, and e.m. phenomena enter into play only as a secondary effect, while adapting their role to the leading constraints imposed by the great endogenous thermal energy.

Hence, whenever the bulk plasma velocity $\boldsymbol{u}$ implies speeds much lower than light's speed, and σ is large, all parts of $\mathbb{C}$ are ultimately almost short-circuited with each other, no $\rho \neq 0$ can occur, transient phenomena are negligible, and *QS* applies.

The same argument can also be applied to every analogous Gedankenexperiment composed of bundles of $\boldsymbol{j}$-loops crossing at some common point where a $\boldsymbol{j}$-generator $\partial\rho(t)/\partial t$ is located, which supplies a total null Coulomb charge $\rho(t) = 0$ (when it is summed up over all the $\boldsymbol{j}$-loops of the bundle). Apart some formal complication - and a few warnings to be suitably considered in every case history - the entire previous argument can be repeated.

However, if the reader prefers, one can also avoid appealing to such a general approach and one can rather consider some simple case histories as follows.

Suppose to deal with no *QS*, and with an axisymmetric $\mathbb{C}$. Use cylindrical coordinates, with $\hat{\boldsymbol{z}}$-axis along λ. Consider a single charged particle alone and choose

$$u_r = 0 \qquad u_\varphi = const \qquad u_z = 0 \qquad (8)$$

The particle moves along a circle. Owing to symmetry, no charge concentration occurs at any particular azimuth φ. Hence, smear out the single particle charge along this circular trajectory, and conclude that, owing to axisymmetry requirements, this case history is reckoned to the aforementioned description in terms of a 3D distribution of closed $\boldsymbol{j}$-loops. Therefore, in this case the same conclusions hold, also independent of *QS*.

However, it is nonsensical to smear the charge of a single particle along a circle, unless one can apply the continuity approximation. The continuity approximation can be applied inside either a star or a planet or a satellite, due to the large ρ, unlike, e.g., in the case of the radiation belts in the magnetosphere. In fact, single particle orbits are considered inside the radiation belts, which are saturated as every extra amount of trapped radiation should imply an excess of particle-particle interaction, whereby their respective trapping orbits are disturbed, and every eventual extra-flux is lost, that is associated to every additional trapped particle.

This general conclusion is the same even when considering an entire 3D set of particles moving along circular $\boldsymbol{j}$-loops of the kind (5), with either identical or different orbit radii, or z co-ordinate. That is, instead of one single particle, consider a full arbitrary 3D axisymmetric distribution $\mathbb{C}$, where, however, every particle, or its respective circular orbit, satisfies the condition (8). Hence, in this case the Cowling theorem holds also for no *QS*, just due to the constraints alone of axial symmetry and of mere azimuthal motion. Note, however, that such a state is *per se* synonymous of *QS*.

The conclusion is different whenever in (8a) it is $u_r \neq 0$, as in general one can imagine that there is an axisymmetric space distribution of charge $\rho(r) \neq 0$, whereby *QS* cannot hold. Nevertheless, even in this case when *QS* cannot be applied, it is possible to deal with a description of the system in terms of a 3D distribution of closed $\boldsymbol{j}$-loops, although it is, instead of $div\, \boldsymbol{j}(t) = 0$,

$$div\, j(t) + \frac{\partial \rho(t)}{\partial t} = 0 \qquad (9)$$

One is tempted to use the same formalism based on (4) and (5). This, however, might lead to wrong results, because a charge density $\rho(r) \neq 0$ can imply a non-negligible electric energy density, whereby (4) and (5) are no more representative of the state of the system.

For simplicity, consider a very simple geometry, in terms of a torus with axis λ and of circular cross section, with a $\boldsymbol{j}$-loop being located on its cross-section with every azimuthal plane around λ. The entire system can uniformly

NCGT Journal
New Concepts in Global Tectonics
New Concepts in Global Tectonics Journal
Volume 14, Number 1, January 2026
ISSN number; ISSN 2202-0039

rotate, or not, around λ. The system can also be modified in term of closed $\boldsymbol{j}$-loops winding up around the torus surface. In every such a configuration, the associated $\boldsymbol{B}$ is toroidal. This torus can even change shape in time. Axisymmetry requires, as above, that $\rho(r) = 0$ as far as the azimuthal charge movement is concerned, while it can be $\rho(r) \neq 0$ whenever either $u_r \neq 0$ as above, or also $u_z \neq 0$.

Summarizing, in general, either for poloidal or for toroidal $\boldsymbol{B}$, the condition *QS* is fundamental for applying (4) and (5). Axisymmetry combined with azimuthal motion alone, means that - under suitable conditions - the charge particle motion must be likened to the slowing down by Joule dispersion of conduction charges within a conductor. Hence, by a matter of definition, no dynamo effect can occur. Whenever no *QS* can be used, reference ought to be made to some modified and more general formulation of the variational relations (4) and (5).

Relation with the classical Cowling theorem

Consider any given arbitrary function $F(\vartheta, \varphi)$, such as, e.g., either the $\boldsymbol{B}$ potential or its associated current function of the Chapman-Bartels (*CB*) algorithm. This *CB* algorithm is the most convenient way to represent the $\boldsymbol{B}$ produced by a continuous 2D $\boldsymbol{j}$-distribution over a spherical surface (e.g., Chapman and Bartels, 1940, p. 628).

Given a pre-chosen $\hat{\boldsymbol{z}}$-axis to be identified with the Earth's spin axis, consider the part of $F(\vartheta, \varphi)$ that is axisymmetric around $\hat{\boldsymbol{z}}$. This is uniquely defined and coincides with the sum of all terms of the spherical harmonic expansion (*SHE*) that have $m = 0$. These terms are called "zonal".

Specifically, refer to the *CB* current function. Consider separately every one of its partial contributions that is associated with one specific $\boldsymbol{j}$-loop alone. This is an equivalent $\boldsymbol{j}$-loop, resulting from an abstraction, which, however, in any case shares the same symmetry properties of the real $\boldsymbol{j}$-distribution that it represents. Hence, the only axisymmetric $\boldsymbol{j}$-loops of such a *SHE* are just terms with $m = 0$. On the other hand, once the base reference frame - or set of base functions, i.e., the spherical harmonics (*SH*s) - has been pre-chosen and fixed, the subsequent expansion is *uniquely* defined. Differently stated, the set of all $\boldsymbol{j}$-loops with $m = 0$ represents the *uniquely defined* part of the *physical* $\boldsymbol{j}$-distribution that has the required axisymmetry.

Moreover, consider the aforementioned $\boldsymbol{j}$-distribution named $\mathbb{Q}$ and appearing in the aforementioned formulation of the generalized Cowling theorem. The theorem was defined by requiring that the system $[\mathbb{C} - \mathbb{Q}]$ must have a minimum U_s. Its equivalent $\boldsymbol{j}$-loops - that are represented by the terms of the aforementioned *SHE* terms of the *CB* argument - do in fact correctly represent the energy content of their respective subsystem.

Moreover, since the base functions of the expansion (i.e., the *SH*s) are orthogonal, it is well known that their U_s is proportional to the sum of the square of their expansion coefficients. That is, all the coefficients of the *SHE* do contribute proportionally to their respective square, independent of their sign.

Therefore, it is concluded that the aforementioned $\boldsymbol{j}$-distribution $\mathbb{Q}$ can be rigorously identified with the $\boldsymbol{B}$ potential associated to the $\boldsymbol{j}$-distribution on the spherical surface of the *CB* algorithm that was defined by all zonal terms alone of its respective *SHE*. In particular, owing to the Cowling theorem, since these zonal terms cannot derive from a self-sustained dynamo, they must be continuously regenerated by the dynamo process, although their fate is to decay according to (5), while (4) can never be applied to them. Hence, they cannot be self-sustaining.

The aforementioned formulation of the generalized Cowling's theorem can thus be completed as follows.

The generalized Cowling's theorem

Assume *QS* and refer to a charge distribution $\mathbb{C}$ in 3D space, which is contained within some volume of finite extension, while $\mathbb{C}$ eventually moves and evolves *vs.* time t. Transient phenomena should be negligible. Also, define some arbitrary pre-chosen axis λ.

(i) – Whenever $\mathbb{C}$ has axial symmetry around λ, and particles move in terms of $\boldsymbol{j}$ that flow azimuthally around λ, and never along λ nor radially, $\mathbb{C}$ cannot be a dynamo, rather it can behave only as an electric heater.

(ii) – Instead, when dealing with any most general configuration, $\mathbb{C}$ can operate eventually as a dynamo, eventually as an electric heater, eventually in both ways. It is possible to subtract from $\mathbb{C}$ some arbitrary charge distribution $\mathbb{Q}$ being axisymmetric around λ, and such that its currents $\boldsymbol{j}$ are directed only azimuthally around λ, and neither along λ nor radially. The system $[\mathbb{C} - \mathbb{Q}]$ acts as a dynamo only as much as $\mathbb{C}$ alone does, while, compared to $\mathbb{C}$ alone, it releases a different amount of Joule heat.

(iii) – The best dynamo performance is attained whenever the system $[\mathbb{C} - \mathbb{Q}]$ has minimum magnetic self-energy.

(iv) – The $\boldsymbol{j}$-system $\mathbb{Q}$ can be chosen as follows. Consider the $\boldsymbol{B}$ observed over some surface that envelops the system, and consider the magnetostatic potential of such a $\boldsymbol{B}$. Express it as a *SHE*, and keep only its zonal terms (i.e., only the terms with $m = 0$). The resulting potential coincides with the uniquely defined potential of the needed $\mathbb{Q}$. Hence, subtract from $\mathbb{C}$ any $\boldsymbol{j}$-system, which is characterized by this potential. Note that $\mathbb{Q}$ cannot be uniquely defined *per se* by means of this physical constraint alone, as different $\boldsymbol{j}$-systems can provide this potential, their real geometry and morphology depending rather on the internal structure of the Earth or planet, or on the internal processes of a star, etc. However, all these physical and structural details are *per se* unessential to define the self-energy of $\mathbb{Q}$, which is the only physical quantity of concern for the energy content and for the generalized Cowling's theorem *per se*. That is, the arbitrary addition of $\boldsymbol{j}$-systems to $\mathbb{Q}$ implies a production of Joule heat that is independent of the dynamo performance of the whole system.

NCGT Journal
New Concepts in Global Tectonics
New Concepts in Global Tectonics Journal
Volume 14, Number 1, January 2026
ISSN number; ISSN 2202-0039

Note that no prescription is required concerning the driver that determines the dynamics of charged particles. Only particles are required that move along closed trajectories, driven by any cause. *The Cowling dynamo always works and transforms kinetic energy into e.m. energy. This is therefore a universal theorem that applies on every spacetime scale, except in the atomic and subatomic domain,* where Maxwell laws do not apply.

Note that this most general formulation of the Cowling's theorem in reality does not include all case histories considered by its previous formulations. In fact, the form here given only relies on consideration of the role of azimuthal $\boldsymbol{j}$, while previous formulations also deal with more general axisymmetric configurations - such as exemplified by the simple case histories of Fig. 1.

Only for comparison purpose, consider, e.g., that the axisymmetric nature of the zonal terms (i.e., with $m = 0$) - compared to the non-axisymmetric nature of the terms with $m \neq 0$ - is the leading rationale for the so-called 2D dynamos reviewed by Fearn (1998), who states that this concept "*denotes models fully resolved in r and ϑ but only with limited resolution in φ ... This essential interaction between nonaxisymmetric ($m \neq 0$) and the mean ($m = 0$) part of the field is the most important role of the non-axisymmetric part of the problem. This will be present if we model the dynamo with its axisymmetric part and only one non-axisymmetric mode - i.e., truncate the summation in m ... to only two terms: $m = 0$ and one other value of m ... The effect and importance of interactions between different non-axisymmetric modes can be explored by gradually increasing azimuthal truncation ... Perhaps our best tool at present is the 2D model ... The hope is that including the essential interaction between axisymmetric and non-axisymmetric parts will model the fundamental physics of the dynamo.*"

It seems reasonable to enquire whether rotation alone is - or can be – essential for dynamo performance. For instance, one can eventually just operate with a reference frame co-rotating with the star or planet and consider whether a dynamo action exists even in this reference frame.

First, when subtracting the zonal *SHE* terms from the *CB* algorithm, all other $\boldsymbol{j}$-loops are unchanged and have a wavy pattern *vs.* longitude φ. Therefore, they interact with rotation. This phenomenon is determinant whenever there is some differential rotation of different parts of the system.

Second, consider the ideal case of one electron that rotates in a plane around an axis, i.e., this is the case of (5). Owing to the continuity approximation of *MHD*, smear its charge along its entire trajectory and consider that it generates a $\boldsymbol{B}$, i.e., this constitutes the most elementary dynamo.

Suppose that we use a reference frame that co-rotates with the electron, whereby $\boldsymbol{B}$ no more exists, rather only an $\boldsymbol{E}$, hence no dynamo exists. Therefore, it is concluded that one must always pre-choose a reference frame, and then, within it, one can discuss about the eventual dynamo action of the system. Rotation is not an option; rather, sometimes it is a crucial ingredient for every dynamo.

The present concern is about the two Gedankenexperimenten representing ideal physical configurations of Fig. 1. Let us discuss whether they fit or not with the aforementioned arguments and rationale.

One configuration imagines a mere poloidal $\boldsymbol{B}$ and mere toroidal $\boldsymbol{j}$-loops (Fig. 1a). It is $curl\ \boldsymbol{B} = 0$, hence $\boldsymbol{B} = grad\ V$, and the potential V can be expressed in terms of a *SHE*. The terms with $m = 0$ cannot be representative of a dynamo, because - according to the aforementioned formulation of the Cowling's theorem - the entire $m = 0$ system of this toroidal $\boldsymbol{j}$-loops (one can consider directly the real rather than the equivalent $\boldsymbol{j}$-loops) coincides with the $\mathbb{Q}$ system itself. In addition, the terms with $m \neq 0$ originate a non-vanishing $\boldsymbol{B}$, although it rapidly decays. In fact, particles are trapped while spiraling around $\boldsymbol{B}$-field lines, and shortly leave the system at a large speed along approximately equipotential trajectories. Hence, this is not a dynamo, as it lacks steadiness. That is, every system with a mere poloidal $\boldsymbol{B}$ and mere toroidal $\boldsymbol{j}$ will never be a dynamo.

The other ideal configuration (Fig. 1b) has a mere toroidal $\boldsymbol{B}$ and mere poloidal $\boldsymbol{j}$. It is $curl\ \boldsymbol{B} \neq 0$, and one should use a vector potential, etc. In addition, owing to completeness and orthogonality of the *CB*'s *SHE* and owing to the intrinsic symmetry properties of every term of the *SHE*, it is concluded that in this case the $\mathbb{Q}$ system of the Cowling theorem must strictly vanish. That is, the system has a maximum dynamo performance. However, independent of the toroidal $\boldsymbol{B}$ and poloidal $\boldsymbol{j}$, if the system has perfect cylindrical symmetry, the system cannot be a dynamo, consistently with to the Cowling theorem in its original formulation, as both $\boldsymbol{B}$ and $\boldsymbol{u}$ are axisymmetric. Hence, the system has a maximum dynamo performance, but its maximum is zero. That is, this invisible dynamo is ruled out in agreement with Kaiser et al. (1994).

For brevity, we call "*Cowling dynamo*" every configuration of the kind of Fig. 1b, and the generalized Cowling theorem can be stated by claiming that Fig. 1a is never a dynamo, and Fig. 1b is a dynamo, although in the case of perfect cylindrical symmetry, the total generated $\boldsymbol{B}$ is null.

Applications

The Cowling dynamo explains several presently unexplained features observed on a wide range of scale sizes, both in space ad time. We highlight a few relevant case histories, as a simple reminder. A very large literature exists, but – owing to brevity purpose – we cannot report the related discussion. A more general discussion is also given in Gregori et al. (2025w).

Water condensation and precipitation in the atmosphere is generally reported as unexplained. Condensation nuclei are certainly provided by cosmic rays (Svensmark effect), which are proven to account for a large fraction of precipitation. An older hypothesis (Bowen hypothesis) appeals to aerosol particles. One should consider also the atomic and molecular ions produced by friction of air flowing over Earth's surface. However, how a condensation nucleus evolves and becomes a droplet is unexplained.

NCGT Journal
New Concepts in Global Tectonics
New Concepts in Global Tectonics Journal
Volume 14, Number 1, January 2026
ISSN number; ISSN 2202-0039

When the droplet is formed, the balance between surface evaporation and surface tension controls the droplet evolution. The Cowling dynamo fills this logical gap as follows.

A water molecule is an electrical dipole. Hence, water molecules are electrostatically attached to an electrified condensation nucleus as shown in Fig. 11. Several layers of water molecules pile up around the condensation nucleus while the whole micro-system keeps the electrical charge of the former nucleus. A similar figure, borrowed from the literature, is shown in Fig. 12.

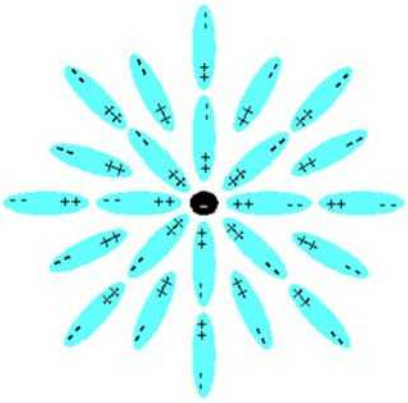

Fig. 11 – Cartoon showing the agglomeration of water molecules like electric dipoles around a condensation nucleus with negative electric charge. A symmetric case history occurs for a positively charged nucleus. See text. Unpublished figure.

Suppose that a local tenuous thermal instability determines some micro-convection process. The Cowling dynamo generates, on the micro-scale, a tenuous e.m. field. Water molecules in the environment are electrically neutral and are not affected by the electric field $\boldsymbol{E}$, unlike condensation nuclei that have a charge. Hence, the condensation nuclei, and their water envelop, move through the environment that is filled with water molecules. The motion acts like a broom that collects water until eventually forming a droplet. Phenomena are extremely tiny and different case histories occur.

The mildest phenomenon is the formation of a tiny droplet that remains suspended in air. This is fog. When driving on a highway with a thick fog, it is well known that the fog fades off while crossing a river. In fact, the thermal contrast determined by the river is such as to enhance the Cowling dynamo. Thus, the tiny droplets increase their motion, collect new water molecules, and precipitate due to increased weight.

Suppose that a local tenuous thermal instability

The next phenomenon is rain or snow precipitation, which occurs whenever the Cowling dynamo is such as to produce heavier water droplets that cannot remain suspended in air.

Hail refers to the case of comparatively larger convection cells inside clouds, by which a droplet – before precipitating – experiences several cycles inside the cell, melting and freezing several times, until a hail grain is formed. See below.

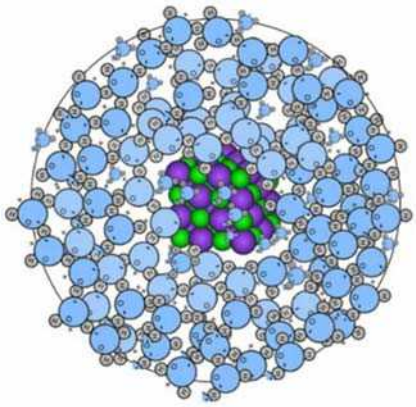

Fig. 12 – Cartoon showing the concept of "ion-induced nucleation". After Ouzounov et al. (2014). With kind EGU permission CC BY 4.0 license.

Anomalous "local" phenomena can represent a valuable test for interpretation of unexplained events. In the middle of September 2022, the Marche Region (Central Italy, Adriatic coast) was hit by a severe flood (Pescara and surrounding towns and villages). The event caused *12* causalities and was unpredicted, and meteorologists stressed that some $\sim 40\ km$ apart it did not even rain. Nobody noticed, however, that during those same days a swarm of instrumental earthquakes hit that area[21] (Fig. 13). The interpretation is that the unnoticed seismic swarm denotes a local crustal fracturing with enhanced soil exhalation that changed the thermal equilibrium, hence the local Cowling dynamos, which caused severe and abrupt precipitations. This interpretation could be confirmed only if local shallow geotherms are eventually available (see Gregori et al., 2025h).

Let us shift to visual phenomena.

Begin from a few ten-centimeter size. Whenever a temporary convection cell is triggered inside an ionized environment – such as it typically occurs, e.g., inside a home fireplace – a Cowling dynamo generates a toroidal **B** that confines like a "plasma bottle" a hot plasma inside a much colder magnetic envelop. The phenomenon emits light and is called "ball lightning" (*BL*). At present, this is generally considered a "mystery" of nature. The phenomenon was checked in the laboratory. Normally a *BL* has a short life, as it lasts as long as an internal heat source supplies convection. When the heat source exhausts, the *BL* fades off, leaving a smell of ozone and nitrogen oxides, due to oxygen and nitrogen in air.

Case histories were reported of *BL*s that cross through the windows of an aircraft with no consequence on the airplane window glass. In fact, while crossing the glass, electrons are exchanged between the $\boldsymbol{j}$-currents of the *BL* plasma bottle and the electrons of the solid structure of the

[21] We are indebted to Claudio Rafanelli for stressing this correlation.

NCGT Journal
New Concepts in Global Tectonics
New Concepts in Global Tectonics Journal
Volume 14, Number 1, January 2026
ISSN number; ISSN 2202-0039

glass, while the mechanical performance of the glass is unaffected.

This possibly leads to a better understanding of the unexplained nature of a spark or of a lightning (see Gregori and Leybourne, 2025e, 2025f, 2025g). Namely, the concern is about explaining why a spark, or a lightning have the shape of an arrow - rather than looking like a diffuse flux of charges between two electrodes.

Fig. 13 – Seismic shocks in Italy, between 14th September 2022 and 17th September 2022 (18:28:14 UTC) showing a swarm in Central Italy in an area that was hit by intense local precipitations, with floods and victims. Meteorologists stressed the impossibility to forecast such an event. Image based on the seismic database of *INGV*, kindly provided by Claudio Rafanelli who stressed this correlation.

Suppose that a *BL* is supplied somewhere in air. It lasts as long as the internal heat sources supplies convection. When the *BL* fades off, it releases the very hot plasma inside a nearby small air volume, where a new *BL* is generated. The phenomenon propagates like a domino play of contiguous *BL*s. This explains why the propagation speed of a lightning bolt is very slow, compared to light speed, and can be measured by a fast motion camera. This is an original explanation of the mysterious phenomena observed inside every spark or lightning. When a lightning is triggered, the discharge ground-cloud-ground is an oscillatory phenomenon; hence, it is irrelevant whether the trigger starts a ground-top lightning or a top-ground discharge. Note that the huge convection inside clouds generates – through Cowling dynamo - an intense e.m. field that, beneath clouds, is related to cloud-ground-cloud oscillatory discharges, and, above clouds, supplies the electric charge of the ionosphere, including phenomena eventually manifested like *TLE*. In addition, the charging of the ionosphere is positive, because the Cowling dynamo – that *per se* can imply either a positive or a negative charging of the ionosphere - must be of one given sign alone, i.e., positive, as the ionosphere already has a positive charge, due to the positive charge of the solar wind (Gregori and Leybourne, 2025b).

Large convection cells inside clouds determine strong e.m. fields that trigger intense cloud- cloud (*CC*) lightning bolts, which are more frequent than cloud-ground (*CG*) lightning. However, a great amount of invisible *CG* discharges is associated to huge air-earth currents.

Consider that, according to the literature, no explanation is available for explaining how a thunderclap is generated. Let us attempt to explain it. A single *BL* is observed inside a closed room (a home fireplace, or the cockpit of an airplane, etc.). A *BL* typically lasts a fraction of a second, or at most a matter of seconds, before vanishing while releasing a gentle noise. One can speculate, e.g., that the domino effect of a huge number of *BL*s originates an almost simultaneous noise that rumbles like a typical spark.

The case history of an *IC* or *CG* discharge derives from huge thermal convection cells of the size of a large cloud. The electrical discharge can be associated – or not – with luminous phenomena. If a luminous emission occurs, a lightning happened. However, in principle no reason requires that every electrical discharge is associated to luminous emission. Hence, whether the luminous emission occurs or not, the *BL* domino effect is the crucial mechanism. When the *BL*s vanish, in a matter of a few seconds they release altogether a noise similar to a spark. However, the noise propagates homogenously, in 3D, through the environment, which is composed of huge convection cells that we visually observe like clouds. The environment is composed of a medium characterized by a large gradient of mass density and of water content, hence also of sound speed. The final effect is therefore the typical rumbling noise of thunderclaps. That is, noise propagates in 3D and the rumbling effect ought to be justified by the varying air mass-density, humidity and temperature, which control the sound speed through air.

Some echo phenomena can occur, such as, typically, inside narrow mountain valleys. A spark noise is omnidirectional in the lab, and a thunderclap is omnidirectional in the atmosphere. Indeed, no lab experiment shows that the noise is stronger, e.g., along the axis of the spark than perpendicularly to it. Similarly, no reason seems to envisage that a thunderclap is stronger, whether the lightning is *IC* or *CG*. My point in the lavaka paper about this, is that if you are located along the axis where the lightning terminates, the sound will appear stronger to the observer on the ground than any lightning up in the clouds. Thus, this ground effect may possibly be related to some harmonics of the lavaka formation, as we discussed in the other paper. Your case history only considers IC and CG lightning, but how can GC lightning be distinguished from CG lightning? Vaisala -a global lightning detection network company- notes that this is

NCGT Journal
New Concepts in Global Tectonics
New Concepts in Global Tectonics Journal
Volume 14, Number 1, January 2026
ISSN number; ISSN 2202-0039

distinguished by the clouds lowering towards the ground before a strike, indicating a ground effect.

With reference to the concern about hail prevention, suppose that an area has a reasonably dense network of lightning rods, which should ensure a steady air-earth current flow, eventually observable like St. Elmo fires. These air-earth currents discharge the energy of the convective system of the cloud. Is this loss of energy sufficient to reduce hail size, or even to prevent it? It is difficult to reply, unless by carrying out experiments.

Moreover, convective cells inside cloud are responsible for three other phenomena.

(i) Transient luminous events (*TLE*s) are a comparatively recent huge chapter of the investigations of observations above clouds.

(ii) The same mechanism is the most credible cause of the well-known positive electric charge of the ionosphere. At present, it is explained by the earlier - although, maybe, not fully convincing - hypothesis (by C.T.R. Wilson)[22] that is fashionable since the 1910s, i.e., charge separation occurs due to the different electrostatic charge of water droplets (inside clouds) depending on droplet radius.

(iii) The third phenomenon is the more recently discovery of the deadly terrestrial gamma flashes (*TGF*s), observed mostly in areas of intense storm activity. The generated $\boldsymbol{E}$ is such as to produce Bremsstrahlung γ-rays, which are released both downward and upward, and are reasonably guessed to explain some air-crash.

Specific laboratory experiments address plasma jets. No detailed mention can be here given. Let us just quote e very recent finding. Bellan (2023) is illustrated by Velasco (2023), who claims that "*in a vacuum chamber, wisps of gas are ionized by several thousand volts. One hundred thousand amps then flow through the plasma, producing strong* $\boldsymbol{B}$ *that mold the plasma into a jet traveling around* $10\ miles\ sec^{-1}$ *(*$\sim 16\ km\ sec^{-1}$*). High-speed recordings show that the jet transitions through several distinct stages in* $a\ few\ 0.1\ \mu sec$*. Bellan says the plasma jet looks like an umbrella growing in length. Once the length reaches one or two feet (*$30-60\ cm$*), the jet undergoes an instability that causes it to transform into a rapidly expanding corkscrew. This rapid expansion triggers a different, faster instability that creates ripples.*

'The ripples choke the jet's $100\ kA$ electric current, much like putting your thumb over a water hose restricts the flow and creates a pressure gradient that accelerates water,' *Bellan says*. 'Choking the jet current creates an electric field strong enough to accelerate electrons to high energy.'

Those high-energy electrons were previously identified in the jet experiment by the X-rays they generate, and Bellan says their presence was a surprise. That's because conventional understanding says the jet plasma was too cold for electrons to be accelerated to high energy … Although this plasma had a temperature of $\sim 20{,}000\ K$ *, … it is nowhere near the temperature of the Sun's corona, which is over* $1{,}000{,}000\ K$*. ….*

Cold plasmas were thought to be incapable of generating high-energy electrons because they are too 'collisional,' meaning an electron cannot travel very far before colliding with another particle. … In the case of a cold plasma, an electron would accelerate only about one micron before colliding and slowing down.

The Bellan group's first attempt at explaining this phenomenon was a model suggesting that some fraction of the electrons manages to avoid colliding with other particles during the first micron of travel. … But while compelling, the theory was wrong, Bellan says.

'It was realized that this argument has a flaw,' *he says,* 'because electrons don't really collide in the sense of hitting something or not hitting something. They are all actually deflecting a little bit all the time. So, there's no such thing as an electron that's colliding or not colliding.' … "

Note that this behavior is closely consistent with the Cowling dynamo confinement. In addition, a very recent finding deals with a new instability that also contributes to a self-collimation of plasma (see Shalaby et al., 2021, 2022, 2023, illustrated by *Leibniz Institute for Astrophysics Potsdam*, 2023).

On a larger scale-size, remind about the self-collimation of solar wind, which is reported unexplained (Gregori and Leybourne, 2025b). That is, the Cowling dynamo generates a magnetic confinement, which the standard *MHD* treatment cannot explain. See Gregori et al. (2025w).

An additional effect must be considered in the solar wind, relying on a study by Park et al. (2018), illustrated by Zyga (2018). The effect reminds about observations of electrical discharges through gases reported in college textbooks on experimental physics. Quoting Zyga (2018), "*the phenomenon of ionic wind has been known for about four (?) centuries: by applying a voltage to a pair of electrodes, electrons are stripped off nearby air molecules, and the ionized air collides with neutral air molecules as it moves from one electrode to the other."*

Park et al. (2018) claim that "…*the electric wind, … supposedly occurs due to the charged particle–neutral coupling in systems of weakly ionized gases, but this mechanism remains unclear.* [They] *report direct evidence that electric wind is caused by an electrohydrodynamic force generated by the charged particle drag as a result of the momentum transfer from electrons/ions to neutrals. The model experiment is based on a pulsed plasma jet as a source of weakly ionized gases generated in the helium gas at atmospheric pressure using Schlieren photography. Studying the helium gas flow trajectories at different discharge parameters allows one to distinguish between the effects of streamer propagation or space charge drift causing the electric wind as well as to determine the role of electrons and (positive) ions in wind generation*." The Schlieren photography is a technique often used to photograph airplanes in flight. Park et al. (2018) synthesize their study by means of Fig. 14.

They carry out a clever theoretical treatment. Refer to their paper. They rely on some approximations, such as n_i (and n_e), j_i (and j_e), and μ_i (and μ_e) that are the number

[22] Charles Thomson Rees Wilson (1869-1959).

NCGT Journal
New Concepts in Global Tectonics
New Concepts in Global Tectonics Journal
Volume 14, Number 1, January 2026
ISSN number; ISSN 2202-0039

density, the current density, and the mobility of ions (and electrons), respectively. They consider the force per unit volume $F_{i;e-n}$ in a weakly ionized gas, and consider that in the non-neutral region it is $n_i \neq n_e$. They call this phenomenon *EHD* (electro-hydro dynamics), while according to the scheme explained in Gregori and Leybourne (2025b), it is more appropriate to call it *EGD* (electro-gas dynamics), which refers to a compressible fluid like a gas, while *EHD* should refer to an incompressible fluid, such as a liquid.

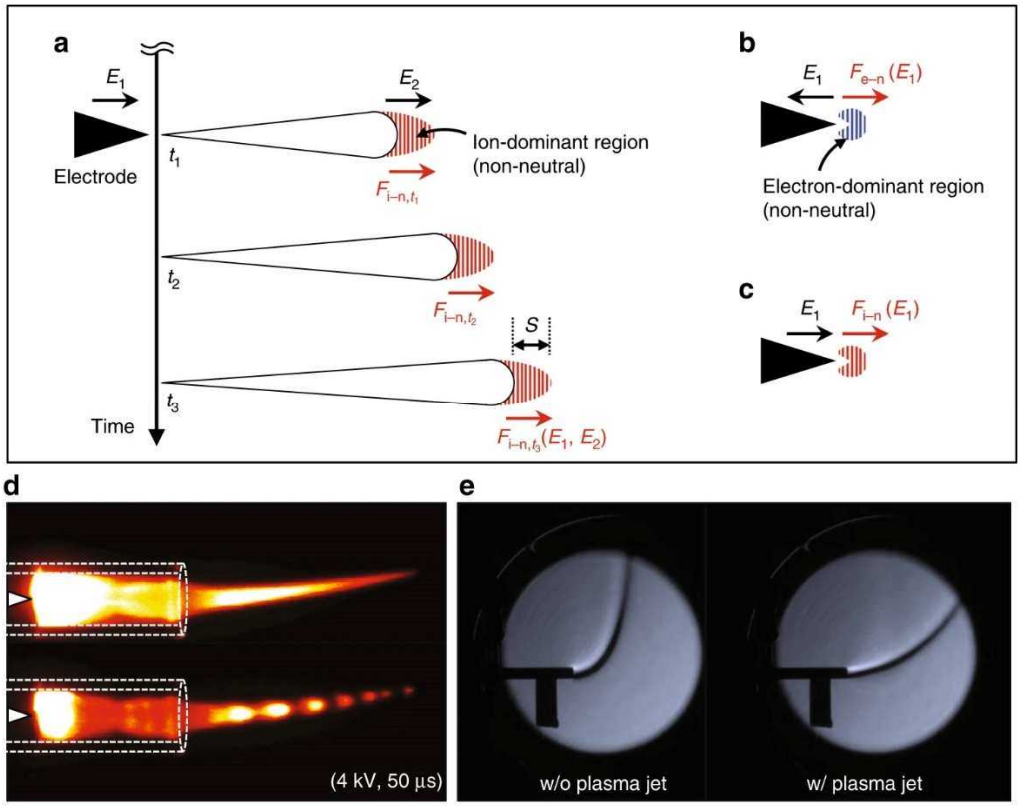

Fig. 14 – "*A simple illustration of* EHD *force generation via different mechanisms. The schematic of* EHD *force generation by* (a) *positive pulsed streamer propagation driven by (positive) ion and the presented space charges behind the moving front, where* E_1 *and* E_2 *represent external and internal electrical fields, respectively. The cases of* EHD *force generation by* (b) *electron drift in negatively pulsed plasma jets or* (c) *ion drift in positively pulsed plasma jets are presented.* (d) *A plasma jet image in continuous mode and composite image of nanosecond-resolved images are presented along with a schematic of the experiment with the glass tubing and electrode.* (e) *The jet of free gas flow without plasma has a flow trajectory or free jet boundary, which is imaged by Schlieren photography, and this trajectory changes when the plasma discharge is turned on, thereby providing information on the flow parameters. The glass tubes with an inner diameter of* $3.5\ mm$ *are used as substitute for scale bars for all images."* See text. Figure and captions after Park et al. (2018). Reproduced with permission of *Nature Communications* ("Open Access").

That is, the phenomenon illustrated by Park et al. (2018) considers a weakly ionized medium, which is not the case of the solar wind. However, consider the great mass difference between protons and positive ions compared to electrons. The solar corona expands radially due to the mass of protons and positive ions, while electrons only ensure the Alfvén frozen-in approximation of the magnetic field. The aforementioned collimation of the solar wind caused by the Cowling dynamo is a mere e.m. effect associated to electrons, while the energy is supplied by the local micro-convection associated to the local temperature gradient due to protons and positive ions. Thus, local toroidal magnetic fields cause compression and collimation of the solar wind.

An additional effect, however, must be considered, due to the enormous mass difference between protons and positive ions, and electrons. The larger mass of protons and positive ions determines a local radial electric current, and an associated circular magnetic field, which results in a spiral motion of the electrons. This motion overlaps to the confinement effect due to the Cowling dynamo, and both effects contribute to the self-collimation of the solar wind.

The luminous blobs in the lower part of Fig. 14d are due to the pulsed injection of He, and every blob is equivalent to a *BL*.

In addition, in this same respect, some features observed in the solar photosphere show extremely thin lineaments. According to Parker (2000), the previous finest optically detected features are called "fibrils" were as detailed as ~ $100\ km$. In this same respect, Yu et al. (2023), illustrated by *New Jersey Institute of Technology* (2023), reported detailed radio observations of an extraordinary aurora-like display, occurring $40{,}000\ km$ above a sunspot. When considering a nebula of a forming star, a large amount of available pictures displays a clear toroidal pattern of $\boldsymbol{B}$.

New Concepts in Global Tectonics Journal
Volume 14, Number 1, January 2026
ISSN number; ISSN 2202-0039

Similarly, stars inside galaxies are observed located along alignments, likewise galaxies inside galactic superclusters (both features, to our knowledge, are unexplained). That is, clear observations are available of unexplained alignments and self-confinements that seem to be ubiquitous on much different scale-sizes, in both space and time. E.g., some mysterious enormous radio wave circles were discovered in 2019 (Coil et al., 2024, illustrated by *University of California - San Diego,* 2024). The Cowling dynamo is a very general and ubiquitous occurrence in the universe. For these and several analogous items see Gregori et al. (2025w).

Molecular phenomena

The Cowling dynamo holds as long as Maxwell laws apply, as the "*principle of magnetic energy variation*" is the basic tool needed to prove the generalized Cowling theorem. Inside atoms and molecules, however, Maxwell laws do not hold, and one must refer to the Schrödinger equation. Owing to several reasons it is reasonable to assume that, in any case, the principle applies by stating that a system tends of maximize the joint energy between components of the natural system, and to minimize the self-energy of every component.

Differently stated, a backcountry exists between the domain where Maxwell laws hold, and the domain where quantum mechanics must apply. In this backcountry the "*principle of magnetic energy variation*" is likely to apply, although after suitable adaptation. This seems crucial when dealing with molecular phenomena, such as crystal physics, or biological phenomena, cell physics, etc. Let us discuss this challenging item in some detail. For this purpose we should look at phenomena from a more general perspective, according to what can be here only concisely outlined (refer to Gregori, 2005, and more extensively to Gregori et al., 2022, 2022a, 2022b, 2022c, 2022d, 2022e, 2023). This is a preliminary short account aims to focus on a few essential items, while a much longer treatment in terms of a wider perspective is given in Gregori et al. (2025w).

Nature is organized in closed domains ("*monads*") that interact and exchange information through quanta (named "*virtues*") released by one monad and received by another monad (this reminds about the Feynman graphs). We can know phenomena that occur inside one monad only if we live inside that monad, while - concerning monads that we can observe only from outside (such as atoms and molecules) - we can observe "*virtues*", and we can only guess some hidden parameters, which are arbitrary. Note that we must rebut several classic concepts, such as action-at-a-distance, force, field, gravitation, etc.

The Schrödinger equation governs phenomena that occur inside the monad atom, or inside the monad molecule. Atoms and molecules, however, display some symmetries. These symmetries are reflected by the "*virtues*" through which various monads interact. This is the leading principle that leads crystallography.

Another key concept deals with the arrow of time, and with the search for equilibrium (Gregori et al., 2022). This is related to the strict need to conceive the whole universe as a unique natural system. This implies the concept of irreversibility of phenomena, which is synonymous of perception of the one-way direction of the arrow of time. Since, owing to the need for "simplicity" by the human mind, we must rather refer to separate subsystems of the whole universe, by this we miss the perception of "irreversibility". Note that the perception of the direction of the arrow of time is shared by every living being, just for a matter of survival. The difference of the humans is that the humans keep memory of the elapsing "time".

The monad represented by the whole universe evolves through states of progressive approach to a final equilibrium, which, however, is never attained. In any case, every system always evolves according to some variation principle. This is the meaning of the golden ratio observed in several phenomena – which is also related to fractal properties. Complete equilibrium is never attained because the golden ratio φ is an irrational number – conversely, with a rational φ the entire universe would soon become a non-evolving world, almost like a dead swamp, and we could not even define "time". Note that, if "irreversibility" (connected with fractal properties) applies also inside the monads atoms and molecules, one should find the golden ratio hidden somewhere also in spectra and/or in the Mendeleev table. In fact, Pellis (2022) shows a close relationship between the golden ratio and the fine structure of atomic spectra, and this proves that the golden ratio is a leading feature inside spectra.

The universe seemingly progresses through a denumerable series of states that can be associated to some number in a sequence, such as, e.g., the Fibonacci sequence. However, as soon the boundary conditions change, a new final equilibrium is defined and the evolution changes accordingly. That is, the perception of the one-way direction of the arrow of time is synonymous of the perception of "irreversibility" (Gregori et al., 2022a).

The evolution, perhaps, occurs and is characterized by a selected set of key numbers in the Fibonacci sequence (Gregori et al., 2022), and this should explain why similar living species, which should be expected to be identical, eventually display a varied morphology. This occurs, e.g., whenever similar vegetables or fruits display a variety of forms (see, e.g., Fig. 15). This should also justify the different shapes of leaves etc. Every form ought to represent a different status of relative maximum joint energy - or minimum self-energy of the constituent parts - and a different typical reference-number characterizes every different morphology.

When similar monads – such as similar molecules - interact each other, they respond to some internal symmetries. This is the principle that governs crystallography. Every micro-crystal is a monad that interacts with other similar monads, always reminding about the innate symmetry, thus composing a larger monad. Every micro-crystal, as a monad, has a shell of electrons that are almost like a cage that isolate the inner from the outer space. These electron shells, maybe, interact according to the "*principle of magnetic energy variation*". Differently stated, the original formation of atoms or molecules occurs through Schrödinger. Then, the

New Concepts in Global Tectonics Journal
Volume 14, Number 1, January 2026
ISSN number; ISSN 2202-0039

subsequent interaction between micro-crystals occurs through links between the outer shells of electrons of every monad. This is the backcountry between quantum mechanics and Maxwell laws. Refer to Gregori et al. (2025w) for additional details.

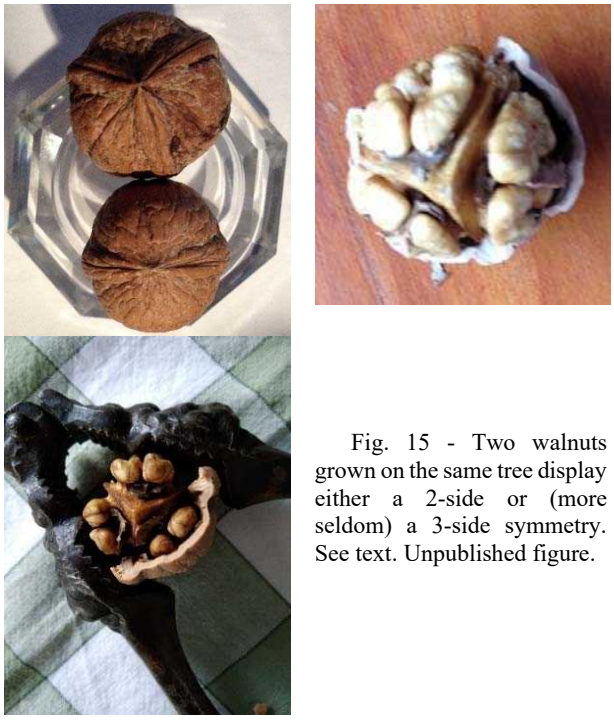

Fig. 15 - Two walnuts grown on the same tree display either a 2-side or (more seldom) a 3-side symmetry. See text. Unpublished figure.

However, it is impossible to enter here into the discussion of these very specific, though crucial, items that, since the times of these old papers, certainly experienced a relevant progress. It is here only stressed that the largest fraction of the fundamental micro-physical and chemical aspects of water condensation and precipitation in the atmosphere remains essentially poorly understood. At the same time, compared to the intrinsic and objectively great difficulty of the problem, a simple approach in terms of thermodynamics and energy balance is certainly partial and understating.

In addition, Biello (2008) and Christner et al. (2008) showed that the biosphere, with its microorganisms, seems to play a role in favoring water condensation. Schiermeier (2008) claims that "*studies on freshly fallen snow suggest that 'bio-precipitation' might be much more common than was suspected.*" Aerobiology is a wide discipline, with specific specialists, with dedicated journals and international meetings, etc. focused on the interaction between air and biosphere.[23]

The role of a thin cover of elementary and very minor organisms (lichens and/or fungi) in the control of rain, was shown by Otterman as specifically discussed in Gregori et al. (2025j). In any case, the biosphere - unlike what is generally assumed - plays a crucial active and not simply passive role. The interaction between wind-blown air and Earth's surface is therefore critical, depending on the biological cover of Earth's surface. That is, it is not only a simple matter of electrostatic interaction. The study of all these items is still in its infancy.

At present, several aspects are unknown of these fundamental processes. The role of quantum processes is the object of specific studies that deal with the so-called "quantum phase transitions", which are defined as the phase transitions that occur at zero temperature. Distinct states of matter coexist at a transition, and quantum fluctuations occur between them, with collective behavior [see the *Nature Physics Focus* issue of March 2008, Vol. 4, No. (3), 167-204.] However, compared to the complication of phenomena that are observed in the natural environment, these investigations appear to be still preliminary.

Summarizing, the very early mechanism of water condensation occurs according to the process sketched in Figs 11 and 12. Then, organic components play an important role, also depending on surface phenomena, which can control the interaction with water molecules by means of peculiar 2D pentagonal or hexagonal molecular rings, etc.

When this trigger stage is in progress, it is usual to state that a water droplet or an ice crystal is formed depending on local temperature. Such a statement is, however, understating as it reflects a mere concern about thermodynamics. On the other hand, at this comparatively early stage, the application is premature of thermodynamics. One should rather consider the role of the Cowling dynamo and of the $\boldsymbol{E}$ field. In addition, the evolution occurs according to the delicate rules of the Nakaya diagram (see Gregori et al., 2025w) that depend on air chemistry and on its pollution, because water molecules, when water is "doped" by a pollutant, behave much differently on different kinds of solid surfaces or of liquid-like surfaces. These phenomena may appear a mere academic curiosity. In reality, these processes play a crucial role in the water behavior in the atmosphere.

Differently stated, the "poetic" fascination of a wonderful snow crystal hides a profound implication for climate control, either for amplifying or for reducing the impact of every different pollutant.

In any case, it is unlikely than thermodynamics alone can give a reliable hint for understating the beginning of water precipitation phenomena, including the cause of atmospheric transparency and - in the final analysis - for the whole radiative energy balance of the atmosphere. A huge discipline exists that deals with these items and is the object of important and learned debates.

A large number of topics cannot here be treated. Several difficult problems remain to be solved, concerning the

[23] At present, satellite monitoring for aerobiology seems not to be available. Also, seasonal variation effects are being investigated. Even wind-blown microplastics were observed in the French Pyrenees (Allen et al., 2019; Zhang et et al.,2020). Also olfactory phenomena seem to be related to bird migration (Abolaffio et al., 2018). Some important satellite monitoring of the biosphere is available inside ocean water, but these items are not discussed here.

ISSN number; ISSN 2202-0039

competing role of microphysics with phenomena averaged over large volumes.

When dealing with other crystals, the unexplained features are increasingly complicated - and even more so when dealing with intricate organic compounds, or with cell physics. We can observe interesting symmetries and self-similarities that envisage an extremely complicated explanation. Refer to Gregori et al. (2025w) for additional details and discussion, including the origin of life.

At present, one can only guess that measurements ought to be carried out of the electric phenomena inside biological systems, because e.m. phenomena (either electrostatics, or Cowling dynamo) are the likely keys to understanding these challenging features. Every final assessment is premature. However, e.m. phenomena are the likely key to promote the understanding of these fascinating aspects of life, including the endemic origin of life in the matter of galaxies - and symmetrically the endemic generation of anti-life in the anti-matter of anti-galaxies (see Gregori et al, 2025w).

Acknowledgement

We acknowledge all co-workers that, during decades, and in different ways contributed to the exploitation of the analyses mentioned in the present study. We especially like to thank Willie Soon and Victor Manuel Velasco Herrera for some relevant information, and in particular concerning their fundamental papers Velasco Herrera et al. (2021, 2022), high-quality figures and permission to use figures. We also warmly thank Dong WenJie and Gao Xiaoqing for providing valuable information on some investigations of the school of the late Professor Tang MaoCang. We also appreciate the warm encouragement we had over the years from several outstanding scientists.

Funding Information

G.P. Gregori is retired since 2005. B.A. Leybourne is a semi-retired self-funded independent researcher. J.R. Wright is retired since 2004.

Author's Contributions

This study derived from a long-lasting cooperation by both authors. The backbone draft was prepared by the first author, although several ideas resulted from the emergence of long-lasting discussions with all coauthors.

Ethics

This article is original and contains unpublished material. Authors declare that there are no ethical issues and no conflict of interest that may arise after the publication of this manuscript.

References

Abolaffio, M., Reynolds, A.M., Cecere, J.G., Paiva, V.H. and Focardi, S., 2018. Olfactory-cued navigation in shearwaters: linking movement patterns to mechanisms, Nature Science Reports, 8 (1): 11590. DOI:10.1038/s41598-018-29919-0

Allen, S., Allen, D., Phoenix, V.R., Le Roux, G., Durántez Jiménez, P., Simonneau, A., Binet, S. and Galop, D., 2019. Atmospheric transport and deposition of microplastics in a remote mountain catchment, Nature Geoscience, 12: 339–344. DOI: 10.1038/s41561-019-0335-5

Babcock, H.W. and Babacock, H.D., 1955. The Sun's magnetic field, 1952-1954, Astrophysical Journal, 121: 349-366; DOI:10.1086/145994

Babcock, H.W. and Babacock, H.D., 1955a. The Sun's magnetic field and corpuscular emission. Nature, 175(4450): 296-296; DOI:10.1038/175296a0

Bellan, P.M., 2023. Energetic electron tail production from binary encounters of discrete electrons and ions in a sub-Dreicer electric field, Physics of Plasmas; DOI:10.1063/5.0167004

Biello, David, 2008. Do microbes make snow? *Scientific American*., 298, February 28th: 6

Biermann, L., 1941. Der gegenwärtige Stand der Theorie konvectiver Sonnenmodelle. Vierteljahrsschrift der Astronomischen Gesellschaft, Leipzig, 76: 194-200. [After 1950 the journal continued as Mitteilungen der Astronomischen Gesellschaft, Hamburg]

Chandrasekhar, S. and Fermi, E., 1953. Problems of gravitational stability in the presence of a magnetic field. Astrophysical Journal, 118: 116-141

Chapman, S. and Bartels, J., 1940. Geomagnetism. 2 vol., Oxford Univ. Press, (Clarendon), London and New York. pp. 1049

Christner, B.C., Morris. C.E., Foreman, C.M., Cai, R. and Sands, D.C., 2008. Ubiquity of biological ice nucleators in snowfall, *Science*, 319 (5867): 1214-. DOI:10.1126/science.1149757

Coil, A.L., S. Perrotta, D.S.N. Rupke, C. Lochhaas, C.A. Tremonti, A. Diamond-Stanic, D. Fielding, J.E. Geach, R.C. Hickox, J. Moustakas, G.H. Rudnick, P. Sell, and K.E. Whalen, 2024. Ionized gas extends over 40 kpc in an odd radio circle host galaxy, Nature; DOI:10.1038/s41586-023-06752-8

Cowling, T.G., 1933 or 1934. The magnetic field of sunspots. Monthly Notices of the. Royal Astronomical Society, 94: 39-48

Elsasser, W M., 1956. Hydromagnetism. 2. A review. American Journal of Physics, 24: 85-110

Fearn, D.R., 1998. Hydromagnetic flow in planetary cores. Reports of Progress in Physics, 61: 175-235

Gregori, G. P., 2002. Galaxy – Sun – Earth relations. The Origin of the Magnetic Field and of the Endogenous Energy of the Earth, with Implications for Volcanism, Geodynamics and Climate Control, and Related Items of Concern for Stars, Planets, Satellites, and Other Planetary Objects. A Discussion in a Prologue and Two Parts. *Beiträge zur Geschichte der Geophysik und Kosmischen Physik*, Band 3, Heft 3: pp. 1-471 [Available at http://ncgtjournal.com/additional-resources.html]

ISSN number; ISSN 2202-0039

Gregori, G. P., and B. A. Leybourne, 2025b. The electrostatic Sun. In press in *New Concepts in Global Tectonics, Journal*

Gregori, G. P., and B. A. Leybourne, 2025e. The physics of electrical discharges – 1. Small-scale phenomena - Fog - atmospheric precipitation – BLs. In press in *New Concepts in Global Tectonics, Journal*

Gregori, G. P., and B. A. Leybourne, 2025f. The physics of electrical discharges – 2. RB & TGFs - Runaway breakdown – terrestrial gamma flashes – GK effect. In press in *New Concepts in Global Tectonics, Journal*

Gregori, G. P., and B. A. Leybourne, 2025g. The physics of electrical discharges – 3. Sparks and lightning - electrostatics of the ionosphere – TLEs - plasma jets collimation – Birkeland currents & sea-urchin spikes - stellar and galactic alignments. In press in *New Concepts in Global Tectonics, Journal*

Gregori, G. P., B. A. Leybourne, Dong Wenjie, and Gao Xaoqing, 2025j. Topics in palæoclimatology - The role of the biosphere for air-earth currents. *New Concepts of Global Tectonics, Journal,* 13, (8): 1234-1331

Gregori, G. P., B. A. Leybourne, Dong Wenjie, and Gao Xaoqing, 2025l. Energy release from *ALB*, *CMB* and *ICB* and secular variation. II – Methods: the "principle of magnetic energy variation" & Joule heat on a spherical shell of currents *New Concepts in Global Tectonics, Journal*, 13, (3): 350-377

Gregori, G. P., B. A. Leybourne, Dong Wenjie, and Gao Xaoqing, 2025o. Energy release from *ALB*, *CMB* and *ICB* and secular variation. V – Results, *New Concepts in Global Tectonics, Journal*, 13, (3): 433-459

Gregori, G. P., B. A. Leybourne, Dong Wenjie, and Gao Xiaoqing, 2025h. Shallow geotherms. *New Concepts in Global Tectonics, Journal,* 13, (8): 1080-1169

Gregori, G. P., C. W. Monckton of Brenchley, W. Soon, R. Tattersall, A. D'Amico†, G. Zimatore, V. M. Velasco Herrera, B. A. Leybourne, and Z. A. Oziewicz†, 2022. The golden Ratio, variational principles, cyclic and wave phenomena, and Quanta. In H. M. Colin Garcia, J-de-J. Cruz Guzman, L. H. Kauffman, and H. Makaruk, (eds), *Scientific Legacy of Professor Oziewicz, selected papers from the International Conference "Applied Category Theory Graph-Operated-Logic"* held in honor of Professor Zbigniew Oziewicz in Memoriam (August 25th to 27th, 2021), World Scientific, Series on Knots and Everything; DOI:10.1142/9789811271151.0018: 363-389; http://ncgtjournal.com/additional-resources.html

Gregori, G. P., M. T. Hovland, B. A. Leybourne, S. Pellis, V. Straser, B. G. Gregori, G. M. Gregori, and A. R. Simonelli, 2025w. Air-earth currents and a universal "law": filamentary and spiral structures - Repetitiveness, fractality, golden ratio, fine-structure constant, antifragility and "statistics" - The origin of life, *New Concepts in Global Tectonics, Journal*, 3, (1): 106-225

Gregori, G. P., W. Soon, V. Straser, and B. A. Leybourne, 2022a. Golden ratio, fractals, and the arrow of time. Irreversibility vs. reversibility - Space, time, antitime - The foundations of physics. *New Concepts in Global Tectonics, Journal*, 10 (3): 158-201

Gregori, G. P., W. Soon, V. Straser, and B. A. Leybourne, 2022b. The foundations of physics and axiomatics. I - Axioms. *New Concepts in Global Tectonics, Journal*, 10 (3): 202-235

Gregori, G. P., W. Soon, V. Straser, and B. A. Leybourne, 2022c. The foundations of physics and axiomatics. II - Algorithms and equations, and a comparison with Einstein's theory of relativity. *New Concepts in Global Tectonics, Journal*, 10(3): 236-262

Gregori, G. P., W. Soon, V. Straser, and B. A. Leybourne, 2022e. The foundations of physics and axiomatics. IV - The geometrical representation of symmetries - Parity, emp, and charge (PEC) "meta-multiverse". *New Concepts in Global Tectonics, Journal*, 10 (3): 284-299

Gregori, G.P., 2005. Relativity, Quanta, Gravitation and Cosmology. A Discussion on the Cognitive Process in Theoretical Physics, Sonderband Beitr. Gesch. Geophy. Kosm. Physik, Science Edition. ISSN: 1615-2824, pp: 1-219

Gregori, G.P., F.C. Wezel†, L.C. Gregori, B.A. Leybourne, W. Soon, and V. Straser, 2023. Archæology of the concept of "time" in the ancient Western, Eastern, and Far Eastern cultures The foundations of physics, *New Concepts in Global Tectonics, Journal*, 11 (1): 3-34

Gregori, G.P., W. Soon, V. Straser, and B.A. Leybourne, 2022d. The foundations of physics and axiomatics. III - Superluminal phenomena, mechanisms, matter-antimatter, cosmological implications. New Concepts in Geoplasma Tectonics, 10(3): 263-283

Griffiths, D.H. and King, R.F., 1965. Applied Geophysics for Engineers and Geologists, Pergamon Press, London. ISBN 9780080107493, pp: 1-223

Hide, R., 1979a. Dynamo theorems, Geophysical and Astrophysical Fluid Dynamics, 14: 183-186

Hide, R., 1981. The magnetic flux linkage of a moving medium: a theorem and geophysical applications. Journal of Geophysical Research, 86(B12): 11,681-11,687

Hide, R., 2000. Generic nonlinear processes in self-exciting dynamos and the long-term behaviour of the main geomagnetic field, including polarity superchrons, Philosophical Transactions of the Royal Society of London, 358A: 943-955

Hide, R., and Palmer, T.N., 1982. Generalisation of Cowling's theorem. Geophysical and Astrophysical Fluid Dynamics, 19: 301-309

Kaiser, R., Schmitt, B.J., and Busse, F.H., 1994. On the invisible dynamo. Geophysical and Astrophysical Fluid Dynamics, 77: 91-109

Larmor, Sir J., 1919. How could a rotating body such as the Sun become a magnet? British Association Report: 159-160, Bournemouth

Larmor, Sir J., 1919a. Possible rotational origin of magnetic fields of Sun and Earth. Electrical Review, 85: 412 (or 512?)

Larmor, Sir J., 1920. How could a rotating body such as the Sun become a magnet?, Report of the British Association for the Advancement of Science,

Bournemouth Meeting, 1919: 159-160, also in Mathematical and physical papers, Vol. II, Cambridge University Press, 1929, p: 611-612

Leibniz Institute for Astrophysics Potsdam, 2023. Riding the cosmic wave: how plasma instability is changing our view of the universe, SciTechDaily, issued December 15, 2023

New Jersey Institute of Technology, 2023. Mysterious aurora-like radio emissions uncovered above a sunspot, SciTechDaily, issued November 16, 2023

Ouzounov, D., Pulinets, S., Hernandez-Pajares, M., Hattori, K. and Garcia-Rigo, A., 2014. Geo-Space Observation of Atmospheric Environmental Effects Associated with 2011 Fukushima Nuclear Accident, (poster), EGU General Assembly 2014.

Park, S., U. Cvelbar, W. Choe, and Se Youn Moon, 2018. The creation of electric wind due to the electrohydrodynamic force, Nature Communications, 9:371-378; DOI:10.1038/s41467-017-02766-9

Parker, E.N., 2000. The physics of the Sun and the gateway to stars. Physics Today, 53 (6): 26-31

Pellis, S., 2022. Fine-Structure Constant from the Golden Angle, the Relativity Factor and the Fifth Power of the Golden Mean, Preprint,·September 2022; DOI:10.13140/RG.2.2.21052.31363/1. See https://www.researchgate.net/publication/363268874

Schiermeier, Q., 2008. 'Rain-making' bacteria found around the world. Some microbes are frequent flyers in clouds. Nature, News, 28th February. DOI:10.1038/news.2008.632

Shalaby, M., R. Lemmerz, T. Thomas, and C. Pfrommer, 2022. The mechanism of efficient electron acceleration at parallel non-relativistic shocks. arXiv:2202.05288

Shalaby, M., T. Thomas, and C. Pfrommer, 2021. A new cosmic-ray-driven instability, The Astrophysical Journal; DOI:10.3847/1538-4357/abd02d

Shalaby, M., T. Thomas, C. Pfrommer, R. Lemmerz, and V. Bresci, 2023. Deciphering the physical basis of the intermediate-scale instability, Journal of Plasma Physics; DOI:10.1017/S0022377823001289

Sharma, P.V., 1976. Geophysical Methods in Geology, Elsevier Scientific Publ. Co., Amsterdam etc., pp: 1-428

University of California - San Diego, 2024. Cosmic puzzles: the mystery behind universe's rare radio circles unveiled, issued January 14, 2024

Velasco, E., 2023. Redefining physics: plasma jets with unexpected X-ray emissions, SciTechDaily, issued December 22, 2023

Yu, Sijie, Bin Chen, R. Sharma, T.S. Bastian, S. Mondal, D.E. Gary, Yingjie Luo, and M. Battaglia, 2023. Detection of long-lasting aurora-like radio emission above a sunspot, 2023, Nature Astronomy; DOI:10.1038/s41550-023-02122-6

Zhang, Y., Kang, S., Allen, S., Allen, D., Gao, T., and Sillanpää, M. 2020. Atmospheric microplastics: a review on current status and perspectives, Earth-Science Reviews, 203: 103118. DOI:10.1016/j.earscirev.2020.103118

Zyga, L., 2018. What causes ionic wind? Phys.org, issued February 7th, 2028

Acronyms

BL – ball lightning
CB - Chapman-Bartels (algorithm)
CC - cloud-to-cloud discharges
CG - cloud-ground discharges
CMB - core mantle boundary (of the Earth)
e.m. electromagnetic
EGD - electro-gas dynamics
EHD - electro-hydro dynamics
IC - inner core (of the Earth)
INGV – Istituto Nazionale di Geofisica e Vulcanologia
MHD – magneto-hydro dynamics
OC - outer core (of the Earth)
QS - quasi-stationarity
SH - spherical harmonic
SHE - spherical harmonic expansion
TGF – terrestrial gamma flashes
TLE – transient luminous phenomena

ISSN number; ISSN 2202-0039

ABOUT THE NCGT JOURNAL

The NCGT Newsletter, the predecessor of the NCGT Journal, was begun as a result of discussions at the symposium "Alternative Theories to Plate Tectonics" held at the 30th International Geological Congress in Beijing in August 1996. The name is taken from an earlier symposium held in association with the 28th International Geological Congress in Washington, D. C. in 1989. The first issue of the NCGT Newsletter was December 1996. The NCGT Newsletter changed its name in 2013 to the NCGT Journal. Aims of the NCGT Journal include:

1. Providing an international forum for the open exchange of new ideas and approaches in the fields of geology, geophysics, solar and planetary physics, cosmology, climatology, oceanography, electric universe, and other fields that affect or are closely related to physical processes occurring on Earth from its core to the top of its atmosphere.
2. Forming an organizational focus for creative ideas not fitting readily within the scope of dominant tectonic models.
3. Forming the basis for the reproduction and publication of such work, especially where there has been censorship or discrimination.